

# Sarah Goes Left and Right Looking Beyond the Standard Model and Meets Susy

Dissertation  
zur  
Erlangung des Doktorgrades (Dr. rer. nat.)  
der  
Mathematisch-Naturwissenschaftlichen Fakultät  
der  
Rheinischen Friedrich-Wilhelms-Universität Bonn

vorgelegt von  
**Toby Oliver Opferkuch**  
aus  
Subiaco, Australien

Bonn, 01.06.2017

Dieser Forschungsbericht wurde als Dissertation von der  
Mathematisch-Naturwissenschaftlichen Fakultät der Universität Bonn angenommen und ist  
auf dem Hochschulschriftenserver der ULB Bonn  
[http://hss.ulb.uni-bonn.de/diss\\_online](http://hss.ulb.uni-bonn.de/diss_online) elektronisch publiziert.

1. Gutachter: Prof. Herbert K. Dreiner Ph.D.  
2. Gutachter: Prof. Dr. Hans-Peter Nilles

Tag der Promotion: 07.07.2017  
Erscheinungsjahr: 2017

# Summary

---

Progress in the search for physics beyond the Standard Model (BSM) proceeds through two main avenues. The first requires the development of models that address the host of theoretical and experimental deficiencies of the Standard Model (SM). The second avenue requires scrutinising these models against all available data as well as checks for theoretical consistency. Unfortunately there exists a large number of strongly motivated models as well as an absence of any signs illuminating the correct path nature has chosen. With the lack of a clear direction, automated tools provide an effective means to test as many models as possible.

In this thesis we demonstrate how the SARAH framework can be used in this context as well as its adaptability for confronting unexpected hints of new physics, such as the diphoton excess, that have arisen at the Large Hadron Collider (LHC) over the previous years. We then turn to more theoretical constraints namely, studying the stability of the electroweak vacuum in minimal supersymmetric models. Here we studied the impact of previously neglected directions when including non-standard vacuum expectation values. In the second half of this thesis we consider low-scale left-right symmetric models both with and without supersymmetry. In the non-supersymmetric case we consider constraints arising from charged lepton flavour violation. We have significantly improved existing parametrisations allowing for the new Yukawa couplings to be determined as a function of the underlying model parameters. The last scenario we consider is a model based on  $SO(10)$  unification at the high-scale. We build a complete model with TeV-scale breaking of the left-right phase studying in detail the phenomenology.



# Acknowledgements

---

The only place to start is by thanking Herbi Dreiner for the opportunity to undertake my PhD studies under his supervision. I believe that it would be nigh on impossible to find anyone else that I'd rather call my 'Doktorvater'. I'd also like to thank Hans-Peter Nilles not only for referring my dissertation, but also for the many insightful discussions during my time in Bonn and the time and effort taken by both Philip Bechtle and Martin Langer to be the final members of my thesis committee.

This brings me to all of my fantastic collaborators. In particular I'd like to thank Florian Staub for taking me under his wing and undertaking a huge amount of responsibility in ensuring I survived the turbulent waters that are known as the PhD studies. Without his patience and support I'm sure I would not be here today! I am also deeply indebted to both Manuel Krauss and Lorenzo Ubaldi, who both at varying times throughout my PhD played significant roles both as collaborators and as emotional support. Last but not least from my local collaborators, with whom I have had a wonderful time with, Stefano Colucci, Daniel Dercks, Annika Reinert and Martin Winkler. This leaves a number of my remaining external collaborators whom I would also like to thank namely, Cesar Bonilla, Guido Festuccia, Martin Hirsch and Werner Porod as well as my collaborators during the exciting diphoton excess times. A very special mention goes to Victor Martin Lozano, Manuel Krauss and Lorenzo Ubaldi for proof reading this thesis.

I would like to thank all the people who have made the BCTP an exceptional place to work. Of course if there wasn't somebody around to keep the physics kindergarten in check and to assist us through the countless bureaucratic hurdles then I'm convinced the BCTP would have ground to a halt. To that end I'd like thank Dagmar Faßbender, Patricia Zündorf, Christa Börsch and Petra Weiß.

I'm also greatly indebted to my family for their support and understanding, especially with the appalling infrequency of my return trips home. Finally, without Stephanie none of this would have been possible. I can't emphasise enough how fortunate I am to have her in my life.



# List of Publications

---

- [1] D. Dercks, H. K. Dreiner, M. E. Krauss, T. Opferkuch, A. Reinert,  
*R-Parity Violation at the LHC*,  
**Submitted to Eur. Phys. J. C**, arXiv:1706.09418 [hep-ph].
- [2] M. E. Krauss and T. Opferkuch and F. Staub,  
*Spontaneous Charge Breaking in the NMSSM - Dangerous or not?*,  
**Eur. Phys. J. C (2017) 77: 331**, arXiv:1703.05329 [hep-ph].
- [3] C. Bonilla, M. E. Krauss, T. Opferkuch, W. Porod,  
*Perspectives for Detecting Lepton Flavour Violation in Left-right Symmetric Models*,  
**JHEP 03 (2017)**, arXiv:1611.07025 [hep-ph].
- [4] H. K. Dreiner, M. E. Krauss, B. O’Leary, T. Opferkuch, F. Staub,  
*Validity of the CMSSM Interpretation of the Diphoton Excess*,  
**Phys. Rev. D94 (2016) 055013**, arXiv:1606.08811 [hep-ph].
- [5] M. E. Krauss, T. Opferkuch, F. Staub, W. Winkler,  
*Soft Gamma Rays from Heavy WIMPs*,  
**Phys. Dark Univ. 14 (2016) 29-34**, arXiv:1605.05327 [hep-ph].
- [6] F. Staub, P. Athron, L. Basso, M. D. Goodsell, D. Harries, M. E. Krauss,  
K. Nickel, T. Opferkuch, L. Ubaldi, A. Vicente, A. Voigt,  
*Precision Tools and Models to Narrow in on the 750 GeV Diphoton Resonance*,  
**Eur. Phys. J. C (2016) 76: 516**, arXiv:1602.05581 [hep-ph].
- [7] M. Hirsch, M. E. Krauss, T. Opferkuch, W. Porod, F. Staub,  
*A Constrained Supersymmetric Left-right Model*,  
**JHEP 03 (2015)**, arXiv:1512.00472 [hep-ph].
- [8] G. Festuccia, T. Opferkuch, L. Ubaldi,  
*Dynamical Generation of the Peccei-Quinn Scale in Gauge Mediation*,  
**Phys. Rev. D92 (2015) 015020**, arXiv:1504.07634 [hep-ph].

The work presented in this thesis contains results from the publications [2-4] and [6-7].



# Contents

---

<b>1</b>	<b>Introduction</b>	<b>1</b>
<b>2</b>	<b>Constraining New Physics Models Using Automated Tools</b>	<b>7</b>
2.1	The SARAH Framework . . . . .	8
2.1.1	SARAH . . . . .	8
2.1.2	SPheno . . . . .	10
2.1.3	Vevacious . . . . .	10
2.1.4	Other Tools . . . . .	11
2.2	The Diphoton Excess . . . . .	12
2.2.1	Experimental Properties of the Diphoton Resonance . . . . .	13
2.2.2	Confronting the Diphoton Excess with Results from Automated Tools . . . . .	16
2.2.3	Diphoton Observables in the SARAH Framework . . . . .	29
2.2.4	Models . . . . .	38
2.3	Conclusion . . . . .	39
<b>3</b>	<b>Vacuum Stability in Minimal Supersymmetric Models</b>	<b>41</b>
3.1	Vacuum Stability in the Constrained MSSM . . . . .	42
3.1.1	Charge and Colour Breaking Minima . . . . .	42
3.1.2	The Diphoton Excess and the CMSSM . . . . .	50
3.1.3	Stop Bound States . . . . .	51
3.1.4	The CMSSM with a 375 GeV Stop . . . . .	55
3.2	Vacuum Stability in the NMSSM . . . . .	58
3.2.1	Spontaneous Charge Breaking Minima in the NMSSM . . . . .	60
3.2.2	Numerical Results . . . . .	65
3.3	Conclusion . . . . .	69
<b>4</b>	<b>Lepton Flavour Violation in Left-Right Symmetric Models</b>	<b>71</b>
4.1	The Minimal Left-Right Symmetric Model . . . . .	73
4.1.1	Model Definition . . . . .	74
4.1.2	Discrete Symmetries . . . . .	75
4.1.3	Scalar Sector and Gauge Symmetry Breaking . . . . .	76

4.2	Neutrino Sector	78
4.2.1	Neutrino masses	78
4.2.2	Parametrisation of the Yukawa Matrices	79
4.3	Results	83
4.3.1	Numerical Set-up	83
4.3.2	Numerical Results	85
4.4	Conclusion	106
<b>5</b>	<b>Supersymmetric Left-Right Models</b>	<b>107</b>
5.1	The Model	108
5.1.1	Superpotential and Particle Content	108
5.1.2	RGE Running of the Sfermions and Gauginos	112
5.1.3	Quark Masses and Mixing	114
5.1.4	Lepton Sector	116
5.2	Phenomenology	117
5.2.1	Higgs Sector	117
5.2.2	Squark Sector	119
5.3	Conclusion	121
<b>6</b>	<b>Conclusions and Outlook</b>	<b>123</b>
<b>A</b>	<b>Supplementary Information for Chapter 5</b>	<b>127</b>
A.1	Scalar Mass Matrices	127

# Chapter 1

## Introduction

---

Particle physics currently stands at an important crossroad. The only laboratory experiment capable of exploring the high energy frontier is the Large Hadron Collider (LHC) at CERN. It has so far collected in excess of  $30 \text{ fb}^{-1}$  at centre-of-mass energies of 13 TeV during run II, closing in on its original design energy of 14 TeV. The most compelling theories constructed to explain new physics insist upon the existence of new physics at the TeV scale. Contrary to this expectation, LHC results contain no direct observation of evidence<sup>1</sup> for new physics beyond the standard model (BSM). We are therefore left with an important question: is the insistence of new physics at the TeV scale incorrect, or is new physics right around the corner potentially hiding under the guise of non-minimal models?

Taking a step back, run I of the LHC has been a huge success. It culminated with the discovery of the Higgs boson in 2012 which forms the final piece of the jigsaw puzzle known as the Standard Model (SM) of particle physics. Over the proceeding years measurements of its properties, such as spin as well as transformations under charge-conjugation and parity, confirmed that this boson carries the quantum numbers expected from the SM Higgs boson. The success of the SM is so significant that it is often exclaimed – whether that be in frustration or admiration – *‘the SM alone explains all the data’*. To give insight into this claim we begin by outlining the typical procedure for building a particle physics model before turning to the specific case of the SM. In particular we emphasise how the ingredients of the SM give rise to such a remarkable description of observed TeV-scale physics.

In any model there are necessarily a number of assumptions that must be made. Here we assume that any model which describes nature at the TeV-scale is described by a quantum field theory that respects Lorentz invariance. Based on these two assumptions a model can then be loosely defined by choosing a set of fields, whose excitations correspond to particles, which transform under a specific set of chosen symmetries. Given the choices made one then simply writes down every type of interaction that is not forbidden by the chosen symmetries.<sup>2</sup>

---

<sup>1</sup> There are currently a number of discrepancies between the Standard Model predictions and  $B$ -meson measurements, such as  $B \rightarrow K^* \mu^+ \mu^-$  as obtained by ATLAS and CMS [1,2]. Taking all  $B$ -meson observables and performing a fit to effective field theory operators can result in a  $4\text{-}5\sigma$  pull from the Standard Model [3]. These results indicate that lepton universality in the Standard Model may be violated. However, the significance of these deviations depends strongly on which effective field theory operators are fit.

<sup>2</sup> One must also make a choice whether or not to enforce the model to be renormalisable. Requiring renormal-

The result necessarily contains a number of free parameters usually in the form of couplings and masses. For the model to make predictions a certain number, if not all, of these parameters must first be determined through experimental measurements or constrained via phenomenological considerations. These experimentally determined values of the SM parameters exhibit peculiarly large hierarchies amongst the couplings that determine the fermion masses. This nevertheless results in a remarkably accurate description of observed high-energy phenomena. We therefore begin by describing the features of the SM field content and symmetries before turning to the specific consequences of the experimentally determined parameter values in the SM.

The SM successfully describes three of the four observed fundamental forces of nature. However, in technical terms the SM is nothing more than a specific type of quantum field theory termed a chiral gauge theory. The foundation of this theory was laid in the 1960's by Glashow, Weinberg and Salam (GWS) [4–7]. In a gauge theory the forces are described through the symmetries of the redundant gauge degrees of freedom. The crux of this model however, is the unification of two of these forces, the electromagnetic and weak forces, called electroweak unification. This is possible through a very particular arrangement of the particle content, namely that left- and right-chiral particles couple differently to the electroweak gauge bosons, described by  $SU(2)_W \times U(1)_Y$  gauge symmetries. These gauge bosons are in fact the exchange particles responsible for the fundamental forces. This arrangement of the particle content in conjunction with the necessary gauge symmetries forbid mass terms for both the fermions and electroweak gauge bosons. An elegant solution to this problem was proposed by Higgs, Brout, Englert, Guralnik, Hagen and Kibble [8–12], typically referred to as the Higgs mechanism. This mechanism, called electroweak symmetry breaking (EWSB) in this specific context, spontaneously breaks the SM gauge symmetries

$$SU(3)_C \times SU(2)_W \times U(1)_Y \xrightarrow{\text{EWSB}} SU(3)_C \times U(1)_{\text{EM}}, \quad (1.1)$$

where  $U(1)_{\text{EM}}$  is the gauge symmetry that describes photons. Consequently this allows for the generation of masses, consistent with experimental observation, for both the fermions and the electroweak gauge bosons whilst ensuring that the photon remains massless. It also predicts the existence of a new massive scalar called the Higgs boson.

The final remaining type of interaction in the SM occurs between colour-charged particles. The theory describing this type of interaction is called quantum-chromodynamics (QCD) [13–17]. It is incorporated into the SM using the gauge group  $SU(3)_C$  where  $C$  is the colour quantum number. The combination of QCD and GWS combined is what has today become known as the SM.

After writing down a model containing the above symmetries and observed particle content we end up with 19 free parameters. These parameters are:

- 3 gauge couplings,
- 9 charged fermion masses,
- 3 mixing angles and 1 phase,

---

isability enforces operators to have mass dimension four or less. Otherwise, one should also consider possible higher mass dimension operators, performing a truncation at a chosen mass dimension.

- 
- Higgs mass and vacuum expectation value,
  - QCD CP-violating vacuum angle  $\bar{\theta}$ .

We therefore require at least 19 independent measurements before predictions can be made. In the SM there is, as of yet, no known reason at a fundamental level why there are for instance, such large mass hierarchies or peculiar mixing patterns in the fermion sector. What is essential to note is that changing any of these parameters, even by tiny amounts, can result in radical changes in the phenomenology of the model. To illustrate this idea, consider the hierarchy in the masses of the lightest generation of quarks. Suppose that the parameters of the theory are slightly modified so that the down-quark becomes lighter than the up-quark. This would have catastrophic implications as the proton would become unstable, decaying to the now lighter neutron, preventing the formation of atoms and therefore life as we know it in our observable universe. While this is a particularly drastic example, shifting any of the SM parameters by even small amounts leads to striking observable consequences [18–20].

The patterns of the SM parameters by themselves raise a number of questions, but in conjunction with observational evidence it is undoubtedly clear that physics beyond the SM is essential. Evidence for BSM physics can be categorised into two groups. Firstly, direct observations that cannot be explained nor accommodated into the SM and secondly, theoretical deficiencies of the SM. Here we begin with the later as many of the theoretical deficiencies of the SM can be tied to its experimentally determined parameters. For instance the measured value of the Higgs mass presents a key challenge to our understanding of quantum field theories. The mass term for a scalar field in quantum field theory appears to be sensitive to the UV theory through quantum corrections [21–23]. If we reject the notion of extreme fine-tuning, these corrections would lead to a Higgs mass that is pushed to the cut-off in the theory. This cut-off is exactly where the SM breaks down and the introduction of new degrees of freedom are required to explain the physics which arises at these energy scales. It is also possible to understand this issue as a naturalness problem. Following 't Hooft's definition of naturalness [24], a parameter is allowed to be much smaller than unity only if setting it to zero enhances the symmetry of the theory. This follows as the radiative corrections in such a scenario are proportional to the breaking parameter. An example of this is the fermions of the SM. When the fermions are massless there exists an additional chiral symmetry. Breaking this chiral symmetry by only the introduction of small fermion masses ensures that the radiative corrections are proportional to these small masses. However, no such additional symmetry arises when setting the Higgs mass to zero and therefore the radiative correction are no longer proportional to this mass term. Therefore the hierarchy between the Higgs mass and the Planck mass is deemed to be unnatural. This phenomenon, known as the *hierarchy problem*, has lain at the centre of model building efforts over the past decades. These efforts have resulted in a number of remarkable types of theories such as supersymmetry [25–28], composite Higgs [29–35], and extra-dimensions [36–39]. Their common theme is that each and every one has predicted that if the hierarchy problem is solved, then there must necessarily be new physics at the TeV scale. However, the absence of TeV-scale physics at the LHC has forced theorists to consider increasingly elaborate models which can solve the hierarchy problem but remain undetectable at the LHC given the current centre-of-mass energies and

collected luminosity.<sup>3</sup>

This sets the stage for the first half of this thesis. Before the LHC began collecting data, there was a strong theoretical bias towards a relatively small number of models. The most widely explored model was the minimal supersymmetric extension of the SM (MSSM) [42–50]. The key reason being that supersymmetry was, and is still today, regarded as the most elegant solution of the hierarchy problem. The solution hinges on extending the Lorentz group to its maximal possible size [51] which allows for the inclusion of fermionic supersymmetry generators. These generators act on particles changing their representations under the Lorentz group, which corresponds to a particles spin. Therefore a theory invariant under supersymmetric transformations requires the introduction of an opposite spin superpartner for each SM particle, namely a spin-1/2 or spin-0 superpartner for a SM boson or fermion respectively. From the non-observation of supersymmetry these superpartners must clearly be heavier than their SM counterparts. However, as the LHC collected more and more data, lower bounds on the masses<sup>3</sup> of the superpartners continued to steadily increase. As it now stands, the most constrained variant of the MSSM not only requires a significant amount of fine-tuning to explain observation [52,53], but has been virtually excluded when one also includes the measurement of the anomalous magnetic moment of the muon,  $(g - 2)_\mu$ <sup>4</sup> [54,55]. There are two main avenues to alleviate this tension: (i) relax the stringent boundary conditions of this constrained model allowing for more freedom in the resulting supersymmetric mass spectra [56–60] or, (ii) introduce additional fields and or symmetries to the theory. Here we will mainly pursue the latter option, as in the MSSM obtaining the correct Higgs mass requires either large mass-splitting between the superpartners of the top-quarks (called stops) or both stops must be very heavy. The first option typically leads to a destabilised electroweak vacuum, which we discuss in detail in Chapter 3, while the second option reintroduces a milder form of the hierarchy problem. Introducing new fields and or symmetries can lead to tree-level contributions to the Higgs mass reducing the need for fine-tuned parameter regions where the radiative corrections are maximised. In Chapter 3 we also explore the impact of new fields on vacuum stability in the simplest extension of the MSSM. However, this next-to-minimal model is simply the tip of the iceberg as there exists no clear theoretical or experimental preference for exactly what type of extension is realised in nature.

The only path forward is to confront the myriad of possibilities with all existing experimental data. This is an enormous task which requires a high level of automation if we wish to leave no stone unturned. This task is further compounded by both the increasing quantity and precision of experimental data that one must consider. Finally, we also want the ability to quickly confront any possible signal of new physics that could arise at any time with the highest possible precision theoretical calculations. So far all possible direct signals of new

---

<sup>3</sup> Many ideas are specifically engineered to produce no signal at the LHC while remaining natural in the sense of fine-tuning. These models can be broadly categorised under the umbrella of *neutral naturalness*. This is where the new BSM physics is not charged under the SM  $SU(3)_C$  gauge symmetry, and hence difficult to produce at the LHC. An example of these types of models is the twin-Higgs model [40] where an entire mirror copy of the SM is added to solve the hierarchy problem. Alternatives exist, such as relaxion models [41], which do not require new observable TeV scale physics. The relaxion mechanism instead utilises axion-like dynamics coupled with an inflaton to dynamically generate the weak scale.

<sup>4</sup> This measurement also deviates from the SM prediction at the  $3\sigma$  level.

---

physics have turned out to be statistical fluctuations. Nevertheless each of these fluctuations has required the construction of completely new models. The most significant of which was the diphoton excess appearing in December 2015 [61,62]. However, sufficiently precise theoretical calculations are typically time consuming and error prone. This led to the development of a meta-code<sup>5</sup> `Mathematica` package called SARAH. It allows for the automated calculation of all ingredients necessary, such as vertices, renormalisation group equations, two-loop Higgs masses as well as the complete one-loop masses of all other scalars and fermions in a given BSM theory. SARAH also produces model files for a vast array of existing high-energy physics tools to perform, for instance, detailed dark matter and collider studies. In Chapter 2 we give an overview of SARAH and the tools it interfaces to. Using the diphoton excess as a case study we then give a detailed introduction into the numerous advantages of these tools as well as the implementation of the relevant observables into the SARAH framework.

While much of the theoretical evidence for BSM physics could conceivably be a product of our lack of understanding, there remains three compelling experimental facts that any extension of the SM should address. These are the observation of at least two massive neutrinos [63–66], indirect evidence for the existence of dark matter [67–69] and finally the observed baryon asymmetry of the universe [70–74]. The second half of this thesis focuses on models where neutrino masses are naturally embedded into the theory. The immediate questions that arises from the neutrino sector are what is the nature of the mass terms and what exactly is the mechanism that allows for the generation of such small masses. One question often raised, is whether or not a neutrino mass mechanism should be part of the usual definition of the SM. The main hurdle being that there exists, much like extensions of the MSSM, numerous mechanisms with which one can produce neutrino masses. The exact details of these mechanisms generally lead to quite striking changes in the phenomenology. This depends firstly on the nature of the neutrinos, be it Majorana or Dirac. And secondly, the additional field content beyond the SM fields required to generate these small masses. As a result physical observables that can distinguish between the neutrino nature are of crucial importance. Meanwhile using both high energy and high intensity experiments, we also seek to either directly or indirectly probe the additional field content required.

Minimal left-right symmetric models automatically provide all the necessary ingredients to explain the observed neutrino masses. These models contain a right-handed neutrino as the phase where the left-right symmetry is unbroken forces both the left- and right-handed fermionic field content to sit in  $SU(2)_L$  and  $SU(2)_R$  doublets, respectively. In this phase the complete gauge symmetries of the theory are  $\mathcal{G}_{LR} \equiv SU(3)_C \times SU(2)_L \times SU(2)_R \times U(1)_{B-L}$ . In particular, this left-right symmetric phase can be at the TeV-scale. Depending on the choice of the extended Higgs sector which breaks this phase down to the SM gauge symmetries, both Majorana and Dirac mass terms for neutrinos can be generated [75–79]. This additional particle content can have a large impact on the rates of charged flavour violation (cLFV). In Chapter 4 we present a complete survey of cLFV in the minimal left-right symmetric model, specifying to the scenario where the left-right symmetric phase is broken by triplets under

---

<sup>5</sup> SARAH is capable of writing complete programs and code interfacing to other high-energy physics programs, hence it is technically a meta-code.

$SU(2)_R$ .<sup>6</sup>

From a top-down approach a compelling motivation for left-right symmetric models arises from their compatibility into an  $SO(10)$  grand unified theory (GUT) [83–85]. Starting with an  $SO(10)$  GUT there exists two main methods to break this group down to the SM gauge group. The first is via  $SU(5)$  (with or without an additional  $U(1)$ ) to the SM and the second is via the left-right symmetric phase.<sup>7</sup> However, in the minimal scenarios the scale of left-right breaking must be at least  $10^{10}$  GeV in order to maintain gauge coupling unification [86]. Introducing supersymmetry, Ref. [87] explores all possible breaking chains to the SM via the various possible left-right symmetric phases. In particular it has been found that there exists a number of possibilities where the left-right phase is broken at the TeV scale while preserving gauge coupling unification.<sup>8</sup> In the final chapter, Chapter 5, we study the phenomenology of the minimal model containing this low-scale left-right broken phase, paying particular attention to the effect of threshold corrections at these scales.

---

<sup>6</sup> The main alternative breaks this symmetry via  $SU(2)_R$  doublets, see for example Ref. [80–82]. However, this does not result in masses for the neutrinos and therefore requires the introduction of additional particles. We therefore consider such a scenario to be disfavoured compared to the triplet case considered.

<sup>7</sup> There exist a number of possibilities for the breaking chain from  $SO(10)$  to the SM gauge group via left-right symmetric phases. For instance a Pati-Salam phase is possible before breaking to the left-right phase as well as breaking the  $SU(2)_R$  in left-right phase to  $U(1)_R$  rather than directly breaking to the SM.

<sup>8</sup> It is also possible to add additional fields to achieve gauge coupling unification without introducing supersymmetry [88].

## Chapter 2

# Constraining New Physics Models Using Automated Tools

---

In the field of particle physics phenomenology there are two main objectives. The first demands that we exhaustively explore all possible classes of extensions to the SM in order to ensure that all promising signatures of these models are properly scrutinised. The second goal is to assess the compatibility of all possible BSM theories with experimental data. This latter objective is not only particularly exciting but becoming increasingly demanding as more and more data becomes available from a vast array of different experiments. To complicate matters further, newly developed extensions of the SM are becoming more and more complicated. The reality of the situation has led over the last years to the development of increasingly sophisticated packages aimed at reducing the labour involved in analysing new models. These packages are designed to automate the calculation of Feynman rules in perturbative quantum field theories which involve spontaneously broken symmetries, gauge or otherwise.

The two prominent tools in this direction are SARAH [89–94] and FeynRules [95]. Both tools perform similar tasks, however SARAH interfaces with a larger number of other complementary particle physics packages. It should be noted that FeynRules is compatible with non-renormalisable operators, whereas SARAH is only compatible with renormalisable theories although work is being undertaken to rectify this deficiency.

In this chapter we begin by giving an overview of the tools involved in what we dub the ‘SARAH framework’. We then discuss the recent diphoton excess reported by ATLAS and CMS using it as an example to highlight the usefulness of these tools. In particular we examine a large number of examples where their use would have helped various authors of diphoton papers to either avoid mistakes or drastically improve the accuracy of their results. Note that many of these examples are very simple applications of quantum field theory. Nevertheless, there was a large array of fundamental errors and overly simplistic assumptions that were made in the diphoton literature. Finally in the latter half of this chapter we consider in detail the implementation of the effective vertices into SARAH and SPheno which are essential for the calculation of the relevant diphoton observables. This sets the stage for the subsequent chapters where we perform detailed studies focusing on many different observables to constrain various BSM theories. To conclude this chapter we provide the full list of diphoton models that were implemented in to SARAH. Here we stress that the main purpose was to

provide a rich array of examples to assist the user in the implementation of their own model.

## 2.1 The SARAH Framework

In this section we give a short introduction into the various tools that are used throughout this thesis to examine the different types of BSM theories. A detailed introduction of the conventions used as well as a comprehensive how-to with numerous examples can be found in Refs. [94, 96].

### 2.1.1 SARAH

The original motivation behind the creation of SARAH [89] was to automate the calculation of the renormalisation group equations (RGEs), mass matrices and vertices from a supersymmetric Lagrangian written in the superspace formalism. In particular the original versions were specifically designed for high-scale supersymmetric models. These are models featuring unification of the gauge couplings at high-energies where boundary conditions on the supersymmetric parameters can be enforced, reducing the number of additional parameters. SARAH has, since this point, evolved into a tool which can handle all renormalisable, perturbative quantum field theories both with and without supersymmetry.

The idea is the user must only give the same information as would be required to define a model on paper. This information namely, the field content, gauge and global symmetries, as well as the symmetry breaking pattern is fed into the SARAH model file. In addition the user must specify which particles mix after symmetry breaking, although there are automated checks that can be run to ensure that no possible mixing has been missed. The model can then be loaded into an interactive `Mathematica` notebook where one has access to all the analytic expressions of the model. Such expressions include the scalar potential, minimisation equations (often termed ‘tadpole equations’), mass matrices, RGEs (at both one- and two-loop level) and vertices. These expressions in the interactive `Mathematica` environment are hugely useful and generally provide the user a first step in analysing a new model. However, the real power of SARAH is its usefulness as a meta-program.

Once a model file for SARAH exists, the SARAH backend<sup>1</sup> can write a complete version of the spectrum generator `SPheno` for the specific model in question as well as model files for other high-energy physics codes. A schematic of these capabilities is shown in Fig. 2.1. This flow-chart also shows what information is exchanged among the different programs. This code includes crucial diagrammatic computations of the two-loop self-energies for the Higgs scalars in the theory for *general* BSM models [97–99]. The incorporation of these two-loop contributions is absolutely crucial in reducing the theory uncertainty on the mass prediction, especially in theories such as the MSSM where large radiative corrections are essential. For example in the next-to-minimal supersymmetric model (NMSSM), it has been shown in

---

<sup>1</sup> Here the SARAH backend refers to the routines in SARAH where the results are not directly accessible in the `Mathematica` interface. Examples include the routines used to write code for `SPheno` and other high-energy physics tools.

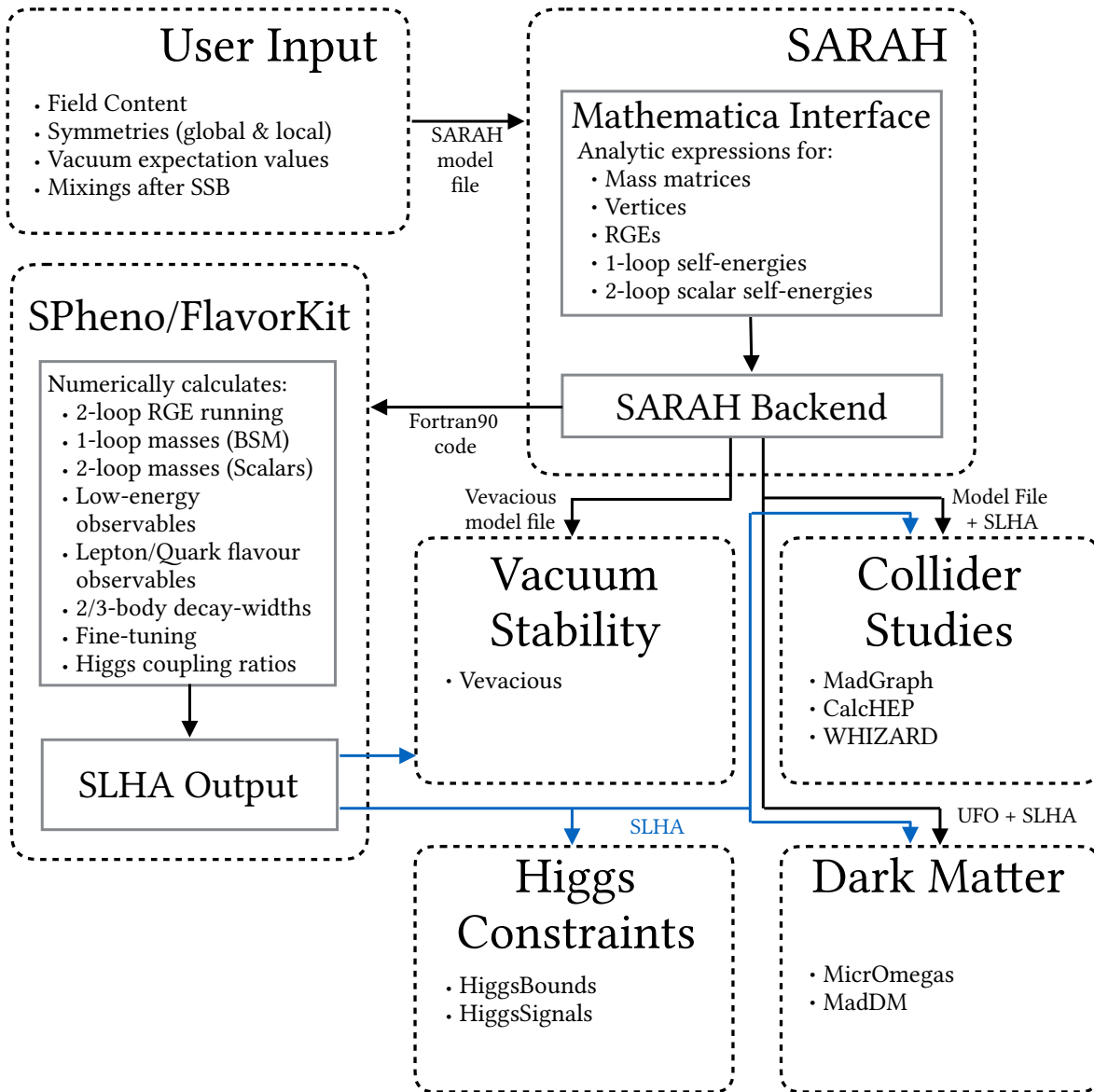


Figure 2.1: Flowchart illustrating the features of SARAH and the SPheno code generated by SARAH as well as how they can both be linked with other important computer tools.

Ref. [100] that the exact details of the two-loop computation and the determination of the running SM parameters can lead to discrepancies of up to 8 GeV in the prediction of the Higgs mass.

One of the most recent extensions of SARAH is FlavorKit which allows for the calculation of generic flavour observables in BSM theories [101]. To do so one considers an effective Lagrangian that contains the operators relevant to the flavour observables of interest. These operators are usually non-renormalisable, each containing pre-factors called Wilson coefficients. FlavorKit takes the masses and vertices of the BSM model and calculates the tree-level and

1-loop contributions to the set of Wilson coefficients. The package, by default included in SARAH, contains a large number of predefined quark and lepton flavour observables. The expressions for the BSM contributions to these observables are passed to SPheno where all the numerical results are calculated. Although not used for the projects contained in this thesis, FlavorKit includes a pre-SARAH module that utilises FeynArts [102] and FormCalc [103] to allow the user to implement new observables into the program chain.

## 2.1.2 SPheno

The first step after the model has been studied using the interactive Mathematica interface is the generation of the SPheno code. SPheno, short for supersymmetry phenomenology, much like SARAH is a tool originally written to study supersymmetric models [104, 105]. The code has been developed as a spectrum generator for the minimal supersymmetric standard model (MSSM) as well as its R-parity violating (RPV) extensions, with various choices implemented for the structure of the high-scale boundary conditions. However, when implementing new models with SARAH, a completely new version of the core code is written thereby allowing the possibility for non-supersymmetric models. This SARAH generated code utilises a number of libraries present in the SPheno distribution, but is largely independent of the original SPheno code.

Using the results of SARAH this code numerically calculates the masses and mixing angles based on the procedure of Ref. [106]. In addition it also calculates low-energy observables (such as  $(g - 2)_\mu$  and various lepton dipole moments), quark and lepton flavour observables from FlavorKit, as well as two- and three-body decay widths. Note that SPheno performs a complete matching of the measured SM parameters to the running parameters using thresholds which depend on the details of the mass spectrum of the model, see Ref. [94] for further information. It also calculates Higgs couplings to SM particles, providing the necessary results to interface with both HiggsBounds [107] and HiggsSignals [108]. Finally, any model can be implemented as either a low- or high-scale model, i.e. with or without RGE-running. The results are written in an output file following the supersymmetry Les Houches accord (SLHA) [109] which is readable by all high-energy physics tools.

## 2.1.3 Vevacious

For a model to be phenomenologically viable it must contain a local minimum of the scalar potential, often called a vacuum, that results in the desired spontaneous electroweak symmetry breaking pattern. However, the existence of such a local minimum does not ensure that other potentially deeper minima cannot co-exist. This is especially problematic in theories containing numerous scalar fields. This often results in complicated scalar potentials where a large number of directions in field space must be considered. In order to deal with this complicated higher-dimensional problem the tool Vevacious has been developed [110].

Vevacious is a tool that determines all minima of the tree-level scalar potential. It then determines the minima of the one-loop effective potential by using the tree-level minima as input. It then allows these points to roll down the potential until the true one-loop minima are

reached. If minima exist which are deeper than the correct electroweak breaking minimum another tool called CosmoTransitions [111] is used to calculate the tunnelling rate to the closest of these deeper minima in field space. Using this result one can then classify a model point based on the following:

- *stable*: electroweak minimum is the global minimum
- *metastable and long-lived*: lifetime of the electroweak minimum is longer than the age of the universe
- *metastable and short-lived*: lifetime of the electroweak minimum is shorter than the age of the universe

A model point is phenomenologically viable if the vacuum is either stable or metastable and long-lived. If the vacuum is metastable and long-lived then an additional mechanism is necessary which ensures we end up in the correct electroweak breaking minimum rather than any of the other possible minima. As a result the more stringent constraint of a stable electroweak vacuum is preferable.

## 2.1.4 Other Tools

The remaining tools that integrate into SARAH and SPheno are used for performing collider studies, checking Higgs constraints and determining dark matter observables. HiggsBounds and HiggsSignals [107, 108, 112, 113] are used to check if a given model is compatible with current data for both the SM Higgs measurements and null-results for searches for additional Higgs bosons. These tools are integrated through the SARAH and SPheno tool chain, which writes dedicated blocks in the SLHA output to be read by the respective programs. These blocks contain information on the couplings of the Higgs bosons to SM particles, the production cross-sections of these Higgs bosons as well as their masses. HiggsBounds uses this information to check against searches for additional Higgs bosons at both the LHC and the Large Electron-Positron collider (LEP). While HiggsSignals checks for compatibility of the SM-like Higgs boson in the model against the measurements of the Higgs boson properties, returning a  $\chi^2$  value.

One of the most useful tools given the wealth of LHC results are Monte-Carlo event generators used for performing collider studies. To that end, SARAH produces a universal FeynRules output file (UFO) [114], which is used to implement new models into a variety of event generators, such as MadGraph [115], GoSam [116], Herwig++ [117–119] and Sherpa [120–122]. The UFO files contain the particles, vertices and free parameters of the model which are used in conjunction with the SLHA output of SPheno to generate events for given model points of a theory. In addition SARAH also writes dedicated model files for the two event generators WHIZARD [123, 124] and CalcHEP [125]. In particular the CalcHEP model file can also be used to perform calculations of dark matter observables using MicrOmegas [126, 127]. These observables include the dark matter relic abundance, cross-sections for scattering off nuclei used in direct-detection experiments as well as gamma-ray spectra used in indirect-direction experiments.

Data samples and hypotheses		15 <sup>th</sup> Dec 2015		17 <sup>th</sup> Mar 2016		5 <sup>th</sup> Aug 2016	
		ATLAS [61]	CMS [62]	ATLAS [128]	CMS [129]	ATLAS [130]	CMS [131]
		3.2 fb <sup>-1</sup>	2.6 fb <sup>-1</sup>	3.2 fb <sup>-1</sup>	3.3 fb <sup>-12</sup>	15.4 fb <sup>-1</sup>	15.2 fb <sup>-1</sup>
Spin-0	Local	3.2σ	-	3.9σ	2.85σ	2.3σ	< 1σ
	Global	2.0σ	-	2.0σ	< 1σ	< 1σ	-
Spin-2	Local	-	2.6σ	3.6σ	2.85σ	-	< 1σ
	Global	-	1.2σ	1.8σ	< 1σ	-	-

Table 2.1: The statistical significance, both local and global, of the resonance observed in the 700-800 GeV mass window. The significances are given in terms of two different signal hypotheses, namely a spin 0 or a spin 2 resonance. Note that the statistical combinations with the  $\sqrt{s} = 8$  TeV data are not shown in this table as the collaborations used different methods to assess the compatibility between the different data sets.

## 2.2 The Diphoton Excess

In December 2016, the first set of analysed LHC data at  $\sqrt{s} = 13$  TeV was presented. It contained what appeared to be an extremely clear signal for BSM physics. Both multi-purpose experiments, ATLAS and CMS, reported a resonance at around 750 GeV in the diphoton channel with local significances of  $3.6\sigma$  (with  $3.2 \text{ fb}^{-1}$  of data) and  $2.6\sigma$  (with  $2.6 \text{ fb}^{-1}$ ), respectively [61, 62]. When including the look-elsewhere-effect, deviations from the SM expectation dropped to  $2.0\sigma$  and  $1.2\sigma$  for the two experiments. This signal was the most significant excess that has been observed by both experiments over the course of both runs at the LHC. It caused an incredible amount of excitement in the theory community for a number of reasons. Firstly, from an experimental point of view, searching for two back-to-back photons can be considered as one of the simplest searches to perform at a hadron collider as there are only two key ingredients in such an analysis: the ability to reconstruct photons in the detectors, and an adequate fit to the background processes. As a result there are no sources of intrinsic uncertainty such as complicated QCD processes. In essence this analysis can be summarised as a bump-hunting exercise in the invariant mass distribution of the two reconstructed photons.

The second reason being, unlike excesses in  $B$ -meson physics, a signal of two photons arising from a 750 GeV resonance is unquestionably a signal for BSM physics. Adding to the excitement, the large width of the resonance implied that an explanation based on well-motivated perturbative BSM theories was highly disfavoured. This led to many papers where one simply took his or her favourite model and retrofitted the required particle content to boost the width of resonance, see for example the models in Section 4 of Ref. [96]. However, in doing so, many authors did not properly study the impact of the additional field content on other sectors of the specific model in question.

Since the excess was first reported there have been two major updates, the first contained

<sup>2</sup> CMS have also included data taken with zero detector magnetic field.

more refined analyses, while the second contained significantly more data than the original analyses. The first update came at the winter conference ‘Moriond’ [128, 129]. This update showed small increases in the significance for both experiments, see Table 2.1, through refinements of the analyses. Both collaborations also checked the compatibility of the signal with data taken at  $\sqrt{s} = 8$  TeV. This demonstrated that a spin-0 resonance led to less tension between the two datasets than the spin-2 hypothesis. At this point many members of the theory community began to take this excess more seriously. Although there were many questions raised by the fact that CMS chose to include data where the magnetic field in their detector was not functioning.

However, five months later at the summer conference ‘ICHEP’, both ATLAS and CMS confirmed that the excess observed in the earlier data was a statistical fluctuation. ATLAS no longer observed an excess at 750 GeV, the most significant bump nearby was at 710 GeV with a  $2.3\sigma$  significance, whereas CMS had no excess above  $1\sigma$  in the 700-800 GeV mass window.

While we now know that the diphoton excess was only a statistical fluctuation, during the eight months where this excess appeared to be a signal of new physics we scrutinised many of the proposed models developed to fit this excess. However, before we discuss these contributions, we first need to know what exactly where the observed properties of this resonance as well as the best-fit cross-section and decay width.

## 2.2.1 Experimental Properties of the Diphoton Resonance

On first sight this excess appears very similar to the early stages of the Higgs discovery. However, there were no other signs of this resonance in other channels. Nevertheless, given the signal in only the diphoton channel one still seeks to ascertain the properties of this resonance, namely:

- *Electric charge*: From charge conservation alone we can deduce that the resonance is necessarily an electrically neutral particle.
- *Spin*: If the final state contains *only* two photons<sup>3</sup> the Landau-Yang theorem [133, 134] eliminates the possibility of a massive spin-1 particle. This leaves only two remaining options: a spin-0 particle, which can be either CP-even or CP-odd, or a spin-2 particle. Spin-0 and spin-2 resonances can be distinguished by considering the angular distribution of the final state photons with respect to the beam axis in the decaying particles rest-frame [135–137]. Here we denote this angle as  $\theta^*$ . A spin-0 resonance decays isotropically resulting in a flat distribution with respect to  $\cos \theta^*$ , while a spin-2 resonance yields a distribution that peaks at  $\cos \theta^* = 1$ . Given sufficient statistics one can discriminate the spin of the resonance in a similar manner to what was performed for the SM Higgs boson.

<sup>3</sup> The caveat here, is that if the final state contains additional photons whereby two collimated photons have been mistakenly reconstructed as a single photon, then a spin-1 resonance is again a possibility. Any concrete realisations of this scenario will lead to distinguishable distributions in the angular observables, see [132] for more details.

- *Charge-parity (CP)*: The CP properties of the resonance directly affect the correlation between the polarisation of the two out-going photons. For instance a pure CP-even state results in a maximal decay rate when the polarisation vectors are parallel, whereas in the CP-odd case it is when they are orthogonal. Such a measurement is conceivable using photons that decay into electron-positron pairs, however as was the case for the measurements of the Higgs CP properties, the CP nature is most easily measurable through other decay modes if they were discovered. For example the decay mode  $S \rightarrow Zh$ , where  $S$  is the resonance, is possible only if  $S$  has CP-odd interactions [138, 139]. Therefore, given the information available at the time both CP states are equally plausible.
- *Production modes*: The dominant production mode of the new resonance is a model dependent question. However, its choice directly influences the compatibility between the 8 TeV and 13 TeV data. Essentially production modes that maximise the increase in cross-section when increasing the centre-of-mass energy will reduce the tension between the datasets. This implies that there is a preference for production via gluon-fusion in comparison to direct first-generation quark production, as the production cross-sections with  $gg$  in the initial state are 4.7 times larger at 13 TeV versus 8 TeV. While  $u\bar{u}$  or  $d\bar{d}$  initial states lead to only a factor 2.5 increase [140]. One must also bear in mind that there is a large disparity between the quantity of data collected at the two different centre-of-mass energies.
- *Best-fit cross-section and width*: To determine the cross-section which fits the combination of 8 TeV and 13 TeV data it is necessary to assume a specific production mode of the resonance. In addition, the final best-fit cross-section will be a function of the width of the resonance. We follow Ref. [141] closely, who provided a best-fit to all data which was available after the very first announcement of an excess [61, 62]. In particular they use 8 TeV and 13 TeV data from both ATLAS and CMS using a uniform method to fit the background. This method is preferred, as ATLAS and CMS have chosen different functions to model the diphoton background. In this analysis a spin-0 resonance produced via gluon fusion is assumed with a number of different scenarios regarding the width of the resonance. The scenarios considered are a narrow, a broad (with both fixed and floating width) and a double resonance, respectively. The latter consists of two narrow resonances with either a fixed ratio of the relative cross-sections or a floated ratio as in the broad resonance scenario. The best-fit values shown in Table 2.2 are obtained by minimising a Poissonian likelihood which is a function of the signal plus background hypotheses. We observe that a resonance with a large width provides a better fit to the data. Typically such large widths are difficult to realise in perturbative models. However, a double resonance results in a quality of fit almost at the same level as the broad resonance. The double resonance effectively mimics a broad resonance if the masses of the two resonances have a small off-set. This last result is especially encouraging for a perturbative explanation of the diphoton excess.

Given the best-fit cross-section and width one can use the narrow-width approximation to estimate the size of the partial widths required to fit the excess. Following Ref. [140]

Resonance Type	$m_S$	$\sigma_{ggS} \times \text{Br}_{\gamma\gamma}$	$\Gamma_S$	Significance
Narrow	744 GeV	2.6 fb	–	$3.3 \sigma$
Broad (fixed width)	744 GeV	5.6 fb	40 GeV	$3.9 \sigma$
Broad (free width)	745 GeV	6.9 fb	62 GeV	$4.0 \sigma$
Double (fixed ratio)	745 GeV (705 GeV)	2.8 fb (1.3 fb)	–	$3.8 \sigma$
Double (free ratio)	745 GeV (706 GeV)	2.5 fb (1.8 fb)	–	$3.9 \sigma$

Table 2.2: Best-fit values for the different assumptions on the width, namely a narrow, broad and double resonance as well as the corresponding local significance of the excess taken from Ref. [141]. For the double resonance the values in parentheses refer to the sub-dominant resonance.

the cross-section, assuming a spin-0 resonance,  $S$  produced via gluon fusion, is given by

$$\sigma_{pp \rightarrow S \rightarrow \gamma\gamma} = \frac{1}{s m_S \Gamma_{\text{tot}}} [k_{gg} C_{gg} \Gamma_{S \rightarrow gg}] \Gamma_{S \rightarrow \gamma\gamma}, \quad (2.1)$$

where  $s$  is the centre-of-mass energy while  $m_S$  and  $\Gamma_{\text{tot}}$  are the mass and width of the spin-0 resonance, respectively.  $k_{gg}$  is the k-factor incorporating next-to-leading order effects, which for the gluon channel takes the value  $k_{gg} \simeq 1.5$  [142]. Finally, the dimensionless partonic integral  $C_{gg}$  is given by

$$C_{gg} = \frac{\pi^2}{8} \int_{m_S^2/s}^1 \frac{dx}{x} f_{g/p}(x, \mu_F) f_{g/p}\left(\frac{m_S^2}{sx}, \mu_F\right), \quad (2.2)$$

where  $x$  is the fraction of the proton's energy that the gluon carries,  $\mu_F$  is the factorisation scale and  $f_{g/p}(x)$  is the parton distribution function (PDF) [143]. This is the probability of finding a parton, which in this case is a gluon, with energy  $xE$ , given that the original proton has an energy  $E$ . Evaluating this integral using the MSTW2008NLO PDFs [143] given the resonance mass  $m_S = 750$  GeV yields  $C_{gg} \simeq 174$  and 2137 for  $\sqrt{s} = 8$  TeV and 13 TeV, respectively. Re-expressing Eq. (2.1) as

$$\frac{\Gamma_{S \rightarrow gg}}{m_S} \frac{\Gamma_{S \rightarrow \gamma\gamma}}{m_S} = \frac{s \Gamma_{\text{tot}}}{k_{gg} C_{gg} m_S} \sigma_{pp \rightarrow S \rightarrow \gamma\gamma} \quad (2.3)$$

allows us to place constraints on the partial widths for the two extreme cases of either a narrow or large total width:

1. *Narrow width:* This implies that

$$\Gamma_{\text{tot}} = \Gamma_{S \rightarrow gg} + \Gamma_{S \rightarrow \gamma\gamma}. \quad (2.4)$$

If one further assumes that  $\Gamma_{S \rightarrow gg} \gg \Gamma_{S \rightarrow \gamma\gamma}$ , which is generically the case for strong versus electroweak processes, then  $\Gamma_{S \rightarrow gg}$  drops out of Eq. (2.3). Plugging

the relevant numbers into Eq. (2.3) in addition to insisting that  $\sigma_{pp \rightarrow S \rightarrow \gamma\gamma} = 2.6$  fb (best-fit value from Table 2.2) yields

$$\frac{\Gamma_{S \rightarrow \gamma\gamma}}{m_S} \simeq 3.5 \times 10^{-7}. \quad (2.5)$$

2. *Large width:* In this case neither partial widths to gluons nor photons are the dominant contribution to the resonances total width. Subsequently, the partial width to gluons does not drop-out of Eq. (2.3) However, the minimal required  $\Gamma_{S \rightarrow \gamma\gamma}$  can be ascertained by choosing the maximal  $\Gamma_{S \rightarrow gg}$  allowed from di-jet constraints [144] for a given total width. Replacing in Eq. (2.1) the partial width  $\Gamma_{S \rightarrow \gamma\gamma}$  by  $k_{gg}\Gamma_{S \rightarrow gg}$  and fixing the width to 40 GeV, the upper bound on the di-jet cross-section of 14 pb at 8 TeV yields the upper limit  $\Gamma_{S \rightarrow gg}/m_S \lesssim 2.2 \times 10^{-2}$ . This results in a required partial width to photons of

$$\frac{\Gamma_{S \rightarrow \gamma\gamma}}{m_S} \simeq 1.9 \times 10^{-6}, \quad (2.6)$$

where we required  $\sigma_{pp \rightarrow S \rightarrow \gamma\gamma} = 5.6$  fb. To emphasise, this value assumes  $\Gamma_{\text{tot}} = 40$  GeV. Reducing this width leads to an increase in the di-jet cross-section and therefore a tightening on the di-jet constraint.

## 2.2.2 Confronting the Diphoton Excess with Results from Automated Tools

Automated tools have mainly been used in the past for detailed studies of *specific* promising BSM candidates such as the MSSM, NMSSM or variants of two-Higgs doublet models (THDMs). There are two main reasons why these tools are usually the preferred method to study these models: (i) it has been shown that there can be large differences between the exact numerical results and any analytic approximations; (ii) writing private programs for specific calculations is not only time consuming but also error prone in comparison to well established codes. Authors are reluctant to adopt computer codes in tackling the diphoton excess because many of these programs are written explicitly for a either a single model or small sub-set of models. Consequently such tools are not adaptable enough to allow the user to tweak an existing model, for example adding vector-like quarks or a new gauge symmetry as is generally required for comparability with the diphoton signal. Due to the meta-code nature of SARAH, extensions of existing model files are easily performed.

We noticed that several studies in the context of the 750 GeV excess have overlooked important subtleties, such as, neglecting crucial higher order corrections, or making simplifying assumptions which are difficult to justify. Using generic software tools in this context can help to address these issues as many of these simplifications will no longer be necessary and important higher order corrections can be taken into account in a consistent manner. In order to illustrate this we comment, in the following subsections, on several problems we became aware of when revisiting results in the literature.

## Calculation of the Diphoton and Digluon widths

A precise calculation of the diphoton rate is of crucial importance. In the validation process of this work, we identified several results in the literature that deviate, often by an order of magnitude or more, in comparison to our results [145–147]. Additionally we observed that in many cases there are important subtleties which we think are highly relevant and were not taken into account.

The first issue is the choice of the renormalisation scale of the running couplings appearing in the calculation. The majority of recent studies use the electromagnetic coupling at the scale of the decaying particle namely  $\alpha_{\text{EM}}(750 \text{ GeV})$ . However, one should rather use  $\alpha_{\text{EM}}(0)$ , i.e. the Thompson limit (see for instance Refs. [148, 149]), which minimises the size of NLO corrections. Taking this into account already amounts to an  $\mathcal{O}(10 \%)$  change of the diphoton rate compared to many studies in the literature. In addition, as we will discuss in the following sections, an important prediction of a model is the ratio  $\text{Br}(S \rightarrow gg)/\text{Br}(S \rightarrow \gamma\gamma)$ . It is well known that the digluon channel receives large QCD corrections. If one neglects these corrections the ratio will be severely underestimated.

To demonstrate these effects we consider toy models based on the simplest idea proposed to explain the diphoton excess. Such models extend the SM by a scalar singlet and vector-like fermions, which serve the purpose of enhancing the diphoton rate via loop contributions, and – in the case of coloured states – also the production via gluon fusion. As discussed above an enhancement of gluon fusion seems to be necessary because a production of the resonance purely by photon fusion is in tension with the 8 TeV data. The increase in the cross section from 8 to 13 TeV is just a factor 2 for photon fusion, while a factor of 5 would be needed to make the results from LHC run-I and II compatible.

To begin with we categorise the toy models according to the CP properties of the involved scalar singlet. There are three possibilities: (i) the singlet is a real CP-even scalar, (ii) a real CP-odd scalar, or (iii) a complex scalar. We further introduce all possible representations of vector-like fermions. These possibilities, following Tables 3 and 4 of Ref. [150], are shown below in Table 2.3. This allows one to study the combinations of different fermion representations for the resonance. All mixings between the extra fermions and SM fermions are neglected through the assumption of a discrete  $\mathbb{Z}_2$  symmetry. Of course in a realistic model the mixings have to be taken into account, as they allow the necessary decays of the coloured vector-like fermions into SM particles.

Field	Generations	$SU(3)_C$	$SU(2)_L$	$U(1)_Y$	$\mathbb{Z}_2$	Ref.
$S$	1	1	1	0	+	
$\Psi_{F_1}$	1	<b>3</b>	<b>2</b>	$\frac{7}{6}$	—	
$\Psi_{F_2}$	1	<b>3</b>	<b>3</b>	$\frac{2}{3}$	—	
$\Psi_{F_3}$	1	<b>3</b>	<b>2</b>	$-\frac{5}{6}$	—	
$\Psi_{F_4}$	1	<b>3</b>	<b>3</b>	$-\frac{1}{3}$	—	
$\Psi_{F_5}$	1	<b>3</b>	1	$\frac{2}{3}$	—	[151, 152]
$\Psi_{F_6}$	1	<b>3</b>	<b>2</b>	$\frac{1}{6}$	—	
$\Psi_{F_7}$	1	<b>3</b>	1	$-\frac{1}{3}$	—	[152]
$\Psi_{F_8}$	1	1	1	1	—	
$\Psi_{F_9}$	1	1	<b>2</b>	$-\frac{3}{2}$	—	
$\Psi_{F_{10}}$	1	1	<b>3</b>	1	—	
$\Psi_{F_{11}}$	1	1	<b>2</b>	$-\frac{1}{2}$	—	
$\Psi_{F_{12}}$	1	1	<b>3</b>	0	—	
$\Psi_{F_{13}}$	1	<b>3</b>	1	$\frac{5}{3}$	—	[153]

Table 2.3: Extra particle content (beyond the SM fields) of the toy models.  $S$  is either the CP-even, CP-odd or complex scalar. The various fermions  $\Psi_{F_i} \equiv \Psi_{F_{iL}}$  each come with a right-handed partner  $\Psi_{F_{iR}}$  with opposite quantum numbers. These models are based on the collection given in Ref. [150], while the last column contains other works where fermions in these specific representations are used. All SM particles have charge ‘+’ under the additional  $\mathbb{Z}_2$  symmetry.

We write the tree-level scalar potentials for the three different types of scalars as

$$\begin{aligned}
 V_{\text{CP-even}} &= \frac{1}{2}m_S^2 S^2 + \frac{1}{4}\lambda_S S^4 - \mu^2 |H|^2 + \frac{1}{2}\lambda_H |H|^4 + \frac{1}{2}\lambda_{HS} S^2 |H|^2 \\
 &\quad + \kappa_{HS} S |H|^2 + \frac{1}{3}\kappa_S S^3, \tag{2.7a}
 \end{aligned}$$

$$\begin{aligned}
 V_{\text{CP-odd}} &= \frac{1}{2}m_S^2 |S|^2 + \frac{1}{4}\lambda_S |S|^4 - \mu^2 |H|^2 + \frac{1}{2}\lambda_H |H|^4 + \frac{1}{2}\lambda_{HS} |S|^2 |H|^2 \\
 &\quad + \left( i\kappa_{HS} S |H|^2 + i\frac{1}{3}\kappa_S S |S|^2 + \text{h.c.} \right), \tag{2.7b}
 \end{aligned}$$

$$\begin{aligned}
 V_{\text{complex}} &= m_S^2 |S|^2 + \frac{1}{2}\lambda_S |S|^4 - \mu^2 |H|^2 + \frac{1}{2}\lambda_H |H|^4 + \lambda_{HS} |S|^2 |H|^2 \\
 &\quad + \left( \kappa_{HS} S |H|^2 + \frac{1}{3}\kappa_S S |S|^2 + \text{h.c.} \right), \tag{2.7c}
 \end{aligned}$$

while the Yukawa interactions are given by

$$-\mathcal{L}_Y = \mathcal{L}_Y^{\text{SM}} + \sum_j \left( m_{F_j} \bar{\Psi}_{F_{jL}} \Psi_{F_{jR}} + \sum_j Y_{F_j} S \bar{\Psi}_{F_{jL}} \Psi_{F_{jR}} \right) + \text{h.c.} \tag{2.8}$$

In the Lagrangian above one should substitute the expression for the relevant scalar field after

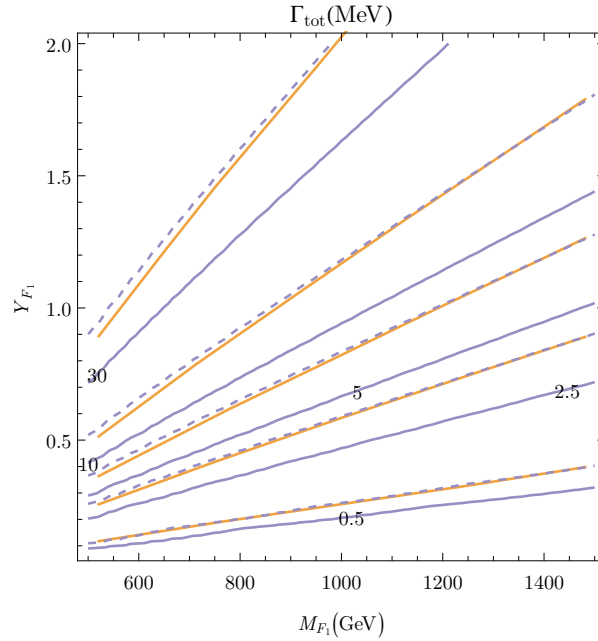


Figure 2.2: The approximate total width (sum of the diphoton and digluon channels) of  $S$  as a function of the coupling  $Y_{F_1}$  and the mass  $m_{F_1}$  of the vector-like particle  $\Psi_{F_1}$ , calculated using SPheno (blue) at LO (dashed) and NLO (solid). The orange contours are the results of the LO calculation from Ref. [150]. Here we assume a single generation of vector-like quarks.

electroweak symmetry breaking

$$S_{\text{CP-even}} = v_S + \phi_S, \quad \text{where } \langle S \rangle = v_S, \quad (2.9a)$$

$$S_{\text{CP-odd}} = i\sigma_S, \quad (2.9b)$$

$$S_{\text{complex}} = \frac{1}{\sqrt{2}}(v_S + \phi_S + i\sigma_S). \quad (2.9c)$$

Note that imposing CP conservation forces  $\kappa_{HS}$  and  $\kappa_S$  to vanish in the CP-odd potential. For both the CP-even and complex singlet models the CP-even component  $\phi_S$  mixes with the neutral Higgs field  $\phi_h$  at tree-level if  $\kappa_{HS} \neq 0$ . As will be discussed below, even if one sets  $\kappa_{HS} = 0$ , mixing between the CP-even states is induced at the loop level.

Using the first model of Table 2.4 we show in Fig. 2.2 the total decay width<sup>4</sup> of the singlet  $S$  as a function of the mass  $M_{F_1}$  and coupling  $Y_{F_1}$ . Table 2.4 contains benchmark points for the partial widths of the digluon and diphoton channels as well as the ratio of these two channels for both CP-even and CP-odd scalar resonances. This table also contains the LO calculations performed using SPheno as a comparison to results previously shown in the literature [150]. We also show the partial widths including NLO corrections for the diphoton channel<sup>5</sup> and

<sup>4</sup> Here, the total width is simply the sum of the diphoton and digluon channels ignoring small contributions from other sub-dominant channels.

<sup>5</sup> NLO corrections in the case of a CP-odd scalar vanish in the limit  $m_f \gg m_S$ , see Section 2.2.3 for more detail.

Model		Br( $gg/\gamma\gamma$ )	$\Gamma_{S \rightarrow gg}$ [MeV]	$\Gamma_{S \rightarrow \gamma\gamma}$ [MeV]
$\Psi_{F_1}$	Ref. [150] LO	11.62/-	6.74/-	0.58/-
	SPheno LO	13.47/12.22	6.78/14.27	0.50/1.17
	SPheno NLO	23.27/20.27	11.04/23.71	0.47/1.17
$\Psi_{F_2}$	Ref. [150] LO	24.42/-	15.14/-	0.62/-
	SPheno LO	28.32/25.70	15.26/32.12	0.54/1.25
	SPheno NLO	48.93/42.67	24.85/52.34	0.51/1.25
$\Psi_{F_3}$	Ref. [150] LO	33.80/-	6.76/-	0.20/-
	SPheno LO	39.20/35.56	6.78/14.27	0.17/0.40
	SPheno NLO	67.72/59.06	11.04/23.71	0.16/0.40
$\Psi_{F_4}$	Ref. [150] LO	49.84/-	14.95/-	0.30/-
	SPheno LO	57.80/52.44	15.26/32.12	0.26/0.61
	SPheno NLO	99.85/87.09	24.85/53.34	0.25/0.61
$\Psi_{F_5}$	Ref. [150] LO	150.0/-	1.50/-	$10.0 \times 10^{-3}/-$
	SPheno LO	177.0/160.6	1.70/3.57	$9.58 \times 10^{-3}/22.22 \times 10^{-3}$
	SPheno NLO	305.8/266.7	2.76/5.93	$9.03 \times 10^{-3}/22.22 \times 10^{-3}$
$\Psi_{F_6}$	Ref. [150] LO	390.0/-	7.80/-	$2.00 \times 10^{-2}/-$
	SPheno LO	453.2/411.1	6.78/14.27	$1.50 \times 10^{-2}/3.47 \times 10^{-2}$
	SPheno NLO	782.8/682.8	11.04/23.71	$1.41 \times 10^{-2}/3.47 \times 10^{-2}$

Table 2.4: Branching fraction ratio, as well as the partial decay widths for the digluon and diphoton channels for the toy model containing only the relevant vector-like fermion pair  $\Psi_{F_i}$ . The above values are for the benchmark points  $Y_{F_i} = 1$  and  $m_{F_i} = 1$  TeV, where the values are for a CP-even/CP-odd scalar resonances, respectively. The SPheno NLO calculation includes up to N<sup>3</sup>LO corrections for the digluon channel, while the diphoton decay width is calculated at NLO and LO for a CP-even and -odd scalar respectively.

up to N<sup>3</sup>LO QCD corrections to the gluon fusion production as implemented in Section 2.2.3. The discrepancies between the LO calculations arise purely through the choice of the renormalisation scale for the gauge couplings. However, the NLO results clearly emphasise that loop corrections at the considered mass scales are the dominant source of errors. To my knowledge, these uncertainties have thus far not received a sufficiently careful treatment in the literature; we give further discussion of this (and the remaining uncertainty in the SARAH calculation) in Section 2.2.3.

## Constraints on a large diphoton width

As discussed in Section 2.2.1, explaining the measured signal requires a large diphoton rate. This necessarily requires a large partial width to photons, namely  $\Gamma_{S \rightarrow \gamma\gamma}/m_S \simeq 3.5 \times 10^{-7}$  assuming a narrow width for  $S$ , while for a large width (40 GeV) one requires  $\Gamma_{S \rightarrow \gamma\gamma}/m_S \simeq 2.3 \times 10^{-6}$ . In weakly-coupled models there are three different possibilities to obtain such a

large partial width:

1. Assuming a large Yukawa-like coupling between the resonance and charged fermions
2. Assuming a large cubic coupling between the resonance and charged scalars
3. Using a large multiplicity and/or a large electric charge for the scalars and/or fermions in the loop

However, all three possibilities are constrained by fundamental theoretical considerations, which we briefly summarise in the following.

1. *Large couplings to fermions:* A common idea to explain the diphoton excess is the presence of vector-like fermion states which enhance the loop-induced coupling of a neutral scalar to two photons or two gluons. This led some authors to consider Yukawa-like couplings of the scalar to the vector-like fermions larger than  $\sqrt{4\pi}$ , which is clearly beyond the perturbative regime<sup>6</sup>. Nevertheless, a one-loop calculation is used in these analyses to obtain predictions for the partial widths [154], despite being in a non-perturbative region of parameter space.

Moreover, even if the couplings are chosen to be within the perturbative regime at the scale  $\mu = 750$  GeV, they can quickly grow at higher energies. This issue of a Landau pole has already been discussed to some extent in the literature [140, 155–159]. Beyond high-scale theoretical considerations for avoiding Landau poles, one should at least ensure that the model does not break down at such low energies such that consistency is retained at observable LHC energies.

2. *Large couplings to scalars:* One possibility to circumvent large Yukawa couplings is to introduce charged scalars, which give large loop contributions to the diphoton/digluon decay rate. A large cubic coupling between the charged scalar and the 750 GeV resonance does not lead to a Landau pole as such a coupling necessarily carries a mass dimension. However, it is known that large cubic couplings can destabilize the scalar potential. If the couplings are too large, the electroweak vacuum could tunnel into a deeper vacuum where  $U(1)_{\text{EM}}$  or  $SU(3)_C$  gauge invariance is spontaneously broken, depending on the considered scenario. The simplest example exhibiting this behaviour is the SM, extended by a real scalar  $S$  as well as a complex scalar  $X$  carrying hypercharge  $Y$ . The scalar potential for this example is

$$V \supset \kappa S |X|^2 + \frac{1}{2} m_S^2 S^2 + m_X^2 |X|^2. \quad (2.10)$$

In Fig. 2.3 the dependence of the diphoton partial width as a function of  $\kappa$  and  $m_X$  is shown, as well as the stability of the electroweak vacuum which has been calculated using *Vevacious* and *CosmoTransitions*. Here we observe that all points which would explain the best-fit cross section are incompatible with the assumption of a stable electroweak vacuum. Note however, that the points right at the border of instability are compatible at the  $2\sigma$  level. For more details about vacuum stability in the presence of

<sup>6</sup> This diphoton excess could be triggered by strong interactions. Of course, in this case one cannot use perturbative methods to understand it.

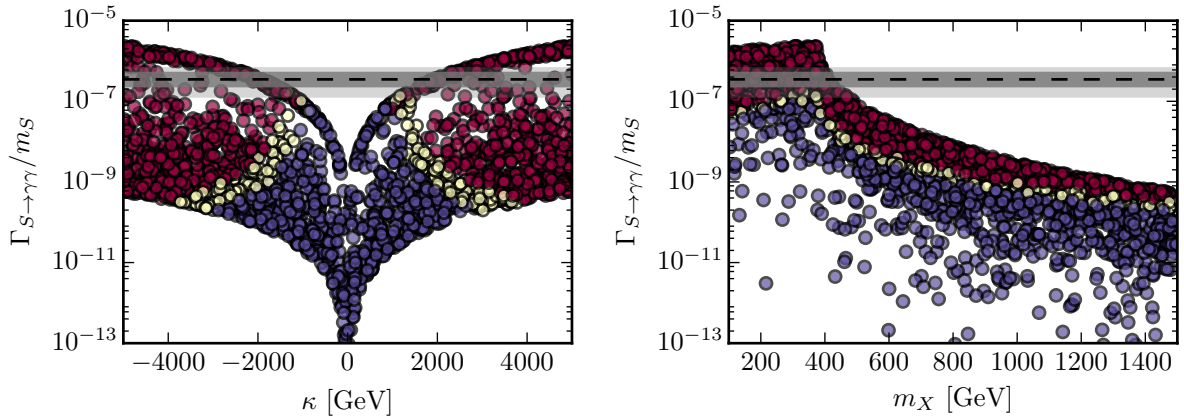


Figure 2.3:  $\Gamma_{S\rightarrow\gamma\gamma}/m_S$  as a function of  $\kappa$  (left) and  $m_X$  (right). In both panels  $\kappa$  and  $m_X$  have been varied randomly in the domains  $\kappa \in [-5, 5]\text{TeV}$  and  $m_X \in [150, 1500]\text{GeV}$ . Blue points have a stable vacuum, yellow points have a meta-stable but long-lived vacuum, while for the red ones the vacuum decays in a short time in comparison to cosmological time scales, with a survival probability below 10%. The black dashed line indicates the best-fit value of  $\Gamma_{S\rightarrow\gamma\gamma}/m_S \simeq 3.5 \times 10^{-7}$ , while the dark/light grey regions are the  $1/2\sigma$  compatible regions assuming a narrow width resonance produced via gluon fusion (see Section 2.2.1 for more details and assumptions). The hypercharge of  $X$  is chosen to be  $Y_X = 1$ .

large scalar cubic terms, we refer to Ref. [159]. The overall conclusion of Ref. [159] is that the maximal possible diphoton width, even when allowing for a meta-stable but sufficiently long-lived electroweak vacuum, is not much larger than in the case of vector-like fermions when requiring that the model is perturbative up to the Planck scale. It is therefore essential to perform these checks when studying a model that postulates large cubic scalar couplings.

3. *Large multiplicities:* To circumvent large Yukawa or cubic couplings, other models introduce a large number of generations of the new BSM fields and/or large electric charges. As a consequence the running of the  $U(1)_Y$  gauge coupling  $g_1$ , gets strongly enhanced at scales well below the Planck scale. Moreover, even before reaching the Landau pole, the model develops large (eventually non-perturbative) gauge couplings. This implies an enhancement of Drell-Yan processes at the LHC, with current data already setting stringent constraints and potentially excluding many of the models proposed to explain the diphoton excess in this manner [160, 161]. For general studies on the running effects in the context of the diphoton excess see [140, 155–158].

We briefly discuss some dramatic examples of these types of models proposed in Refs. [162] and [163]. These models feature approximately  $\sim 100$  and 6000–9000 generations of doubly-charged scalar fields respectively. In the model of Ref. [163] the SM particle content is enlarged by:

- a vector-like doubly-charged fermion  $E$
- a majorana fermion  $N_R$

- a singlet scalar  $S$
- a singly-charged scalar  $h^+$
- $N_k$  generations of the doubly-charged scalar field  $k^{++}$

At the one-loop level the running of  $g_1$  is governed by the renormalisation group equation (RGE)

$$\frac{dg_1}{dt} = \frac{1}{16\pi^2} \beta_{g_1}^{(1)}, \quad (2.11)$$

where  $t = \log \mu$ , given  $\mu$  is the renormalisation scale, and

$$\beta_{g_1}^{(1)} = \frac{g_1^3}{10} (75 + 8 N_k), \quad (2.12)$$

is the one-loop beta function. A large value of  $N_k$  necessarily leads to a very steep increase of  $g_1$  with respect to the renormalisation scale, quickly leading to a Landau pole. This is shown in Fig. 2.4, obtained by setting the masses of all the charged BSM states to  $\mu_{\text{NP}} = 2.5 \text{ TeV}$ , which is the largest mass considered in Ref. [163]. The running up to  $\mu_{\text{NP}}$  is governed by the SM RGEs, where the result for  $g_1$  given by the black dashed line. For scales above  $\mu_{\text{NP}} = 2.5 \text{ TeV}$ , the contributions from BSM fields become relevant. Fig. 2.4 shows that a Landau pole can be reached at relatively low energies once we allow for such large values of  $N_k$ . In fact, for  $N_k = 9000$ , we find that a Landau pole appears already at  $\mu \simeq 2.6 \text{ TeV}$ . In this specific example the appearance of a Landau pole below  $10^{16} \text{ GeV}$  is unavoidable as soon as  $N_k > 10$ .

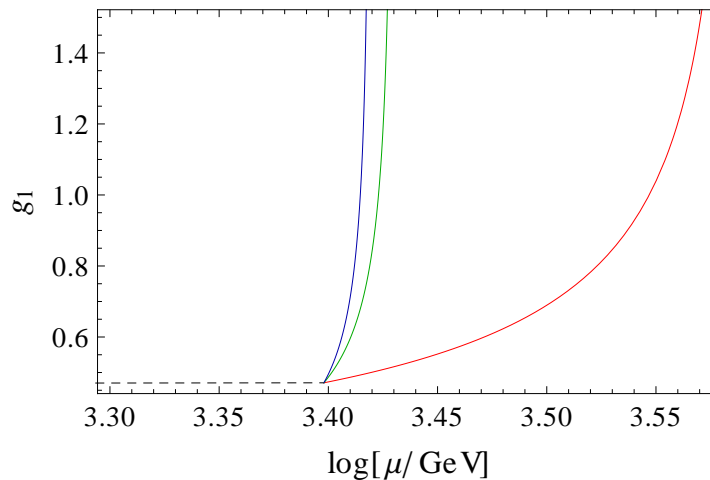


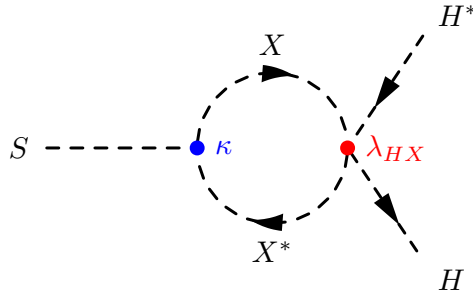
Figure 2.4: Running of the  $U(1)_Y$  gauge coupling,  $g_1$ , in the model presented in Ref. [163] for  $N_k = 1000$  (red),  $N_k = 6000$  (green) and  $N_k = 9000$  (blue). The black dashed line corresponds to the SM running below  $\mu_{\text{NP}} = 2.5 \text{ TeV}$ .

## Properties of the 750 GeV Scalar

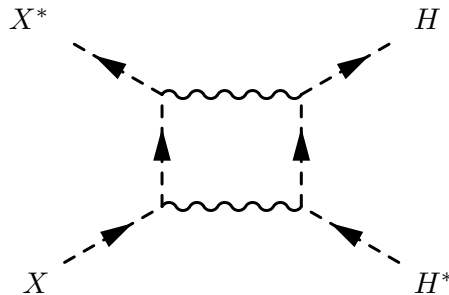
- *Mixing with the SM Higgs:* It is often assumed that  $S$ , although it is a CP-even scalar, does not mix with the SM-like Higgs  $h$ . However, if no symmetry argument is invoked, this assumption is not stable under radiative corrections. To illustrate this, consider the scalar potential

$$V = \frac{1}{2}m_S S^2 + m_X |X|^2 + \mu^2 |H|^2 + \kappa S |X|^2 + \kappa_S S^3 + \lambda_S S^4 + \lambda_{SX} S^2 |X|^2 + \lambda_{HX} |H|^2 |X|^2 + \lambda |H|^4, \quad (2.13)$$

where  $H$  is the SM Higgs  $SU(2)_L$ -doublet, containing the Higgs  $h$ . This potential contains all the necessary ingredients to obtain a large diphoton decay rate where  $S$  decays via a loop involving the charged scalar  $X$ . Note that the potentially dangerous term  $\kappa_H S |H|^2$  has been omitted. Such a term generates a tree-level mixing between  $S$  and  $h$  once the Higgs doublet  $H$  acquires a VEV. However, this term is generated radiatively by the one-loop diagram:



Here, we observe that the parameter  $\kappa$  enters in the loop diagram, which is also the parameter which must be maximised in order to fit the diphoton signal. It is also impossible to circumvent this diagram by forbidding the  $\lambda_{HX}$  term.  $H$  is charged under  $SU(2)_L \times U(1)_Y$  while  $X$  must be charged under either or both  $SU(2)_L$  and  $U(1)_Y$  so that it couples to photons. As a result the  $\lambda_{HX} |H|^2 |X|^2$  term is also generated radiatively via diagrams involving the gauge bosons of  $SU(2)_L$  and or  $U(1)_Y$ :

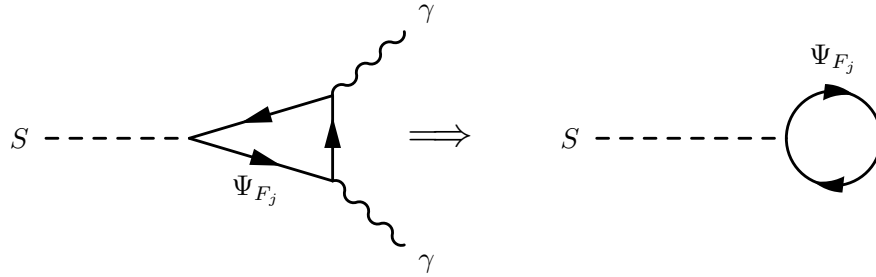


If both  $\lambda_{HX}$  and  $\kappa$  are not present at tree-level then mixing with the SM Higgs occurs only at two-loop order and beyond. However, such a mixing has important con-

sequences since it opens the decay channels  $S \rightarrow hh$  as well as  $S \rightarrow ZZ, S \rightarrow W^+W^-$  at tree-level, which are tightly constrained via experimental measurements, as will be discussed below.

Thus, in general, it is very difficult to justify the assumption that the 750 GeV scalar does not mix with the SM-like Higgs if there is no fundamental symmetry to forbid this mixing. However, this mixing can be forbidden using an unbroken CP symmetry in the scalar sector. For example if the resonance is a CP-odd scalar then there is zero mixing as long as the CP symmetry remains unbroken. While, in the case of a CP-even particle, it is crucial to include the mixing effects and to determine how large the tuning of the parameters must be to avoid all experimental limits.

- *To VEV or not to VEV:* The possibility that the new scalar receives a vacuum expectation value (VEV) is also often neglected. However, as we have just discussed, it often occurs that  $h$ - $S$  mixing will be induced, at least radiatively, in many models. Such radiative effects immediately lead to a non-zero VEV for the new scalar.<sup>7</sup> Even in cases where there is a symmetry which prevents a mixing with the SM Higgs, the 750 GeV particle will still receive a VEV. This arises due to the introduced couplings to charged particles which are necessary to achieve sufficient diphoton and digluon decay rates. More specifically, these couplings will generate one-loop tadpole diagrams for  $S$  via the diagrams:



Note that in the above diagrams one can replace the loop of fermions by loops of CP-even scalars. The resulting tadpole equation reads at the one-loop level

$$\frac{\partial V^{(1L)}}{\partial v_S} = T^{(1L)} = T^{(T)} + \delta T = 0, \quad (2.14)$$

where  $v_S$  is the VEV of the 750 GeV particle  $S$  and  $T^{(T)}$  is the tree-level tadpole, given by

$$\frac{\partial V^{(T)}}{\partial v_S} = T^{(T)} = c_1 v_S + c_2 v_S^2 + c_3 v_S^3 = 0. \quad (2.15)$$

<sup>7</sup> Note that if the spin-0 resonance is a singlet under *all* symmetries both gauge and global, then the VEV can be absorbed via a field redefinition and is therefore negligible.

$e^+e^- + \mu^+\mu^-$	$\tau^+\tau^-$	$Z\gamma$	$ZZ$	$Zh$	$hh$	$W^+W^-$	$t\bar{t}$	$b\bar{b}$	$jj$	inv.
0.6	6	2	6	10	20	20	300	500	1300 <sup>8</sup>	400

Table 2.5: Upper limits on  $\Gamma_{S \rightarrow XX}/\Gamma_{S \rightarrow \gamma\gamma}$  assuming the production of  $S$  via gluon fusion or heavy quarks. Values are taken from Ref. [140].

We have parametrised the tree-level expression so that the general form has the solution  $v_S = 0$ . The one-loop corrections take the form

$$\delta T = \begin{cases} \kappa A(m_X^2), & \text{for a scalar loop,} \\ 2Y_{F_j} m_{F_j} A(m_{F_j}^2), & \text{for a fermion loop,} \end{cases} \quad (2.16)$$

with  $A(x^2) = \frac{1}{16\pi^2} x^2 [1 + \log(\mu^2/x^2)]$  where  $\mu$  is again the renormalisation scale. Taking  $m_{F_j}$ ,  $\kappa$ ,  $m_X$  of the order 1 TeV, results in a VEV which is of order  $1 \text{ TeV}^3/(16\pi^2 c_1)$ . As a result, the simplifying assumption that  $v_S$  vanishes is in general hard to justify. It is therefore important to check how the conclusions made about the model depend on this assumption. Here, the numerical tools discussed can help significantly, as including the non-vanishing VEV  $v_S$  is no more difficult than assuming the VEV vanishes.

- *Additional decay channels:* Many analyses concentrate only on the decay  $S \rightarrow \gamma\gamma$  and completely neglect other potential decay channels. However, there are stringent experimental constraints on the branching ratios of  $S$  into other SM final states, which are summarised in Table 2.5. Therefore, any model which attempts to explain the excess via additional coloured states in the loop must necessarily worry about limits from dijet searches [144]. Consequently, an accurate calculation of the digluon decay rate is a necessity. As an example that illustrates why both additional channels and the diphoton/digluon width calculation are important, we consider the model presented in Refs. [164, 165].

This model extends the SM by introducing a scalar singlet as well as a scalar SU(2)-doublet which is also a colour octet. As an approximation the ratio of the singlet decays to gluons and to photons is

$$\frac{\Gamma_{S \rightarrow gg}}{\Gamma_{S \rightarrow \gamma\gamma}} \simeq \frac{9}{2} \frac{\alpha_S^2}{\alpha_{\text{EM}}^2}, \quad (2.17)$$

where  $\alpha_S$  and  $\alpha_{\text{EM}}$  are the strong and electromagnetic coupling, respectively. In [164] this ratio is quoted as  $\simeq 715$ . Before any NLO corrections are applied, we find 700 which is in good agreement. However, once we include all of the N<sup>3</sup>LO corrections this is enhanced to 1150, near the bound for constraints on dijet production at 8 TeV and significantly squeezing the parameter space of the model.

<sup>8</sup> Since Ref. [140] was published a mistake has been discovered in the ATLAS di-jet analysis of Ref. [144]. The excluded cross-section for a 750 GeV resonance has shifted from 2.5 pb to 14 pb for  $\Gamma_{\text{tot}}/m_S \simeq 6\%$ . The resulting bound is therefore relaxed to  $\Gamma_{S \rightarrow jj}/\Gamma_{S \rightarrow \gamma\gamma} \lesssim 8140$ .

Additionally in many works we observed that potential decay channels of the resonance were missed. For instance in Ref. [166], the authors, who considered the Georgi-Machacek model [167], missed the decay of the scalar into  $W^\pm H^\mp$ , which can be the dominant mode when kinematically allowed.

## Considering a complete model

- *Additional constraints in a complete model:* There are several studies which extend an already existing model by adding vector-like states and then assume that this new part of the model is decoupled from the rest. It is then clear that the results from toy models, with the minimal particle content will be reproduced. However, it is often not obvious if this decoupling will hold without invoking specific structures in the choice of parameters, and if they persist at the one-loop level.

On the other hand, if model-specific features are used to explain the diphoton excess, it is likely that there will be important constraints on the model coming from other sectors. For instance, there might be bounds from flavour observables, dark matter, Higgs searches, neutrino mixing, electroweak precision observables, searches for BSM particles at colliders, and so on. All of these constraints must be checked to be sure that any benchmark point presented is indeed a valid explanation for all observations. Such a wide range of constraints are much easier to address by making exhaustive use of tools which provide a high level of automation.

- *Theoretical uncertainties of other predictions:* Even if the attempts are made to include the effects of the new states on other sectors of the model, it is important to be aware that there are large uncertainties involved in certain calculations. If the level of uncertainty is underestimated, this can have an impact on what is inferred from the calculation. The large uncertainty in a LO calculation of the diphoton and digluon rate has already been addressed in Section 2.2.2. However, there are also other important loop corrections especially in supersymmetric models. For example the accurate calculation of the Higgs mass is a long lasting endeavour where for even the simplest supersymmetric model only now are the dominant three-loop corrections being tackled [168]. The current estimate of the remaining uncertainty is 3 GeV.

It is clear that the MSSM alone cannot explain the excess<sup>9</sup>, hence it must be extended. A common choice is to add additional pairs of vector-like superfields together with a gauge singlet, for a concrete example see Ref. [141]. These new fields can also be used to increase the SM-like Higgs mass. However, this will in general also increase the theoretical uncertainty in the Higgs mass prediction, because these new corrections are not calculated with the same precision as the MSSM corrections. For instance, Ref. [169] has taken into account the effect of the new states on the SM-like Higgs. There, they use a one-loop effective potential approach considering the new Yukawa couplings to be  $\mathcal{O}(1)$

<sup>9</sup> There are many claims that the excess can be fit in the MSSM by turning to highly fine-tuned splitting between certain masses, resulting in a potentially large enough diphoton rate. We will return to this question in Section 3.1.2.

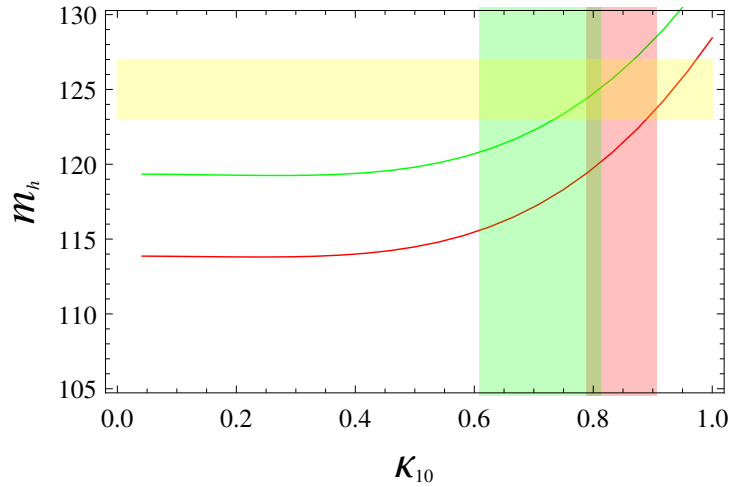


Figure 2.5: Comparison of the two-loop Higgs mass calculation of Ref. [169] with the results obtained by SPheno as a function of the coupling  $\kappa_{10}$ . This is a Yukawa-like coupling of the vector-like quarks to the MSSM Higgs doublets. The parameter values are those of Fig. 4 in Ref. [169], where we consider the slice of parameter space with  $X_{\kappa_{10}} = 0$ . This parameter  $X_{\kappa_{10}}$ , is a parametrisation of contributions to Higgs mass corrections depending on the vector-like masses, the supersymmetry breaking scale and the soft-breaking trilinear terms. The lines are the results from SPheno where the red line corresponds to  $X_t = 4$  and the green line to  $X_t = 2$ . The green and red shaded areas are the ranges of  $\kappa_{10}$  which predict  $m_h = [123, 127]$  GeV according to Ref. [169] for the two different  $X_t$  values. The yellow shaded region shows the band of 2 GeV uncertainty for the Higgs mass calculation from SPheno.

or below, while also including the dominant two-loop corrections from the stop quark. They assumed that including these corrections is sufficient in order to achieve an uncertainty of 2 GeV in the Higgs mass prediction. One can compare their results from Fig. 7 of Ref. [169] with a calculation including, in addition to the corrections stated above, the full momentum dependence and electroweak corrections at the one-loop level, as well as the additional two-loop corrections arising from all newly introduced states. These corrections can be important, as was shown for instance in Ref. [170]. The result of the comparison is shown in Fig. 2.5. We find a similar behaviour, but observe that there are several GeV difference between both calculations. For  $\kappa_{10} = 0.8$  and  $X_t = 4$ , according to Ref. [169] the point would be within the interesting range for  $m_h = [123, 127]$  GeV, while the more sophisticated SPheno calculation predicts a mass below 120 GeV. Thus, the assumed uncertainty of 2 GeV in Ref. [169], which would even be optimistic in the MSSM, is completely unrealistic without including all the aforementioned higher order corrections.

### 2.2.3 Diphoton Observables in the SARAH Framework

#### Calculation of the Effective Diphoton and Digluon Vertices

For the calculation of the partial widths of a neutral scalar  $S$  decaying into two gluons or two photons we follow closely Ref. [148] for both the LO and NLO contributions. The partial widths at LO are given by

$$\Gamma(S \rightarrow \gamma\gamma)_{\text{LO}} = \frac{G_F \alpha_{\text{EM}}^2(0) m_S^3}{128 \sqrt{2} \pi^3} \left| \sum_f N_c^f Q_f^2 r_f^S A_f(\tau_f) + \sum_s N_c^s r_s^S Q_s^2 A_s(\tau_s) + \sum_V N_c^V r_V^S Q_V^2 A_V(\tau_V) \right|^2, \quad (2.18)$$

$$\Gamma(S \rightarrow gg)_{\text{LO}} = \frac{G_F \alpha_S^2(\mu) m_S^3}{36 \sqrt{2} \pi^3} \left| \sum_f \frac{3}{2} D_2^f r_f^S A_f(\tau_f) + \sum_s \frac{3}{2} D_2^s r_s^S A_s(\tau_s) + \sum_V \frac{3}{2} D_2^V r_V^S A_V(\tau_V) \right|^2. \quad (2.19)$$

Here, the sums are over all fermions  $f$ , scalars  $s$  and vector bosons  $V$  which carry electromagnetic charge or are coloured and which couple to the scalar  $S$ .  $Q_i$  is the electromagnetic charge of the fields,  $N_c$  are the colour factors and  $D_2$  is the quadratic Dynkin index of the colour representation which is normalised to  $\frac{1}{2}$  for the fundamental representation. We note that the electromagnetic fine structure constant  $\alpha_{\text{EW}}$  must be taken at the scale  $\mu = 0$ , since the final state photons are real [142]. In contrast,  $\alpha_S$  is evaluated at  $\mu = m_S$  which, for the case of interest here, is  $\mu = 750$  GeV.  $r_i^S$  are the so-called reduced couplings, the ratios of the couplings of the scalar  $S$  to the particle  $i$  normalised to SM values. These are calculated as

$$r_f^S = \frac{v}{2m_f} (C_{ffS}^L + C_{ffS}^R), \quad (2.20a)$$

$$r_s^S = \frac{v}{2m_s^2} C_{ss^*S}, \quad (2.20b)$$

$$r_V^S = -\frac{v}{2m_V^2} C_{VV^*S}. \quad (2.20c)$$

Here,  $v$  is the electroweak VEV and  $C$  are the couplings between the scalar and the different fields with mass  $m_i$  ( $i = f, s, V$ ). Furthermore we define the following mass ratio as

$$\tau_x = \frac{m_S^2}{4m_x^2}, \quad (2.21)$$

while the functions appearing in Eqs. (2.18) and (2.19) are given by

$$A_f = 2 \frac{\tau + (\tau - 1)f(\tau)}{\tau^2}, \quad (2.22a)$$

$$A_s = -\frac{\tau - f(\tau)}{\tau^2}, \quad (2.22b)$$

$$A_V = -\tau^2 [2\tau^2 + 3\tau + 3(2\tau - 1)f(\tau)], \quad (2.22c)$$

with

$$f(\tau) = \begin{cases} \arcsin^2 \sqrt{\tau} & \text{for } \tau \leq 1, \\ -\frac{1}{4} \left( \log \frac{1+\sqrt{1-\tau^{-1}}}{1-\sqrt{1-\tau^{-1}}} - i\pi \right)^2 & \text{for } \tau > 1. \end{cases} \quad (2.23)$$

For a pure pseudo-scalar state only fermions contribute within the loop, i.e. the LO widths read

$$\Gamma(A \rightarrow \gamma\gamma)_{\text{LO}} = \frac{G_F \alpha_{\text{EM}}^2 m_A^3}{32\sqrt{2}\pi^3} \left| \sum_f N_c^f Q_f^2 r_f^A A_f^A(\tau_f) \right|^2, \quad (2.24)$$

$$\Gamma(A \rightarrow gg)_{\text{LO}} = \frac{G_F \alpha_S^2 m_A^3}{36\sqrt{2}\pi^3} \left| \sum_f 3D_2^f r_f^A A_f^A(\tau_f) \right|^2, \quad (2.25)$$

where

$$A_f^A = \frac{f(\tau)}{\tau}, \quad (2.26)$$

and  $r_f^A$  takes the same form as  $r_f^S$  in Eq. (2.20a), replacing  $C_{\bar{f}fS}^{L,R}$  by  $C_{\bar{f}fA}^{L,R}$ .

These formulae are used by SPheno to calculate the full LO contributions of any CP-even or -odd scalar present in a model including all possible loop contributions at the scale  $\mu = m_S$ . However, it is well known, that higher order corrections are important, especially for the production cross-sections [171–175]. Therefore, NLO, NNLO and even N<sup>3</sup>LO corrections from the SM are adapted and used for any model under consideration. In the case of heavy colour fermionic triplets, the included corrections for the diphoton decay are

$$r_f^S \rightarrow r_f^S \left( 1 - \frac{\alpha_S}{\pi} \right), \quad (2.27)$$

$$r_s^S \rightarrow r_s^S \left( 1 + \frac{8\alpha_S}{3\pi} \right). \quad (2.28)$$

These expressions are obtained in the limit  $\tau_f \rightarrow 0$  and thus applied only when  $m_S < m_f$ .  $r_f^A$  does not receive any corrections in this limit. For the case  $m_S > 100m_f$ , we have included

the NLO corrections in the light quark limit given by [148]

$$r_f^X \rightarrow r_f^X \left( 1 + \frac{\alpha_S}{\pi} \left[ -\frac{2}{3} \log 4\tau + \frac{1}{18} (\pi^2 - \log^2 4\tau) + 2 \log \left( \frac{\mu_{\text{NLO}}^2}{m_f^2} \right) + \frac{i\pi}{9} (\log 4\tau + 6) \right] \right) \quad (2.29)$$

for  $X = S, A$ .  $\mu_{\text{NLO}}$  is the renormalisation scale used for these NLO corrections, chosen to be  $\mu_{\text{NLO}} = m_S/2$ . In the intermediate range of  $100m_f > m_S > 2m_f$ , no closed expressions for the NLO correction exist. Our approach in this range was to extract the numerical values of the corrections from HDECAY [176] and to fit them. For the digluon decay rate, the corrections up to N<sup>3</sup>LO are included and parametrised by

$$\Gamma(X \rightarrow gg) = \Gamma(X \rightarrow gg)_{\text{LO}} \left( 1 + C_X^{\text{NLO}} + C_X^{\text{NNLO}} + C_X^{\text{N}^3\text{LO}} \right), \quad (2.30)$$

with [148, 171–175, 177]

$$C_S^{\text{NLO}} = \left( \frac{95}{4} - \frac{7}{6} N_F \right) \frac{\alpha_S}{\pi}, \quad (2.31)$$

$$C_S^{\text{NNLO}} = \left( 370.196 + (-47.1864 + 0.90177 N_F) N_F + (2.375 + 0.666667 N_F) \log \frac{m_S^2}{m_t^2} \right) \frac{\alpha_S^2}{\pi^2}, \quad (2.32)$$

$$C_S^{\text{N}^3\text{LO}} = \left( 467.684 + 122.441 \log \frac{m_S^2}{m_t^2} + 10.941 \left( \log \frac{m_S^2}{m_t^2} \right)^2 \right) \frac{\alpha_S^3}{\pi^3}, \quad (2.33)$$

and

$$C_A^{\text{NLO}} = \left( \frac{97}{4} - \frac{7}{6} N_F \right) \frac{\alpha_S}{\pi}, \quad (2.34)$$

$$C_A^{\text{NNLO}} = \left( 171.544 + 5 \log \frac{m_S^2}{m_t^2} \right) \frac{\alpha_S^2}{\pi^2}, \quad (2.35)$$

where  $N_F$  is the number of quark flavours and  $m_t$  is the top quark mass. For pseudo-scalars we include only corrections up to NNLO as the N<sup>3</sup>LO are not known for CP-odd scalars.

One has to keep in mind that the NLO up to N<sup>3</sup>LO corrections are calculated in the SM under the assumption that only a (fermionic) colour triplet and the gluons play any role in the loops. Of course, in BSM theories this must not necessarily be the case. For instance, in supersymmetric models gluinos would also contribute at NLO. The impact of these additional corrections is estimated in the following section. Another possible effect is the presence of a scalar triplet, such as the supersymmetric top partners. However, it was found that the higher-

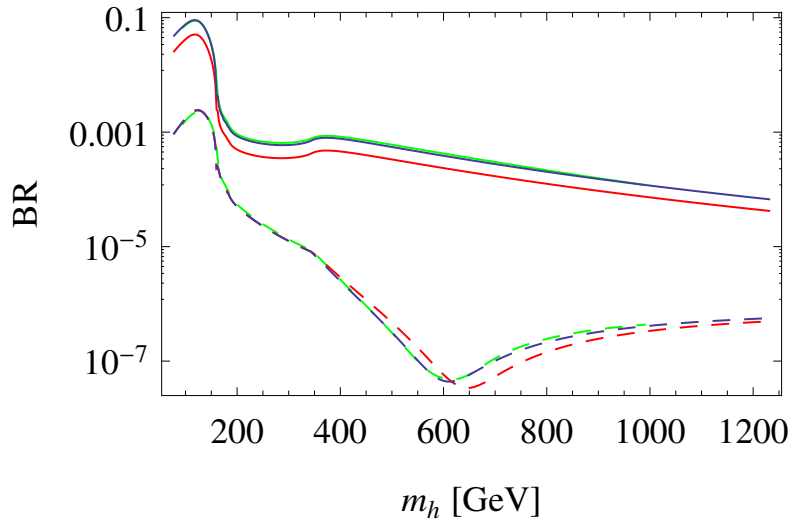


Figure 2.6: Comparison of  $\text{Br}(h \rightarrow gg)$  (full lines) and  $\text{Br}(h \rightarrow \gamma\gamma)$  (dashed lines) as calculated by SPheno at LO (red) and including higher order corrections as described in the text (blue). The green line shows the values of the Higgs cross-section working group.

order corrections for this case can be well approximated by the SM results, see Ref. [178]. Finally, other colour representations beyond triplets can induce an effective digluon coupling in BSM theories. To our knowledge, NLO and higher order corrections for these cases have not yet been discussed in the literature. We consider the SM corrections to also give the dominant effect at NLO and beyond for the cases at hand. This is motivated by the observation of Ref. [178] that the  $k$ -factor for the higher-order corrections in the MSSM is nearly identical to the SM which arises as the largest contributions by-far come from final state gluons. However, we also provide a flag in SPheno that allows users to turn-off these corrections, if they think that such corrections are not appropriate for the case at hand.

In order to check the accuracy of our implementation, we compared the results obtained with SARAH-SPheno for the SM Higgs boson decays with the ones given in the CERN yellow pages [179]. In Fig. 2.6 we show the results for the Higgs branching ratios into two photons and two gluons with and without the inclusion of higher order corrections. One sees that good agreement is generally found when including higher order corrections. Fig. 2.7 shows the relative difference of the partial widths  $\Gamma_{h \rightarrow \gamma\gamma}$  and  $\Gamma_{h \rightarrow gg}$  as calculated by SPheno and FlexibleSUSY<sup>10</sup> compared to the benchmark values provided by the Higgs cross-section working group. While the results obtained from the two codes are not identical, there is good agreement between them for both partial widths.

The differences between SPheno and FlexibleSUSY originate mainly from a different treatment of unknown higher-order corrections to the pole mass spectrum. In Fig. 2.8 we show the ratio  $\text{Br}(h \rightarrow gg)/\text{Br}(h \rightarrow \gamma\gamma)$  and compare it again with the recommended numbers by the Higgs cross-section working group [179]. Allowing for a 10% uncertainty, we find that our calculation including higher order corrections agrees well within the errors, while the LO calculation predicts a ratio that is over a wide range much too small. The important range

<sup>10</sup> FlexibleSUSY is a spectrum generate that has recently been developed which also links to SARAH [180].

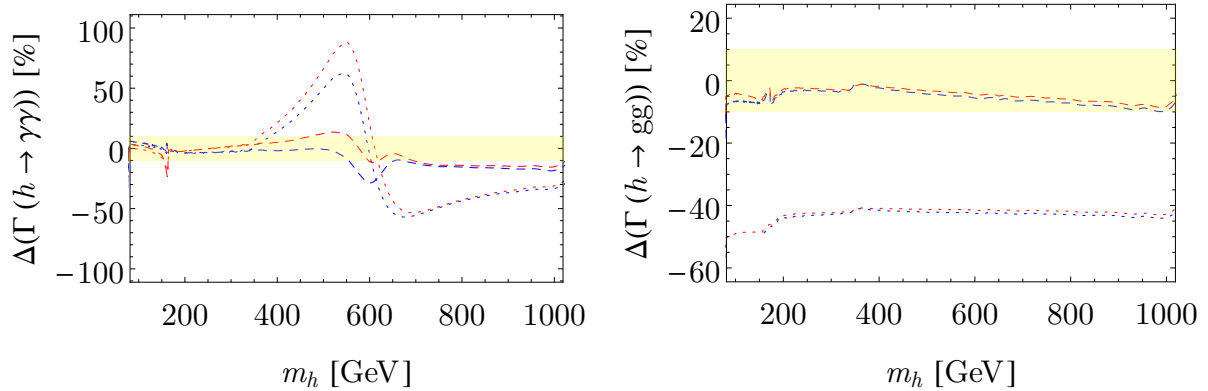


Figure 2.7: On the left: comparison of the relative difference in the partial width  $\Gamma(h \rightarrow \gamma\gamma)$  as calculated by SPheno (in red) and FlexibleSUSY (in blue) to the benchmark values provided by the Higgs cross-section working group. The LO results are shown by the dotted lines, while the NLO results are shown by the dashed lines. The yellow rectangle indicates  $\pm 10\%$  errors compared to the results from the Higgs cross section working group. On the right: the same for the partial width  $\Gamma(h \rightarrow gg)$ .

to look at is not the one with  $m_h \simeq 750$  GeV because this corresponds to a large ratio of the scalar mass compared to the top mass. Important for most diphoton models is the range where the scalar mass is smaller than twice the quark mass. In this mass range we find that the NLO corrections are crucial and can change the ratio of the diphoton and digluon rate by up to a factor of 2. We also note that if we had used  $\alpha_{\text{EM}}(m_h)$  instead of  $\alpha_{\text{EM}}(0)$  in the LO calculation, the difference would have been even larger, with a diphoton rate overestimated by a factor  $(\alpha_{\text{EM}}(m_h)/\alpha_{\text{EM}}(0))^2 \simeq (137/124)^2 \simeq 1.22$ .

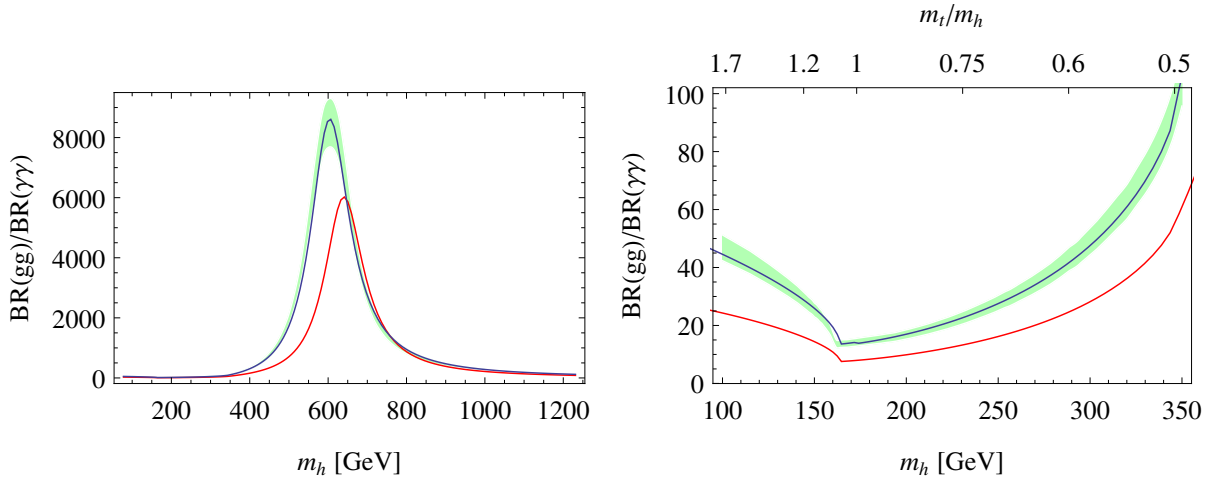


Figure 2.8:  $\text{Br}(h \rightarrow gg)/\text{Br}(h \rightarrow \gamma\gamma)$  as calculated by SPheno at LO (red) and including higher order corrections (blue) as described in the text. The green band shows the values of the Higgs cross section working group including a 10% uncertainty. On the right we zoom into the interesting range  $m_h \in [0.5, 2] m_t$

## Accuracy of the diphoton calculation

Before concluding this section, we should draw the reader's attention to the question of how accurate the results are from SARAH in combination with SPheno and FlexibleSUSY. While every possible correction has been included, there are still some irreducible sources of uncertainty, as we shall discuss below.

- *Loop corrections to  $ZZ, WW, Z\gamma$  final states:* In the 2016 version of SARAH, loop-level decays were only computed for processes where the tree-level process is absent. This is to avoid the technical issue of infra-red divergences. If the particle that explains the 750 GeV excess is a CP-even scalar, then it must mix with the Higgs and therefore acquire tree-level couplings to the  $Z$  and  $W$  bosons. The respective decays are fully taken into account at tree level. However, due to the existence of such terms, the loop corrections to the decays into  $Z$ - and  $W$ -bosons were therefore not yet available in SARAH. These technical issues do not apply for CP-odd scalars, for which the decays into vector bosons are only possible at the loop level. Nevertheless these decays are also not yet available at the loop level. This gap has now been filled with the current release of SARAH [181]. This update allows all possible decay widths at the one-loop level to be automatically calculated.

The lack of complete one-loop corrections in these decay channels can trigger two issues the user has to keep in mind. First, there are limits on the decays  $S \rightarrow WW$  and  $S \rightarrow ZZ$  which could be violated if the loop induced couplings between  $S$  and two massive vector bosons are too large. Therefore, one has to be careful when studying models with large additional SU(2) representations. The second issue is that the prediction for the BR into two photons suffers from an additional uncertainty because of the missing contribution of the  $ZZ$  and  $WW$  decays to the total width.

To estimate the uncertainty incurred by their absence, let us assume that the 750 GeV resonance  $S$  couples to the U(1)<sub>Y</sub> and SU(2)<sub>L</sub> gauge bosons via the effective operators  $SB_{\mu\nu}B^{\mu\nu}$  and  $SW_{\mu\nu}W^{\mu\nu}$ . If we can neglect the tree-level contributions to the decays and assume that the dominant contribution originates from a set of particles in the loops, which have the hypercharge  $Y$ , Dynkin index  $D_2(W)$  and dimension of the SU(2) representation  $d_2$ , then the decay widths are approximately given by

$$\begin{aligned} \frac{\Gamma(S \rightarrow ZZ)}{\Gamma(S \rightarrow \gamma\gamma)} &\simeq \frac{(\frac{D_2}{t_W^2} + t_W^2 d_2 Y^2)^2}{(d_2 Y^2 + D_2)^2}, & \frac{\Gamma(S \rightarrow Z\gamma)}{\Gamma(S \rightarrow \gamma\gamma)} &\simeq \frac{2}{t_W^2} \frac{(D_2 - t_W^2 d_2 Y^2)^2}{(d_2 Y^2 + D_2)^2}, \\ \frac{\Gamma(S \rightarrow WW)}{\Gamma(S \rightarrow \gamma\gamma)} &\simeq \frac{2D_2^2 \text{cosec}^4 \theta_W}{(d_2 Y^2 + D_2)^2}. \end{aligned} \quad (2.36)$$

where we abbreviated  $t_W$  for  $\tan \theta_W$ . Put together, the uncertainty that we find for the decay  $S \rightarrow \gamma\gamma$  reads

$$\frac{\delta\Gamma(S \rightarrow \text{anything})}{\Gamma(S \rightarrow \text{anything})} \simeq \left[ \frac{55D_2^2 - 2d_2 Y^2 D_2 + 0.69d_2^2 Y^4}{(d_2 Y^2 + D_2)^2} \right] \times \text{Br}(S \rightarrow \gamma\gamma). \quad (2.37)$$

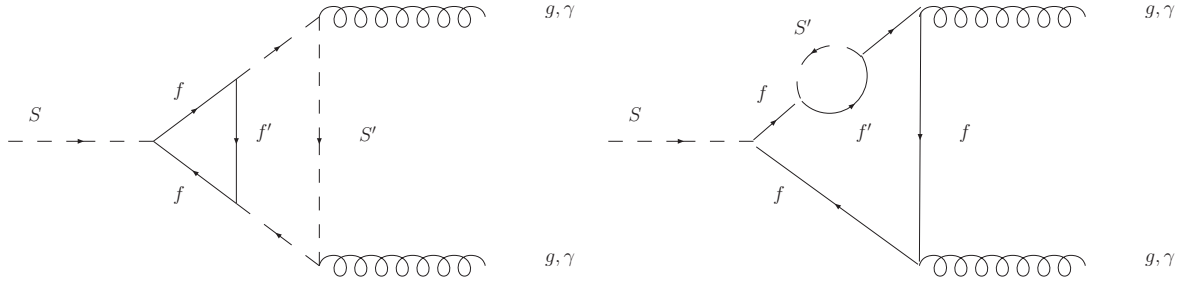


Figure 2.9: Example Feynman graphs of potentially important NLO corrections. Here  $f$  and  $f'$  would typically be vector-like quarks.  $S$  is the 750 GeV resonance, while  $S'$  represents possible models where scalars run in the loop to enhance the diphoton rate.

The factor in square brackets is largest for fields that only couple to  $SU(2)_L$  gauge bosons, giving a factor of  $\sim 55$ , and for  $SU(2)$  doublets with hypercharge  $1/2$  it is 13, although the former case yields too many  $W$  bosons (the limit from run 1 searches is  $\frac{\Gamma(S \rightarrow WW)}{\Gamma(S \rightarrow \gamma\gamma)} \lesssim 20$ ). Thus, provided that  $\text{Br}(S \rightarrow \gamma\gamma) \lesssim 10^{-3}$ , the relative uncertainty is guaranteed to be less than 10%. In such cases, the proportional error in the total width transfers directly into the proportional error in the total cross-section:

$$\frac{\delta\sigma(pp \rightarrow S \rightarrow \gamma\gamma)}{\sigma(pp \rightarrow S \rightarrow \gamma\gamma)} \simeq \frac{\delta\Gamma(S \rightarrow \text{anything})}{\Gamma(S \rightarrow \text{anything})} \quad (2.38)$$

On the other hand, for models where the dominant decay channel of the singlet is into gluons, it is not possible to have  $\text{Br}(S \rightarrow \gamma\gamma) \lesssim 10^{-3}$  without violating constraints from dijet production, and the reader should be careful about the possible errors incurred. Fortunately, provided that the loop particles have a hypercharge the error is much smaller. For example in the case that  $D_2 = 0$  the coefficient above is less than one, thus giving an error of  $\sim 10^{-3}$  for  $\text{Br}(S \rightarrow \gamma\gamma) = 10^{-3}$ .

- *BSM NLO corrections:* As discussed above, SARAH includes the leading-order computation of the diphoton and digluon decay amplitudes including the effects of all SM and BSM particles in the loops. Furthermore, it also includes the leading-log corrections to the digluon rate at NLO, NNLO and  $N^3\text{LO}$  order in  $\alpha_S$  in the SM, and some NLO corrections due to diagrams with an extra gluon to both the digluon and diphoton rates. However, the NLO corrections are absent for all other particles, which in the case of large Yukawa couplings or hierarchies could be sizeable. Two examples of such diagrams are given in Fig. 2.9. In the context of supersymmetric theories, particularly important are diagrams involving the gluino, which (if it is a Majorana particle) would not couple to a singlet at leading order. Naively their contribution is

$$\frac{\delta\Gamma(S \rightarrow gg/\gamma\gamma)}{\Gamma(S \rightarrow gg/\gamma\gamma)} \simeq \frac{\alpha_S}{\pi} \log \frac{m_{\tilde{g}}^2}{\mu_{\text{NLO}}^2} \xrightarrow{m_{\tilde{g}}=2 \text{ TeV}} \approx 10\% . \quad (2.39)$$

Model	Name	Reference
<b>Toy models with vector-like fermions</b>		
CP-even singlet	SM+VL/CPevenS	
CP-odd singlet	SM+VL/CPoddS	
Complex singlet	SM+VL/complexS	
<b>Models based on the SM gauge-group</b>		
Portal dark matter	SM+VL/PortalDM	[153, 184]
Scalar octet	SM-S-Octet	[164, 165] $\triangle$ <sup>(1)</sup>
SU(2) triplet quark model	SM+VL/TripletQuarks	[185]
Single scalar leptoquark	LQ/ScalarLeptoquarks	[186]
Two scalar leptoquarks	LQ/TwoScalarLeptoquarks	[145] $\triangle$ <sup>(3)</sup>
Georgi-Machacek model	Georgi-Machacek	[166, 187]
THDM w. colour triplet	THDM+VL/min-3	[188]
THDM w. colour octet	THDM+VL/min-8	[188]
THDM-I w. exotic fermions	THDM+VL/Type-I-VL	[189, 190]
THDM-II w. exotic fermions	THDM+VL/Type-II-VL	[189, 190]
THDM-I w. SM-like fermions	THDM+VL/Type-I-SM-like-VL	[191]
THDM-II w. SM-like fermions	THDM+VL/Type-II-SM-like-VL	[191]
THDM w. scalar septuplet	THDM/ScalarSeptuplet	[192, 193]

Table 2.6: Part I of the overview of proposed models to explain the diphoton excess which are now available in SARAH. The warning ( $\triangle$ ) shows that we found serious problems with the model during the implementation. The reasons are as follows. (1): the model is in conflict with limits from dijet constraints; (2): we changed the quantum numbers and/or the potential because the original model had charge violating interactions; (3): we find disagreement with the diphoton rate as calculated in the original reference. For simplicity, we used the abbreviations LQ for LeptoQuarks and U1Ex for U1Extensions.

- *Presence of light fermions:* The higher order corrections to the Higgs production and decay via the effective digluon coupling is calculated in the SM using an effective-field-theory (EFT) approach. This is possible because the top mass is sufficiently heavy compared to the Higgs boson. The presence of vector-like quarks with masses below 750 GeV is already tightly constrained by direct searches at the LHC [182]. Therefore, for realistic scenarios the EFT approximation is also typically valid. Even so, one might wonder how large the additional uncertainty is due to the presence of light quarks. For a detailed discussion of this, we refer to Ref. [183]. The overall result is that the additional uncertainty is larger than the one stemming from the choice of the QCD scale. Nevertheless, it was found that the EFT computation still gives a good estimate for the overall  $k$ -factor.

Model	Name	Reference	
<b>U(1) Extensions</b>			
Dark U(1)'	U1Ex/darkU1	[194]	
Hidden U(1)	U1Ex/hiddenU1	[195]	
Simple U(1)	U1Ex/simpleU1	[196]	
Scotogenic U(1)	U1Ex/scotoU1	[197]	$\triangle$ <sup>(2)</sup>
Unconventional U(1) <sub>B-L</sub>	U1Ex/BL-VL	[198]	
Sample of U(1)'	U1Ex/VLsample	[199]	
flavour-nonuniversal charges	U1Ex/nonUniversalU1	[147]	$\triangle$ <sup>(3)</sup>
Leptophobic U(1)	U1Ex/U1Leptophobic	[200]	$\triangle$ <sup>(1)</sup>
Z' mimicking a scalar resonance	U1Ex/trickingLY	[132]	
<b>Non-abelian gauge-group extensions of the SM</b>			
LR without bidoublets	LRmodels/LR-VL	[201–203]	$\triangle$ <sup>(2)</sup>
LR with U(1) <sub>L</sub> × U(1) <sub>R</sub>	LRmodels/LRLR	[204]	$\triangle$ <sup>(2)</sup>
LR with triplets	LRmodels/tripletLR	[205]	
Dark LR	LRmodels/darkLR	[206]	
331 model without exotic charges	331/v1	[207]	
331 model with exotic charges	331/v2	[208]	
Gauged THDM	GTHDM	[209]	
<b>Supersymmetric models</b>			
NMSSM with vectorlike top	NMSSM+VL/VLtop	[154]	$\triangle$ <sup>(1)</sup>
NMSSM with 5's	NMSSM+VL/5plets	[169, 210, 211]	
NMSSM with 10's	NMSSM+VL/10plets	[169, 210, 211]	
NMSSM with 5's & 10's	NMSSM+VL/10plets	[211]	
NMSSM with 5's and RpV	NMSSM+VL/5plets+RpV	[169]	
Broken MRSSM	brokenMRSSM	[212]	
U(1)'-extended MSSM	MSSM+U1prime-VL	[213, 214]	
E <sub>6</sub> with extra U(1)	E6MSSMalt	[215]	

Table 2.7: Part II of the overview of proposed models to explain the diphoton excess which are now available in SARAH. The warning ( $\triangle$ ) shows that we found serious problems with the model during the implementation. The reasons are as follows. (1): non-perturbative couplings needed to explain diphoton excess; (2): we changed the quantum numbers and/or the potential because the original model had charge violating interactions; (3): we find disagreement with the diphoton rate as calculated in the original reference.

## 2.2.4 Models

A large variety of models have been proposed to explain the diphoton excess at 750 GeV. We have selected and implemented several possible models in SARAH. Our selection is not exhaustive, but we have tried to implement a sufficient cross-section which are representative of many of the ideas put forward in the context of renormalisable models. All model files are available for download at:

[http://sarah.hepforge.org/Diphoton\\_Models.tar.gz](http://sarah.hepforge.org/Diphoton_Models.tar.gz)

In addition an overview of all implemented models is given in Tabs. 2.6 and 2.7. Models where we found inconsistencies are marked with a danger sign with the specific issue mentioned in the caption of the relevant table. The main goal of implementing so many models is to give the user a vast array of examples in order to assist with their own model implementation.

All SARAH model files which have been created, as well as the numerical codes derived thereof, have been validated by us using the following procedure:

1. First, the SARAH files themselves have been tested for consistency using basic SARAH commands. We have checked every model for anomalies as well as for invariance under all gauge and discrete symmetries. Furthermore, the `CheckModel` command was executed which in addition checks for consistency of all field and parameter definitions as well as whether all possible particle admixtures have been correctly taken into account.
2. Whenever analytic formulas such as mass matrices were presented in the original studies, we have reproduced and checked the respective expressions with SARAH.
3. For each model, we have produced and successfully compiled the tailor-made code for the spectrum generators `SPheno` and `FlexibleSUSY`.
4. Whenever the reference proposing the model has presented the necessary information to reproduce their results, we have done so. Differences are noted in Tabs. 2.6 and 2.7.
5. The model files for `MadGraph` and `CalcHEP` have been produced for all models and checked for consistency using the internal routines of the respective tools. Furthermore, we have computed representative processes like the production and/or decay of the candidate for the diphoton resonance and compared the obtained branching ratios between `MadGraph`, `CalcHEP` and `SPheno/FlexibleSUSY`.
6. For each model, we provide a set of input parameters which can be used to produce a valid spectrum which itself can then serve as an input for programs like `MadGraph` or `CalcHEP`.

Lastly, we want to mention other proposals which we have not dealt with here due to their incompatibility with SARAH. Many authors [140, 216–234] have studied the excess with effective (non-renormalisable) models, which is sensible given that there are thus far no other striking hints of new physics at the LHC. As more data becomes available and the evidence for new physics becomes more substantial, one might want to UV complete these models, at which point the tools we are advertising become relevant and necessary. Other authors [156, 235–250] considered strongly coupled models, in which the resonance is a com-

posite state. This possibility would be favoured by a large width of the resonance, as first indications seemed to suggest. Another possibility is to interpret the signal in the context of extra-dimensional models [251–261], with the resonance being a scalar, a graviton, a dilaton, or a radion, depending on the scenario. In supersymmetry, the scalar partner of the goldstino could provide an explanation to the diphoton signal [262–265]. Other ideas, slightly more exotic, include: a model with a space-time varying electromagnetic coupling constant [266], Gluionia [267], Squarkonium/Diquarkonium [268], flavons [269], axions in various incarnations [146, 270–274], a natural Coleman-Weinberg theory [275, 276], radiative neutrino mass models [162, 163, 277], and string-inspired models [278–282].

## 2.3 Conclusion

In this chapter we have given an overview of the `Mathematica` tool SARAH as well as the other high-energy physics codes that it interfaces with. We dub this the ‘SARAH framework’, which is the main tool used in the forthcoming chapters. This framework equips a phenomenologist with a powerful tool-kit allowing a large number of models to be studied when compared to the usual time consuming process performing such computations by hand. As a result we are able to confront numerous possible BSM theories with data not only in a finite period of time but also using theory calculations with a high level of precision. For example, the combination of SARAH and SPheno allow the calculation of the Higgs mass at two-loop level in arbitrary BSM theories. This is of particular interest as the theoretical uncertainty on the Higgs mass prediction is usually significantly larger than the experimental uncertainty on the Higgs mass measurement.

In the second half of this chapter we have used the recent diphoton excess as an example of how these tools can be used to confront signals of new physics. We observed that many theorists were retrofitting additional particle content, for instance vector-like quarks, to existing BSM theories without regarding the consequences of these additions on other sectors of the model. As a result we have included a lengthy motivation exactly how these tools can aid the perspective author in avoiding many of the pitfalls we observed initially in the diphoton literature. We then discussed the implementation of the required observables into SARAH as well as the sources of uncertainty in the calculations. Note that since this work was completed, the calculation of all possible one-loop decay widths have since been implemented into SARAH [181]. This supersedes the implementation discussed here. We implemented a large cross-section of different types of models, approximately 40 in total, into SARAH to serve as templates for future users implementing their own models.



## Chapter 3

# Vacuum Stability in Minimal Supersymmetric Models

---

Supersymmetry [42–50] is one of the most theoretically appealing solutions to the hierarchy problem of the SM [51]. However, as with all possible solutions to the hierarchy problem, invoking supersymmetry also comes with a large number of downsides. The first, most obvious downside to supersymmetry is the large number of parameters that are necessarily introduced in addition to the 19 of the SM. This follows from the necessity that supersymmetry cannot be an unbroken exact symmetry at current observable energies as this symmetry enforces exact mass degeneracy between the SM particles and their respective supersymmetric partners. As we have not yet observed any of these superpartners, supersymmetry must therefore be broken at some higher, as yet unobservable, energy scales. The problem of additional parameters arises as there exist a plethora of different methods to break supersymmetry softly.<sup>1</sup> Therefore, one typically adds all possible soft-breaking terms to the Lagrangian in order to remain as generic as possible. The consequence, is an additional 105 parameters in the theory [42, 46]. These parameters can then be chosen to correspond to specific models of supersymmetry breaking.

The second problem arises through the introduction of a large number of new scalar fields, forming the superpartners to the SM fermion content. This results in a scalar potential that has significantly larger number of directions in field space. In comparison the SM scalar potential contains only a single real degree of freedom.<sup>2</sup> In the SM, the problem therefore reduces to ensuring that the potential remains bounded from below as, given the structure of the SM potential at tree-level, additional minima cannot co-exist with the required minimum for electroweak symmetry breaking. This implies that if one chooses the parameters of the SM such that the correct electroweak breaking minimum exists, then this precludes the existence

---

<sup>1</sup> Breaking supersymmetry softly refers to adding only supersymmetry breaking operators of mass dimension three or less to the Lagrangian so that the quadratic divergence in the corrections to the Higgs mass do not reappear [283–285]. This condition on an operator being *soft* is necessary but not always sufficient. For example if a supersymmetric theory contains a scalar singlet  $\Phi$  then an operator of the form  $\Phi^* \Phi^2$ , although satisfying the above condition, actually reintroduces a quadratic divergence to the theory [285].

<sup>2</sup> One can show that through an  $SU(2)$  gauge transformation the complex Higgs doublet can be brought into the unitary gauge where the physical Higgs boson is the only remaining degree of freedom in the scalar sector.

of other minima which may not lead to the correct symmetry breaking pattern. Returning to supersymmetric models, one typically obtains a scalar potential that can easily have  $\mathcal{O}(20)$  directions in field space. The determination of the stability and subsequent phenomenological viability of such potentials forms the basis for the work that follows in this chapter.

The first section of this chapter focuses on the most constrained variant of the minimal supersymmetric standard model (MSSM), referred to as the CMSSM [23, 286–289]. We demonstrate that this model cannot explain the diphoton excess that appeared in the 2015 LHC dataset while also containing a sufficiently stable electroweak breaking vacuum. In the second section we consider the next-to-minimal supersymmetric standard model (NMSSM) which contains a gauge singlet coupling to the Higgs doublets of the MSSM. This coupling allows for non-trivial configurations of the potential leading to minima which spontaneously break  $U(1)_{EM}$ . We study these destabilising effects at both tree and one-loop level.

## 3.1 Vacuum Stability in the Constrained MSSM

### 3.1.1 Charge and Colour Breaking Minima

In this section we introduce the MSSM potential and illustrate the procedure to determine the stability of the electroweak vacuum which is used in `Vevacious`. Any supersymmetric model begins with the definition of the superpotential.<sup>3</sup> This specifies all interactions in the theory that do not arise from the gauge sector of the model, for example the Yukawa interactions. In addition its exact form is strongly constrained by the requirement of invariance underneath supersymmetry transformations. This leads to two important consequences: (i) the superpotential can only contain holomorphic operators<sup>4</sup> and (ii) superpotential operators do not receive renormalisation at any order in perturbation theory [291, 292]. The superpotential of the MSSM is

$$W_{\text{MSSM}} = Y_u \hat{Q} \hat{H}_u \hat{U} + Y_d \hat{Q} \hat{H}_d \hat{D} + Y_e \hat{L} \hat{H}_d \hat{E} + \mu \hat{H}_u \hat{H}_d, \quad (3.1)$$

where generational, colour and  $SU(2)_L$  indices have all been suppressed, and the quantum numbers under the SM gauge symmetries can be found in Table 1.1 of Ref. [49]. Here, the hatted fields correspond to chiral superfields which each contain physical complex scalar and Weyl fermion degrees of freedom. The Yukawa couplings  $Y_u$ ,  $Y_d$  and  $Y_e$  are each  $3 \times 3$  complex matrices, while  $\mu$  is referred to as the Higgsino mass term. The form of the superpotential is fixed by the introduction of a discrete symmetry called either R-parity or matter-parity [49] in conjunction with the SM gauge symmetries from Eq. (1.1). These discrete symmetries enforce conservation of both lepton and baryon number as is required for sufficient stability of the

---

<sup>3</sup> In this thesis we have omitted a detailed introduction to the general structure of supersymmetric Lagrangians. This is discussed in complete detail in a number of excellent reviews and textbooks, see for example [42, 49, 290].

<sup>4</sup> Here, holomorphic refers to the fact that if an operator  $\Phi_i \Phi_j$  was present in the superpotential, then the term  $\Phi_i^\dagger \Phi_j^\dagger$  would be non-holomorphic and therefore forbidden in the superpotential.

proton.<sup>5</sup> The soft-breaking terms in the Lagrangian are

$$-\mathcal{L}_{\text{soft}} = V_{\text{soft}} + \mathcal{L}_{\tilde{\lambda}\text{-mass}}, \quad (3.2)$$

$$V_{\text{soft}} = \sum_i m_i^2 |\phi_i|^2 + \left( B_\mu H_u H_d + T_u \tilde{Q} H_u \tilde{U} + T_d \tilde{Q} H_d \tilde{D} + T_e \tilde{L} H_d \tilde{E} + \text{h.c.} \right), \quad (3.3)$$

$$\mathcal{L}_{\tilde{\lambda}\text{-mass}} = \sum_j \frac{1}{2} M_j \bar{\lambda}_j \lambda_j, \quad (3.4)$$

where the tilde indicates the scalar, supersymmetric component of the superfield while  $H_u$  and  $H_d$  correspond to the scalar components. The index  $i$  runs over *all* scalar fields of the theory, while the index  $j$  runs over the supersymmetric partners of the  $U(1)_Y$ ,  $SU(2)_L$  and  $SU(3)_C$  gauge bosons called gauginos. Here, the gauginos  $\lambda_j$  have been written as four-component Majorana fermions.  $T_u$ ,  $T_d$  and  $T_e$  are the trilinear soft-breaking terms which are conventionally written in terms of the respective Yukawa couplings  $T_\alpha \equiv A_\alpha Y_\alpha$ , with  $\alpha = u, d, e$ . Using these expressions one can determine the tree-level scalar potential of any renormalisable supersymmetric theory

$$V_{\text{tree}} = V_F + V_D + V_{\text{soft}}, \quad (3.5)$$

$$V_D = \frac{1}{2} \sum_A g_A^2 \left( \sum_{i,j} \phi_i^\dagger T_{Ar}^a \phi_j \bar{\delta}_{ij} \right)^2, \quad (3.6)$$

$$V_F = \sum_i \left| \frac{\partial W}{\partial \hat{\Phi}_i} \right|_{\hat{\Phi}_i \rightarrow \phi_i}^2. \quad (3.7)$$

The contributions arising in  $V_D$  are called  $D$ -terms. Here, the index  $A$  runs over all gauge symmetries of the model, where  $T_A^a$  are the generators of the gauge group for the particular representation  $r$  that  $\phi_i$  transforms under. In this expression  $\bar{\delta}_{ij}$  equals 1 if  $\phi_i$  and  $\phi_j$  have exactly the same transformation properties under all symmetries and 0 otherwise. Likewise contributions arising in  $V_F$  are called  $F$ -terms. The derivatives are with respect to the superfields of the theory. Once performed the superfields are replaced by their respective scalar components.

With an expression for the scalar potential one can then determine all minima of the theory by looking for the stationary points

$$\left. \frac{\partial V_{\text{tree}}}{\partial \phi_i} \right|_{\phi_i(x) \rightarrow \frac{1}{\sqrt{2}}(v_i + \phi'_i(x))} \stackrel{!}{=} 0. \quad (3.8)$$

Here, the partial derivative of the potential is taken with respect to all scalar fields  $\phi_i$  in the

<sup>5</sup> These discrete symmetries only forbid lepton and baryon number violating terms at the renormalisable level. They do not forbid dimension 5 terms nor do they preclude the possibility of baryon and or lepton number violation through non-perturbative physics. Dimension 5 operators can also be dangerous for proton decay (c.f Ref. [293]), therefore for complete stability of the proton discrete symmetries such as proton hexality are required [294].

theory. Choosing a particular solution of this set of  $i$  equations, referred to as the *minimisation conditions* or *tadpole equations*, physically corresponds to choosing a minimum. This is nothing other than a choice of the vacuum around which we expand the physical fields. This is indicated in the above expression by the replacement  $\phi_i(x) \rightarrow \frac{1}{\sqrt{2}}(v_i + \phi'_i(x))$ , where  $v_i$  are called the vacuum expectation values (VEVs) of the fields and  $\phi'_i$  are the shifted fields. This set of minimisation conditions can be used to eliminate  $N$ , where  $i = 1, \dots, N$ , Lagrangian parameters of the theory, hence constraining the remaining parameters so that one is always in the desired vacuum of the theory under consideration.

Returning to the case of the MSSM, electroweak symmetry breaking occurs when the electrically neutral components of the Higgs doublets acquire VEVs. However, unlike the SM which contains only a single physical scalar field direction, the MSSM has numerous other scalar field directions. If any of these additional scalar fields acquire VEVs then the pattern of spontaneous symmetry breaking will be altered. For example, if in addition to the neutral Higgs VEVs the scalar superpartners of the top, called stops, acquired VEVs then both the symmetries  $SU(3)_C$  and  $U(1)_{EM}$ , which we require to be unbroken on phenomenological grounds, would be spontaneously broken.<sup>6</sup> As a result such VEVs where the field carries colour and electrical charge are referred to as charge-and-colour-breaking (CCB) vacua. The procedure typically performed disregards these additional directions beyond the real neutral Higgs scalars. This amounts to setting all additional VEVs by hand to zero, which in many scenarios is unfounded [295].

In what follows we are interested in whether or not there exist undesirable CCB minima that can co-exist with the required electroweak symmetry breaking vacuum. Once these additional minima are located, they must then be compared against the depth of the electroweak breaking vacuum. However, it has been shown that one-loop corrections can significantly alter any conclusions drawn from the tree-level potential, c.f. Refs. [295–297].

As an introduction, using the MSSM as an example, we give details on the procedure that is performed when using the tool `Vevacious`. The procedure is as follows:

1. Determine the minimisation equations for the desired electroweak symmetry breaking vacuum disregarding any other scalar directions. For the MSSM, if we express the complex  $SU(2)_L$  Higgs-doublets as

$$H_u = \begin{pmatrix} H_u^+ \\ H_u^0 \end{pmatrix}, \quad H_d = \begin{pmatrix} H_d^0 \\ H_d^- \end{pmatrix}, \quad (3.9)$$

then the corresponding tree-level potential is given by

$$\begin{aligned} V_{\text{tree}}^{H^0}(H_u^0, H_d^0) &= (\mu^2 + m_{H_u}^2) |H_u^0|^2 + (\mu^2 + m_{H_d}^2) |H_d^0|^2 \\ &+ \frac{1}{8}(g_1^2 + g_2^2) (|H_d^0|^2 - |H_u^0|^2)^2 - (B_\mu H_u^0 H_d^0 + \text{h.c.}) . \end{aligned} \quad (3.10)$$

In this expression we have considered only the parts consisting purely of neutral Higgs fields. The resulting minimisation conditions for successfully breaking electroweak

<sup>6</sup> The remaining gauge symmetries after the stops acquired VEVs would depend upon the  $SU(3)_C$  structure of the left- and right-stop VEVs.

symmetry are

$$\frac{\partial V_{\text{tree}}^{H^0}}{\partial \Re(H_u^0)} = v_u m_{H_u}^2 - \frac{1}{8}(g_1^2 + g_2^2)v_u(v_d^2 - v_u^2) + v_u|\mu|^2 - v_d \Re(B_\mu) \stackrel{!}{=} 0, \quad (3.11a)$$

$$\frac{\partial V_{\text{tree}}^{H^0}}{\partial \Re(H_d^0)} = v_d m_{H_d}^2 + \frac{1}{8}(g_1^2 + g_2^2)v_d(v_d^2 - v_u^2) + v_d|\mu|^2 - v_u \Re(B_\mu) \stackrel{!}{=} 0, \quad (3.11b)$$

where after taking the derivatives we have expanded the fields around the minimum, corresponding to the replacement in Eq. (3.8)

$$H_u^0 = \frac{1}{\sqrt{2}} [v_u + \phi_u(x) + i\sigma_u(x)], \quad H_d^0 = \frac{1}{\sqrt{2}} [v_d + \phi_d(x) + i\sigma_d(x)]. \quad (3.12)$$

In this expression we have written the complex components in terms of their VEV ( $v$ ), CP-even ( $\phi$ ) and CP-odd ( $\sigma$ ) components. Contrary to the above expression when the Higgs doublet components are expanded around a minimum one obtains in complete generality

$$\begin{aligned} H_u^0 &= \frac{1}{\sqrt{2}} [v_u e^{i\varphi_u} + \phi_u(x) + i\sigma_u(x)], & H_d^0 &= \frac{1}{\sqrt{2}} [v_d e^{i\varphi_d} + \phi_d(x) + i\sigma_d(x)], \\ H_u^+ &= \frac{1}{\sqrt{2}} [v_p e^{i\varphi_p} + h_u^+(x)], & H_d^- &= \frac{1}{\sqrt{2}} [v_m e^{i\varphi_m} + h_d^-(x)]. \end{aligned}$$

However, one is able to perform an  $SU(2)_L$  rotation to remove three real degrees of freedom, for instance  $v_m = \varphi_m = \varphi_d = 0$ . Performing a field redefinition of the other Higgs doublet allows one to set  $\varphi_u = 0$ . As a result the remaining degrees of freedom that one should consider are  $v_u, v_d, v_p$  and  $\varphi_p$ . However, it can then be shown at tree-level that the global minimum of two-Higgs-doublet models is charge conserving if a correct electroweak breaking minimum exists [298–300]. As the MSSM is simply a special type of two-Higgs-doublet model, we focus on the more prominent effect induced by the stop quark sector of the model. We revisit the case of non-zero charged Higgs VEVs in Section 3.2.

Returning to Eqs. (3.11a) and (3.11b) and solving for  $|\mu|^2$  and  $B_\mu$  we obtain

$$-2(B_\mu)_{\text{min}} = (m_{H_d}^2 - m_{H_u}^2) \tan 2\beta + M_Z^2 \sin 2\beta, \quad (3.13a)$$

$$|\mu|_{\text{min}}^2 = (\cos 2\beta)^{-1} (m_{H_u}^2 \sin^2 \beta - m_{H_d}^2 \cos^2 \beta) - \frac{1}{2} M_Z^2, \quad (3.13b)$$

where  $\tan \beta = v_u/v_d$ ,  $v = \sqrt{v_u^2 + v_d^2}$  is the value of the electroweak VEV and  $M_Z^2 = \frac{1}{4}(g_1^2 + g_2^2)v^2$  is the Z-boson mass. Hence we can express  $|\mu|^2$  and  $B_\mu$  in terms of the input parameters namely, the two Higgs soft-masses,  $\tan \beta$  and the Z-boson mass. This fixes the value of  $|\mu|^2$  and  $B_\mu$  so that we ensure the existence of an electroweak breaking minimum. In what follows we utilise the subscript ‘min’ to indicate when  $\mu$  and  $B_\mu$  are constrained via Eqs. (3.13a) and (3.13b).

As an aside, from the solution of Eqs. (3.13a) and (3.13b) we can now define the parameters of the constrained minimal supersymmetric model (CMSSM) [23, 286–289], which will be the focus of this section. This model has not only been a benchmark for experimental supersymmetry searches due to its small number of parameters but is also strongly motivated when considering supergravity UV completions [45]. It is defined by the parameters

$$M_1 = M_2 = M_3 = M_{1/2}, \quad (3.14a)$$

$$(m_Q^2)^{ij} = (m_U^2)^{ij} = (m_D^2)^{ij} = (m_L^2)^{ij} = (m_E^2)^{ij} = m_0^2 \delta^{ij}, \quad (3.14b)$$

$$m_{H_u}^2 = m_{H_d}^2 = m_0^2, \quad (3.14c)$$

$$A_u = A_d = A_e = A_0, \quad (3.14d)$$

at the unification scale,  $M_{\text{GUT}} \simeq 10^{16}$  GeV, where  $T_k = Y_k A_k$ . Here  $m_0, M_{1/2}$  are the universal scalar and gaugino masses,  $A_0$  is the universal trilinear scalar interaction.  $\tan \beta$  is defined below Eq. (3.13b) and the sign of the  $\mu$  parameter is ambiguous when solving the minimisation conditions. To summarise the CMSSM is defined by the SM parameters plus the additional five parameters

$$m_0, \quad M_{1/2}, \quad A_0, \quad \tan \beta, \quad \text{sign}(\mu). \quad (3.15)$$

2. Now that we have guaranteed an electroweak breaking minimum, one would in principle return to the full potential of the theory containing all scalar fields. However, the expression for the complete scalar potential of the MSSM even at tree-level is too lengthy to provide a useful example. Here, we instead consider the scenario where only the stops can acquire VEVs in addition to the above neutral Higgses. This is a well motivated scenario as additional new minima appear for large terms which are cubic functions of the VEVs. For the MSSM cubic terms arise only from the soft-breaking trilinear terms, which are largest when considering the stops due to the size of the top Yukawa coupling. The potential in this case is given by

$$\begin{aligned} V_{\text{tree}}^{H^0 + \tilde{t}}(H_u^0, H_d^0, \tilde{t}_L^r, \tilde{t}_R^r) &= V_{\text{tree}}^{H^0}(H_u^0, H_d^0) + m_Q^2 |\tilde{t}_L^r|^2 + m_u^2 |\tilde{t}_R^r|^2 \\ &+ |Y_t|^2 (|H_u^0|^2 (|\tilde{t}_L^r|^2 + |\tilde{t}_R^r|^2) + |\tilde{t}_R^r \tilde{t}_L^r|^2) + (T_t H_u^0 \tilde{t}_R^{r*} \tilde{t}_L^r - \mu Y_t^* H_d^0 \tilde{t}_L^{r*} \tilde{t}_R^r + \text{h.c.}) \\ &+ \frac{g_3^2}{6} (|\tilde{t}_L^r|^4 + |\tilde{t}_R^r|^4 + 3|\tilde{t}_L^{r*} \tilde{t}_R^r|^2 - |\tilde{t}_L^r|^2 |\tilde{t}_R^r|^2) \\ &+ \frac{g_2^2}{8} (|\tilde{t}_L^r|^4 - 2|\tilde{t}_L^r|^2 |H_u^0|^2 + 4|\tilde{t}_L^{r*} H_d^0|^2 - 2|\tilde{t}_L^r|^2 |H_d^0|^2) \\ &+ \frac{g_1^2}{72} \left( |\tilde{t}_L^r|^4 + 2|\tilde{t}_L^r|^2 (3|H_u^0|^2 - 3|H_d^0|^2 - 4|\tilde{t}_R^r|^2) \right. \\ &\left. + 8|\tilde{t}_R^r|^2 (3|H_d^0|^2 - 3|H_u^0|^2 + 2|\tilde{t}_R^r|^2) \right), \end{aligned} \quad (3.16)$$

where we have neglected all Yukawa couplings besides from the top-quark Yukawa  $Y_t$ ,

while  $m_Q^2$  and  $m_u^2$  are the soft masses for the quark-doublet and up-type singlet respectively. In this expression we have expanded the colour triplets, considering only the *red-coloured* direction, namely

$$\tilde{t}_L \equiv \begin{pmatrix} \tilde{t}_L^r \\ \tilde{t}_L^b \\ \tilde{t}_L^g \end{pmatrix} \rightarrow \begin{pmatrix} \tilde{t}_L^r \\ 0 \\ 0 \end{pmatrix}, \quad (3.17)$$

and equivalently for  $\tilde{t}_R$ . This has significant implications only for the  $D$ -terms of the theory. The other parts of the potential are diagonal in colour space. Determining the stationary points and expanding around these points (again neglecting CP-violating VEVs) using Eq. (3.12) and

$$\tilde{t}_L^r = \frac{1}{\sqrt{2}} (v_{\tilde{t}_L} + \phi_{\tilde{t}_L}(x) + i\sigma_{\tilde{t}_L}(x)), \quad \tilde{t}_R^r = \frac{1}{\sqrt{2}} (v_{\tilde{t}_R} + \phi_{\tilde{t}_R} + i\sigma_{\tilde{t}_R}), \quad (3.18)$$

yields

$$\begin{aligned} \frac{\partial V_{\text{tree}}^{H^0+\tilde{t}}}{\partial \Re(H_u^0)} &= \frac{\partial V_{\text{tree}}^{H^0}}{\partial \Re(H_u^0)} + \frac{g_1^2}{24} v_u (v_{\tilde{t}_L}^2 - 4v_{\tilde{t}_R}^2) - \frac{g_2^2}{8} v_u v_{\tilde{t}_L}^2 \\ &\quad + \frac{1}{2} |Y_t|^2 v_u (v_{\tilde{t}_L}^2 + v_{\tilde{t}_R}^2) + \frac{\sqrt{2}}{2} \Re(T_t) v_u v_{\tilde{t}_L} v_{\tilde{t}_R} \stackrel{!}{=} 0, \end{aligned} \quad (3.19)$$

$$\frac{\partial V_{\text{tree}}^{H^0+\tilde{t}}}{\partial \Re(H_d^0)} = \frac{\partial V_{\text{tree}}^{H^0}}{\partial \Re(H_d^0)} + \frac{g_1^2}{24} v_d (4v_{\tilde{t}_R}^2 - v_{\tilde{t}_L}^2) + \frac{g_2^2}{8} v_d v_{\tilde{t}_L}^2 - \frac{\sqrt{2}}{2} |Y_t^* \mu| v_{\tilde{t}_L} v_{\tilde{t}_R} \stackrel{!}{=} 0, \quad (3.20)$$

$$\begin{aligned} \frac{\partial V_{\text{tree}}^{H^0+\tilde{t}}}{\partial \Re(\tilde{t}_L^r)} &= v_{\tilde{t}_L} m_Q^2 + \frac{g_1^2}{72} v_{\tilde{t}_L} (3v_u^2 - 3v_d^2 + v_{\tilde{t}_L}^2 - 4v_{\tilde{t}_R}^2) + \frac{g_2^2}{8} (v_{\tilde{t}_L}^3 + v_{\tilde{t}_L} (v_d^2 - v_u^2)) \\ &\quad + \frac{g_3^2}{6} (v_{\tilde{t}_L}^3 - v_{\tilde{t}_L} v_{\tilde{t}_R}^2) + \frac{1}{2} |Y_t|^2 v_{\tilde{t}_L} (v_u^2 + v_{\tilde{t}_R}^2) \\ &\quad + \frac{\sqrt{2}}{2} v_{\tilde{t}_R} (\Re(T_t) v_u - v_d |Y_t^* \mu|) \stackrel{!}{=} 0, \end{aligned} \quad (3.21)$$

$$\begin{aligned} \frac{\partial V_{\text{tree}}^{H^0+\tilde{t}}}{\partial \Re(\tilde{t}_R^r)} &= v_{\tilde{t}_R} m_u^2 + \frac{g_1^2}{18} (3v_d^2 - 3v_u^2 - v_{\tilde{t}_L}^2 + 4v_{\tilde{t}_R}^2) + \frac{g_3^2}{6} (v_{\tilde{t}_R}^2 - v_{\tilde{t}_L}^2) \\ &\quad + \frac{1}{2} |Y_t|^2 v_{\tilde{t}_R} (v_u^2 + v_{\tilde{t}_L}^2) + \frac{\sqrt{2}}{2} v_{\tilde{t}_L} (\Re(T_t) v_u - v_d |Y_t^* \mu|) \stackrel{!}{=} 0. \end{aligned} \quad (3.22)$$

One can now solve for the four VEVs of the system of equations as a function of the input parameters. However, this would not guarantee that any of the resulting minima satisfy Eqs. (3.13a) and (3.13b), which are the minimisation conditions to ensure that the theory contains an electroweak symmetry breaking minimum. The required minimum which results in electroweak symmetry breaking is often referred to as the *desired symmetry breaking* (DSB) minimum. To ensure that the DSB minimum exists we make the substitution  $|\mu| \rightarrow |\mu|_{\min}$  and  $B_\mu \rightarrow (B_\mu)_{\min}$  before solving for the VEVs. The resulting stationary points would therefore co-exist with the DSB minimum. The only downside

is that without making additional approximations the above system of equations is no longer analytically solvable.

Vevacious solves the system of polynomials using the homotopy continuation method [301,302], see also Ref. [303] for a more pedestrian introduction. This works by starting with a set of polynomials with known solutions, continuously deforming the system and updating the respective roots until the required solution is reached. The key advantage to this approach is that it is still sufficiently fast when considering systems with more than a few degrees of freedom. This method is implemented in the code HOM4PS [304], which is used by Vevacious.

3. The next step is to substitute the values of the VEVs for the different minima back into the potential and compare their respective depths to the depth of the DSB minima. Before Vevacious, the typical approach to vacuum stability was to consider  $D$  or  $F$ -flat directions in the tree-level potential, namely  $V_D = 0$  and  $V_F = 0$  respectively. For the case at hand the  $D$ -flat directions are most relevant. The logic being that the  $D$ -terms provide a stabilising effect as they are always functions of the VEVs squared. If one considers the direction  $v_d = 0$  and  $v_X \equiv v_u = v_{\tilde{t}_L} = v_{\tilde{t}_R}$ , then all  $D$ -terms in Eq. (3.16) vanish leaving a potential of the form

$$V_{\text{tree}} = \frac{1}{2} (m_{H_u}^2 + m_Q^2 + m_u^2 + |\mu|^2) v_X^2 + \frac{T_t}{\sqrt{2}} v_X^3 + \frac{3|Y_t|^2}{4} v_X^4. \quad (3.23)$$

Determining the stationary points with respect to  $v_X$  yields

$$v_X^{\text{min}} = \frac{\sqrt{3}A_t + \sqrt{3A_t^2 - 8(m_{H_u}^2 + m_Q^2 + m_u^2 + |\mu|^2)}}{2\sqrt{6}Y_t}, \quad (3.24)$$

ignoring the trivial solution  $v_X^{\text{min}} = 0$ . Here  $T_t = A_t Y_t$ , namely  $A_t$  is the trilinear soft-breaking coupling at the supersymmetry breaking scale after RGE evolution down from the high-scale where one imposes  $A_0 = A_t$  in the CMSSM. Substituting the expression for  $v_X$  back into the potential and insisting that the  $V_{\text{tree}} > 0$  yields one of the typically used *rule-of-thumb* expressions for vacuum stability [305–309]

$$A_t^2 < 3(m_{H_u}^2 + m_Q^2 + m_u^2 + |\mu|^2). \quad (3.25)$$

However, this expression only considers a single direction in field space. Although slightly more generic conditions have been derived in Refs. [310,311], these analyses are far from general and give no insight into what exactly is the global minimum of the potential, see also Refs. [297,312]. In addition it has been shown in Refs. [296,297] that the one-loop corrections can significantly alter the relative depths of the minima.

In Vevacious the numerically determined tree-level minima are used as starting points. Using the full one-loop effective potential in the vicinity of these tree-level solutions, the true one-loop minima are determined by allowing these starting points to roll down the potential. The resulting one-loop minima are then substituted back into the effective

potential and compared against the depth of the DSB vacuum. If the DSB vacuum is the global minimum then the parameter point is *stable*, while if other deeper minima exist then the point is termed *metastable*.

Using this approach the CMSSM was studied in detail using Vevacious in Ref. [295]. It was found that the lowest stop mass, assuming a Higgs mass of 125 GeV, possible in the CMSSM which has a stable electroweak (EW) vacuum is around 600 GeV, when setting  $M_{1/2} = 500$  GeV. Note however, that this value is now in conflict with the limits from gluino searches, i.e. the lower bound on the stop mass is even higher. In addition, this limit does not include the constraint from the Higgs mass. When including this constraint, the lightest possible stop mass with a stable vacuum increases to 800 GeV [313].

4. The limits quoted so far on the stop mass only checked if there existed a minimum with non-zero stop VEVs which is deeper than the DSB vacuum. However, it is possible that the EW vacuum is metastable but long-lived on cosmological time scales. This leads to a weaker constraint compared to the requirement that the DSB vacuum is the global minimum used above. The expression for the decay rate  $\Gamma$  per unit volume for a false vacuum is given in [314, 315] as

$$\Gamma/\text{vol.} = Ae^{-\frac{B}{\hbar}}(1 + \mathcal{O}(\hbar)), \quad (3.26)$$

where  $A$  is a factor which depends on the eigenvalues of a functional determinant and  $B$  is the bounce action.  $A$  is usually taken to be of order the renormalisation scale, typical the supersymmetry breaking scale or top quark mass for non-supersymmetric theories, and is less important for the tunnelling rate which is dominated by the exponent  $B$ . In a multi-dimensional space one must calculate  $B$  numerically as any approximations, analytic or otherwise, are not accurate enough due to the huge sensitivity of  $\Gamma$  on  $B$  [314]. The most widely used tool for calculating  $B$  is CosmoTransitions [111]. In this context one has to keep in mind several effects which could alter the lifetime as calculated with CosmoTransitions:

- (i) It is not guaranteed that CosmoTransitions always finds the optimal path for tunnelling.
- (ii) There might be other directions in the VEVs when including more scalar fields beyond the Higgs doublets and stops, which could cause a faster decay of the EW vacuum [295], see also Ref. [316] for a recent discussion.
- (iii) The inclusion of thermal effects can reduce the likelihood that the Universe is still in a metastable but long-lived vacuum [317].
- (iv) Planck suppressed operators can cause a decrease in the lifetime of the EW vacuum [318, 319].

All of these effects can only *decrease* the lifetime of the EW vacuum if it is metastable. Therefore the limits that we present below are conservative estimates.

We show in Fig. 3.9 an example CMSSM parameter point which illustrates how quickly

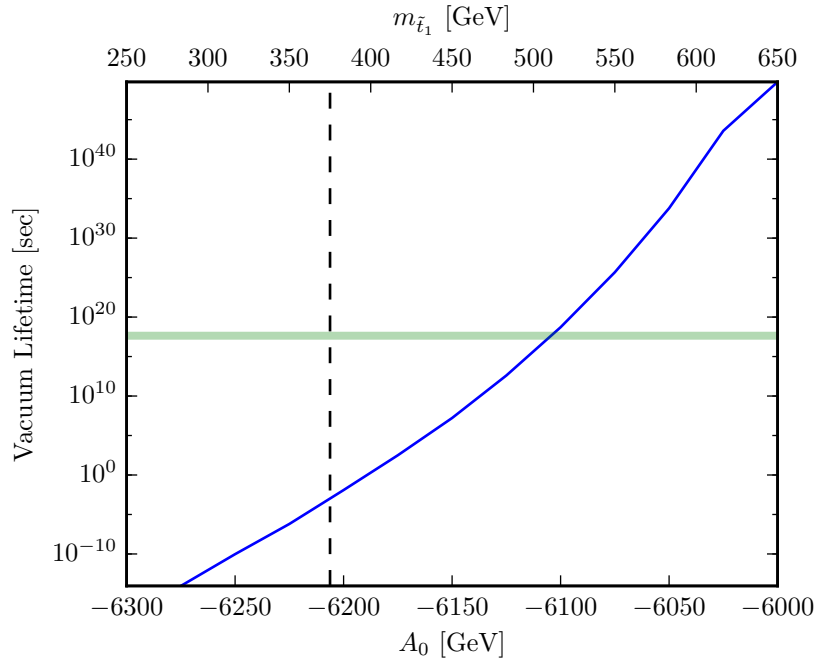


Figure 3.1: The lifetime of the EW vacuum as a function of  $A_0$ . The other CMSSM parameters are chosen as  $m_0 = 2.75$  TeV,  $M_{1/2} = 750$  GeV,  $\tan \beta = 15$ , and  $\mu > 0$ . Also shown along the top  $x$ -axis is the mass of the light stop for the given  $A_0$  values. The black dashed line corresponds to  $m_{\tilde{t}_1} = 375$  GeV while the green line corresponds to a lifetime of 13.8 billion years.

the EW vacuum lifetime decreases with increasing  $|A_0|$ , and therefore decreasing stop mass. This point has a completely stable EW vacuum for  $A_0 \simeq 5.5$  TeV which corresponds to a stop mass of 850 GeV. Allowing the EW vacuum to be metastable, and enforcing that the lifetime of the EW vacuum is at least as long as the current age of the universe allows one to decrease the stop mass to about 525 GeV. However, the point with  $m_{\tilde{t}_1} = 375$  GeV has a lifetime of only a fraction of a second and is therefore ruled out beyond doubt. Moreover, we have not taken into account thermal corrections to the tunnelling process which typically reduce the lifetime [295].

### 3.1.2 The Diphoton Excess and the CMSSM

The diphoton excess seen at the LHC at 750 GeV in the first data set of the 13 TeV run [62, 320] was the first and only striking signal of BSM physics, see Section 2.2 for a detailed overview.<sup>7</sup> Many different explanations for this excess were proposed. In weakly coupled theories usually a new fundamental scalar with a mass of 750 GeV is introduced. One alternative possibility in weakly coupled theories was pointed out in Ref. [322]: it was shown that bound states of

<sup>7</sup> The data collected in 2016 [130, 321] do not confirm this excess. Combining the 2015 and 2016 data sets, the local significance is reduced from  $\sim 3 - 4\sigma$  to no more than  $\sim 2\sigma$  at both ATLAS and CMS. See also Section 2.2 for more details.

a pair of coloured scalars or fermions with masses of about 375 GeV can explain this excess while being in agreement with all other constraints from direct searches. Ref. [322] finds that the new particles should have charge  $4/3$  or  $5/3$  to have a sufficiently large diphoton production cross section. This is based on the assumption that the binding energies are small enough for the relativistic calculations to hold. In Ref. [323] it was claimed that the same idea works in the CMSSM. Here, the bound states are formed by a pair of stops. In order to be in agreement with the production rate a large binding energy was assumed, which leads to a large uncertainty on the calculation of the production cross section [322].

The CMSSM is experimentally already extremely challenged, if not excluded, when including the constraints for  $(g - 2)_\mu$  [54]. In the perturbatively calculable regions of the CMSSM, it is well known that light stops can no longer be obtained when including all existing constraints. The main reason for this is the Higgs mass which is bounded from above at the tree level requiring large radiative corrections, mainly from stops. This is only possible in the case of one light stop eigenstate if a large mass splitting in the stop sector is present. This large splitting is severely constrained by bounds from vacuum stability: if the trilinear coupling is responsible for enhancing the Higgs mass and for splitting the two stops, minima in the scalar potential can appear where charge and colour get broken via stop VEVs [295]. Therefore, we critically re-analyse the possibility of explaining the diphoton excess within the CMSSM when including these constraints.

In this context we also comment on the possibility of obtaining very large binding energies of the stoponium which might render both perturbative Higgs mass calculations, as well as standard checks of the vacuum stability inappropriate. Even if it is questionable that the changes in the Higgs mass would be so dramatic to be in agreement with the measurements, there is an even stronger argument to rule out these parameter regions: the branching ratio of the stoponium into a pair of Higgs bosons would be much larger than into a pair of photons.

### 3.1.3 Stop Bound States

#### Estimate of the binding energy

It has been pointed out in Ref. [324] that in the case of large trilinear couplings the stops can form bound states (“stoponium”,  $\sigma_{\bar{t}}$ ) via the exchange of Higgs bosons. A rough approximation for the mass of the bound state was given as

$$M_B = 2m_{\bar{t}_1} \sqrt{1 - \frac{1}{(16\pi)^2 4n^2} \left( \frac{T_t \cos \alpha \sin 2\Theta_{\bar{t}}}{\sqrt{2}m_{\bar{t}_1}} \right)^4}. \quad (3.27)$$

Here,  $\Theta_{\bar{t}}$  and  $\alpha$  are the stop and Higgs mixing angles, respectively, whereas  $n$  counts the bound state modes. One can see from this equation that two conditions are necessary to have a small bound state mass or a large binding energy which can even be of the order of the EW scale: very large trilinear couplings  $T_t$  and a large stop mixing  $\Theta_{\bar{t}} \sim \pi/4$ . This was also pointed out in Ref. [325]. The strong dependence on the mixing angle is depicted in Fig. 3.2. Thus, only for mixing above about 0.3 can the binding energy be in the multi-GeV range, for

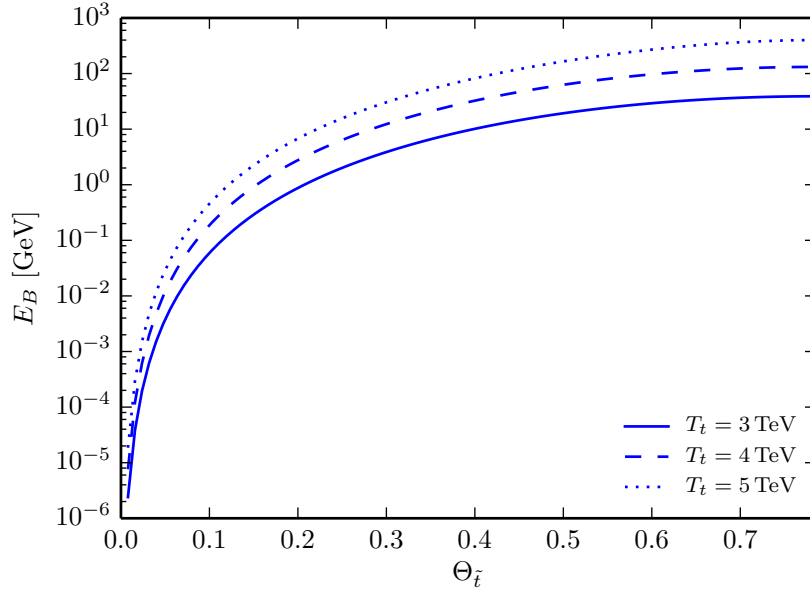


Figure 3.2: The binding energy of two stops with  $m_{\tilde{t}_1} = 375$  GeV for  $T_t = 3$  TeV (solid line), 4 TeV (dashed line), and 5 TeV (dotted line) as a function of the stop mixing angle  $\Theta_t$ .

$T_t$  of order a few TeV. That large binding energy would then impact the study of the vacuum stability and one might need to take these effects into account. However, for smaller mixing angles, the binding energy is tiny compared to the stop mass scale, which is the important scale also for the tunnelling processes. In these cases one can safely expect that the standard calculations hold.

### Correlation between the stoponium binding energy and the light Higgs mass

We can make a rough estimate to see if the binding energy in the parameter space of interest is expected to be large. For this purpose we assume the stop mixing matrix at tree level to be parametrized by

$$m_{\tilde{t}}^2 = \begin{pmatrix} m_{LL}^2 & m_t X_t \\ m_t X_t^* & m_{RR}^2 \end{pmatrix}, \quad (3.28)$$

where  $m_{LL}^2$ ,  $m_{RR}^2$  are the sums of soft supersymmetry-breaking  $F$ - and  $D$ -terms and  $X_t \equiv T_t/Y_t - \mu \cot \beta$ . For  $\tan \beta \gg 1$  the first term dominates, and we assume this limit for the following discussion. We will always refer to mass-ordered eigenstates,  $\tilde{t}_{1(2)}$  being the lighter (heavier) stop eigenstate. Together with the well-known expression for the one-loop corrections to the Higgs mass via (s)tops in the decoupling limit  $M_A \gg M_Z$  [49, 326–330],

$$\delta m_h^2 = \frac{3}{2\pi^2} \frac{m_t^4}{v^2} \left[ \log \frac{M_S^2}{m_t^2} + \frac{X_t^2}{M_S^2} \left( 1 - \frac{X_t^2}{12M_S^2} \right) \right], \quad (3.29)$$

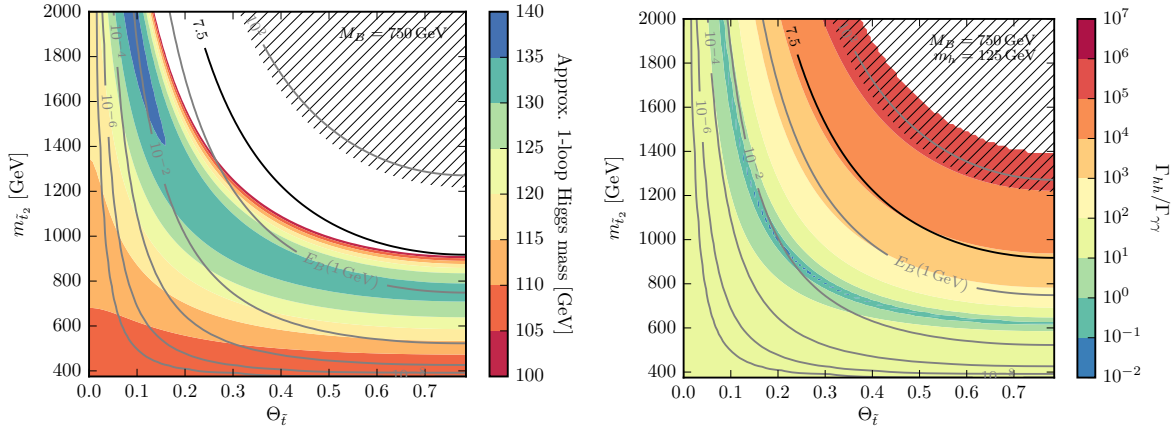


Figure 3.3: Left: estimate of the one-loop corrected Higgs mass (coloured contours) in the  $(\Theta_{\tilde{t}}, m_{\tilde{t}_2})$  plane. Right: the ratio of the partial decay widths of the stoponium into a pair of Higgs bosons (for fixed  $m_h = 125$  GeV) and a pair of photons. We have set  $M_B = 750$  GeV, respectively. In both figures, the lines are contours of constant  $E_B/\text{GeV}$ , the black line indicates the contour where  $E_B$  reaches 1% of  $M_B$ . The hatched region corresponds to parameter space where the perturbative calculation is no longer reliable, namely  $E_B \geq 0.1M_B$ .

with  $M_S = \sqrt{m_{\tilde{t}_1} m_{\tilde{t}_2}}$ , one can express the one-loop corrected Higgs mass as a function of  $m_{\tilde{t}_2}$  and  $\Theta_{\tilde{t}}$ , when fixing the stoponium mass at  $M_B = 750$  GeV. For the same parameters, we also compute the binding energy. The combined results are shown in the left panel of Fig. 3.3. One can see that for light stop masses,  $m_{\tilde{t}_2}$ , the maximal enhancement for the Higgs mass appears, as expected, for maximal stop mixing. However, for heavier stops, a smaller stop mixing is preferred. One can also see that, in the interesting region with the largest corrections to the Higgs mass, the stoponium binding energy is usually small and often even below the GeV range. Very large binding energies of order the EW scale only appear in parameter regions in which the light Higgs would even become tachyonic, because of huge negative one-loop corrections. Thus, in general one can assume that for parameter regions which lead to the correct Higgs mass using the standard calculations, also the standard checks for the vacuum stability do indeed hold. Moreover, the production rate can be calculated using the expressions for a pure QCD bound state which turns out to be too small to explain the observed diphoton excess.

### Strongly coupled stoponium: Di-Higgs decays

These arguments are valid as long as we are situated in a ‘normal’ environment, where perturbative calculations hold and the Higgs boson is a pure elementary particle. Even in the set up of the MSSM, however, it may be possible to find regions with very large stoponium binding energies. One might argue that one cannot trust perturbative evaluations of the Higgs mass in the regions where it becomes tachyonic due to the large trilinear couplings involved and subsequently lattice calculations would be more appropriate for a calculation of  $m_h$ .<sup>8</sup> In

<sup>8</sup> This was actually *not* the Ansatz of Ref. [323], which made use of the standard Higgs mass calculations.

Fig. 3.3, we hatch the regions where the perturbative calculation can no longer be trusted, where we have conservatively taken this region to begin at  $E_B \gtrsim 0.1M_B$ . Let us assume for the time being that we are in this strongly coupled phase and that a 125 GeV Higgs mass is possible with large  $E_B$  due to the Higgs exchange. This immediately raises the question how important the decay of the stoponium into a pair of Higgs bosons becomes with respect to the desired diphoton decay, as these regions feature very large trilinear couplings. Fortunately, all partial widths scale in the same way with the wave function at the origin (and subsequently with the binding energy); therefore, this factor drops out when calculating ratios so that reliable predictions can be made. The respective formulas can, for instance, be taken from Ref. [331]; for earlier work see also [332]. In the right-hand panel of Fig. 3.3 we show the resulting ratio of  $\Gamma_{hh}/\Gamma_{\gamma\gamma}$  in the same plane as in the left-hand panel. Following the outlined argument, we assume here that the perturbative computation does not reproduce the correct Higgs mass because of the large trilinear couplings involved. Therefore, we fix the physical Higgs mass to 125 GeV in the computation of the branching ratio in order to obtain the correct decay kinematics in the entire plane. As expected, the di-Higgs decay rate is much larger than the diphoton decay rate in the regions where the binding energy due to Higgs exchange becomes large, i.e., in regions with large  $|X_t|$ . Interestingly, all of the parameter space which features a tachyonic Higgs, assuming standard perturbative calculations, has a ratio of the partial widths  $\Gamma_{hh}/\Gamma_{\gamma\gamma}$  larger than  $10^3$ . For regions where the binding energy reaches a percent of the bound state mass the partial width ratio is larger than  $10^4$ .

Let us now compare the results to the experiment. In Ref. [333], a search for resonant Higgs pair production in the  $b\bar{b}b\bar{b}$  final state was performed, setting limits of  $\sim 12$  fb at  $\sqrt{s} = 8$  TeV. Assuming gluon fusion for the production mechanism of the stoponium and taking the most conservative best-fit value for the necessary diphoton cross section at  $\sqrt{s} = 13$  TeV from Ref. [141], we arrive at the experimental bound  $\Gamma_{hh}/\Gamma_{\gamma\gamma} < 64$ .<sup>9</sup> This eliminates all of the parameter space where the stoponium has large binding energy, in clear contradiction to Ref. [323].

## Stoponium-Higgs mixing

Thus far, we have assumed that the 125 GeV Higgs is an elementary particle and solely a mixture of the MSSM fields  $H_u$  and  $H_d$ . We drop this assumption now in order to see if this would alter the conclusions of the previous sections. The situation becomes more complicated as soon as the stoponium mixes with the Higgs and takes part in electroweak symmetry breaking through the acquisition of a VEV. Although this situation is highly disfavored, given the almost perfect agreement of the Higgs signal strength and coupling measurements with the SM, let us assume for the sake of argument that this situation is possible. In this case, the stoponium is a new scalar degree of freedom in the theory, introducing a new direction in the scalar potential which is not calculable using perturbative methods. Such a scenario arises for very large values of  $|X_t/M_S|$  [335], corresponding to such a tightly bound state that a lattice calculation is the only reliable technique. Unfortunately, these calculations have not yet been

---

<sup>9</sup> Other reference values for the diphoton cross section (see, for instance, Ref. [334]) suggest even more constrained ratios of  $\Gamma_{hh}/\Gamma_{\gamma\gamma} < 42$ .

performed. However, for our purposes such precise predictions are not necessary as the rough order of magnitude of the relative partial decay widths into  $hh$  and  $\gamma\gamma$  will not be affected. In particular, the rate into a pair of light Higgs bosons would still be huge due to the necessarily large  $|X_t|$  values. A conservative estimate would be to parametrize the two scalar states at 125 and 750 GeV as  $\Phi_{125} = h \cos \phi + \sigma_{\tilde{t}} \sin \phi$  and  $\Phi_{750} = -h \sin \phi + \sigma_{\tilde{t}} \cos \phi$ . Projecting out only the  $\sigma_{\tilde{t}}$  production followed by the  $\sigma_{\tilde{t}} \rightarrow hh$  decay, the respective partial width roughly scales as  $\cos^6 \phi$ , leading to a suppression of  $\frac{1}{8}$  in the case of maximal mixing.<sup>10</sup> Even allowing for another order of magnitude uncertainty due to the now undetermined VEV structure cannot rescue the points with  $E_B/M_B > 10^{-2}$  from being experimentally excluded. As a result, the regions in parameter space which could potentially feature a stoponium condensate participating at EW symmetry breaking, i.e., those regions with binding energies of the order of the EW scale, are excluded by many orders of magnitude, far beyond any imaginable source of uncertainty for the ratio  $\Gamma_{hh}/\Gamma_{\gamma\gamma}$ .

The entire discussion has so far neglected the high-scale boundary conditions present in the CMSSM. We find that in regions of parameter space where  $|X_t/M_S| \gtrsim 15$ , which is the range where the critical coupling for EW symmetry breaking through stop condensates is reached [335], the lightest stau always becomes tachyonic.<sup>11</sup>

## The possible stoponium binding energy

We briefly summarize our discussion of the possible stoponium binding energy. Very large binding energies are immediately ruled out by the di-Higgs decay rate. Consequently, the maximal binding energy of a 750 GeV stoponium from pure Higgs exchange is less than 1%. Therefore, it is of the order of, or smaller than, the typical binding energy from perturbative QCD [332]. Such a QCD bound state, as has been discussed in Ref. [323], is insufficient to produce the required diphoton rate. Moreover, these small binding energies render the usual vacuum stability considerations, which involve much higher scales, fully consistent.

### 3.1.4 The CMSSM with a 375 GeV Stop

Even though this scenario is already highly disfavoured by a production rate which is too small, we nevertheless discuss the impact of vacuum stability constraints in more detail. The reason is that the calculation of the production cross section still includes uncertainties, potentially increasing the production cross section such that the resulting signal is consistent to within  $2\sigma$  of the observed excess. In addition, one might consider the case that there are other contributions to the diphoton rate in the CMSSM-like sbottomium in the large  $\tan \beta$  limit. Here, we aim to exclude light stoponium bound states within the CMSSM, independently of the diphoton cross section, leaving the results also applicable in the currently more realistic case that the diphoton excess turns out to be a statistical fluctuation, which we now

<sup>10</sup> This is a very conservative estimate as it only corresponds to the decay shown in the figure, neglecting all contributions from the  $h \rightarrow \sigma_{\tilde{t}}\sigma_{\tilde{t}}$  projection as well as the mixed projections.

<sup>11</sup> This assumes the standard renormalisation group equation evaluation, but is also rather robust against deviations in the SM Yukawa couplings, which could be caused by the stoponium-Higgs mixing.

know to be the case. Therefore, we perform a numerical analysis of the CMSSM in the remaining parameter space with  $M_B \simeq 2m_{\tilde{t}_1}$ , where, in contrast to Fig. 3.9, the standard calculations reproduce the observed Higgs mass and the vacuum should be sufficiently stable. The results we find also apply to the CMSSM parameter space with light stops in that ballpark which do not necessarily form bound states. For this purpose we use a SARAH [89–94] generated SPheno [104, 105] version to calculate the mass spectrum, including the full one-loop corrections to the stops and the dominant two-loop corrections to the Higgs states [97, 98]. To check the vacuum stability we use Vevacious [110]. Vevacious finds the global minimum of the one-loop corrected effective potential and calls CosmoTransitions to calculate the lifetime if necessary. For our checks we used Vevacious with the model files for the MSSM with real VEVs for the neutral Higgs doublets and the two stops which were also generated by SARAH.

In order to check if it is possible to have a 375 GeV stop in the CMSSM with the correct Higgs mass we perform a scan in the following ranges:

$$m_0 = [1, 3.5] \text{ TeV}, \quad M_{1/2} = [0.6, 1.0] \text{ TeV},$$

where we fix both  $\tan\beta = 15$  and  $\mu > 0$ .  $A_0$  is fit at each point to ensure a light stop at 375 GeV. For larger  $M_{1/2}$  values it is not possible to find points with the correct Higgs mass without going to even larger  $m_0$  values. However, if  $m_0$  is too large the performed fixed order calculation of the Higgs mass suffers from a large uncertainty. We therefore restrict ourselves to values within this range. It turns out that the lifetime of the EW vacuum quickly drops with increasing  $M_{1/2}$ ; i.e., this restriction does not affect the generality of our results. One also expects that the results are robust against changes of  $\tan\beta$ . However, for very large  $\tan\beta$  the vacuum stability issue becomes more severe, due to the possible appearance of stau and sbottom VEVs. The results are summarized in Fig. 3.4.

One can see that the entire region of the parameter space which is consistent with the Higgs mass measurements and accommodates a light stop has a metastable vacuum. In this range, the lifetime of the metastable vacuum is always very short on cosmological time scales. Moreover, the region with small  $M_{1/2}$  where the lifetime exceeds one second is in conflict with the current limits from gluino searches which exclude masses up to  $\sim 1.8$  TeV (see, e.g., Refs. [336, 337] for recent LHC Run-II results). Thus, even when assigning a generous theoretical error to the lifetime calculation, the conclusion does not change. Additionally for low  $M_{1/2}$ , one can see that the binding energy of the stoponium lies at most in the 100 MeV range; i.e., this effect cannot have an impact on the validity of the vacuum stability results. Finally, because of this small binding energy, the standard calculation of the cross section of stoponium production, followed by the decay to two photons, is also expected to be valid in the entire plane. This results in an insufficient diphoton cross section for the entire  $(m_0, M_{1/2})$  plane.

The results of the previous section show that both the binding energies and vacuum lifetimes for particular combinations of CMSSM parameters are small. Here we demonstrate that small binding energies are indeed a generic feature under the assumption of the CMSSM boundary conditions. Shown in Fig. 3.5 is the logarithm of the ratio  $E_B/2m_{\tilde{t}_1}$  as a function of  $A_0$  and  $m_0$  for fixed values of  $M_{1/2}$ . For each parameter point,  $(m_0, A_0)$ , the largest value of  $R = \log_{10}(E_B/2m_{\tilde{t}_1})$  is taken as  $\tan\beta$  is varied between the values (2, 60) including the

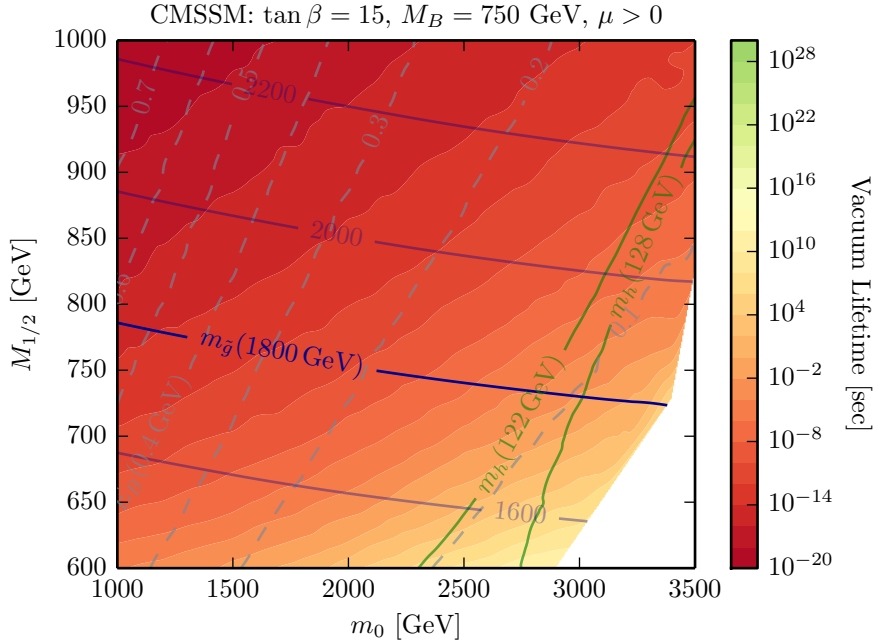


Figure 3.4: The lifetime of the EW vacuum in seconds (coloured contours) as calculated with the combination SPheno-Vevacious-CosmoTransitions. For comparison, the age of the universe is  $\sim 4.35 \times 10^{17}$  s. Between the two green contour lines, the Higgs mass lies in the range  $125 \pm 3$  GeV. The stoponium binding energy from Higgs exchange in GeV is shown as grey dashed contours, while the dark blue contours indicate the gluino mass in GeV. The line for  $m_{\tilde{g}} = 1800$  GeV is highlighted, as it roughly corresponds to the current lower experimental bound on the gluino mass.

following constraints: (i)  $m_{\tilde{\tau}_R}^2 > 0$ , (ii)  $m_{\tilde{t}_R}^2 > 0$ , (iii)  $m_{\tilde{t}_1} > 75$  GeV.<sup>12</sup> Regions where these conditions are not satisfied for any value of  $\tan \beta$  correspond to the hatched regions. The results of these show that the binding energy never exceeds 4% of the mass of the bound state. The reason is that large  $A_0$  values are required for sizeable binding energies. However, these large  $A_0$  values also enter the renormalisation group equations and split the stop-left and stop-right soft SUSY-breaking masses. This results in a reduced stop mixing angle. Finally large  $A_0$  values also lead to negative singlet soft masses for the staus and stops in the case of small  $M_{1/2}$ . In general, one can find for larger  $\tan \beta$  values larger binding energies because of a smaller mass splitting between  $m_{\tilde{\tau}_R}$  and  $m_{\tilde{b}_L}$ , i.e., larger stop mixing. However, at some points the staus become tachyonic and prevent a further increase of  $\tan \beta$ .

In Ref. [323], three benchmark points with a light stop were proposed, which are consistent with the Higgs mass and the dark matter relic density. For completeness, we use our numerical set-up to check the stability of these three points as well. The results are summarized in Table 3.1 and confirm the previous discussion.

We see that all three points have a global minimum where charge and colour are broken

<sup>12</sup> The value of 75 GeV is a rather arbitrary but very conservative choice. More realistic cuts of 175 GeV to circumvent search limits, or even 375 GeV, in order to have a bound state of around 750 GeV lead to an even smaller upper limit of  $R$ .

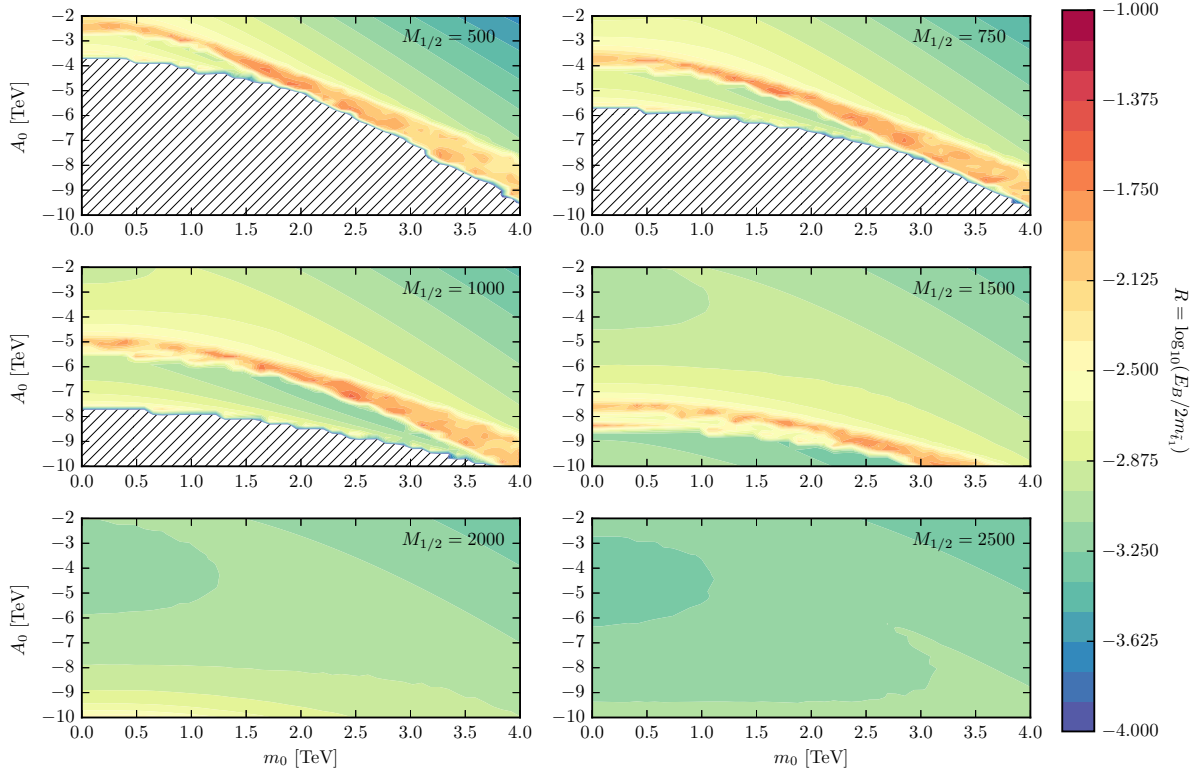


Figure 3.5: The logarithm of the ratio  $E_B/2m_{\tilde{t}_1}$  as a function of  $A_0$  and  $m_0$ , where  $\tan\beta$  is chosen point-wise to maximize the logarithm. Note that each panel represents a different choice of  $M_{1/2}$ . The hatched regions correspond to parameter space where the constraints  $m_{\tilde{\tau}_R}^2 > 0$ ,  $m_{\tilde{t}_R}^2 > 0$  and  $m_{\tilde{t}_1} > 0$  are not satisfied.

via stop VEVs in the TeV range. The depth of colour breaking minima is 5 to 6 orders of magnitude deeper than the EW vacuum. This also explains the very fast decay of the EW vacuum: all three points have a lifetime which is a tiny fraction of a second. Thus, one sees that the energy scales which are important in this calculation are several orders of magnitude above the binding energy of the stoponium. Moreover, the calculated tunnelling rate is so huge that not even the assumption of a large uncertainty on the coefficient  $A$  in Eq. (3.26) could possibly alter the above conclusion.

## 3.2 Vacuum Stability in the NMSSM

At first glance, the discovery of a SM-like Higgs boson with a mass of approximately 125 GeV [339, 340] appears to be a huge success of supersymmetry and in particular of the MSSM. In contrast to other ideas to extend the SM, supersymmetry predicts that the Higgs boson shouldn't be significantly heavier than the  $Z$ -boson if new physics is around the TeV scale, see e.g. Ref. [49] and references therein. Other avenues such as technicolor prefer the natural mass range for the Higgs to lie at scales well above the measured mass. On the other hand,

	BP1	BP2	BP3
$m_0$ [GeV]	2855	3199	3380
$M_{1/2}$ [GeV]	755	860	910
$\tan \beta$	15	15	15
$A_0$ [GeV]	$-6405^*$	$-7205^*$	$-7620^*$
$m_{\tilde{t}_1}$ [GeV]	375	425	444
$m_{\tilde{t}_2}$ [GeV]	2226	2495	2632
$m_{\tilde{g}}$ [GeV]	1837	2070	2181
$m_h$ [GeV]	122	122	122
$T_t$ [GeV]	$-2960$	$-3333$	$-3520$
$\Theta_{\tilde{t}}$	0.118	0.106	0.101
$E_B$ [GeV]	0.108	0.078	0.067
$V_{EW}$ [GeV <sup>4</sup> ]	$-9.8 \times 10^7$	$-9.8 \times 10^7$	$-9.7 \times 10^7$
$V_{CCB}$ [GeV <sup>4</sup> ]	$-3.7 \times 10^{12}$	$-6.4 \times 10^{12}$	$-8.2 \times 10^{12}$
$v_d, v_u$ [TeV]	0.9, 2.8	1.1, 3.2	1.2, 3.4
$v_{\tilde{t}_L}, v_{\tilde{t}_R}$ [TeV]	2.2, $-3.0$	$-2.7, -3.7$	2.7, 3.7
$\tau$ [s]	$2.6 \times 10^{-4}$	$5.9 \times 10^{-4}$	$3.9 \times 10^{-4}$

Table 3.1: The benchmark points proposed by Ref. [323].  $V_{EW}$  is the depth of the EW vacuum,  $V_{CCB}$  the depth of the global vacuum with the given Higgs and stop VEVs  $v_x$  (with  $x = d, u, \tilde{t}_L, \tilde{t}_R$ ).  $\tau$  is the life-time of the EW vacuum. Note: we slightly adjusted the input values of  $A_0$  in order to get the same stop masses as given in Ref. [323]. Since SPheno uses different matching conditions than Suspect [338] to calculate the top Yukawa coupling, the running stop mass parameters for the same input are slightly different. Since we had to *decrease*  $|A_0|$  compared to Ref. [323], the life-time using the original values would be even shorter.

closer investigation shows that the situation is more complicated in the MSSM as the Higgs mass requires large radiative corrections to be compatible with experimental data. The main source of these corrections are the superpartners of the top, the stops. In order to maximise their contributions to the Higgs mass, one needs to consider scenarios in which they are maximally mixed [106, 341–343]. This can be dangerous because it can lead to the presence of charge- and colour-breaking vacua whereby the stops receive VEVs [295, 317, 344, 345], as also discussed in the previous section. Since the tunnelling rate to these vacua is typically large, this results in tension between an acceptable Higgs mass and a sufficiently long-lived EW breaking vacuum. Consequently, supersymmetric models which can enhance the Higgs mass at tree-level are especially appealing. The simplest such extension is to add a scalar singlet, resulting in the next-to-minimal supersymmetric standard model (NMSSM), yielding  $F$ -term contributions, which raise the tree-level Higgs mass [346, 347]. This significantly reduces the need for large loop corrections. As a result, large stop mixing is no longer necessary. There-

fore, the vacuum stability problems of the MSSM are cured as well as reducing the EW fine-tuning [348–355]. However, the extended Higgs sector in the NMSSM introduces new couplings which can potentially destabilize the EW vacuum. The vacuum stability in the NMSSM has been studied in the past at tree-level [356–360], and also with one-loop corrections [361]. Potentially dangerous parameter ranges have been identified in these works. However, all these studies made the assumption that charge is conserved at the global minimum of the scalar potential, i.e. the charged Higgs boson VEVs were neglected. This was motivated to some extent as it has been shown that the global minimum of two-Higgs-doublet models, if they have a minimum with correct electroweak symmetry breaking, is always charge conserving at tree-level [298–300]. However, for non-vanishing singlet–doublet interactions this is no longer the case [362] and one must in principle always take these VEVs into account. The aim of this section is to discuss the impact of charged Higgs VEVs on the vacuum stability in the NMSSM. We begin in Sec. 3.2.1 with a discussion of the scalar potential, before we show the numerical results in Sec. 3.2.2.

### 3.2.1 Spontaneous Charge Breaking Minima in the NMSSM

We consider in the following the NMSSM with a  $\mathbb{Z}_3$  to forbid all dimensionful parameters in the superpotential, which reads

$$W_{\text{NMSSM}} = \lambda \hat{H}_u \hat{H}_d \hat{S} + \frac{1}{3} \kappa \hat{S}^3 + W_Y, \quad (3.30)$$

with the standard Yukawa interactions  $W_Y$  as in the MSSM, i.e. Eq. (3.1) without the Higgsino mass term. The additional soft-terms for the scalars in comparison to the MSSM are

$$-V_{\text{soft}} \supset \left( T_\lambda H_u H_d S + \frac{1}{3} T_\kappa S^3 + \text{h.c.} \right) + m_s^2 |S|^2, \quad (3.31)$$

where we have used the common parametrisation for the trilinear soft terms  $T_\lambda = A_\lambda \lambda$ ,  $T_\kappa = A_\kappa \kappa$ . Note, we assume in the following that all  $A$ -terms in the sfermion MSSM sector vanish or are sufficiently small such that they do not destabilise the scalar potential. After electroweak symmetry breaking, the scalar singlet  $S$  obtains a VEV  $v_S$  which generates an effective Higgsino mass term

$$\mu_{\text{eff}} = \frac{\lambda v_S}{\sqrt{2}}. \quad (3.32)$$

Using the three minimisation conditions of the potential, the Higgs sector in the NMSSM is specified at tree-level by six parameters:

$$\lambda, \quad \kappa, \quad A_\lambda, \quad A_\kappa, \quad \mu_{\text{eff}}, \quad \tan \beta, \quad (3.33)$$

where again  $\tan \beta = v_u/v_d$ , namely the ratio of the doublet VEVs.

However, we have so far neglected the possibility that charged Higgs bosons can acquire VEVs. In order to include this possibility, one needs to check for the global minimum of the

scalar potential resulting from the following VEVs:

$$\begin{pmatrix} \langle H_d^0 \rangle \\ \langle H_d^- \rangle \end{pmatrix} = \frac{1}{\sqrt{2}} \begin{pmatrix} v_d \\ v_m \end{pmatrix}, \quad \begin{pmatrix} \langle H_u^+ \rangle \\ \langle H_u^0 \rangle \end{pmatrix} = \frac{1}{\sqrt{2}} \begin{pmatrix} v_p \\ v_u \end{pmatrix}, \quad \langle S \rangle = \frac{v_S}{\sqrt{2}} \quad (3.34)$$

One can reduce this five-dimensional problem via an  $SU(2)$  gauge transformation to eliminate one of the charged Higgs VEVs. This turns out to be more robust for the numerical evaluation, but for the current discussion we keep the more intuitive form with all five VEVs.

The scalar potential of the Higgs sector in the NMSSM with these five VEVs consists of  $F$ -,  $D$ - and soft-terms

$$V_{\text{tree}} = V_F + V_D + V_{\text{soft}}, \quad (3.35)$$

with

$$\begin{aligned} V_F = \frac{1}{4} & \left( \lambda v_S^2 (\lambda (v_d^2 + v_m^2 + v_p^2 + v_u^2) + 2\kappa(v_m v_p - v_d v_u)) \right. \\ & \left. + \lambda^2 (v_m v_p - v_d v_u)^2 + \kappa^2 v_S^4 \right), \end{aligned} \quad (3.36)$$

$$\begin{aligned} V_D = \frac{1}{32} & \left( g_1^2 (v_d^2 + v_m^2 - v_p^2 - v_u^2)^2 + g_2^2 (v_d^4 + v_m^4 + 2v_d^2 (v_m^2 + v_p^2 - v_u^2) \right. \\ & \left. - 2v_m^2 (v_p^2 - v_u^2) + (v_p^2 + v_u^2)^2) \right), \end{aligned} \quad (3.37)$$

$$\begin{aligned} V_{\text{soft}} = \frac{1}{2} & \left( m_{H_d}^2 (v_d^2 + v_m^2) + m_{H_u}^2 (v_p^2 + v_u^2) + m_S^2 v_S^2 \right) \\ & + \frac{v_S}{6} \left( \sqrt{2} T_\kappa v_S^2 + 3\sqrt{2} T_\lambda (v_m v_p - v_d v_u) \right). \end{aligned} \quad (3.38)$$

In the above expressions we have already substituted in the VEVs using Eq. (3.34). In what follows we shall always use the equations which determine the stationary points with respect to  $v_u, v_d$  and  $v_S$  (while simultaneously setting  $v_m = v_p = 0$ ) to eliminate the soft SUSY-breaking masses  $m_{H_u}^2, m_{H_d}^2$  and  $m_s^2$  from the potential. In doing so we insist upon the existence of an appropriate electroweak vacuum through the introduction of the input parameters  $\mu_{\text{eff}}$ ,  $\tan \beta$  and the electroweak VEV  $v$ . These input parameters *only* fix the soft SUSY-breaking masses and *retain the same values* irrespective of the specific minimum under consideration. To emphasise, if one considers a generic minimum of the potential, these input parameters only enter in the scalar potential as a substitute for the soft SUSY-breaking masses while the free directions in field space,  $v_{u,d,p,m,S}$ , are varied to determine other minima of the theory. Consequently, all minima which we find in addition to the desired EW vacuum configuration occur simultaneously.

Before we continue, we can check if parameter points exist, for which the global minimum of the potential is charge breaking. In order to do so, we compute

$$\Delta V = V_{\text{tree}} - V_{\text{tree}} \Big|_{v_m=v_p=0}. \quad (3.39)$$

Together with the relation between  $A_\lambda$  and the charged Higgs mass  $m_{H^\pm}$

$$A_\lambda = \frac{\lambda t_\beta (4m_{H^\pm}^2 - v^2 (g_2^2 - 2\lambda^2)) - 4\kappa\mu_{\text{eff}}^2 (t_\beta^2 + 1)}{4\lambda\mu_{\text{eff}} (t_\beta^2 + 1)}, \quad (3.40)$$

where  $t_\beta = \tan \beta$ , we get in the limit  $t_\beta \rightarrow 1$ ,  $v_m \rightarrow 0$ <sup>13</sup>

$$\begin{aligned} \Delta V = \frac{1}{32} v_p^2 & \left[ g_2^2 (2v_d^2 - 2v^2 + v_p^2 + 2v_u^2) - 16\mu_{\text{eff}}^2 + 8\lambda^2 v_S^2 \right. \\ & \left. + g_1^2 (v_p^2 - 2v_d^2 + 2v_u^2) + 8m_{H^\pm}^2 \right]. \end{aligned} \quad (3.41)$$

Thus, one can see that for large  $\mu_{\text{eff}}$  it is possible to get very deep charge-breaking (CB) minima below those which are charge-conserving (CC).

We now seek to gain some additional insight into the behaviour of the potential and, in particular, regions where the CB minima are potentially dangerous. The most promising directions in field space to discover deep minima are those in which either the  $F$ - or  $D$ -terms vanish. Since we are in general interested in points with sizeable  $\lambda$  couplings in order to get a large enhancement for the Higgs mass, the most stabilising effect of the potential can be expected to come from the  $F$ -terms. It is actually not possible to find any  $F$ -flat directions which are charge conserving. However, in the charge-breaking case the  $F$ -terms vanish for

$$v_m = v_u, \quad v_p = v_d, \quad v_S = 0. \quad (3.42)$$

In this direction in VEV space the value of the potential is

$$V = \frac{1}{8} (v_d^2 + v_u^2) [4m_{H_d}^2 + 4m_{H_u}^2 + g_2^2 (v_d^2 + v_u^2)], \quad (3.43)$$

which can be related in the limit  $\tan \beta \rightarrow 1$  to the input parameters

$$V = \frac{1}{8} (v_d^2 + v_u^2) \left[ 8A_\lambda \mu_{\text{eff}} + g_2^2 (v_d^2 + v_u^2) + 8\mu_{\text{eff}}^2 \left( \frac{\kappa}{\lambda} - 1 \right) - 2\lambda^2 v^2 \right]. \quad (3.44)$$

Defining  $x^{\text{CB}} = \sqrt{v_d^2 + v_u^2 + v_m^2 + v_p^2}$ , we find that new minima develop in the direction  $v_u = v_m, v_d = v_p$  at the point

$$x_{\text{min}}^{\text{CB}} = \pm \frac{\sqrt{2} \sqrt{-4A_\lambda \lambda \mu_{\text{eff}} + 4\mu_{\text{eff}}^2 (\lambda - \kappa) + \lambda^3 v^2}}{g_2 \sqrt{\lambda}}, \quad (3.45)$$

at which the value of the potential is

$$V(x_{\text{min}}^{\text{CB}}) = - \frac{(-4A_\lambda \lambda \mu_{\text{eff}} + 4\mu_{\text{eff}}^2 (\lambda - \kappa) + \lambda^3 v^2)^2}{8g_2^2 \lambda^2}. \quad (3.46)$$

---

<sup>13</sup> Again, the choice  $v_m \rightarrow 0$  can always be made using a  $SU(2)$  gauge transformation.

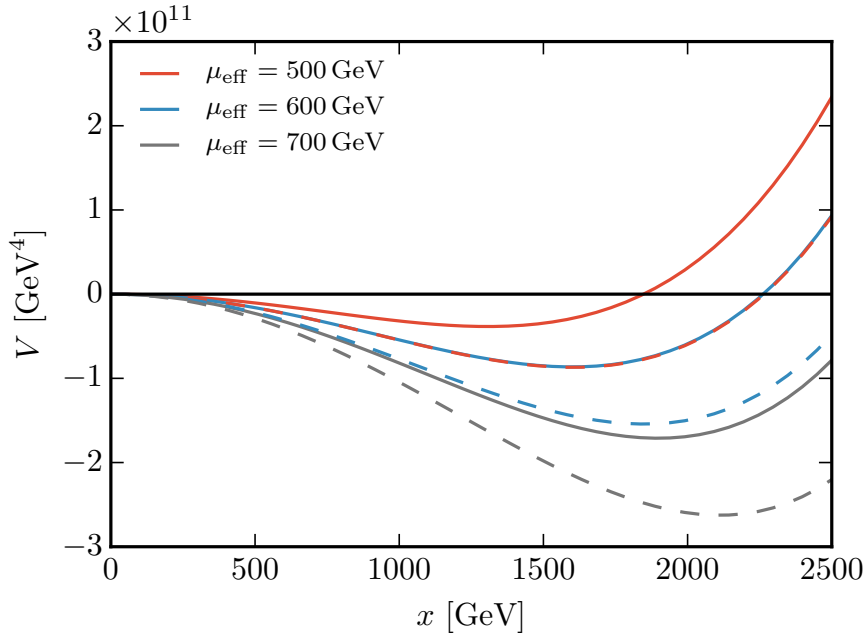


Figure 3.6: Value of the scalar potential in the direction of vanishing  $F$ -terms for three different values of  $\mu_{\text{eff}}$ . Here, we have chosen  $\kappa = \frac{1}{2}\lambda$ ,  $A_\lambda = 100$  as well as  $\lambda = -1$  (full lines) and  $\lambda = -2$  (dashed lines).

From these expressions one sees that the following conditions characterise the potentially dangerous regions in which CB minima might develop: (i) large  $|\lambda|$  and  $|\mu_{\text{eff}}|$ , (ii) either opposite signs for  $\lambda$  and  $\kappa$  or  $|\kappa/\lambda| < 1$  as well as (iii) opposite signs for  $A_\lambda$  and  $\mu_{\text{eff}}$ . Eq. (3.44) has to be combined with the condition that all Higgs masses are non-tachyonic at the electroweak vacuum. The condition to have a positive charged Higgs mass is

$$0 < \frac{1}{4}v^2 (g_2^2 - 2\lambda^2) + 2\frac{\kappa}{\lambda}\mu_{\text{eff}}^2 + 2\mu_{\text{eff}}A_\lambda, \quad (3.47)$$

which for large  $\mu_{\text{eff}}^2$ , prefers  $\lambda$  and  $\kappa$  of same signs and also either equal signs for  $A_\lambda$  and  $\mu_{\text{eff}}$  or small  $A_\lambda$  compared to  $\mu_{\text{eff}}$ . From the positivity condition on the pseudo-scalar masses one can further see that opposite signs for  $A_\kappa$  and  $\mu_{\text{eff}}$  are preferable. Therefore, combined with Eq. (3.44), we see that CB minima are likely to occur if:

- $|\lambda|$  and  $|\mu_{\text{eff}}|$  are large
- $|\kappa/\lambda| < 1$  with  $\text{sign}(\kappa) = \text{sign}(\lambda)$
- $|A_\lambda/\mu_{\text{eff}}| < 1$
- $\text{sign}(A_\kappa) = -\text{sign}(\mu_{\text{eff}})$

It is important to note that in these regions, the mostly singlet-like scalar is heavy, therefore the SM-like Higgs is always the lightest CP-even scalar state.

In Fig. 3.6, we show the behaviour of the potential in the direction  $x = \sqrt{v_d^2 + v_u^2 + v_m^2 + v_p^2}$

for different values of  $\mu_{\text{eff}}$ . We see in these examples that the minima are in the multi-TeV range and move quickly to larger values with increasing  $\mu_{\text{eff}}$ . Thus, it needs to be checked how efficient the tunnelling to these minima is. In addition, one also needs to compare the tunnelling to these minima with the tunnelling to potential CC minima which don't coincide with the electroweak breaking vacuum.

One important VEV direction in this context is the one with

$$v_u = v_m = v_p = v_S = 0, \quad v_d \equiv x^{\text{CC}} \neq 0, \quad (3.48)$$

in which the potential is given by

$$V = \frac{v_d^2}{2} \left[ A_\lambda \mu_{\text{eff}} + \frac{v_d^2}{16} (g_1^2 + g_2^2) + \mu_{\text{eff}}^2 \left( \frac{\kappa}{\lambda} - 1 \right) - \frac{1}{4} \lambda^2 v^2 \right]. \quad (3.49)$$

In this direction, new minima appear at

$$x_{\text{min}}^{\text{CC}} = \pm \frac{\sqrt{2} \sqrt{-4A_\lambda \lambda \mu_{\text{eff}} + 4(\lambda - \kappa) \mu_{\text{eff}}^2 + \lambda^3 v^2}}{\sqrt{(g_1^2 + g_2^2) \lambda}}, \quad (3.50)$$

at which the depth of the potential is

$$V(x_{\text{min}}^{\text{CC}}) = - \frac{(-4A_\lambda \lambda \mu_{\text{eff}} + 4\mu_{\text{eff}}^2 (\lambda - \kappa) + \lambda^3 v^2)^2}{8\lambda^2 (g_1^2 + g_2^2)}. \quad (3.51)$$

The second derivatives of the scalar potential in both the CB and the CC but non-EW cases are given by

$$\left. \frac{\partial^2 V^{\text{CB/CC}}}{\partial x^2} \right|_{x=x^{\text{CB/CC}}} = 2\mu_{\text{eff}}^2 \left( 1 - \frac{\kappa}{\lambda} \right) + \frac{v^2 \lambda^2}{2} - 2A_\lambda \mu_{\text{eff}}, \quad (3.52)$$

which, given the above conditions on the parameters, always turns out to be positive, ensuring that the configurations we consider here indeed correspond to minima of the potential.

Thus, we find that the conditions to develop additional charge conserving and charge breaking minima in addition to the one with the correct EWSB are very similar and both kind of minima can appear simultaneously for given input values. Comparing Eqs. (3.45-3.46) with Eqs. (3.50-3.51), we find that the CB minima are deeper than the CC ones by a factor  $(g_1^2 + g_2^2)/g_2^2$ . At the same time, the CB minimum is further away in field space by a factor  $\sqrt{g_1^2 + g_2^2}/g_2$ . A one-dimensional comparison between the behaviour of the potential in this direction and in the direction defined via Eq. (3.42) is shown in Fig. 3.7. As a result, we observe in typical regions of parameter space that CB and CC minima occur at the same time and, both are usually deeper than the correct electroweak vacuum. Furthermore, the behaviour indicated in Eqs. (3.45-3.46) and (3.50-3.51) can be seen from Fig. 3.7 where the CB minimum is deeper than the non-EW but CC as expected. However, the latter appears at slightly smaller  $x$  values. Consequently, it is not a priori clear to which minimum the electroweak state would tunnel to more effectively – to the deeper one or the nearer one – as the field space is highly non-trivial. In these cases, one needs to calculate the tunnelling rate to the different

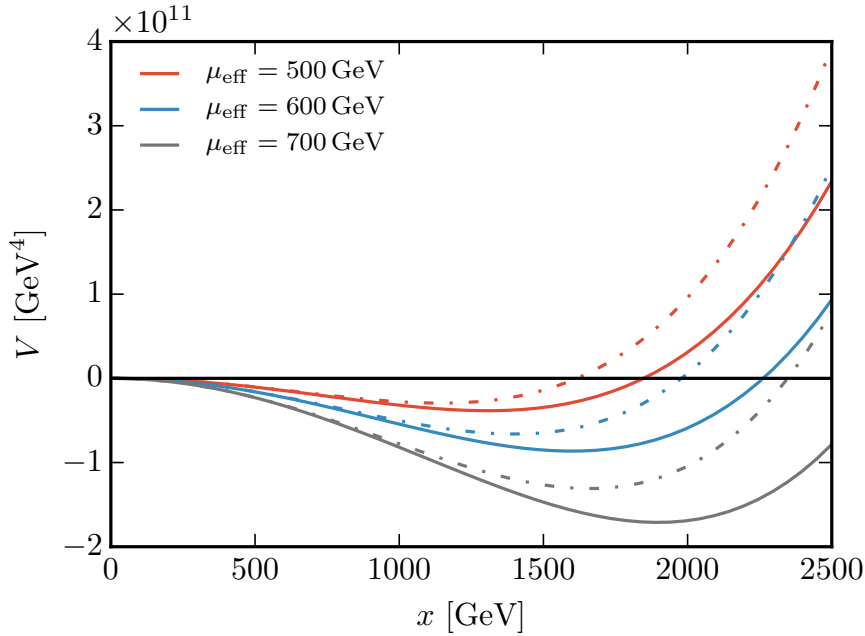


Figure 3.7: Comparison of the potential in the charge conserving (dash-dotted) and charge-breaking direction (full) defined by Eqs. (3.42) respectively (3.48). The same parameter choices as in Fig. 3.6 were made and we show here the case  $\lambda = -1$ .

minima in order to be able to judge if the inclusion of charged Higgs VEVs yields additional constraints. However, an analytical discussion of all these cases doesn't give further insights. We therefore turn directly to the numerical results.

### 3.2.2 Numerical Results

As we have seen so far, one can find new vacua in the NMSSM when including the possibility of spontaneous charge breaking. However, it needs to be clarified how important the study of these minima is. Therefore, we are going to make a numerical analysis not only of the tree-level potential but also of the one-loop effective potential with and without the consideration of charge-breaking VEVs. For doing that, we use `Vevacious` [110] for which we have generated model files with `SARAH` [89–94]. We also used `SARAH` to generate a `SPheno` module [104, 105] for the NMSSM. With this module we calculate the SUSY and Higgs masses including NMSSM-specific two-loop corrections [97–99] which are important in particular for large  $|\lambda|$  [100, 363]. Consequently, the accuracy in the Higgs mass prediction is similar to the MSSM and we use 3 GeV for the theoretical uncertainty in the following. The spectrum file generated by `SPheno` is passed to `HiggsBounds` [107, 112] and is also used as input for `Vevacious`. `Vevacious` finds all solutions to the tree-level tadpole equations by using a homotopy continuation implemented in the code `HOM4PS2` [364]. These extrema are used as the starting points to find the minima of the one-loop effective potential using `minuit` [365]. If it finds deeper minima than the EW one, `Vevacious` calls `CosmoTransitions` [111] to determ-

ine the tunnelling rate. However, in the standard `Vevacious` package, the calculation for the tunnelling rate is not done for all minima, but only for the so called ‘panic’ vacuum. This is the one closest to the EW minimum in field space. We have modified `Vevacious` to calculate the tunnelling rate to all minima in order to be able to compare the different sets of vacua. We are going to distinguish two cases in the following: (i) cases in which only CB minima exist which are deeper than the EW one; (ii) cases in which both deeper CB and CC minima exist. The results that we show below are particular points of interest obtained by scans over the parameter space:

- $\tan \beta \in [1, 4]$
- $\lambda \in [-2, 2]$
- $\kappa \in [-2, 2]$
- $A_\lambda \in [-5, 5]$  TeV
- $A_\kappa \in [-5, 5]$  TeV
- $\mu_{\text{eff}} \in [-2, 2]$  TeV

Also note that in the following numerical examples, we will minimise the impact of the stop- and sbottom-sector on both Higgs mass and vacuum stability by assuming negligible trilinear couplings.

### Charge-breaking minima only

Although it is not reflected in the analytical example discussed in Sec. 3.2.1, there also exist parameter points for which the EW minimum is only metastable once the possibility of charge breaking is included. Without the consideration of charged-Higgs-VEVs, the wrong impression of a stable EW minimum would be obtained. An example is shown in Fig. 3.8 where the blue region features a global CB minimum while the next-deepest minimum is the desired EW one. In the green region, the EW vacuum is stable whereas in the yellow region, other CC minima corresponding to Eq. (3.48) are also deeper than the desired EW one. In this figure, no parameter point which predicts the correct Higgs mass features a stable vacuum once the CB direction is taken into account. As a side remark we note that one can also see in this example that loop corrections to the scalar potential can be important when discussing the vacuum stability: if one would not have included charged Higgs VEVs, the conclusion whether stable regions in agreement the Higgs mass measurement exist would have changed from tree- to loop-level.

When checking all cases which we found in our scans, there were no points featuring only CB minima deeper than the desired EW one which turned out to be short-lived on cosmological time scales. All points had a life-time which was many orders of magnitude longer than the life-time of the universe. We therefore conclude that such points are phenomenologically viable, albeit significantly less appealing compared with regions where the vacuum is entirely stable.

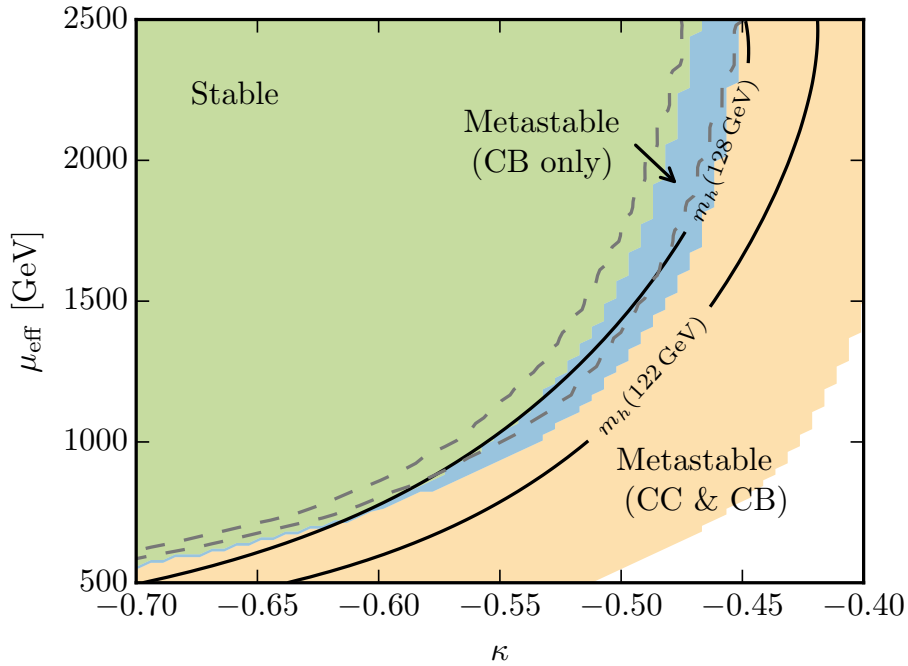


Figure 3.8: Stability of the EW vacuum considering the full one-loop effective potential. Regions shaded in green are stable, indicating that the desired electroweak breaking minimum is the global minimum. The yellow and blue regions correspond to metastability of the desired electroweak breaking minimum. In particular, the blue region contains only CB minima that are deeper, while the yellow regions contains both CB and CC minima. The dashed-grey contours show the equivalent of the blue CB metastable region assuming only a tree-level potential. Finally, the region between the black solid contours corresponds to an acceptable Higgs mass, namely  $m_h \in [122, 128]$  GeV. Here we have chosen  $\lambda = -0.68$ ,  $\tan \beta = 1.02$ ,  $A_\kappa = -700$  GeV and  $A_\lambda = -300$  GeV.

### Charge-breaking and charge-conserving minima

This part aims to answer the question whether or not CB minima can further destabilise already metastable regions of parameter space, reducing the EW vacuum to be dangerously short-lived on cosmological time scales. As discussed before, this is not the case in regions where only CB minima are deeper than the EW minimum, which is why we turn to regions where also other CC minima are deeper. Indeed we find many regions of parameter space where the CB vacuum configuration corresponds to the global minimum, with potential values up to  $\mathcal{O}(30\%)$  deeper compared to the next deepest CC minimum, in accordance with the discussion in section 3.2.1. However, as already seen in Fig. 3.7, other non-EW CC vacua are nearer to the EW vacuum configuration in field space, which means that the tunnelling path is reduced compared to the tunnelling to the global, CB minimum. In practice, it turns out that this effect is more important than the relative depth of the minima. Although the global minimum is often CB, we find that the tunnelling-time to the slightly nearer shallower CC configuration of Eq. (3.48) is either shorter or of comparable size in the regions where the

lifetime of the vacuum is comparable to the lifetime of the Universe.<sup>14</sup> Furthermore, we find that in those few cases where the tunnelling to the CB minimum indeed results in a shorter lifetime, the differences are typically small. This behaviour is shown Fig. 3.9. The background colours depict the ratio of the lifetimes when considering both CC and CB minima (denoted as  $\tau_{4\text{-VEV}}$ ) versus when considering only CC minima ( $\tau_{3\text{-VEV}}$ ). Purple ( $\tau_{4\text{-VEV}}/\tau_{3\text{-VEV}} \simeq 1$ )

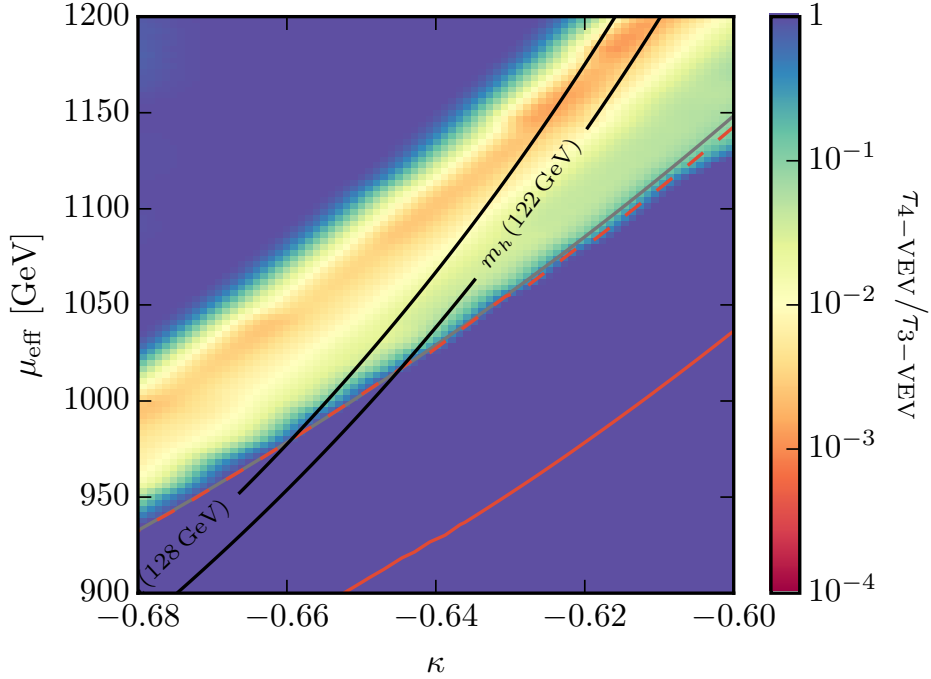


Figure 3.9: Ratio of the lifetimes  $\tau_{4\text{-VEV}}$  and  $\tau_{3\text{-VEV}}$ . Here,  $\tau_{4\text{-VEV}}$  and  $\tau_{3\text{-VEV}}$  are the lifetimes for the most unstable minima of the respective systems. The regions above the red (both solid and dashed) and grey lines correspond to at least 99% survival probabilities of the DSB vacuum. The dashed red and solid grey contours correspond to the most unstable minima of the 3 and 4 VEV systems respectively. The solid red contour corresponds to the stability of the panic vacuum (the minimum closest in field space to the DSB vacuum) in the 3 VEV system. Once again the the region between the black solid contours corresponds to an acceptable Higgs mass,  $m_h \in [122, 128]$  GeV. Here we use  $\lambda = -0.81$ ,  $\tan \beta = 1.02$ ,  $A_\kappa = -1400$  GeV and  $A_\lambda = -580$  GeV.

correspond to regions where the tunnelling rate of the EW vacuum is unchanged when also considering the charged-Higgs VEVs. Deviations from the purple background colour indicate that including the charged-Higgs direction leads to a more effective tunnelling than only considering the neutral Higgs directions. Regions above and to the left of the red dashed and grey lines correspond to parameter space where the vacuum is sufficiently long-lived for the 3- and 4-VEV systems respectively. Here, we have used a 99% survival probability to calculate these lines. To emphasise regions in this plane below the dashed red and grey lines corres-

<sup>14</sup> Note that one can not generalise the statement that tunnelling to the nearer minimum is more effective: if we were to always consider the nearest minimum to the EW one, we would often underestimate the actual tunnelling rates by several orders of magnitude, as is also reflected in the numerical example shown in Fig. 3.9.

pond to model points where the EW vacuum lifetime is too small such that the probability of the EW vacuum surviving as long as the age of the universe is below 99%.

Note that we see a slight difference between the grey and red-dashed lines in the upper right part of the figure. This is where the tunnelling to the CB minimum is more efficient than the tunnelling to the CC one. The area which the two lines enclose is, however, very small. Therefore the inclusion of the charged-Higgs direction in the vacuum stability calculation results in only a tiny strip of parameter space where the EW vacuum lifetime *decreases* below the 99% survival probability threshold. In contrast, other regions of parameter space (red regions in Fig. 3.9) show significant changes when including the charged Higgs direction. However, the charged Higgs direction does not decrease the EW vacuum lifetime below the survival probability threshold and is therefore, on phenomenological grounds, uninteresting. Finally, the red solid line depicts the instability bound we would arrive at if we considered only the panic vacuum, i.e. the minimum nearest to the EW one in field space. It is therefore evident that a naïve check for the vacuum stability can severely underestimate the excluded parameter ranges.

In the parameter space scanned, we find that although the global minimum of an NMSSM parameter point can feature a global minimum where the charged Higgs develops a VEV, it is not necessary to check for this extra field direction as the constraints on the model parameters remain approximately unchanged if one ensures that the tunnelling rate to all possible minima are calculated.

### 3.3 Conclusion

In this chapter we have considered two very particular scenarios in minimal supersymmetric models investigating the effect of vacuum stability. In the first scenario we have reviewed an explanation of the diphoton excess via stop bound states in the CMSSM, as proposed in Ref. [323]. Stops in the CMSSM with masses of 375 GeV cause charge and colour breaking minima. This is necessarily the case when the constraints from the Higgs mass measurement are included. This arises as such a 125 GeV Higgs mass requires large mass splitting between the stops, which can only arise from dangerously large soft-breaking trilinear couplings of the stops. We have summarized results in the literature which find that the lower limit on the stop mass in the CMSSM is about 800 GeV if one requires the electroweak vacuum to be the global minimum. These limits are certainly weaker if the possibility of a metastable but long-lived electroweak minimum is considered. These conclusions are not affected by the appearance of bound state effects because the binding energy in the experimentally allowed parameter region is very small compared to the other relevant scales in the calculation. In addition, due to this small binding energy, the cross section to produce the diphoton signal is too small. The *ad hoc* assumption of large binding energies which makes the calculation of the Higgs mass, as well as the checks for the vacuum stability more difficult is also ruled out by the much too large decay rate of the stoponium into a pair of Higgs bosons.

Taking all these effects into account, it is not possible to explain the diphoton signal in the CMSSM. At the time of the original publication it was unclear whether the general MSSM would survive, given the existence of the diphoton excess. There was the claim that it might

be possible to obtain a sufficient diphoton cross section in fine-tuned parameter regions of the MSSM with a large  $\mu$  term [366]. However, this possibility also lacked a concrete proof of existence since so far no valid parameter regions consistent with the constraints from vacuum stability were presented.

In the second scenario we considered the possibility of spontaneous charge breaking in the NMSSM via VEVs of the charged Higgs components. We found that in contrast to models without singlets it is possible that charge is broken at the global minimum of the potential. We could identify two different kinds of parameter regions. First, regions in which all vacua deeper than the EW minimum have broken electric charge. These points would give the wrong impression of a stable EW vacuum if charged Higgs VEVs were not included in the study. However, in all examples we found for these scenarios, the life-time of the EW vacuum is sufficiently long on cosmological time-scales. The second possibility is that charge-breaking and -conserving minima beside the EW one are present at the same time. Here, the charge-breaking minima could be significantly deeper than the charge-conserving ones. However, we found that the parameter regions which are excluded due to an increased tunnelling rate to these deeper vacuum states are hardly affected when considering the extra charged Higgs field direction. Thus, the inclusion of charge-breaking minima doesn't drastically change the conclusion of a 'long-lived' vacuum to a 'short-lived' one. All in all, despite the presence of deep charge-breaking minima in the NMSSM, their phenomenological impact is rather limited. However, we want to stress that the usual practice of checking only the tunnelling rate to the deeper minimum nearest to the EW vacuum is insufficient for obtaining reliable bounds on the NMSSM parameter space.

## Chapter 4

# Lepton Flavour Violation in Left-Right Symmetric Models

---

Massive neutrinos are clearly a requirement of any extension of the SM. The most economical extension that achieves this goal is the addition of at least two generations of right-handed neutrinos  $\nu_{R_j}$  that are singlets under the gauge symmetries of the SM. However, this is a purely phenomenological argument for extending the SM field content. An appealing theoretical motivation for including this singlet arises from grand unified theories (GUTs). Assuming an SO(10) GUT allows for an entire generation of SM matter fields to reside in the 16-dimensional spinor SO(10) representation [83]. Interestingly the decomposition of this spinor representation under the SM gauge symmetries results in exactly the required components in addition to a SM gauge singlet which can be identified as the right-handed neutrino. There are two main avenues for breaking SO(10) to the SM gauge symmetries [367]. The first proceeds via SU(5)

$$\text{SO}(10) \xrightarrow{M_{\text{GUT}}} \text{SU}(5) (\times \text{U}(1)_X) , \quad (\text{flipped}) \text{SU}(5) , \quad (4.1)$$

while the second possibility, via a left-right symmetric phase will be the focus of the following chapters. This breaking chain is:

$$\text{SO}(10) \xrightarrow{M_{\text{GUT}}} \text{SU}(4)_C \times \text{SU}(2)_L \times \text{SU}(2)_R \quad \text{Pati-Salam} \quad (4.2)$$

$$\xrightarrow{M_{\text{PS}}} \text{SU}(3)_C \times \text{SU}(2)_L \times \text{SU}(2)_R \times \text{U}(1)_{B-L} \quad \text{left-right symmetric} \quad (4.3)$$

$$\xrightarrow{M_R} \text{SU}(3)_C \times \text{SU}(2)_L \times \text{U}(1)_R \times \text{U}(1)_{B-L} \quad \text{U}(1)_R\text{-left-right} \quad (4.4)$$

In the above expressions the scales at which the symmetries are broken are free parameters, with the exception of the GUT scale  $M_{\text{GUT}}$ . They are however, constrained by the requirement that the gauge couplings unify at  $M_{\text{GUT}}$ . Here, we observe that the second possibility opens up a wide range of possibilities for intermediate scales all of which can be broken either directly to the SM gauge symmetries or via additional steps in this chain. In this chapter we are interested in the left-right (LR) symmetric phase that arises from the breaking of SO(10) via the maximal subgroup called the Pati-Salam phase [368]. A further attractive feature of

models containing a LR symmetric phase is parity restoration which occurs in conjunction with the discrete symmetries of the theory [369].

The scale where this LR symmetric phase is broken could be anywhere between the TeV and GUT scale. In Ref. [87], under the assumption of a minimal model, it was shown that requiring gauge coupling unification (GCU) places a lower bound on the breaking of the LR phase of approximately  $10^{10}$  GeV. In this same work the authors categorise all possible extensions of the particle content of these minimal models consistent with  $SO(10)$  unification which can have breaking scales down to  $\mathcal{O}(\text{TeV})$ , see also Ref. [370].<sup>1</sup> Adding additional field content is not the only way out. For instance it was shown that this problem can be solved if discrete LR parity is broken at a higher scale [376, 377]. Here, we take a bottom-up approach insisting on a TeV-scale realisation of this LR symmetric phase ignoring the issue of GCU. As we will see this is well motivated as we are interested in the low-energy phenomenology. Our results will therefore remain as general as possible. In Chapter 5 we will return to the issue of building complete GUT compatible models.

Models featuring these LR symmetric gauge symmetries automatically contain the correct ingredients to explain the observed neutrino masses and mixings. Not only is the right-handed neutrino field  $\nu_R$  required to build  $SU(2)_R$  doublets and hence gauge invariant operators, but the breaking of the LR symmetry by  $SU(2)_R$  triplets generates a Majorana mass term for the  $\nu_R$  fields and thus a see-saw mechanism [75–79]. However, in a LR symmetric model one would also expect that the Higgs sector respects the LR symmetry particle-wise. This implies that there should be a one-to-one correspondence between the additional Higgs bosons charged under  $SU(2)_L$  and  $SU(2)_R$ , respectively. In the simplest model with Majorana mass terms for the neutrinos one requires that the electroweak breaking Higgses form doublets under both  $SU(2)$  factors, referred to as a bi-doublet. In addition one must also introduce  $SU(2)_L$  triplets to go along with the  $SU(2)_R$  triplets that break  $SU(2)_R \times U(1)_{B-L}$  [378]. The introduction of these triplets leads to a combination of see-saw type I and type II and induces lepton flavour violating (LFV) decays at tree-level [379]. LFV decays are already heavily constrained by existing data, for example  $\text{BR}(\mu \rightarrow 3e) \leq 10^{-12}$  [380] which will be further constrained by upcoming experiments like Mu3e [381]. If the new scalar particles are at the TeV scale, one can therefore expect measurable rates in the near future. In Table 4.1 we give an overview of the relevant LFV observables and their current bounds as well as expected future sensitivities.

Many variants of left-right symmetric models with a TeV-scale breaking in have been considered in the past. The following aspects have been previously investigated:

- lepton flavour and lepton number violation [378, 382–387]
- CP violation [388]
- bounds on the heavy additional vector bosons [371, 389–391]
- potential Higgs signals at the LHC [392–395]
- lepton flavour and number violating signals at the LHC [387, 396–399].

---

<sup>1</sup> In many supersymmetric realizations, a TeV-scale LR symmetry is even preferred from both vacuum stability considerations [371], and GCU [372, 373]. There also exists an intimate connection between the LR- and supersymmetry-breaking scales [374, 375].

Beside the constraints due to LFV processes further constraints arise from observables in the  $K$ - and  $B$ -meson sector, see e.g. [400, 401] for recent updates. These observables lead to stringent constraints when the model is invariant under discrete parity or charge-conjugation due to a direct correspondence between the left and right CKM matrices. Ref. [401] also considers direct LHC searches for new states leading to a bound of 2.9 TeV on the mass of the  $W_R$  [402, 403], which is the charged gauge boson arising from the  $SU(2)_R$  gauge symmetry. Note, however, that such bounds are model dependent and can be weaker if additional decay channels of the  $W_R$  and/or  $\nu_R$  are present as discussed e.g. in Ref. [371]. In addition, the  $\rho$  parameter [404, 405], or more generally the oblique parameters [406, 407], constrain the vacuum expectation value (VEV) of the  $SU(2)_L$  scalar triplet to be no larger than approximately 1 GeV [408–411]. Note that in the majority of these works only parts of a complete model have been considered, e.g. only the lepton sector or the Higgs sector. Features of these specific sectors were then investigated without checking whether the other parts are consistently implemented.

In this chapter we discuss the minimal model which is particle-wise LR symmetric and where the different scales of the  $SU(2)_L$  and  $SU(2)_R$  breaking occur dynamically. We will assume true LR-symmetry in the Yukawa sector of the model where parity restoration is implemented via discrete parity symmetry or charge conjugation. As a result of these discrete symmetries, it is possible to parametrise the triplet Yukawa couplings as a function of only the underlying model parameters and the measured neutrino data [412]. Here we expand upon this method and show how a simple analytic expression for the solution can be obtained. The existing data on lepton masses and mixing is not sufficient to uniquely specify these couplings even in this restricted context. Consequently we will discuss how LFV decays further constrain these couplings. However, the results depend on the details of the Higgs sector, in particular on the value of the masses of the heavier Higgs bosons as well as on  $v_L$ , the vacuum expectation values of the  $SU(2)_L$  triplet  $\Delta_L$ .

We begin in Section 4.1 by presenting the complete details of the considered model. In Section 4.2 we discuss particularities in the neutrino sector. Here we focus on our method of parametrising the Yukawa couplings. We stress that this section is crucial for understanding the subsequent parts of this chapter. In Section 4.3 we present our numerical results. Here we begin by discussing in detail the different contributions to the numerous LFV observables and their behaviour as a function of the free parameters. The main results are located in Section 4.3.2. This is where we show the complementarity of the different LFV observables as a function of the key model parameters.

## 4.1 The Minimal Left-Right Symmetric Model

We consider the minimal phenomenologically acceptable model with left-right (LR) symmetry at the Lagrangian level. This means that, in addition to promoting  $SU(2)_L$ -singlet fields to  $SU(2)_R$  multiplets, there has to be an additional sector which breaks  $SU(2)_R \times U(1)_{B-L} \rightarrow U(1)_Y$ . The most economical choice for the LR breaking which also at the same time leads to neutrino mass generation via a see-saw mechanism is  $SU(2)$  triplets.

LFV Process	Present Bound	Future Sensitivity
$\mu \rightarrow e\gamma$	$4.2 \times 10^{-13}$ [413]	$6 \times 10^{-14}$ [414]
$\tau \rightarrow e\gamma$	$3.3 \times 10^{-8}$ [415]	$\sim 3 \times 10^{-9}$ [416]
$\tau \rightarrow \mu\gamma$	$4.4 \times 10^{-8}$ [415]	$\sim 10^{-9}$ [416]
$\mu \rightarrow eee$	$1.0 \times 10^{-12}$ [380]	$\sim 3 \times 10^{-16}$ [381]
$\tau \rightarrow eee$	$2.7 \times 10^{-8}$ [417]	$\sim 5 \times 10^{-10}$ [416, 418]
$\tau \rightarrow \mu\mu\mu$	$2.1 \times 10^{-8}$ [417]	$\sim 4 \times 10^{-10}$ [416, 418]
$\tau^- \rightarrow e^- \mu^+ \mu^-$	$2.7 \times 10^{-8}$ [417]	$\sim 5 \times 10^{-10}$ [416, 418]
$\tau^- \rightarrow \mu^- e^+ e^-$	$1.8 \times 10^{-8}$ [417]	$\sim 3 \times 10^{-10}$ [416, 418]
$\tau^- \rightarrow \mu^+ e^- e^-$	$1.5 \times 10^{-8}$ [417]	$\sim 3 \times 10^{-10}$ [418]
$\tau^- \rightarrow e^+ \mu^- \mu^-$	$1.7 \times 10^{-8}$ [417]	$\sim 3 \times 10^{-10}$ [418]
$\mu^- \rightarrow e^-, \text{Ti}$	$4.3 \times 10^{-12}$ [419]	$\sim 10^{-18}$ [420, 421]
$\mu^- \rightarrow e^-, \text{Au}$	$7 \times 10^{-13}$ [422]	-
$\mu^- \rightarrow e^-, \text{Al}$	-	$10^{-16} - 3 \times 10^{-17}$ [423–425]
$\mu^- \rightarrow e^-, \text{SiC}$	-	$10^{-14}$ [426]

Table 4.1: Current experimental bounds and future sensitivities for low-energy LFV observables.

### 4.1.1 Model Definition

The minimal particle content of the model as well as their respective irreducible representations, using the notation  $(\text{SU}(3)_c, \text{SU}(2)_L, \text{SU}(2)_R, \text{U}(1)_{B-L})$ , are given by:

Fermions:

$$Q_L = \begin{pmatrix} u_L \\ d_L \end{pmatrix} \in (\mathbf{3}, \mathbf{2}, \mathbf{1}, 1/3), \quad Q_R = \begin{pmatrix} u_R \\ d_R \end{pmatrix} \in (\mathbf{3}, \mathbf{1}, \mathbf{2}, 1/3), \quad (4.5a)$$

$$L_L = \begin{pmatrix} \nu_L \\ \ell_L \end{pmatrix} \in (\mathbf{1}, \mathbf{2}, \mathbf{1}, -1), \quad L_R = \begin{pmatrix} \nu_R \\ \ell_R \end{pmatrix} \in (\mathbf{1}, \mathbf{1}, \mathbf{2}, -1). \quad (4.5b)$$

Scalars:

$$\Phi = \begin{pmatrix} \phi_1^0 & \phi_1^+ \\ \phi_2^- & \phi_2^0 \end{pmatrix} \in (\mathbf{1}, \mathbf{2}, \mathbf{2}, 0), \quad (4.5c)$$

$$\Delta_L = \begin{pmatrix} \frac{\delta_L^+}{\sqrt{2}} & \delta_L^{++} \\ \delta_L^0 & -\frac{\delta_L^+}{\sqrt{2}} \end{pmatrix} \in (\mathbf{1}, \mathbf{3}, \mathbf{1}, 2), \quad \Delta_R = \begin{pmatrix} \frac{\delta_R^+}{\sqrt{2}} & \delta_R^{++} \\ \delta_R^0 & -\frac{\delta_R^+}{\sqrt{2}} \end{pmatrix} \in (\mathbf{1}, \mathbf{1}, \mathbf{3}, 2). \quad (4.5d)$$

Here we use the convention that the electric charge is given by

$$Q_{\text{em}} = T_{3L} + T_{3R} + \frac{B-L}{2}. \quad (4.6)$$

The Yukawa interactions can be split into interactions of the quark and lepton fields with the bi-doublet,  $\mathcal{L}_Y^\Phi$ , leading to Dirac-type masses for all fermions after electroweak symmetry

breaking, as well as interactions with the triplets,  $\mathcal{L}_Y^\Delta$ , leading to Majorana-type mass terms for the neutrinos after LR-symmetry-breaking. The respective terms are

$$-\mathcal{L}_Y^\Phi = \overline{Q}_L \left( Y_{Q_1} \Phi + Y_{Q_2} \tilde{\Phi} \right) Q_R + \overline{L}_L \left( Y_{L_1} \Phi + Y_{L_2} \tilde{\Phi} \right) L_R + \text{h.c.}, \quad (4.7)$$

where  $\tilde{\Phi} \equiv -\sigma_2 \Phi^* \sigma_2$ . For the interaction terms with the triplet fields we explicitly write the hermitian-conjugate terms as they assist in identifying possible discrete symmetries of the theory. This yields

$$\begin{aligned} -\mathcal{L}_Y^\Delta &= \overline{L}_L^C Y_{\Delta_L} (i\sigma_2) \Delta_L L_L + \overline{L}_L Y_{\Delta_L}^* (i\sigma_2) \Delta_L^* L_L^C \\ &\quad + \overline{L}_R^C Y_{\Delta_R} (i\sigma_2) \Delta_R L_R + \overline{L}_R Y_{\Delta_R}^* (i\sigma_2) \Delta_R^* L_R^C, \end{aligned} \quad (4.8)$$

where  $\overline{\Psi}^C = \Psi^T C$  and  $C = i\gamma_2 \gamma_0$ . This result follows from

$$\begin{aligned} (\overline{\Psi}^C Y (i\sigma_2) \Delta \Psi)^\dagger &= -\Psi^\dagger \Delta^\dagger (i\sigma_2) Y^\dagger (\overline{\Psi}^C)^\dagger = -\overline{\Psi} \gamma_0 \Delta^\dagger (i\sigma_2) Y^\dagger \gamma_0 \Psi^C = -\overline{\Psi} \Delta^\dagger (i\sigma_2) Y^\dagger \Psi^C, \\ &= \overline{\Psi} (i\sigma_2) \Delta^* Y^* \Psi^C, \end{aligned} \quad (4.9)$$

where the last equality holds as  $Y^T = Y$  and the specific structure of  $\Delta$  (c.f Eq. (4.5d)) which results in  $\Delta^\dagger i\sigma_2 = -i\sigma_2 \Delta^*$ .

## 4.1.2 Discrete Symmetries

There are two possible phenomenologically viable<sup>2</sup> discrete symmetries, discrete parity [376, 377], and charge conjugation symmetry, denoted as  $\mathcal{P}$  and  $\mathcal{C}$  in the following (see also Ref. [427] and references therein).

### 1. Parity symmetry $\mathcal{P}$ :

Parity symmetry exchanges  $L$  and  $R$ , hence, the symmetry operation is

$$L_L \leftrightarrow L_R, \quad \Delta_L \leftrightarrow \Delta_R, \quad \Phi \leftrightarrow \Phi^\dagger. \quad (4.10)$$

Requiring invariance of the Lagrangian yields the following constraints on the model parameters:

$$Y_{\alpha_i} = Y_{\alpha_i}^\dagger, \quad Y_{\Delta_L} = Y_{\Delta_R}, \quad (4.11)$$

where  $\alpha = Q, L$  and  $i = 1, 2$ .

### 2. Charge conjugation symmetry $\mathcal{C}$ :

<sup>2</sup> In addition to these two discrete symmetries that are an additional two possibilities,  $\Phi \rightarrow \tilde{\Phi}^\dagger$  and  $\Phi \rightarrow \tilde{\Phi}^T$ . However, both of these symmetries lead to unrealistic relations between the up- and down-type quark mass matrices, namely  $M_u = M_d^\dagger$  and  $M_u = M_d^T$  for the two symmetry transformations respectively.

Charge conjugation symmetry exchanges

$$L_L \leftrightarrow L_R^C, \quad \Delta_L \leftrightarrow \Delta_R^*, \quad \Phi \leftrightarrow \Phi^T. \quad (4.12)$$

Once again invariance of the Lagrangian yields

$$Y_{\alpha_i} = Y_{\alpha_i}^T, \quad Y_{\Delta_L} = Y_{\Delta_R}^*. \quad (4.13)$$

### 4.1.3 Scalar Sector and Gauge Symmetry Breaking

The most general  $\mathcal{C}$ - and  $\mathcal{P}$ -conserving renormalisable Higgs potential is given by [378]

$$\begin{aligned} V_{LR} &= -\mu_1^2 \text{Tr}(\Phi^\dagger \Phi) - \mu_2^2 \left[ \text{Tr}(\tilde{\Phi} \Phi^\dagger) + \text{Tr}(\tilde{\Phi}^\dagger \Phi) \right] - \mu_3^2 \left[ \text{Tr}(\Delta_L \Delta_L^\dagger) + \text{Tr}(\Delta_R \Delta_R^\dagger) \right] \quad (4.14) \\ &+ \lambda_1 \left[ \text{Tr}(\Phi^\dagger \Phi) \right]^2 + \lambda_2 \left\{ \left[ \text{Tr}(\tilde{\Phi} \Phi^\dagger) \right]^2 + \left[ \text{Tr}(\tilde{\Phi}^\dagger \Phi) \right]^2 \right\} \\ &+ \lambda_3 \text{Tr}(\tilde{\Phi} \Phi^\dagger) \text{Tr}(\tilde{\Phi}^\dagger \Phi) + \lambda_4 \text{Tr}(\Phi^\dagger \Phi) \left[ \text{Tr}(\tilde{\Phi} \Phi^\dagger) + \text{Tr}(\tilde{\Phi}^\dagger \Phi) \right] \\ &+ \rho_1 \left\{ \left[ \text{Tr}(\Delta_L \Delta_L^\dagger) \right]^2 + \left[ \text{Tr}(\Delta_R \Delta_R^\dagger) \right]^2 \right\} \\ &+ \rho_2 \left[ \text{Tr}(\Delta_L \Delta_L) \text{Tr}(\Delta_L^\dagger \Delta_L^\dagger) + \text{Tr}(\Delta_R \Delta_R) \text{Tr}(\Delta_R^\dagger \Delta_R^\dagger) \right] \\ &+ \rho_3 \text{Tr}(\Delta_L \Delta_L^\dagger) \text{Tr}(\Delta_R \Delta_R^\dagger) + \rho_4 \left[ \text{Tr}(\Delta_L \Delta_L) \text{Tr}(\Delta_R^\dagger \Delta_R^\dagger) + \text{Tr}(\Delta_L^\dagger \Delta_L^\dagger) \text{Tr}(\Delta_R \Delta_R) \right] \\ &+ \alpha_1 \text{Tr}(\Phi^\dagger \Phi) \left[ \text{Tr}(\Delta_L \Delta_L^\dagger) + \text{Tr}(\Delta_R \Delta_R^\dagger) \right] \\ &+ \left\{ \alpha_2 e^{i\delta_2} \left[ \text{Tr}(\tilde{\Phi} \Phi^\dagger) \text{Tr}(\Delta_L \Delta_L^\dagger) + \text{Tr}(\tilde{\Phi}^\dagger \Phi) \text{Tr}(\Delta_R \Delta_R^\dagger) \right] + \text{h.c.} \right\} \\ &+ \alpha_3 \left[ \text{Tr}(\Phi \Phi^\dagger \Delta_L \Delta_L^\dagger) + \text{Tr}(\Phi^\dagger \Phi \Delta_R \Delta_R^\dagger) \right] + \beta_1 \left[ \text{Tr}(\Phi \Delta_R \Phi^\dagger \Delta_L^\dagger) + \text{Tr}(\Phi^\dagger \Delta_L \Phi \Delta_R^\dagger) \right] \\ &+ \beta_2 \left[ \text{Tr}(\tilde{\Phi} \Delta_R \Phi^\dagger \Delta_L^\dagger) + \text{Tr}(\tilde{\Phi}^\dagger \Delta_L \Phi \Delta_R^\dagger) \right] + \beta_3 \left[ \text{Tr}(\Phi \Delta_R \tilde{\Phi}^\dagger \Delta_L^\dagger) + \text{Tr}(\Phi^\dagger \Delta_L \tilde{\Phi} \Delta_R^\dagger) \right]. \end{aligned}$$

The neutral scalar fields in the above potential can be expressed in terms of their CP-even and -odd components:

$$\phi_1^0 = \frac{1}{\sqrt{2}} (v_1 + \sigma_1 + i\varphi_1), \quad \delta_L^0 = \frac{1}{\sqrt{2}} (v_L + \sigma_L + i\varphi_L), \quad (4.15a)$$

$$\phi_2^0 = \frac{1}{\sqrt{2}} (v_2 + \sigma_2 + i\varphi_2), \quad \delta_R^0 = \frac{1}{\sqrt{2}} (v_R + \sigma_R + i\varphi_R), \quad (4.15b)$$

where we use the generic symbols  $\sigma$  and  $\varphi$  to label the CP-even and -odd states, respectively. For the vacuum expectation values, which we assume to be real, we use the following

parametrisation:

$$v_1 = v \cos \beta, \quad v_2 = v \sin \beta, \quad t_\beta \equiv \tan \beta = \frac{v_2}{v_1}, \quad (4.16)$$

where  $v_L \ll v \ll v_R$  so that  $v$  can be identified as the SM VEV. The masses of the new gauge bosons therefore read

$$M_{Z_R} \simeq \sqrt{g_R^2 + g_{BL}^2} v_R, \quad M_{W_R} \simeq \frac{g_R}{\sqrt{2}} v_R. \quad (4.17)$$

Due to LR symmetry, we take the SU(2) gauge coupling to be equal, namely  $g_R = g_L$ . Solving the four minimisation conditions for the potential we eliminate the following four parameters:

$$\begin{aligned} \mu_1^2 = v^2 & \left( \lambda_1 - 2\lambda_4 \frac{t_\beta}{t_\beta^2 + 1} \right) + v_L v_R (\beta_1 - 2\beta_3 t_\beta) \frac{t_\beta}{(t_\beta^2 - 1)} + \frac{v_L^2 v_R^2}{v^2} (\rho_3 - 2\rho_1) \frac{(t_\beta^2 + 1)}{(t_\beta^2 - 1)} \\ & + (v_L^2 + v_R^2) \left( \alpha_1 + \alpha_3 \frac{t_\beta^2}{t_\beta^2 - 1} \right), \end{aligned} \quad (4.18a)$$

$$\begin{aligned} \mu_2^2 = v^2 & \left( \frac{\lambda_4}{2} - (2\lambda_2 + \lambda_3) \frac{t_\beta}{1 + t_\beta^2} \right) + \frac{v_L^2}{4} \left( 2\alpha_2 + \alpha_3 \frac{t_\beta}{t_\beta^2 - 1} \right) + \frac{v_L v_R}{4} \left( (\beta_1 - 2\beta_3 t_\beta) \frac{t_\beta^2 + 1}{t_\beta^2 - 1} \right) \\ & - \frac{v_L^2 v_R^2}{2v^2} \left( (2\rho_1 - \rho_3) \frac{t_\beta(t_\beta^2 + 1)}{t_\beta^2 - 1} \right) + \frac{v_R^2}{2} \left( \alpha_2 + \frac{\alpha_3}{2} \frac{t_\beta}{t_\beta^2 - 1} \right), \end{aligned} \quad (4.18b)$$

$$\mu_3^2 = \frac{v^2}{2} \left( \alpha_1 + (\alpha_3 t_\beta - 4\alpha_2) \frac{t_\beta}{t_\beta^2 + 1} \right) + (v_L^2 + v_R^2) \rho_1, \quad (4.18c)$$

$$\beta_2 = (\beta_1 - \beta_3 t_\beta) t_\beta - \frac{v_L v_R}{v^2} (2\rho_1 - \rho_3) (1 + t_\beta^2). \quad (4.18d)$$

From the last expression above one can derive the VEV see-saw relation as noted in [378]. Using the above expressions  $\mu_i^2$ , where  $i = 1, 2, 3$ , and  $\beta_2$  can be eliminated from the potential and the scalar mass matrices of the theory can be derived. These expressions are given in full detail in Appendix A.1. Here we only quote the results after diagonalisation of the mass matrices, see Appendix A.1 for details on all assumptions made. Firstly, the bi-doublet-like scalar masses:

$$m_h^2 \simeq 2\lambda_1 v^2 - \frac{8\lambda_4^2 v^4}{\alpha_3 v_R^2}, \quad m_H^2 \simeq 2(2\lambda_2 + \lambda_3) v^2 + \frac{\alpha_3}{2} v_R^2, \quad (4.19a)$$

$$m_A^2 \simeq 2\alpha_3 v_R^2 + 2(\lambda_3 - 2\lambda_2) v^2, \quad m_{H^\pm}^2 \simeq \frac{1}{4} \alpha_3 (v^2 + 2v_R^2). \quad (4.19b)$$

Here,  $h$  corresponds to the SM-like Higgs boson;  $H$ ,  $A$  and  $H^\pm$  are the bi-doublet-like heavier neutral scalar and pseudoscalar states as well as the mostly bi-doublet-like charged Higgs.

The triplet-scalar sector masses are:

$$m_{H_L}^2 \simeq \frac{1}{2} (\rho_3 - 2\rho_1) v_R^2 \quad m_{H_R}^2 \simeq 2\rho_1 v_R^2, \quad (4.20a)$$

$$m_{A_L}^2 \simeq \frac{1}{2} (\rho_3 - 2\rho_1) v_R^2, \quad m_{H_L^\pm}^2 \simeq \frac{1}{2} v_R^2 (\rho_3 - 2\rho_1), \quad (4.20b)$$

$$m_{H_1^{\pm\pm}}^2 \simeq 2\rho_2 v_R^2 + \frac{1}{2} \alpha_3 v^2, \quad m_{H_2^{\pm\pm}}^2 \simeq \frac{1}{2} ((\rho_3 - 2\rho_1) v_R^2 + \alpha_3 v^2). \quad (4.20c)$$

Particles with an index  $L(R)$  mostly consist of  $\Delta_{L(R)}$  components. The doubly-charged Higgses can in general be strongly mixed which is why we only label them as  $H_{1/2}^{\pm\pm}$ .

## 4.2 Neutrino Sector

Using information from neutrino oscillation experiments, we can determine the neutrino mass matrix  $m_\nu$  which we express as follows

$$m_\nu^{\text{light}} = U_{\text{PMNS}}^* \text{diag}(m_{\nu_1}, m_{\nu_2}, m_{\nu_3}) U_{\text{PMNS}}^\dagger, \quad (4.21)$$

where  $U_{\text{PMNS}} = U_{\text{PMNS}}(\theta_{12}, \theta_{13}, \theta_{23}; \delta_{\text{CP}})$  is the lepton mixing matrix and  $m_i$  are the neutrino masses. Using the standard parametrisation in a basis where the lepton mass matrix is flavour-diagonal, the neutrino mixing matrix is given by

$$U_{\text{PMNS}} = \begin{pmatrix} c_{12}c_{13} & c_{13}s_{12} & s_{13}e^{i\delta_{\text{CP}}} \\ -c_{23}s_{12} - c_{12}s_{13}s_{23}e^{i\delta_{\text{CP}}} & c_{23}c_{12} - s_{12}s_{13}s_{23}e^{i\delta_{\text{CP}}} & c_{13}s_{23} \\ s_{23}s_{12} - c_{12}c_{23}s_{13}e^{i\delta_{\text{CP}}} & -c_{12}s_{23} - c_{23}s_{12}s_{13}e^{i\delta_{\text{CP}}} & c_{13}c_{23} \end{pmatrix} K. \quad (4.22)$$

Here  $c_{ij} = \cos \theta_{ij}$ ,  $s_{ij} = \sin \theta_{ij}$ ,  $\delta_{\text{CP}}$  corresponds to the Dirac CP-violating phase and  $K$  is a complex diagonal matrix which contains the two Majorana phases. From global fits of neutrino oscillation parameters [428–430] the best fit values and the  $3\sigma$  intervals for a normal neutrino mass hierarchy (NH) are:

$$\sin^2 \theta_{13} = 0.0234_{-0.0057}^{+0.0060}, \quad \Delta m_{21}^2 = 7.60_{-0.49}^{+0.58} \times 10^{-5} \text{ eV}, \quad (4.23a)$$

$$\sin^2 \theta_{12} = 0.323_{-0.045}^{+0.052}, \quad \Delta m_{31}^2 = 2.48_{-0.18}^{+0.17} \times 10^{-3} \text{ eV}, \quad (4.23b)$$

$$\sin^2 \theta_{23} = 0.567_{-0.076}^{+0.175}. \quad (4.23c)$$

### 4.2.1 Neutrino masses

From Eq. (4.7) and (Eq. (4.8)) the neutrino mass matrix follows as

$$-\mathcal{L}_Y \supset \frac{1}{2} \begin{pmatrix} \bar{\nu}_L & \bar{\nu}_R^C \end{pmatrix} M_\nu \begin{pmatrix} \nu_L^C \\ \nu_R \end{pmatrix} + \text{h.c.}, \quad (4.24)$$

where

$$\mathcal{M}_\nu = \begin{pmatrix} M_L^* & M_D \\ M_D^T & M_R \end{pmatrix}. \quad (4.25)$$

In the above expression we have used the following definitions

$$M_L = \sqrt{2} Y_{\Delta_L} v_L, \quad M_R = \sqrt{2} Y_{\Delta_R} v_R, \quad \text{and} \quad M_D = \frac{1}{\sqrt{2}} (Y_{L_1} v_1 + Y_{L_2} v_2). \quad (4.26)$$

Note the conjugate of  $M_L$  in the (1,1) entry of Eq. (4.25). This conjugate is crucial in the case of non-zero phases but is however usually forgotten in the literature. Since  $v_R \gg v_L, v_{1,2}$ , the see-saw approximation can be used to determine the light-neutrino mass eigenstates, yielding

$$m_\nu^{\text{light}} = (M_L^* - M_D M_R^{-1} M_D^T). \quad (4.27)$$

As shown in Eq. (4.26), the Dirac neutrino mass matrix  $M_D$  arises as the sum of two different Yukawas multiplied with their respective VEVs. Consequently at loop-level, corrections are proportional to the individual Yukawa coupling values rather than  $M_D$ . Therefore, in regions where  $\tan \beta \simeq 1$ , loop corrections to these two Yukawas spoil the cancellation required for small  $M_D$  values if imposed at tree-level. As  $\tan \beta$  has negligible impact on the lepton flavour-violating operators discussed below, we choose to restrict our analysis to the small  $\tan \beta$  scenario in the following numerical studies. In this limit  $M_D \propto Y_{L_1} v$ , while the charged lepton masses are  $M_\ell \propto Y_{L_2} v$ .

## 4.2.2 Parametrisation of the Yukawa Matrices

Under the discrete symmetries of the theory, namely parity  $\mathcal{P}$  and charge-conjugation  $\mathcal{C}$ , the resulting light-neutrino mass matrices can be re-expressed as

$$m_\nu^{\text{light}} \stackrel{\mathcal{C}}{=} \begin{pmatrix} \frac{v_L}{v_R} M_R - M_D M_R^{-1} M_D \end{pmatrix}, \quad (4.28)$$

$$m_\nu^{\text{light}} \stackrel{\mathcal{P}}{=} \begin{pmatrix} \frac{v_L}{v_R} M_R^* - M_D M_R^{-1} M_D^* \end{pmatrix}. \quad (4.29)$$

Both discrete symmetries exhibit favourable structures, relating  $M_L$  to  $M_R$ . In particular, this enables an elegant parametrisation for fitting the neutrino masses.

In the following we describe in detail the method used to determine the triplet-Yukawa couplings as well as the requirement of invoking different symmetries in the presence of CP phases. The parametrisation, first proposed in Ref. [412], allows one to explicitly solve for the triplet-Yukawa couplings  $Y_{\Delta_L}$  and  $Y_{\Delta_R}$  given a specific input for  $M_D$ . The parametrisation relies on solving a quadratic polynomial for each diagonal entry of Eq. (4.28) or Eq. (4.29) after diagonalisation. Here, our method differs slightly to Ref. [412]. We have exploited the fact that Eqs. (4.28) and (4.29) can both be manipulated into a form requiring only a single unitary rotation matrix  $R$  to bring both sides into their respective diagonal forms. Here we give the

full details of the procedure, where the final result can be found in Eq. (4.40).

For the charge conjugation symmetric case Eq. (4.28) we multiply the left- and right-hand side by  $M_D^{-1/2}$ , while for the parity symmetric case Eq. (4.29) multiplication from the right-hand side requires an additional conjugation, yielding

$$M_D^{-1/2} m_\nu^{\text{light}} M_D^{-1/2} \stackrel{\mathcal{C}}{=} \frac{v_L}{v_R} M_D^{-1/2} M_R M_D^{-1/2} - M_D^{1/2} M_R^{-1} M_D^{1/2}, \quad (4.30)$$

$$M_D^{-1/2} m_\nu^{\text{light}} M_D^{*-1/2} \stackrel{\mathcal{P}}{=} \frac{v_L}{v_R} M_D^{-1/2} M_R^* M_D^{*-1/2} - M_D^{1/2} M_R^{-1} M_D^{*1/2}, \quad (4.31)$$

which if we make the following definitions

$$\alpha \equiv \frac{v_L}{v_R}, \quad A \equiv M_D^{(*)-1/2} M_R M_D^{-1/2}, \quad B \equiv M_D^{-1/2} m_\nu^{\text{light}} M_D^{(*)-1/2}, \quad (4.32)$$

where (\*) refers to the additional conjugation required for the parity symmetric scenario, allows one to write

$$B \stackrel{\mathcal{C}}{=} \alpha A - A^{-1}, \quad (4.33)$$

$$B \stackrel{\mathcal{P}}{=} \alpha A^* - A^{-1}. \quad (4.34)$$

However, in what follows we exploit the fact that the matrices  $A$  and  $B$  are either: (i) real symmetric ( $\delta_{\text{CP}} = 0$ ), or (ii) complex symmetric ( $\delta_{\text{CP}} \neq 0$ ). As a result,  $B$  and subsequently  $A$  are diagonalised by  $R$  which is either: (i) a real orthogonal matrix, or (ii) a complex unitary matrix.<sup>3</sup> For case (i), if the matrix  $R$  diagonalizes  $A$  then this same matrix also diagonalizes the inverse matrix  $A^{-1}$ . As a result Eq. (4.33) can be written as

$$B \stackrel{\mathcal{C} \text{ or } \mathcal{P}}{=} \alpha A - A^{-1} = R (\alpha A_D - A_D^{-1}) R^T, \quad (4.35)$$

where the subscript  $D$  indicates the matrix is in a real diagonal form. Here we observe that both charge-conjugation and parity invariance are equivalent if  $A$  is real. As requiring real  $A_D$  necessitates a unitary  $R$ , we cannot simultaneously diagonalise both  $A$  and  $A^{-1}$  for case (ii) as

$$B \stackrel{\mathcal{C}}{=} \alpha A - A^{-1} = R^* \alpha A_D R^\dagger - R A_D^{-1} R^T \neq R (\alpha A_D - A_D^{-1}) R^T. \quad (4.36)$$

However, here this procedure indeed applies for  $A^*$  and  $A^{-1}$  namely

$$B \stackrel{\mathcal{P}}{=} \alpha A^* - A^{-1} = R (\alpha A_D - A_D^{-1}) R^T, \quad (4.37)$$

so that one can find a suitable parametrisation of the triplet-Yukawa in the  $\mathcal{P}$ -symmetric case also with  $\delta_{\text{CP}} \neq 0$ , as we shall see in what follows. Eqs. (4.33) and (4.34) are identical in their

---

<sup>3</sup> For more details regarding the various diagonalisation procedures see appendix D of Ref. [431].

respective real diagonal forms, namely

$$B_D^{(i,i)} = \alpha A_D^{(i,i)} - \left(A_D^{(i,i)}\right)^{-1}, \quad (4.38)$$

where  $i = 1, 2, 3$ . Solving the decoupled quadratic equations for  $A_D^{(i,i)}$  yields

$$A_D^{(i,i)} = \frac{B_D^{(i,i)} \pm \sqrt{\left(B_D^{(i,i)}\right)^2 + 4\alpha}}{2\alpha}. \quad (4.39)$$

Using the definitions in Eqs. (4.26) and (4.32) we arrive at expressions for the triplet Yukawas

$$Y_{\Delta}^{(\pm\pm\pm)} \equiv Y_{\Delta_{L/R}}^{(\pm\pm\pm)} = \frac{1}{2\sqrt{2}v_L} M_D^{(*)1/2} R^* \text{diag} \left( B_D^{(i,i)} \pm \sqrt{\left(B_D^{(i,i)}\right)^2 + 4\alpha} \right) R^\dagger M_D^{1/2}, \quad (4.40)$$

where  $B_D = R^\dagger M_D^{-1/2} m_\nu^{\text{light}} M_D^{(*)-1/2} R^*$  is a diagonal  $3 \times 3$  matrix,  $R$  is the aforementioned rotation matrix and  $\alpha = v_L/v_R$ . Finally  $(*)$  is an additional conjugation of  $M_D$  required in the case of a parity symmetric neutrino sector. Eq. (4.40) is valid for:

- (i) both possible discrete left-right symmetries if  $\delta_{\text{CP}} = 0$ ,
- (ii) all possible CP phases if the Lagrangian is  $\mathcal{P}$ -symmetric.

Eq. (4.39) leads to an eightfold degeneracy in the solutions due to the choice of sign for each diagonal entry of  $A_D$ , as first noted in Ref. [412]. However, these eight solutions can be categorized into two distinct cases. The differences between these two cases is best illustrated through an example where we choose  $M_D$  to be diagonal and real. In this case  $B \propto m_\nu^{\text{light}}$  which, for realistic choices of the neutrino oscillation parameters and large enough  $v_L$ , leads to the hierarchy  $\alpha \gg (B_D^{(i,i)})^2$ . Subsequently, expanding Eq. (4.39) for small  $B_D^{(i,i)}$  yields

$$A_D^{(i,i)} = \pm\alpha^{-1/2} + \mathcal{O}\left(B_D^{(i,i)}\right). \quad (4.41)$$

Therefore the principle difference between the degenerate solutions is simply a sign choice. But, this sign choice has large ramifications on the resulting triplet Yukawa matrices. To demonstrate this consider the two neutrino generation case, where we examine both mixed and same-sign choices for the cases  $\delta_{\text{CP}} = 0$  and  $\delta_{\text{CP}} \neq 0$ .

**$\delta_{\text{CP}} = 0$ :** For the same-sign scenario we have

$$A^{(++)} = R A_D R^T = \begin{pmatrix} \cos \theta & \sin \theta \\ -\sin \theta & \cos \theta \end{pmatrix} \begin{pmatrix} \alpha^{-1/2} & 0 \\ 0 & \alpha^{-1/2} \end{pmatrix} \begin{pmatrix} \cos \theta & -\sin \theta \\ \sin \theta & \cos \theta \end{pmatrix} = A_D. \quad (4.42)$$

whereas for the mixed sign case we obtain

$$A^{(+-)} = R \begin{pmatrix} \alpha^{-1/2} & 0 \\ 0 & -\alpha^{-1/2} \end{pmatrix} R^T = \alpha^{-1/2} \begin{pmatrix} \cos 2\theta & \sin 2\theta \\ \sin 2\theta & -\cos 2\theta \end{pmatrix}. \quad (4.43)$$

We therefore see that in this example the choice of sign dictates whether or not there are flavour violating off-diagonal entries at leading order. Note that the above argumentation generalizes to the realistic scenario of three neutrino generations. This argumentation is, of course, still valid if  $M_D$  is non-diagonal as it relies on already-diagonalised quantities. However, when plugging Eq. (4.41) into the full expression, Eq. (4.40), one sees that the impact of the above-mentioned effect is weakened comparatively when  $M_D$  itself contains a flavour-violating structure. Therefore, in this situation the solution for  $Y_\Delta$  with different sign choices in general contains larger off-diagonal elements than the solution with equal signs, the relative difference of these off-diagonals is small compared to the case in which  $M_D$  is diagonal.

Shown in Fig. 4.2 are numerical results of the branching ratio for  $\mu \rightarrow 3e$  as a function of the triplet VEV  $v_L$ . Here, all possible sign choices are considered in two extreme scenarios, namely diagonal  $M_D$  and  $M_D = V_{\text{CKM}}^\dagger M_{\text{up-type}} V_{\text{CKM}}$ . As illustrated in the toy two-generation example, same-sign choices for the diagonal  $M_D$  lead to highly suppressed off-diagonals in the resulting triplet Yukawas in comparison to the mixed-sign case. However, in the scenario that  $M_D$  is no longer diagonal then the effect between same or mixed-sign solutions is comparatively smaller.

$\delta_{\text{CP}} \neq 0$ : Here we demonstrate that there is a significant difference in the same-sign scenario when introducing this phase. As  $B$  is now a complex symmetric matrix  $R$  must necessarily be a unitary matrix. Therefore for the same-sign case we obtain

$$\begin{aligned} A^{(++)} &= R^* A_D R^\dagger, \\ &= e^{-2i\phi_3} \begin{pmatrix} e^{-i\phi_1} \cos \theta & e^{-i\phi_2} \sin \theta \\ -e^{-i\phi_2} \sin \theta & e^{i\phi_1} \cos \theta \end{pmatrix} \begin{pmatrix} \alpha^{-1/2} & 0 \\ 0 & \alpha^{-1/2} \end{pmatrix} \begin{pmatrix} e^{-i\phi_1} \cos \theta & e^{-i\phi_2} \sin \theta \\ e^{-i\phi_2} \sin \theta & e^{i\phi_1} \cos \theta \end{pmatrix}, \\ &= \alpha^{-1/2} e^{2i\phi_3} \begin{pmatrix} e^{-2i\phi_1} (\cos^2 \theta + e^{-2i(\phi_2-\phi_1)} \sin^2 \theta) & i \sin 2\theta \sin(\phi_1 - \phi_2) \\ i \sin 2\theta \sin(\phi_1 - \phi_2) & e^{2i\phi_1} (\cos^2 \theta + e^{2i(\phi_2-\phi_1)} \sin^2 \theta) \end{pmatrix}, \end{aligned} \quad (4.44)$$

where  $\phi_i$  are the three phases of a generic unitary  $2 \times 2$  matrix. We observe, in contrast to the case with the same-sign solution and  $\delta_{\text{CP}} = 0$ , that there is a complex off-diagonal generated at leading order even in the case that  $M_D$  is proportional to the unit matrix. This off-diagonal is in general non-zero as the three phases  $\phi_1$ ,  $\phi_2$  and  $\phi_3$  must be chosen such that the matrix  $A$  is brought into its real diagonal form. The resulting structure shares similarities to the case with mixed sign and  $\delta_{\text{CP}} = 0$ . Namely, we see an off-diagonal entry, which in this case is complex, proportional to  $\sin 2\theta$ .

This results of this parametrisation form the basis of our subsequent numerical studies. By choosing a form for  $M_D$  and requiring that  $m_\nu^{\text{light}}$  satisfies Eq. (4.21), one can determine  $R$  such that  $B_D$  is diagonal.  $R$  therefore contains the information from the experimental neutrino data. From Eq. (4.40) we see that there does not exist a unique solution to the triplet-Yukawa. Rather for each diagonal entry there appears a sign choice in front of the square-root. Considering the possible permutations, there are in total eight unique solutions. This parametrisation is therefore advantageous in comparison to the Casas-Ibarra-like parametrisations [432] as it by construction respects the discrete symmetries of the theory. This is crucial, as the finite number of solutions is a direct consequence of invariance under a discrete left-right symmetry.

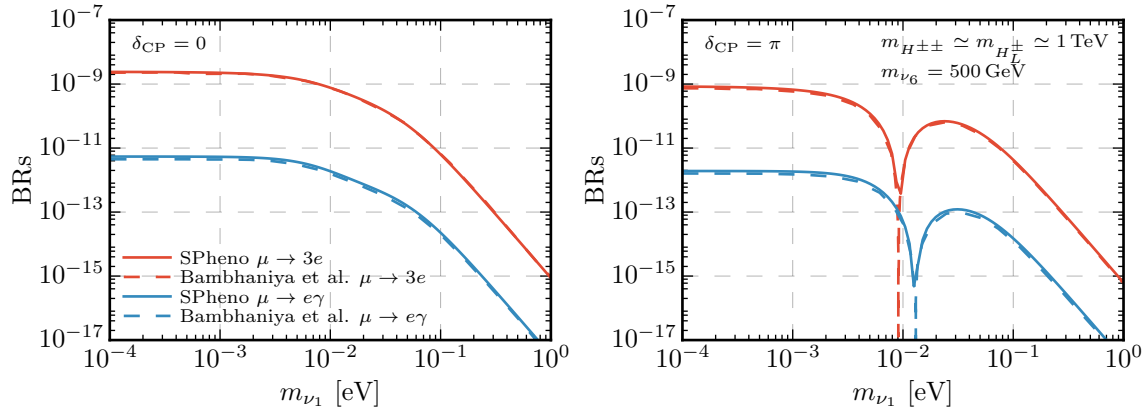


Figure 4.1: Comparison of the SPHeno code with results in Fig. 3.4 from Ref. [386].

## 4.3 Results

### 4.3.1 Numerical Set-up

In this section we present a numerical study of the model. In order to do so we have used the Mathematica package SARAH [89–94] for which we have created the necessary model files. The respective code is available from the [SARAH model database](#). SARAH interfaces to the spectrum generator SPHeno [104, 105] which enables the computation of the mass spectrum and particle decays as well as quark and lepton flavour violating observables via the link to FlavorKit [101].

As a first step we have compared the  $\mu \rightarrow 3e$  and  $\mu \rightarrow e\gamma$  branching ratios with those from Ref. [386]. To do so we consider a similar set up where  $M_L = 0$  and  $M_D \propto \mathbb{1}$  leading to a pure type-I see-saw mechanism where the light neutrino masses and mixings are encoded in  $Y_{\Delta_R}$  couplings. In addition, Ref. [386] neglected contributions arising from both neutral scalars and  $W_L - W_R$  mixing which is a well justified approximation. Shown in Fig. 4.1 are the rates for  $\mu \rightarrow 3e$  and  $\mu \rightarrow e\gamma$  from this work (solid lines) and, for comparison, the results from Fig. 3.4 of Ref. [386] (dashed lines), where the triplet masses are set to 1 TeV. We observe good agreement between the respective results, with only small deviations in the rates for  $\mu \rightarrow e\gamma$ . The main reason for these small deviations is that our analysis considers a complete model where the scalar masses are a function of the model parameters. This prevents one from varying the scalar masses independently. Therefore the resulting spectrum does not correspond exactly to the mass choices of Ref. [386]. As both of the observables are highly sensitive functions of the scalar masses, a 5% deviation in the mass spectrum leads to the observed small mismatch in the flavour observables.

In the subsequent analysis we study lepton flavour violating rare decays based on the best-fit NH oscillation parameters given in Eq. (4.23a) choosing the lightest mass to be  $m_{\nu_1} = 10^{-4}$  eV. We also consider the impact of varying these two choices. Lastly, we choose  $\delta_{CP} = 0$ , but consider non-zero choices and  $\delta_{CP} = 3\pi/2$ , as suggested by recent global fits [433], in later sections. The model parameters used, unless otherwise stated, are given in Table 4.2.

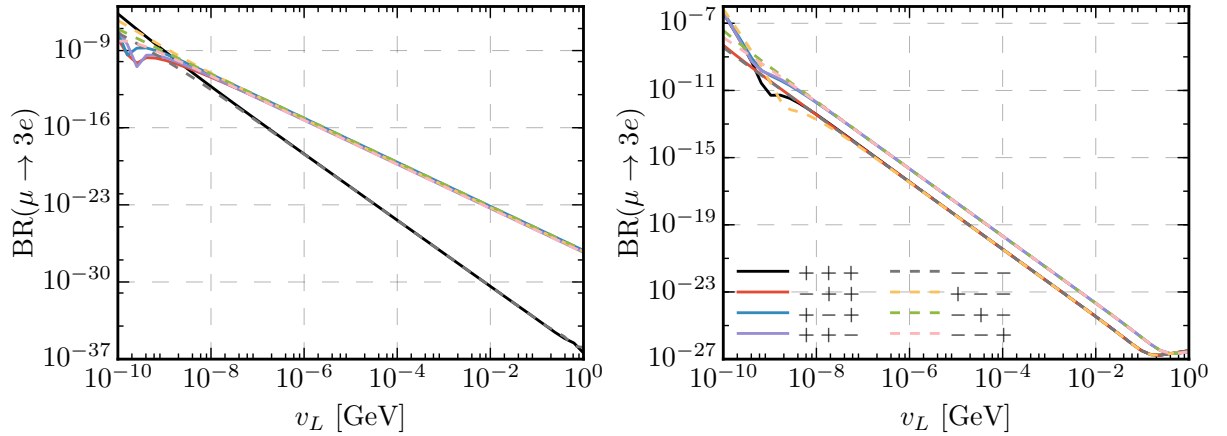


Figure 4.2: Dependence of the observable  $\text{BR}(\mu \rightarrow 3e)$  on the eightfold degenerate solutions in the cases that  $M_D = x\mathbb{1}$  [GeV] (left-hand panel) and  $M_D = xV_{\text{CKM}}^\dagger M_{\text{up-type}} V_{\text{CKM}}$  (right-hand panel), where in both cases  $x = 10^{-4}$ .

The value chosen for  $v_R$  leads to  $W_R$  and  $Z_R$  masses which are outside of the reach of the LHC. However, in the presence of a low-scale discrete  $\mathcal{C}$  symmetry, the  $K$ - and  $B$ -meson constraints only allow the heavy bidoublet Higgs to be as ‘light’ as 20 TeV [401] which, in combination with a perturbativity constraint on  $\alpha_3$ , dictates a lowest possible  $v_R$  value of  $\sim 15$  TeV, cf. Eq. (4.19a). This can lead to scalar triplet masses of  $\mathcal{O}(1 \text{ TeV})$  and therefore within the LHC reach, it however pushes  $M_{W_R, Z_R}$  to  $\mathcal{O}(10 \text{ TeV})$ .

The remaining parameters and choices which we investigate are as follows:

- $v_L$ , which we typically vary between 0.1 eV and 1 GeV.
- $M_D$ , the Dirac neutrino mass matrix which in our parametrisation is an input parameter. We study three different possibilities:
  1.  $M_D = x\mathbb{1}$  GeV,
  2.  $M_D = xM_{\text{up-type}}$ ,
  3.  $M_D = xV_{\text{CKM}}^\dagger M_{\text{up-type}} V_{\text{CKM}}$ ,

where  $M_{\text{up-type}}$  is the diagonal up-type quark-mass matrix. For each choice we have also added the parameter  $x$ , which we use to vary the overall mass scale of the matrix  $M_D$ .

- Sign choice of the diagonal  $\pm$  signs appearing in Eq. (4.40). In the numerical studies we investigate two different choices of the possible eight, namely  $(+++)$  and  $(+-+)$ . This is well motivated as these eight solutions can be divided into two subgroups, whereby each subgroup leads to similar results. This is demonstrated in Fig. 4.2, where we show the branching ratio for  $\mu \rightarrow 3e$  for all eight sign choices varying  $v_L$ , with two different extreme examples of  $M_D$ . Here we clearly see the grouping of the eight solutions into the two classes (i) *same-sign* and (ii) *mixed-sign* solutions.

Model Parameters			
$\lambda_1$	0.13	$v_L$	$10^{-10} \dots 1 \text{ GeV}$
$\lambda_2$	1.0	$v_R$	20 TeV
$\lambda_3$	1.0	$\tan \beta$	$10^{-4}$
$\lambda_4$	0	$\alpha_1$	0
$\rho_1$	$3.2 \times 10^{-4}$	$\alpha_2$	0
$\rho_2$	$2.5 \times 10^{-4}$	$\alpha_3$	2.0
$\rho_3$	$1.8 \times 10^{-3}$	$\beta_1$	0
$\rho_4$	0	$\beta_2$	$3.83 \times 10^{-4}$
$\mu_1^2$	$7.87 \times 10^3 \text{ GeV}^2$	$\beta_3$	0
$\mu_2^2$	$-2.00 \times 10^4 \text{ GeV}^2$	$\mu_3^2$	$1.28 \times 10^5 \text{ GeV}^2$
Resulting Mass Spectrum			
$m_h$	125.5 GeV	$m_H$	20 TeV
$m_A$	20 TeV	$m_{H^\pm}$	20 TeV
$m_{H_L}$	482 GeV	$m_{H_R}$	506 GeV
$m_{A_L}$	482 GeV	$m_{H_L^\pm}$	512 GeV
$m_{H_1^{\pm\pm}}$	511 GeV	$m_{H_2^{\pm\pm}}$	541 GeV
$M_{W_R}$	9.37 TeV	$M_{Z_R}$	15.7 TeV

Table 4.2: Benchmark point used in the subsequent LFV study. All parameters and masses are compatible with the constraints derived in Refs. [401, 411].

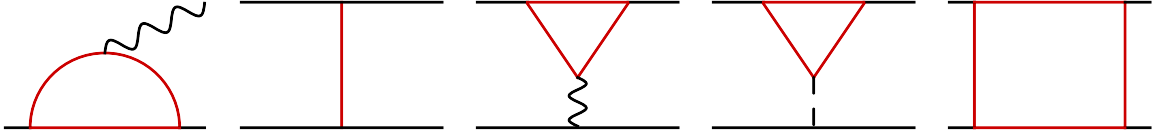


Figure 4.3: Representative lepton flavour violating Feynman diagrams. Here, red solid lines represent particles of all spins. Diagrams of the left-hand type lead to the radiative lepton decays  $\ell_\alpha \rightarrow \ell_\beta \gamma$ . The other four diagrams induce LFV three-body decays as well as  $\mu - e$  conversion in nuclei. We shall label them “tree-level scalar”, “vector penguin”, “scalar penguin” as well as “box” contributions.

### 4.3.2 Numerical Results

As pointed out beforehand, the free parameters in our study which determine the neutrino sector are  $M_D$ ,  $v_L$  as well as  $\delta_{\text{CP}}$ . As we shall see, they are crucially important for determining which type of diagram dominates the lepton flavour violating process. We decompose the relevant diagrams into different categories which are depicted in Fig. 4.3.

The radiative decays  $\ell_\alpha \rightarrow \ell_\beta \gamma$  are described by the first type of diagram, the vector line corresponding to an on-shell photon whereas the particles running in the loop can be (i)  $H_i^{\pm\pm} - \ell_\delta^\mp$ , (ii)  $H_i^0 - \ell_\delta^\pm$ , (iii)  $H_i^\pm - \nu_j$ , (iv)  $W_{L/R}^\pm - \nu_j$  (where  $j = 1, \dots, 6$ ).

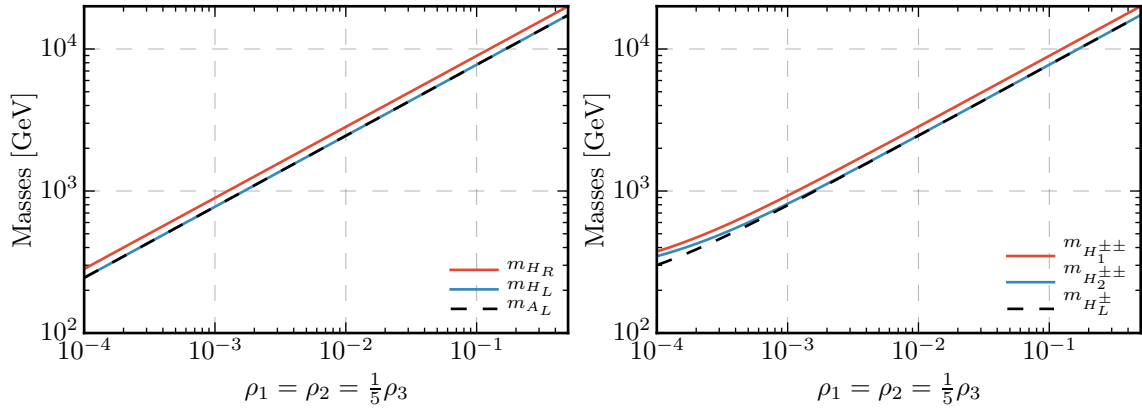


Figure 4.4: Variation of the neutral and charged triplet scalar masses that are used in subsequent figures. Here, the values of the additional parameters not shown in the figure are given in Table 4.2. The light and heavy neutral bi-doublet masses are fixed to 125.5 GeV and 20 TeV, respectively.

The three-body decays as well as  $\mu-e$  conversion processes receive contributions from both tree-level as well as one-loop diagrams. As the heavy neutral bidoublet-like Higgs  $H$  couples to both leptons and quarks generically in a flavour-non-conserving manner, it contributes to both  $\mu-e$  conversion as well as  $\ell_\alpha \rightarrow \ell_\beta \ell_\gamma \ell_\delta$ . Depending on the flavour structure of the lepton Dirac Yukawa couplings, this contribution can be both sizeable or small (in case of a flavour-diagonal  $M_D$ , its contribution is zero). The tree-level diagram mediated by the doubly-charged scalars vanishes for the  $\mu-e$  conversion processes since the triplet doesn't couple to quarks. In case of the LFV three-body decays one can expect in large portions of the parameter space a dominance of those tree-level diagrams since  $Y_\Delta$  is typically much larger than the Dirac Yukawas. It is interesting to note that the  $\tau$  three-body decays with a mixed  $e/\mu$  final state,  $\tau^\pm \rightarrow \ell_\alpha^\mp \ell_\beta^\pm \ell_\beta^\pm$  are much more frequent than  $\tau^\pm \rightarrow \ell_\alpha^\pm \ell_\beta^\mp \ell_\beta^\pm$  whenever the triplet tree-level diagram is dominating the LFV observables and the flavour-violating  $Y_\Delta$  entries are small; this is simply because of the doubly-charged mediator: the process  $\tau^\pm \rightarrow \ell_\alpha^\pm \ell_\beta^\mp \ell_\beta^\pm$  needs a flavour-violating coupling at each vertex whereas  $\tau^\pm \rightarrow \ell_\alpha^\mp \ell_\beta^\pm \ell_\beta^\pm$  contains one flavour-violating and one flavour-conserving vertex. This is in contrast to the loop-induced contributions including virtual neutral or singly-charged bosons which, in order for a  $\tau^\pm \rightarrow \ell_\alpha^\mp \ell_\beta^\pm \ell_\beta^\pm$  decay to happen, require at least two flavour-violating vertices in the dominant contributions [434].

The remaining diagrams are scalar and vector penguins as well as box diagrams. It is known from studies in other models with low-scale see-saw mechanisms that the boxes and vector penguins with  $W_L$  bosons and right-handed neutrinos running in the loop can be very important [434–438]. In left-right symmetric theories, other very important contributions arise from triplet scalars and neutrinos/leptons in the loop as well as  $W_R - \nu_R$  diagrams. Diagrams including a  $W_{L/R}$  and a right-handed neutrino in the loop are expected to be important in the case of small  $Y_\Delta$ . While penguin diagrams featuring triplet-scalars in the loop are loop-suppressed with respect to the corresponding tree-level diagrams, certain flavour structures of  $Y_\Delta$  may suppress the tree-level w.r.t. the loop-level diagrams. We shall see examples of this behaviour later on; see, for instance, Section 4.3.2.

We now start the discussion by looking at the different contributions to the LFV observ-

ables as a function of the model parameters. In particular, we will vary the masses of the triplet scalars while keeping the bidoublet masses constant. We will do so choosing different parametrisations of  $M_D$  and values for  $v_L$ . The reader should be reminded that  $v_L$  not only determines the size of the see-saw-II contribution to the neutrino masses, see Eq. (4.25), but also feeds into the determination of  $Y_\Delta$  for a given  $M_D$  following Eq. (4.40).

### Case I: $M_D \propto \mathbb{1}$

Let us first examine the simplest case where the Dirac neutrino mass is diagonal and flavour-universal. This results in, for the majority of the parameter space, an almost degenerate spectrum of right-handed neutrinos due to almost degenerate diagonal  $Y_\Delta^{(i,i)}$  entries. More importantly, all the lepton flavour violation arises through the triplet Yukawas, meaning that the bidoublet states have only lepton flavour-conserving interactions. Quite generically, this also means that the rather uniform structure of neutrino mixing is translated to the triplet Yukawas. Hence, there is no large hierarchy between the Yukawa matrix elements which mix the 1st, 2nd or 3rd generation.<sup>4</sup>

(+ + +) **Solution.** As a numerical example, choosing  $v_L = 2 \times 10^{-7}$  GeV,  $M_D = 1$  MeV Eq. (4.40), yields

$$Y_\Delta^{(+++)} = \begin{pmatrix} 1.12 \times 10^{-2} & -1.41 \times 10^{-5} & 2.97 \times 10^{-6} \\ -1.41 \times 10^{-5} & 1.12 \times 10^{-2} & -3.78 \times 10^{-5} \\ 2.97 \times 10^{-6} & -3.78 \times 10^{-5} & 1.12 \times 10^{-2} \end{pmatrix}. \quad (4.45)$$

From here we can already draw some conclusions: (i) the doubly-charged Higgs as the tree-level mediator dominates the LFV three-body decays, which means that (ii) the magnitudes of the  $\mu$  and  $\tau$  LFV decays are of comparable size (within at most an order of magnitude or two) and that (iii) the three-body decays are much more abundant than the radiative decays  $\ell_\alpha \rightarrow \ell_\beta \gamma$ . A LFV process observed at the Mu3e experiment with no evidence for  $\mu \rightarrow e \gamma$  would therefore be a smoking gun for these scenarios with LFV triplet scalar interactions.

We will now move to discussing numerical examples starting with the dependence of various LFV observables on the triplet scalar sector. Unless noted otherwise, all model parameters are chosen as given in Table 4.2. We therefore vary the model parameters  $\rho_1, \rho_2$  and  $\rho_3$ , where we show the resulting masses in Fig. 4.4.

In the left upper panel of Fig. 4.5 the magnitude of  $\mu \rightarrow 3e$  is shown using the parametrisation of Eq. (4.45) with the different diagrammatic contributions split according to Fig. 4.3. As discussed above, the tree-level diagram with a doubly-charged mediator completely dominates over other contributions. In the lower left panel we also show the other LFV three-body decays. The radiative decays, shown on the upper right panel, are smaller by roughly two orders of magnitude which is due to the loop suppression w.r.t. the three-body decays. The reason why  $\text{BR}(\tau \rightarrow e \gamma) \ll \text{BR}(\tau \rightarrow \mu \gamma)$ ,  $\text{BR}(\mu \rightarrow e \gamma)$  as well as  $\text{BR}(\tau \rightarrow 3e) \ll \text{BR}(\tau \rightarrow 3\mu)$ ,  $\text{BR}(\mu \rightarrow 3e)$  is simply the order of magnitude difference

<sup>4</sup> In this context, ‘no large hierarchy’ means no more than an order of magnitude of difference, therefore small compared to the hierarchy in quark flavour mixing.

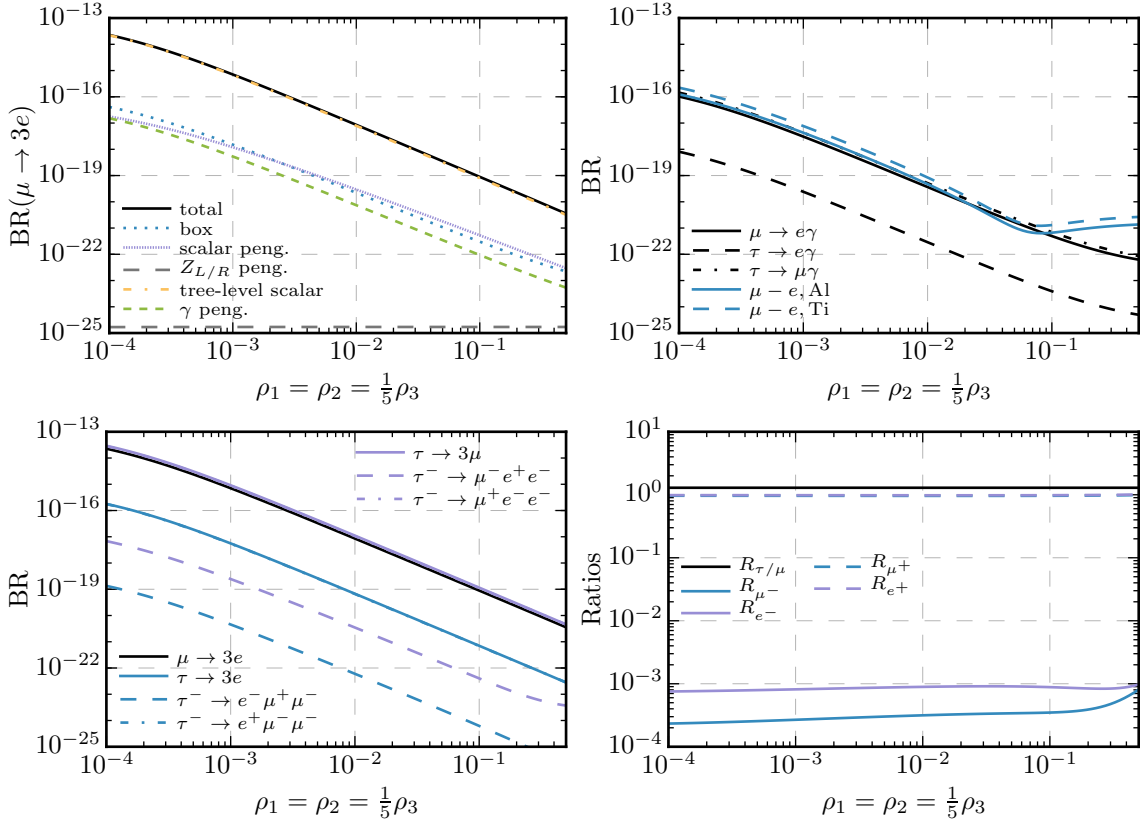


Figure 4.5: A cross-section of different LFV observables for the choice  $v_L = 2 \times 10^{-7}$  GeV,  $M_D = 1$  MeV and the Yukawa solution sign choice  $(+++)$ . Top left: Total branching ratio of  $\mu \rightarrow 3e$  and the different contributing types of diagrams. Top right:  $\ell_\alpha \rightarrow \ell_\beta \gamma$  and  $\mu - e$  conversion in different nuclei. Bottom left: Different 3-body decay channels of muons and taus, note that the channels  $\tau^- \rightarrow e^+ \mu^- \mu^-$  and  $\tau^- \rightarrow \mu^+ e^- e^-$  cannot be seen as they lie very close to the branching ratios  $\tau \rightarrow 3\mu$  and  $\mu \rightarrow 3e$ , respectively. Bottom right: Ratios of the different 3-body decay modes, see Eq. (4.46) for a description of the labels.

between  $Y_\Delta^{(1,3)}$  and the other two off-diagonal Yukawa entries. For the  $\mu - e$  conversion observables we first see a decrease of the conversion rate with an increasing mass scale of the triplet scalar sector. The reason is that for this choice of parameters, for triplet masses up to 5 TeV the  $\gamma$ -penguin diagrams with triplets running in the loop are dominating. For higher scalar masses, the  $W_{L/R} - \nu_R$ -mediated box diagrams which are independent of the scalar sector parameters become more important (as the triplets don't couple to quarks, the most important  $\mu - e$  conversion box contribution is always coming from these internal particles). For a heavy scalar sector, we can therefore even have  $\text{CR}(\mu - e) > \text{BR}(\mu \rightarrow e\gamma)$ ; this could be interesting for future experiments which have better prospects for sensitivity in  $\mu - e$  conversion than for the radiative muon decay. For  $\mu \rightarrow 3e$ , the size of the boxes is determined by the triplets for all of the parameter regions shown. Finally in the lower right panel of Fig. 4.5

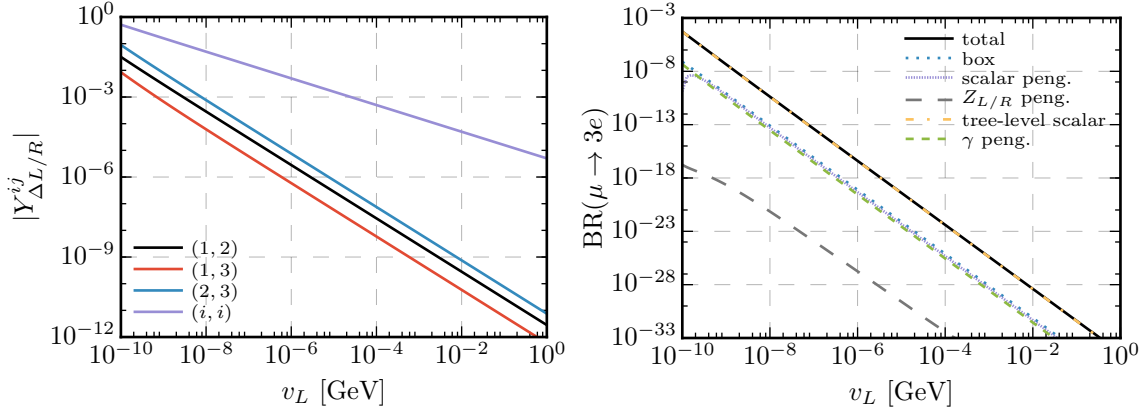


Figure 4.6: Dependence of the triplet Yukawa coupling on left triplet VEV  $v_L$  using the  $(+++)$  solution of Eq. (4.40) (left) and the consequential decoupling of the different contributions to  $\mu \rightarrow 3e$  (right).

we show ratios of the three-body branching ratios. The labels in the figure correspond to

$$R_{\tau/\mu} = \frac{\text{BR}(\tau \rightarrow 3\mu)}{\text{BR}(\mu \rightarrow 3e)}, \quad R_{e^\mp} = \frac{\text{BR}(\tau^- \rightarrow e^\mp \mu^\pm \mu^-)}{\text{BR}(\tau \rightarrow 3e)}, \quad R_{\mu^\mp} = \frac{\text{BR}(\tau^- \rightarrow \mu^\mp e^\pm e^-)}{\text{BR}(\tau \rightarrow 3\mu)}. \quad (4.46)$$

Let us now fix the scalar sector to the benchmark values of Table 4.2 and consider the dependence of the LFV rates on the input parameter  $v_L$  which we vary from 0.1 eV to 1 GeV. It is important to realize that, for these parameter values,  $\sqrt{v_L/v_R} \gg B_D^{(i,i)}$ , where  $B_D = R^T M_D^{-1/2} m_\nu^{\text{light}} M_D^{-1/2} R$  as used in Eq. (4.40). Therefore the diagonal elements of  $Y_\Delta$  approximately scale with  $1/\sqrt{v_L}$ . The off-diagonal  $Y_\Delta$  elements, however, vanish to zeroth order in  $\sqrt{v_L/v_R}/B_D^{(i,i)}$  for diagonal  $M_D$  and both the  $(+++)$  or  $(---)$  solutions, see Section 4.2.2 for further details. Therefore, they are generated by the terms proportional to  $B_D$ . With the overall  $1/v_L$  pre-factor in Eq. (4.40), the off-diagonal  $Y_D$  entries decouple like  $1/v_L$ . This is numerically shown in the left-hand panel of Fig. 4.6. On the right-hand panel we show the corresponding decoupling behaviour of the muon three-body decay. The other observables scale accordingly.

**$(+ - +)$  Solution.** Let us now consider another possibility out of the eight different solutions for  $Y_\Delta$  according to Eq. (4.40). As illustrated in detail in Section 4.2.2, the choice of the solution is of particular importance in the case where  $M_D$  is diagonal: while the flavour-conserving  $Y_\Delta$  elements get reduced by less than an order of magnitude when switching from a  $(+++)$  or  $(---)$  solution to one with differing sign choices, the flavour-violating entries get enhanced sizeable. The reason is that for  $Y_\Delta^{(k,l)}$  the entries with  $k \neq l$  do not vanish at zeroth order in  $\sqrt{v_L/v_R}/B_D^{(i,i)}$ . For comparison, using the chosen benchmark point, the Yukawa matrix from the  $(+++)$  case in Eq. (4.45) reads for the  $(+ - +)$  case

$$Y_\Delta^{(+ - +)} = \begin{pmatrix} -3.61 \times 10^{-3} & -8.53 \times 10^{-3} & -6.27 \times 10^{-3} \\ -8.53 \times 10^{-3} & 6.33 \times 10^{-3} & -3.65 \times 10^{-3} \\ -6.27 \times 10^{-3} & -3.65 \times 10^{-3} & 8.56 \times 10^{-3} \end{pmatrix}. \quad (4.47)$$

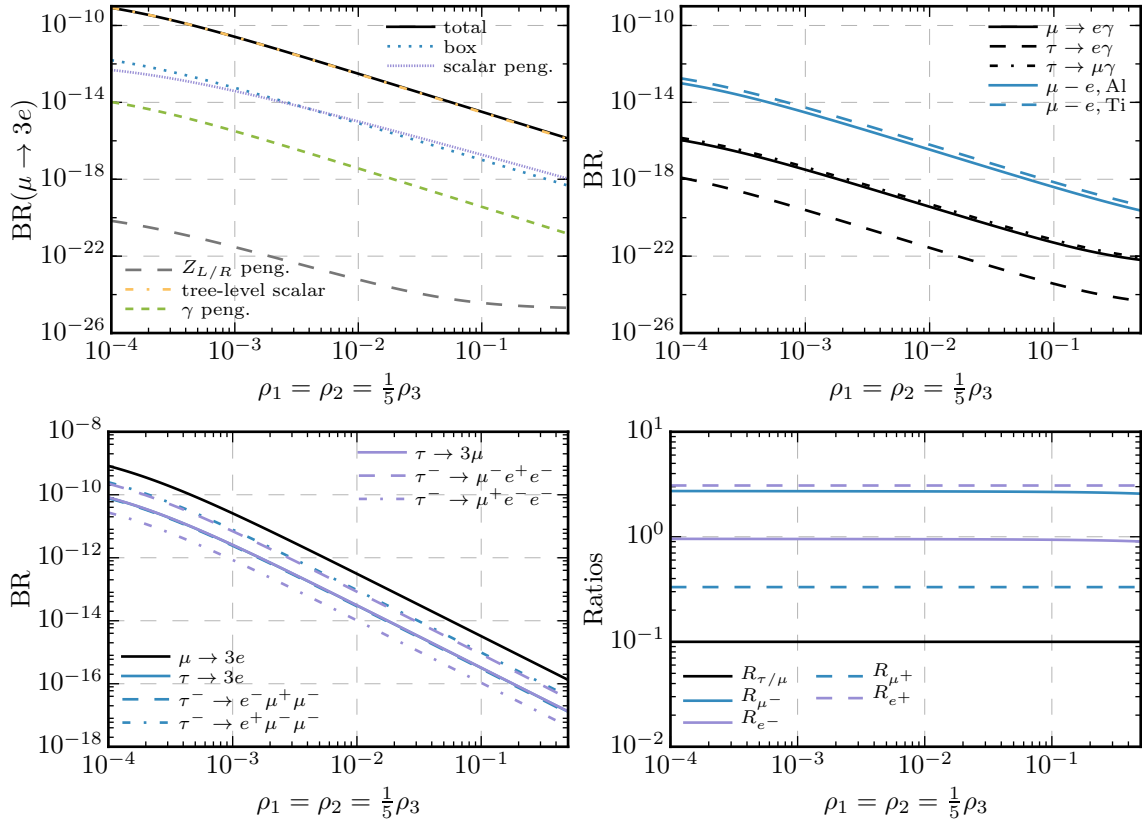


Figure 4.7: A variety of different LFV observables for the choice  $v_L = 2 \times 10^{-7}$  GeV,  $M_D = 1$  MeV and the Yukawa solution sign choice  $(+ - +)$ . For an explanation of the four panels see Fig. 4.5. Note, that the cases with  $\rho_1 \lesssim 6 \times 10^{-3}$  are excluded by the bounds on  $\mu \rightarrow 3e$ .

Naturally, this results in a rate enhancement of the LFV observables by many orders of magnitude. In Fig. 4.7 we show the analogue to Fig. 4.5 but this time using the  $(+ - +)$  solution. We see an interesting effect here: while  $\mu \rightarrow 3e$  is enhanced by roughly four orders of magnitude,  $\mu - e$  conversion observables are only enhanced by three orders. The radiative decays, in turn, are hardly changed at all. The reason for this is as follows. The three-body decays are still dominated by the tree-level  $H^{\pm\pm}$  mediation; therefore their amplitude scales with the respective off-diagonal  $Y_\Delta$  entry which is enhanced by three orders of magnitude from Eq. (4.45) to Eq. (4.47). For the radiative decays, the diagrams with a charged lepton and a doubly-charged Higgs in the loop dominate. For each decay, the internal lepton can be electron, mu or tau flavoured. Taking as an example the decay  $\mu \rightarrow e\gamma$ , the coupling combination entering the amplitude is therefore  $Y_\Delta^{(2,1)} Y_\Delta^{(1,1)} c_e + Y_\Delta^{(2,2)} Y_\Delta^{(2,1)} c_\mu + Y_\Delta^{(2,3)} Y_\Delta^{(3,1)} c_\tau$ , where  $c_i$  denotes the loop function depending on  $m_{\ell_i}$  and  $m_{H^{\pm\pm}}$ . For the photonic dipole loop functions we find that  $c_e \simeq c_\mu \simeq c_\tau$ . Taking the respective  $Y_\Delta^{(k,l)}$  entries from Eq. (4.47) we then observe a cancellation between the different terms so that the sum is actually almost as small as the respective combination using the values from the  $(+++)$  parametrisation. This leads to an almost unchanged magnitude of the radiative decays from one case to the other. The  $\mu - e$  conversion rates are also dominated by the photon penguin; however, what enters here

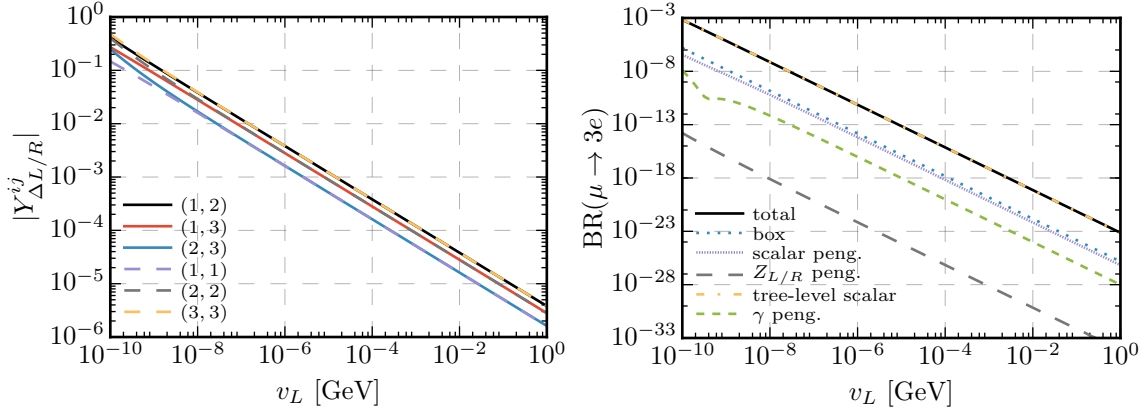


Figure 4.8: Dependence of the triplet Yukawa coupling on left triplet VEV  $v_L$  using the  $(+ - +)$  solution of Eq. (4.40) (left) and the consequential decoupling of the different contributions to  $\mu \rightarrow 3e$  (right).

is the monopole contribution. While the aforementioned cancellation also holds for the diagram where the photon couples to the doubly-charged Higgs, the monopole loop functions differ significantly between the lepton flavours for the diagram where the photon couples to the charged lepton in the loop – therefore spoiling the cancellation. As a result, there is only a partial cancellation and the increase of the conversion rate from the  $(+ + +)$  case to the  $(+ - +)$  case is only about an order of magnitude smaller than for the three-body decays. This observation generalises to the five other sign choices where one sign is different from the two others.

Another consequence of switching to a mixed-sign solution for  $Y_\Delta$ , besides the size of the off-diagonal elements, is the dependence on  $v_L$ : while for the same-sign solutions, the off-diagonals vanished to first approximation, leading to a scaling with  $1/v_L$ , they do not vanish in the mixed-sign case – leading to the same parametric dependence of  $1/\sqrt{v_L}$  as for the diagonal elements. This is depicted in Fig. 4.8 where at the same time we show the decoupling of all contributions to  $\text{BR}(\mu \rightarrow 3e)$ .

Case II:  $M_D \propto M_{\text{up-type}}$

Let us now consider the case where  $M_D$  is proportional to the up-type quark matrix. This choice is motivated from SO(10) unification, where one typically expects unification of the up-and down-type Yukawas. While the individual couplings run differently when evolved from the high to the low scale,<sup>5</sup> let us assume for simplicity that the hierarchy in the diagonal Yukawa entries remains approximately unchanged. In an SO(10) unification context, one would also expect a non-trivial flavour structure in the up-type Yukawa couplings. We will address this case in the next subsection 4.3.2 and first consider a diagonal  $M_D$  here. Obviously, because of the large hierarchy in  $M_{\text{up-type}}$  any solution to Eq. (4.40) also requires a hierarchical structure of  $Y_\Delta$ , resulting in  $m_{\nu_R}^{(e)}/m_u \simeq m_{\nu_R}^{(\mu)}/m_c \simeq m_{\nu_R}^{(\tau)}/m_t$ .

<sup>5</sup> This of course depends on details of the intermediate symmetry breaking steps and the scales where this occurs.

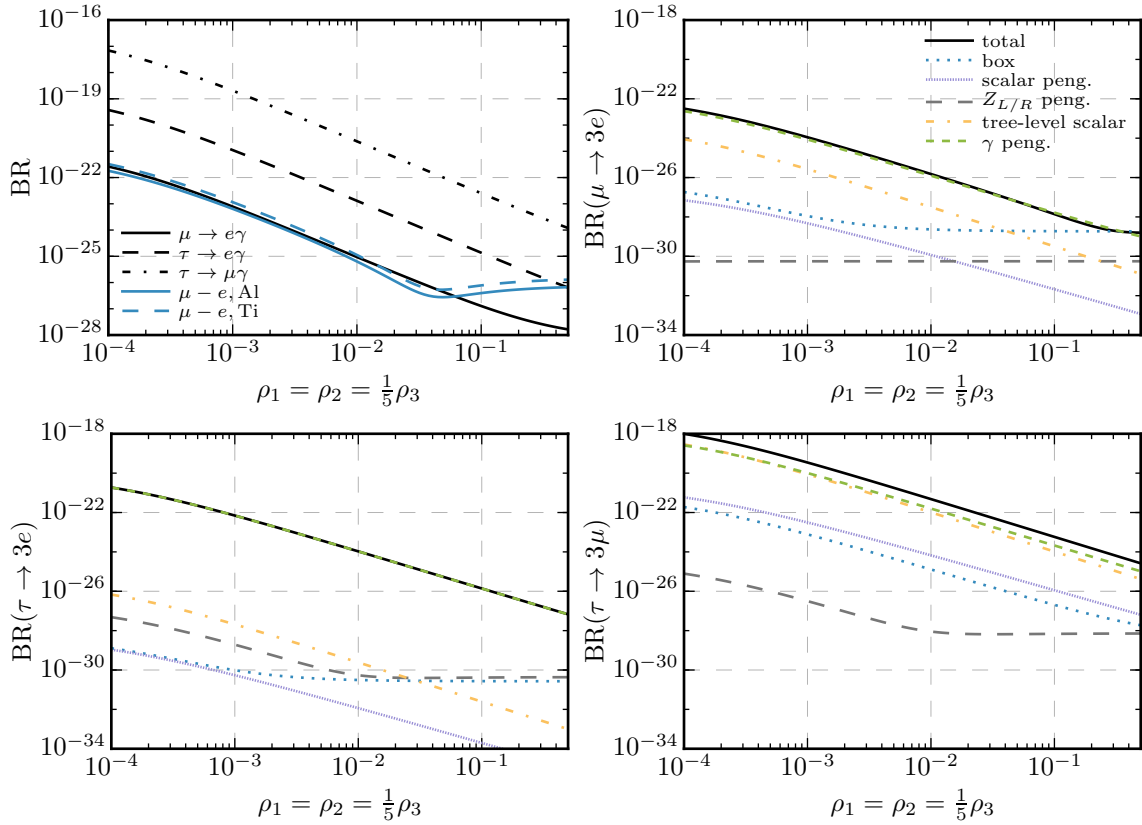


Figure 4.9: A cross-section of different LFV observables for the choice  $M_D = xM_{\text{up-type}}$ , with  $x = 10^{-2}$ ,  $v_L = 5 \times 10^{-5}$  GeV and the Yukawa solution sign choice  $(+++)$ .

$(+++)$  **Solution.** As an explicit example, for  $v_L = 5 \times 10^{-5}$ ,  $x = 10^{-2}$  and this sign choice the triplet Yukawa reads

$$Y_{\Delta}^{(+++)} = \begin{pmatrix} 1.77 \times 10^{-5} & -5.63 \times 10^{-8} & 1.18 \times 10^{-8} \\ -5.63 \times 10^{-8} & 8.98 \times 10^{-3} & -1.50 \times 10^{-7} \\ 1.18 \times 10^{-8} & -1.50 \times 10^{-7} & 1.23 \end{pmatrix}. \quad (4.48)$$

Compared to the case with flavour-universal  $M_D$ , the resulting off-diagonal structure of  $Y_{\Delta}$  is far less intuitive as the solutions to the respective matrix elements of Eq. (4.40) are more involved.<sup>6</sup>

What one can already deduce for the relative magnitude of LFV decays is that  $\tau \rightarrow 3\mu$  will have the largest rates: for this decay, the combination of couplings which enter the tree-level decay mediated by  $H^{\pm\pm}$  is  $Y_{\Delta}^{(2,3)}Y_{\Delta}^{(2,2)}$ . For  $\tau \rightarrow 3e$ , in turn, it is  $Y_{\Delta}^{(1,3)}Y_{\Delta}^{(1,1)}$ .

<sup>6</sup> Note that this Yukawa structure leads to a lightest right-handed neutrino which is lighter than the  $\tau$ . However, due to the suppression of the corresponding  $\tau$  decay by the scale of the  $W_R$  boson, the  $\tau$  branching ratios will not be changed in an observable way. Similarly, the decays of heavy mesons also do not yet place any constraints on this scenario.

As  $Y_{\Delta}^{(1,1)} \simeq m_u/m_c Y_{\Delta}^{(2,2)}$ , there is a large hierarchy to be expected between these observables. Furthermore, we can have the case that for three-body decays ending in a  $e^+e^-$  pair, loop-induced diagrams dominate over the tree-level mediation for the same reason. Consider again  $\tau \rightarrow 3e$ : the small  $Y_{\Delta}^{(1,3)}Y_{\Delta}^{(1,1)}$  factor always enters the tree-level amplitude, making it small. In the vector penguins, there is for instance a contribution which involves a  $H^{\pm\pm} - e$  loop, scaling with the same combination of matrix entries. In addition, however, there's the  $H^{\pm\pm} - \tau$  loop, scaling with  $Y_{\Delta}^{(3,3)}Y_{\Delta}^{(1,3)}$ . The respective amplitude can therefore become even larger than the tree-level contribution despite the loop suppression. For the decay  $\tau \rightarrow 3\mu$ , not only is the tree-level contribution correspondingly larger but also the vector penguin as  $Y_{\Delta}^{(3,3)}/Y_{\Delta}^{(2,2)} \simeq m_t/m_c \simeq \mathcal{O}(16\pi^2)$ . Therefore the corresponding one-loop amplitude is as important as the tree-level contribution. This is explicitly seen in Fig. 4.9 where we show the dependence of various LFV observables<sup>7</sup> on the mass scale of the scalar sector using the  $(+++)$  solution for  $Y_{\Delta}$ , in analogy to Fig. 4.5. Since the LFV  $\mu$  decays are suppressed w.r.t. the LFV  $\tau$  decays due to the smaller Yukawa couplings involved, those diagrams which involve gauge couplings and which are hence independent of the scale of the scalar sector become relevant much earlier. This is most prominently seen in the  $\mu \rightarrow 3e$  as well as  $\mu - e$  conversion rates which are dominated by  $W_{L/R} - \nu_R$  box diagrams for  $\rho_1 \gtrsim 0.3$  and  $0.1$ , respectively. Note that the small dip of the  $\mu - e$  conversion rates around  $\rho_1 \simeq 4 \times 10^{-2}$  is a result of a destructive interference between the box diagrams and the  $\gamma$  penguins. The rates however approach a constant value once the photonic contribution decouples and the box diagrams dominate which is seen at larger  $\rho_1$  values.

In Fig. 4.10 we then show the decoupling behaviour for two different choices of  $x$  as the triplet Yukawa VEV  $v_L$  is varied over the allowed domain.<sup>8</sup> The case that  $x = 10^{-2}$  corresponds to the parameter choice used for the discussion to this point, and the same arguments hold in what concerns the dominance of the  $\gamma$  penguins for the entire range of  $v_L$ , as explicitly depicted for  $\mu \rightarrow 3e$  in Fig. 4.10. Here we have the situation that  $B_D^{(i,i)} \ll \sqrt{v_L/v_R}$  for all shown  $v_L$  choices. As discussed before for the  $M_D \propto 1$  case and illustrated in Section 4.2.2, for the sign choice  $(+++)$  all off-diagonal terms vanish at leading order. Subsequently, the numerical calculation yields heavily suppressed off-diagonal entries that scale as  $1/v_L$ . In the case that  $x = 10^{-5}$ , all off-diagonal  $Y_{\Delta}$  entries still scale with  $1/v_L$ . The diagonal elements, however, show differences: the approximation  $B_D^{(i,i)} \ll \sqrt{v_L/v_R}$  only holds for  $i = 3$  over the entire range of  $v_L$ . For  $i = 1, 2$ ,  $B_D^{(i,i)} \simeq \mathcal{O}\left(\sqrt{v_L/v_R}\right)$  for small values of  $v_L$ . Therefore, just like the off-diagonal terms which are generated by the first non-vanishing order in  $B_D^{(i,i)}/\sqrt{v_L/v_R}$ , also the diagonal  $Y_{\Delta}^{(i,i)}$  elements scale as  $1/v_L$  for small  $v_L$  values. For increasing  $v_L$ , first the  $(2, 2)$  and then also the  $(1, 1)$  elements fall into the limit  $B_D^{(i,i)} \ll \sqrt{v_L/v_R}$ , eventually resulting in a decoupling at a rate proportional to  $1/\sqrt{v_L}$ . As a result, the  $\gamma$  penguin

<sup>7</sup> Note that the overall size of the different flavour observables is typically unobservable even with the upcoming projections noted in Table 4.1. However, this particular choice of  $x$  and  $v_L$  serves as a useful benchmark point to highlight the differences when considering both the different  $M_D$  choices proportional to  $M_{\text{up-type}}$  and different sign choices of the Yukawa solutions in the forth-coming sections.

<sup>8</sup> The  $v_L$  domains between the different choices of  $x$  differ due to the triplet Yukawa parametrisation. For  $x = 10^{-2}$  values of  $v_L$  smaller than approximately  $10^{-5}$  GeV lead to non-perturbative couplings, while for both cases values of  $v_L$  greater than  $\mathcal{O}(1 \text{ GeV})$  are not permitted due to constraints from the rho-parameter.

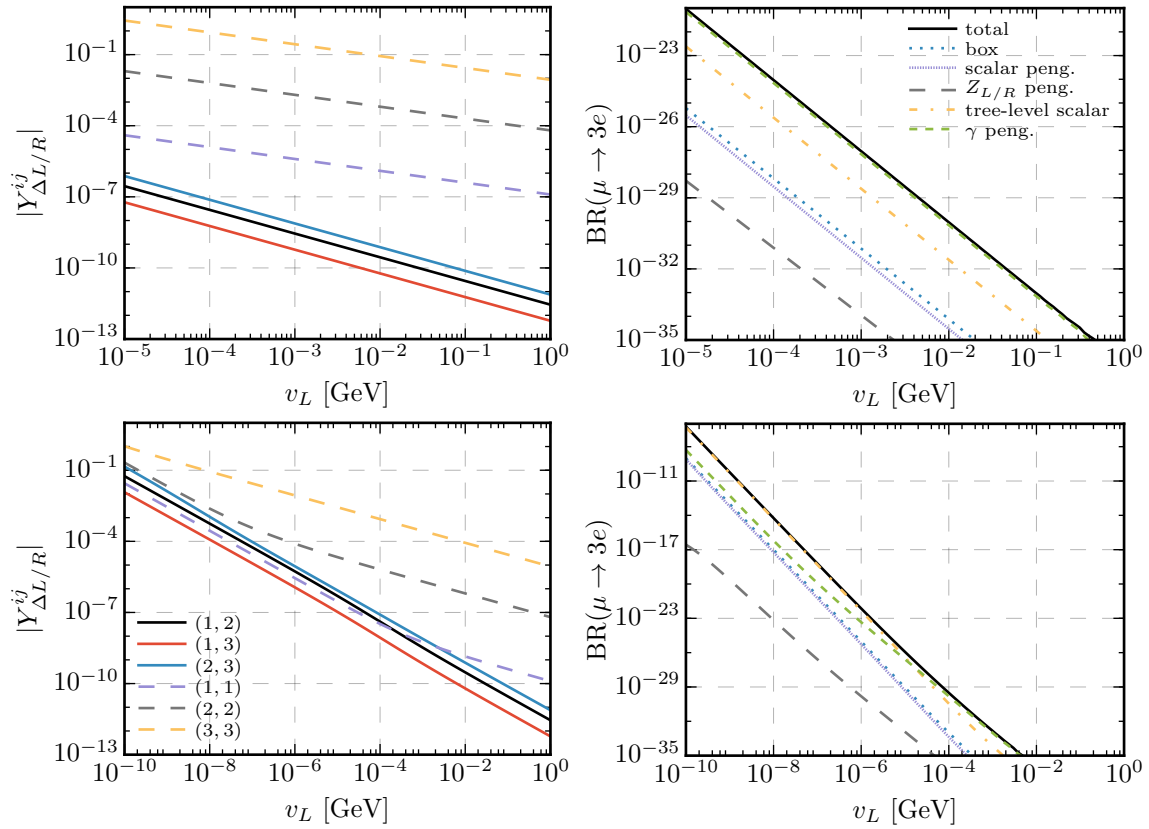


Figure 4.10: Illustration of the different decoupling behaviour resulting from varying  $v_L$  for different  $x$  values, using  $M_D = M_{\text{up-type}}$  and the  $(+++)$  sign choice. Here  $v_L$  is varied between the allowed regions, where the lower bound arises from non-perturbative couplings and the upper bound  $v_L = 1$  GeV from the rho-parameter. The top and bottom rows correspond to  $x = 10^{-2}$  and  $x = 10^{-5}$  respectively.

dominance in  $\mu \rightarrow 3e$  only kicks in for  $v_L \gtrsim 10^{-5}$  GeV. Before that,  $Y_{\Delta}^{(1,1)} \gg m_u/m_c Y_{\Delta}^{(2,2)}$ , giving a boost to the tree-level contribution.

**(+ - +) Solution.** As for the  $M_D \propto \mathbb{1}$  case, we now turn to a different solution to  $Y_{\Delta}$  for the same input parameters. As described in Section 4.2.2, the effect of switching to a  $(+ - +)$  solution rather than the  $(+++)$  solution is not qualitatively different to the case  $M_D \propto \mathbb{1}$  given that  $B_D^{(i,i)} \ll \sqrt{v_L/v_R}$ . First we consider varying the scalar sector choosing  $x = 10^{-2}$  and  $v_L = 5 \times 10^{-5}$  GeV. This results in a triplet Yukawa that reads

$$Y_{\Delta}^{(+ - +)} = \begin{pmatrix} 1.74 \times 10^{-5} & -7.00 \times 10^{-5} & 9.25 \times 10^{-5} \\ -7.00 \times 10^{-5} & -8.61 \times 10^{-3} & 2.33 \times 10^{-2} \\ 9.25 \times 10^{-5} & 2.33 \times 10^{-2} & 1.20 \end{pmatrix}. \quad (4.49)$$

The results of these choices are shown in Fig. 4.11 as a function of the triplet-scalar masses. In comparison to Fig. 4.9, many of the flavour observables are within reach of current or upcoming experiments. In this region of parameter space the change of sign does not modify

the relative size of the  $Y_{\Delta}^{(1,1)}$  or  $Y_{\Delta}^{(2,2)}$  entries. Correspondingly, for  $\mu \rightarrow 3e$  and  $\tau \rightarrow 3e$  the dominant modes remain the  $\gamma$  penguins. These observables are however far larger as the corresponding off-diagonal Yukawas  $Y_{\Delta}^{(1,2)}$  and  $Y_{\Delta}^{(1,3)}$  are typically four orders of magnitude larger compared to the  $(+++)$  sign choice. Additionally, since  $Y_{\Delta}^{(2,3)}$  has changed by five orders w.r.t. to the  $(+++)$  choice, the ratio of  $\text{BR}(\tau \rightarrow 3\mu)/\text{BR}(\mu \rightarrow 3e)$  is increased by two orders of magnitude.

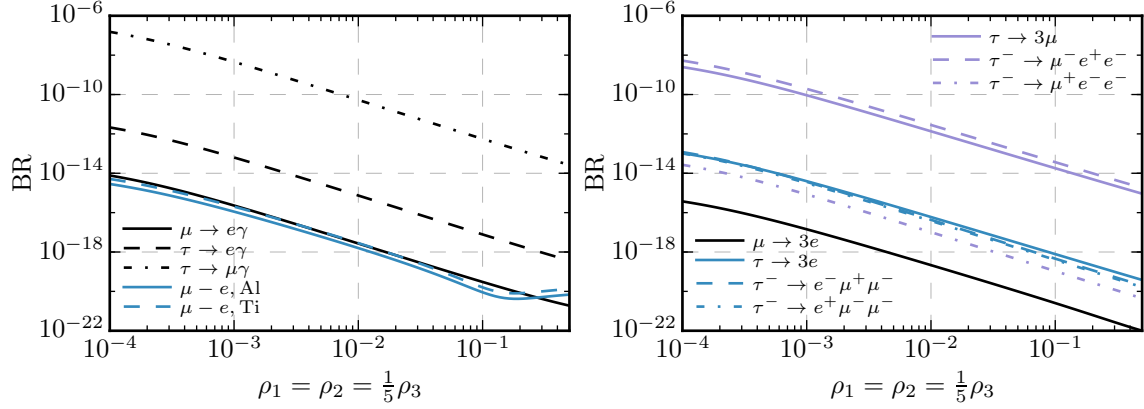


Figure 4.11: A cross-section of different LFV observables for the choice  $M_D = xM_{\text{up-type}}$ , with  $x = 10^{-2}$ ,  $v_L = 5 \times 10^{-5}$  GeV and the Yukawa solution sign choice  $(+ - +)$ .

Case III:  $M_D \propto V_{\text{CKM}}^\dagger M_{\text{up-type}} V_{\text{CKM}}$

Let us now go ahead and consider  $M_D = xV_{\text{CKM}}^\dagger M_{\text{up-type}} V_{\text{CKM}}$ , which is motivated by Yukawa unification due to the intimate connection between the up- and down-type Yukawas.<sup>9</sup> We once again start by considering the  $(+++)$  sign choice,  $v_L = 5 \times 10^{-5}$  GeV and  $x = 10^{-2}$ , completely analogous to the previous subsection. This results in a triplet Yukawa of the form

$$Y_{\Delta}^{(+++)} = \begin{pmatrix} 4.87 \times 10^{-4} & 2.14 \times 10^{-3} & 4.12 \times 10^{-3} \\ 2.14 \times 10^{-3} & 1.06 \times 10^{-2} & 5.01 \times 10^{-2} \\ 4.12 \times 10^{-3} & 5.01 \times 10^{-2} & 1.22 \end{pmatrix}. \quad (4.50)$$

Multiplication of the CKM matrix on both sides results in a slight decrease of the hierarchy amongst the diagonal entries and an increase in the size of the off-diagonal entries, similar to the case where  $M_D = M_{\text{up-type}}$  with the  $(+ - +)$  sign choice. Shown in Fig. 4.12 is the effect of varying the triplet scalar sector with this choice of the triplet-Yukawa. Note that all of the parameter space shown in this figure could be probed by the proposed PRISM/PRIME experiment for  $\mu - e$  conversion [420, 421]. In Fig. 4.13, we further decompose the rate into the dif-

<sup>9</sup> In LR-symmetric theories, the up-type mass matrix can be written as  $m_u = V_{\text{CKM}}^{L\dagger} m_u^{\text{diag}} V_{\text{CKM}}^R$ , where  $m_u^{\text{diag}} = M_{\text{up-type}}$ ,  $V_{\text{CKM}}^L = V_{\text{CKM}}$  is the usual CKM matrix and  $V_{\text{CKM}}^R$  is the according quantity in the  $\text{SU}(2)_R$  sector. Parity symmetry relates  $V_{\text{CKM}}^R = V_{\text{CKM}}^L$  (up to a diagonal matrix of free phases on either side which we choose to set to zero here) so that  $m_u = V_{\text{CKM}}^\dagger M_{\text{up-type}} V_{\text{CKM}}$ . See also the Appendix A in Ref. [401].

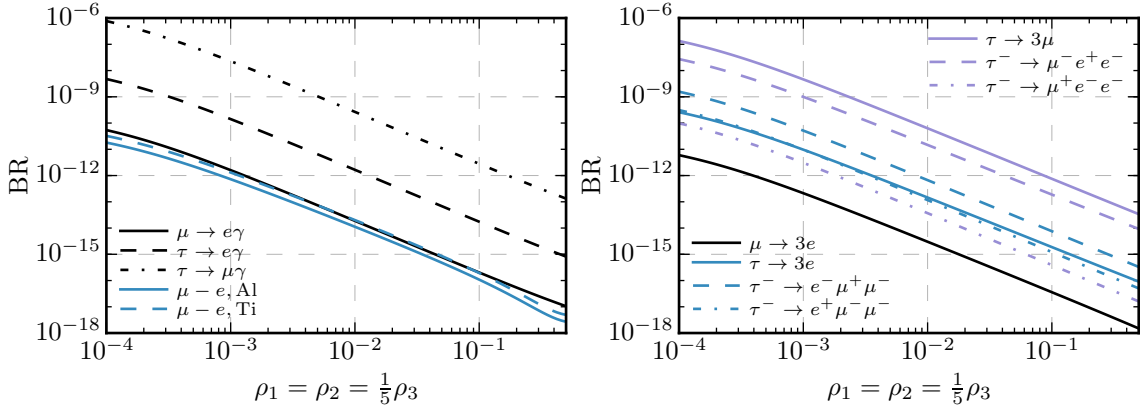


Figure 4.12: A cross-section of different LFV observables for the choice  $M_D = x V_{\text{CKM}}^\dagger M_{\text{up-type}} V_{\text{CKM}}$ , with  $x = 10^{-2}$ ,  $v_L = 5 \times 10^{-5}$  GeV and the Yukawa solution sign choice  $(+++)$ .

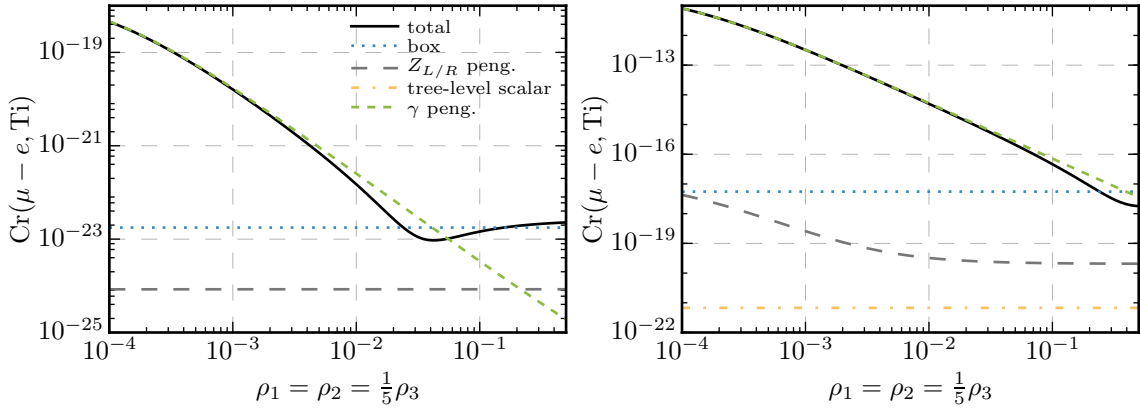


Figure 4.13: The  $\mu - e$  conversion rates in Ti when varying the triplet scalar sector for the choice  $v_L = 10^{-6}$  GeV and the sign choice  $(+++)$  for the solution of the triplet-Yukawa. Two different choices of  $M_D$  are made:  $M_D = x M_{\text{up-type}}$  on the left-hand panel and  $M_D = x V_{\text{CKM}}^\dagger M_{\text{up-type}} V_{\text{CKM}}$  on the right-hand panel, where in both cases  $x = 10^{-3}$ .

ferent contributions, directly comparing the  $M_D = M_{\text{up-type}}$  and  $M_D = V_{\text{CKM}}^\dagger M_{\text{up-type}} V_{\text{CKM}}$  scenarios. Here, the size of the  $\gamma$  penguin contribution is determined by the sum of the product of couplings  $\sum_i Y_\Delta^{(2,i)} Y_\Delta^{(i,1)}$  which increases from the former to the latter  $M_D$  choice. Note that, due to the large off-diagonal entries in Eq. (4.50), the combination  $Y_\Delta^{(2,3)} Y_\Delta^{(3,1)}$  becomes sizeable, two orders of magnitude larger than  $Y_\Delta^{(2,2)} Y_\Delta^{(2,1)} + Y_\Delta^{(2,1)} Y_\Delta^{(1,1)}$  which is the relevant contribution for the  $M_D \propto M_{\text{up-type}}$  choice. Additionally, multiplication by the CKM matrix also introduces contributions arising from the bidoublet scalar sector. However, under the given constraints that the heavy bidoublet Higgs mass is around 20 TeV, these contributions are extremely sub-dominant. This contribution can nevertheless be seen in the right-hand panel of Fig. 4.13.

In the considered case  $M_D \propto V_{\text{CKM}}^\dagger M_{\text{up-type}} V_{\text{CKM}}$ , the effect of switching to a different sign

choice is less drastic than in the diagonal  $M_{\text{up-type}}$  case. The reason is that with the inherently flavour-violating nature of  $M_D$ , there is already a direct flavour-violating insertion into  $Y_\Delta$ . A change from a same-sign to a mixed-sign solution still has an impact here, but it is no longer as pronounced as in the case with diagonal  $M_D$ . As a result, while all LFV observables are generically two orders of magnitude larger than in the  $(+++)$  case, the relative magnitude of the observables remains almost unchanged. A parameter point with a certain value of  $v_L$  and the  $(+++)$  solution is therefore almost indistinguishable from the same point with larger  $v_L$  but the  $(+-+)$  solution.

To conclude this section we show in Fig. 4.14 the equivalent of Fig. 4.10 for the choice  $M_D = V_{\text{CKM}}^\dagger M_{\text{up-type}} V_{\text{CKM}}$ , namely the variation of  $v_L$  given two different choices of  $x$ . For the choice  $x = 10^{-2}$  we see that all entries of  $Y_\Delta$  decrease at the same rate. This is a direct consequence of the multiplication by the CKM matrix. Subsequently we see that the  $\gamma$  penguins and tree-level contributions to  $\mu \rightarrow 3e$  are of comparable size. Additionally we observe that the box and  $Z_{L/R}$ -penguin diagrams do not completely decouple with increasing  $v_L$ . This is due to the  $W_{L/R} - \nu_R$  loops which are independent of  $v_L$ . However, the actual rates in this region of parameter space will not be directly probed in upcoming experiments. Lastly we consider the case where  $x = 10^{-5}$ . Here, we observe that we end up in regions where the triplet Yukawa entries change sign (seen as the dips in the figure) in addition to the change in decoupling behaviour due to the relative sizes of  $B_D$  and  $\sqrt{v_L/v_R}$  as was already observed for the case  $M_D = M_{\text{up-type}}$ .

## Impact of the CP phase

So far we have always assumed the CP phase to be zero. However, this need not be the case. Actually, recent fits even slightly prefer an angle of  $\delta_{\text{CP}} \simeq 3\pi/2$  [433]. Therefore we discuss here the impact of the CP phase on the LFV observables and consider scenarios which are parity-symmetric. When looking at the parametrization of  $Y_\Delta$  according to Eq. (4.40) one readily sees that  $B_D$  becomes complex, requiring the rotation matrix  $R$  to be a complex unitary matrix. As explained in Section 4.2.2, the effect is similar to switching from a  $(\pm\pm\pm)$  solution to a mixed-sign solution namely. This holds even in the case where  $M_D$  is diagonal and  $\sqrt{v_L/v_R} \gg B_D^{(i,i)}$ , off-diagonal  $Y_\Delta$  entries are already induced at the zeroth order in  $B_D/\sqrt{v_L/v_R}$ . Therefore, when turning on  $\delta_{\text{CP}}$  in the case of diagonal  $M_D$  and a  $(\pm\pm\pm)$  choice, large differences of the LFV observables are expected w.r.t. the  $\delta_{\text{CP}} = 0$  case. In those cases, however, where there is either a mixed-sign choice or a non-diagonal  $M_D$  such as in Section 4.3.2, the effect is far less pronounced.

We show this behaviour in Fig. 4.15 with the parametrisation  $M_D \propto \mathbb{1}$ , both the  $(+++)$  and  $(+-+)$  solutions. While there are many orders of magnitude difference between the cases of zero and maximal CP phase when applying the  $(+++)$  solution, the differences are only of  $\mathcal{O}(1)$  in case of  $(+-+)$ . The same arguments hold for the other  $M_D$  parametrisations; we observe large differences in LFV rates between different CP phases for the diagonal  $M_{\text{up-type}}$  and  $(+++)$  choice but only comparably small changes in the other cases. This is clearly illustrated in the next subsection where we show our main results in the cases where  $\delta_{\text{CP}} = 0$  and  $\delta_{\text{CP}} = 3\pi/2$ .

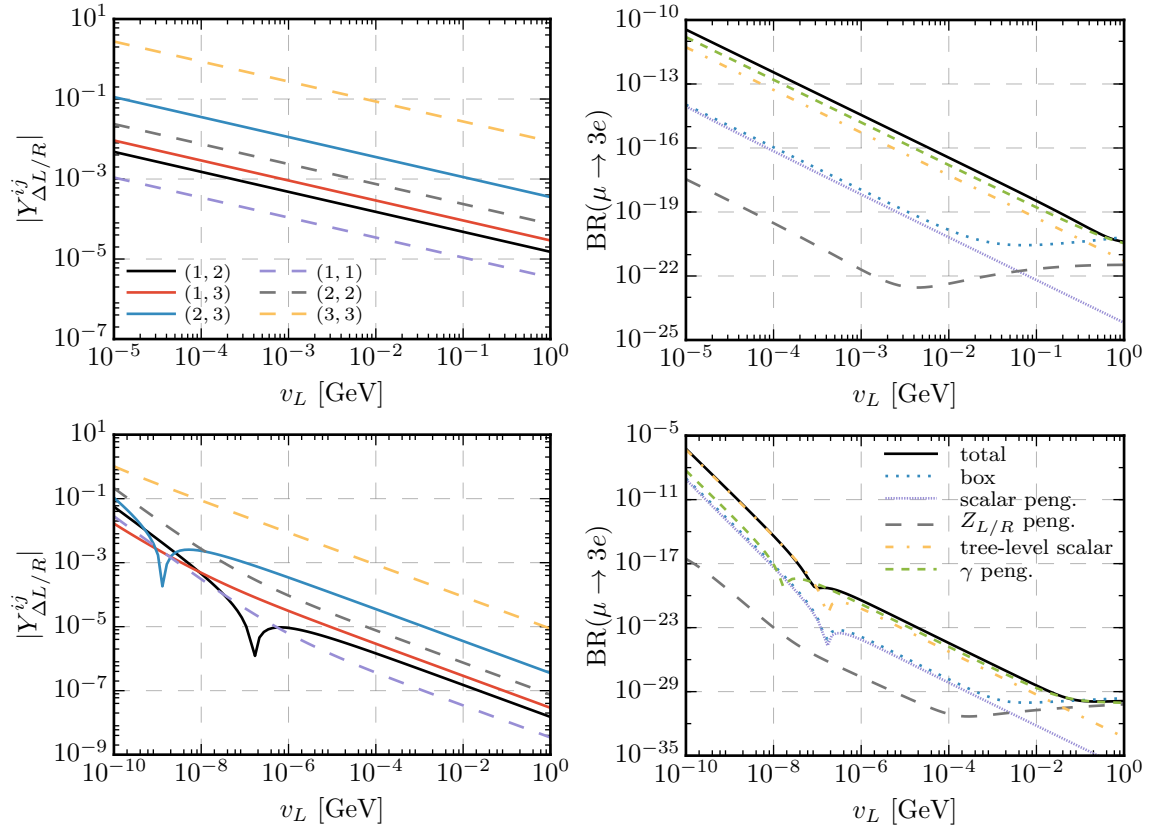


Figure 4.14: Illustration of the different decoupling behaviour resulting from varying  $v_L$  with  $M_D = V_{\text{CKM}}^\dagger M_{\text{up-type}} V_{\text{CKM}}$  using different  $x$  values and the (+ + +) choice. Here  $v_L$  is varied between the allowed regions, where the lower bound arises from non-perturbative couplings and the upper bound  $v_L \sim \mathcal{O}(\text{GeV})$  from the rho-parameter. The top and bottom rows correspond to  $x = 10^{-2}$  and  $x = 10^{-5}$  respectively.

Clearly, allowing for complex phases in the neutrino and, thus, in the Yukawa sector will give rise to an electric dipole moment (edm) for the leptons. Here in particular the bound on the electron is rather severe as its edm must be below  $8.7 \times 10^{-29} \text{ ecm}$  [405]. In the parameter region of Fig. 4.15 we find values of up to approximately  $10^{-33}$  where the main contribution is due to the doubly charged Higgs bosons. However, this contribution is suppressed as one can show that in the limit  $m_F/m_B \rightarrow 0$  the contribution to the edm vanishes [439], where  $m_F$  and  $m_B$  are the masses of the fermion and the boson in the loop. The other potentially dangerous contribution due to the singly charged Higgs boson is suppressed because the lighter one is essentially the  $\Delta_L$  and, thus, the corresponding fermion is the left-handed neutrino. The contribution of the heavier state is suppressed by its mass of around 20 TeV. As a result the electron edm will likely not be testable at the upgraded ACME experiment [440].

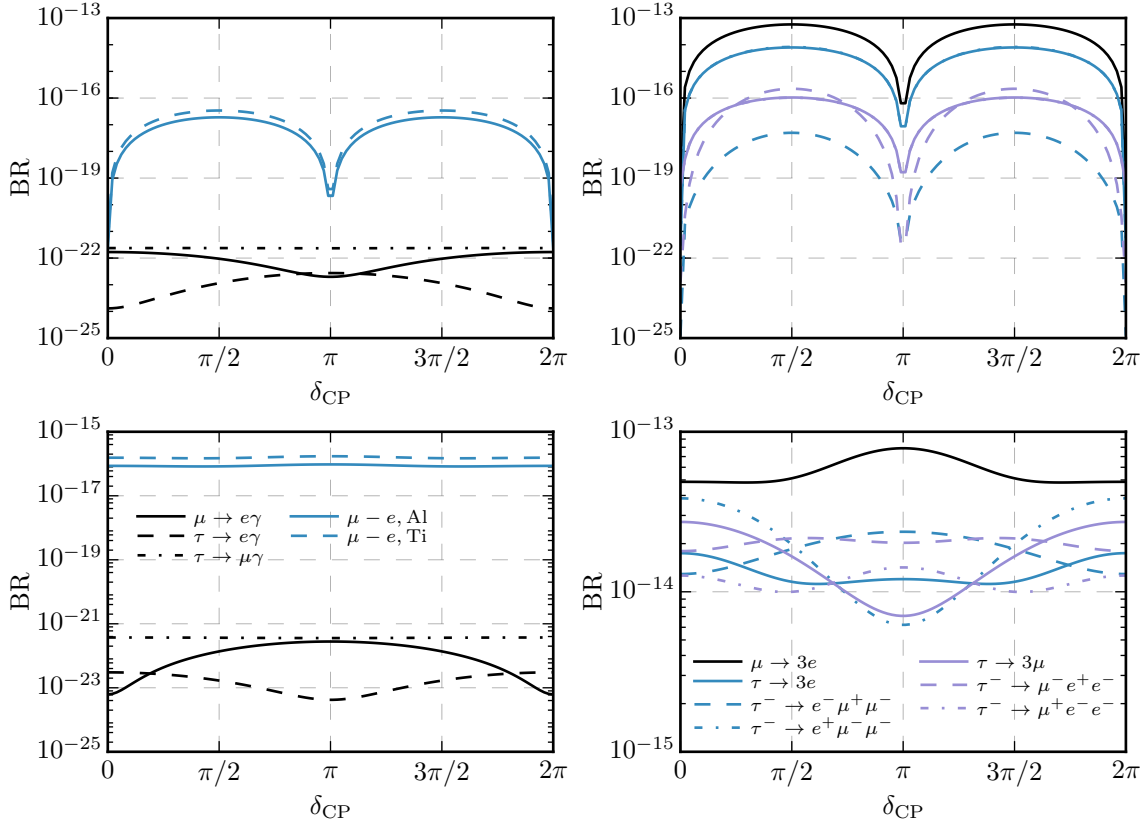


Figure 4.15: The main LFV observables varying the  $\delta_{\text{CP}}$  phase for  $M_D = 1 \text{ MeV}$ , and  $v_L = 10^{-5} \text{ GeV}$ . The top row corresponds to the  $(+ + +)$  solution while the bottom row corresponds to the  $(+ - +)$  solution.

## Measurement prospects

In this section we ask the question: what are the prospects of measuring a signal of lepton flavour violation given a triplet scalar sector with masses at the TeV scale? Here, we choose the scalar sector and model parameters according to Table 4.2. For each parametrisation of  $M_D$  we perform 2D scans in both  $v_L$  as well as the overall scale of  $M_D$  which we define, as before, by the continuous parameter  $x$ . While the structure of  $Y_\Delta$  is determined by the parametrisation of  $M_D$  as well as by the choice of one of the eight possible solutions to Eq. (4.40), the overall  $Y_\Delta$  magnitude is governed by the sizes of  $v_L$  and  $M_D$ . Therefore, by scanning these two quantities for the different  $M_D$  parametrisations one obtains a robust prediction as to the extent of the parameter space which is probe-able by current and future experiments. It should be noted that the choice of the scalar sector maximises the rates of the flavour observables. In this sense these projections are a best case scenario, as the LHC will begin to increase the bounds on the masses of the triplet-scalar sector.

The results for  $\delta_{\text{CP}} = 0$  are presented in Fig. 4.16: in each panel, we shade the region excluded by current experiments for the most sensitive channels.<sup>10</sup> We also depict the sensit-

<sup>10</sup> All flavour observables that were shown in Section 4.3.2 are considered in Fig. 4.16, however to improve

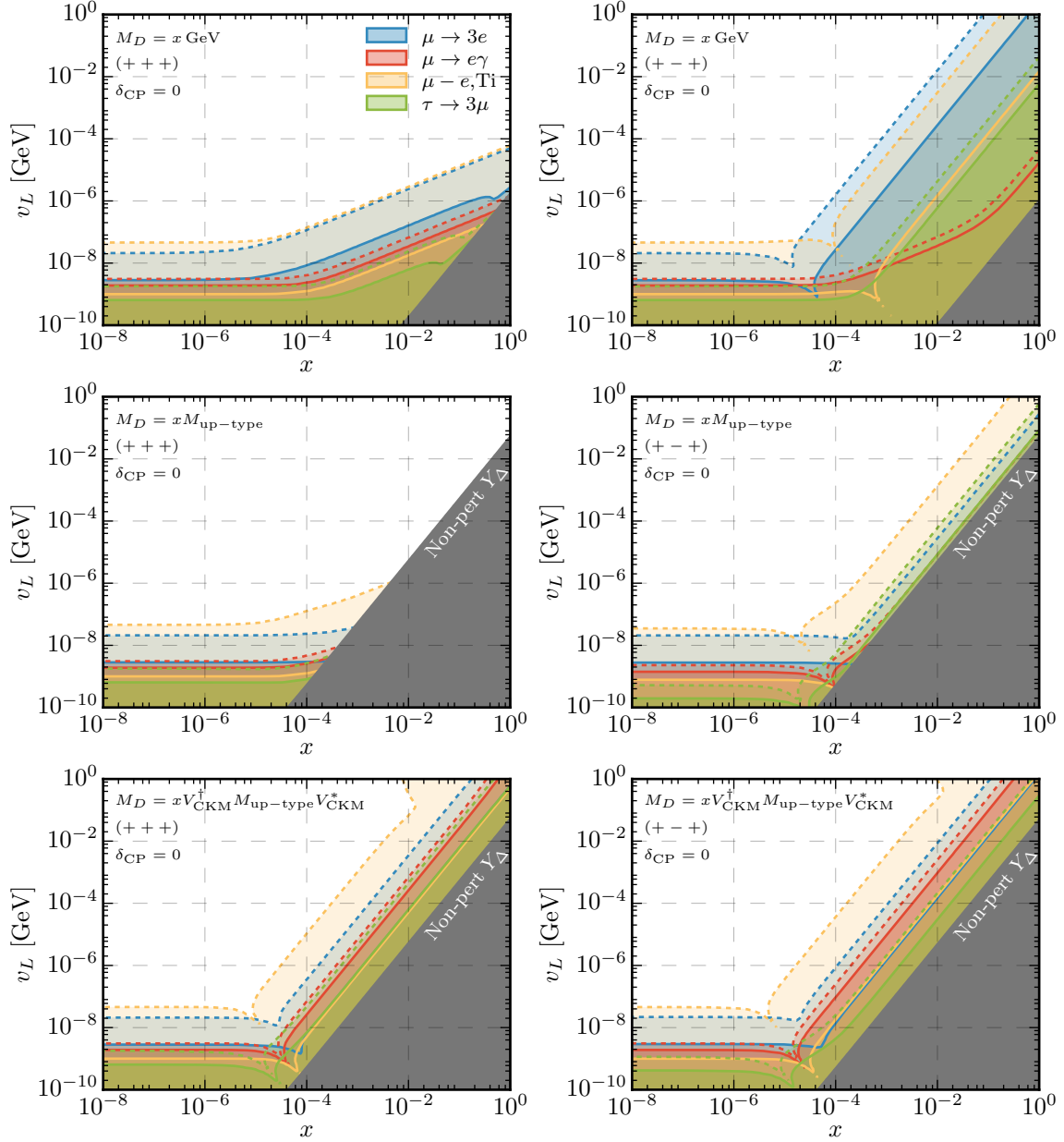


Figure 4.16: Sensitivity of current and future experiments in the  $(x, v_L)$  plane. Solid lines are the current bounds, while the dashed lines are the projected sensitivities of upcoming experiments, see Table 4.1 for the numerical values. The colour scheme for the shaded regions is  $\mu \rightarrow 3e$  (blue),  $\mu \rightarrow e\gamma$  (red),  $\mu - e, \text{Ti}$  (yellow) and finally  $\tau \rightarrow 3\mu$  (green). The non-perturbative regions (grey) correspond to  $\text{Max}(|Y_\Delta|) \geq \sqrt{4\pi}$ .

ivity for future experiments with the lighter shaded regions with a dashed border. The plots have to be read as follows: in the upper left-hand corner of each figure (shown in white), the LFV rates are too small to be measured in the near future. Going to smaller  $v_L$  and larger  $x$  values, the rates increase and many of the current or near-future experiments start to become sensitive.

A generic feature of all plots, irrespective of the  $M_D$  parametrisation or the sign choice, is that the LFV rates are almost independent of  $x$  in the small  $x$  regime. However, at a certain  $x$ -value, depending on both the  $M_D$  choice and the particular observable, the LFV rates begin to increase. The reason is as follows. For small  $x$ ,  $B_D^{(i,i)}$  is of the order of  $\sqrt{v_L/v_R}$  or even larger.<sup>11</sup> This means that the  $M_D$  dependence in

$$Y_\Delta = \frac{1}{2\sqrt{2}v_L} M_D^{(*)1/2} R^* (B_D \pm \sqrt{B_D^2 + 4\alpha}) R^\dagger M_D^{1/2}, \quad (4.51)$$

cancels to first order and the off-diagonal  $Y_D$  structure is determined by the PMNS matrix which enters in the rotation matrix  $R$ . With increasing  $x$ , however, we enter the limit  $\sqrt{v_L/v_R} \gg B_D^{(i,i)}$  and therefore the arguments outlined in Section 4.3.2 hold:

1. if  $M_D$  is diagonal, then for the  $(\pm\pm\pm)$  choices, the  $Y_\Delta$  off-diagonal elements scale with  $x/v_L$
2. for mixed sign choices the entries scale as<sup>12</sup>  $x/\sqrt{v_L}$
3. If, in turn,  $M_D$  contains non-diagonal elements, then the same-sign choices also scale like  $x/\sqrt{v_L}$ . The only difference with respect to the mixed-sign choice being an overall smaller LFV rate.

Let us begin with the parametrisation  $M_D = x\mathbb{1}$  GeV. In the top row of Fig. 4.16 we show the respective planes for both the  $(+++)$  and  $(+-+)$  solutions. As discussed in some detail in Section 4.3.2,  $\mu \rightarrow 3e$  is the observable with the best prospects of being measured in the near future, as there exists no real hierarchy between the  $Y_\Delta$  entries. However, if the PRISM/PRIME experiment reaches the expected sensitivity of  $10^{-18}$  for  $\mu - e$  conversion in Ti, then the future reach will be comparable with the projected sensitivity of the Mu3e experiment [381] for the  $(+++)$  sign choice. Nevertheless, for very small  $x$ -values,  $\mu - e$  conversion is more sensitive for both sign choices. The case  $M_D \propto \mathbb{1}$  also leads to the most drastic change in the region which is experimentally probe-able when changing between the sign choices. Here we see that the change in sign choice drastically increases the rate of the observables in the regime where  $x \gtrsim 10^{-3}$ .

For the case that  $M_D = M_{\text{up-type}}$ , the coverage of both current and upcoming experiments is limited. The vast majority of the sensitive region occurs in the small  $x$  and  $v_L$  regime. For the sign choice  $(+++)$ , there is no prospect of future experiments probing perturbative parameter regions where  $x \geq 2 \times 10^{-3}$  irrespective of the  $v_L$  choice. Whereas, for the mixed

---

readability only the four most sensitive channels are shown in subsequent figures.

<sup>11</sup> Recall that  $B_D = R^\dagger M_D^{-1/2} m_\nu^{\text{light}} M_D^{(*)-1/2} R^*$ .

<sup>12</sup> The LFV amplitudes scale quadratically with  $Y_\Delta$ . However, this is typically the product of a diagonal with an off-diagonal entry of  $Y_\Delta$ . As mentioned above the diagonal entries scale with  $x/\sqrt{v_L}$  in the limit  $\sqrt{v_L/v_R} \gg B_D^{(i,i)}$ , meaning the LFV rates scale with either  $x^4/v_L^3$  or  $x^4/v_L^2$  in the majority of the parameter space.

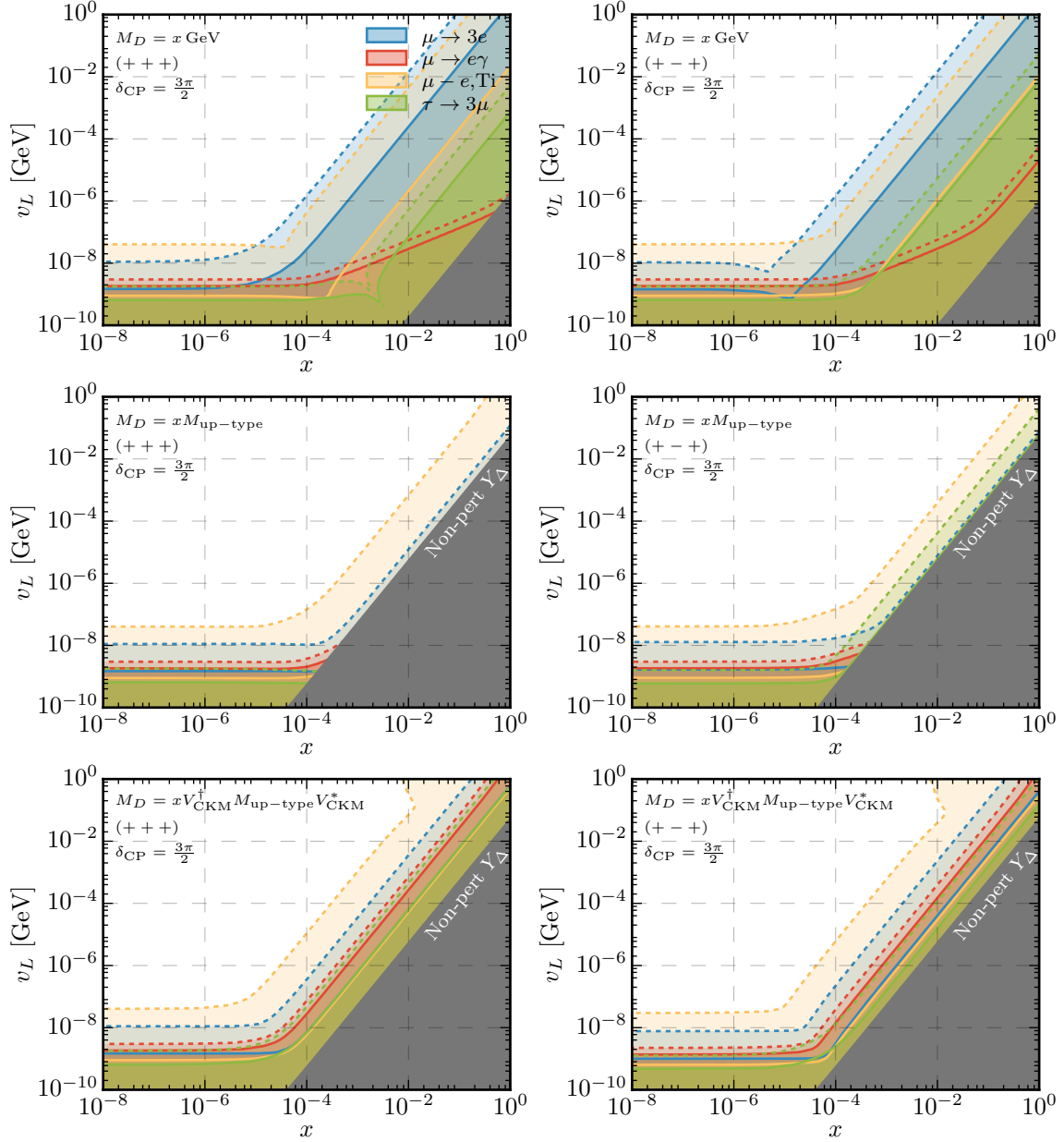


Figure 4.17: Sensitivity of current and future experiments in the  $(x, v_L)$  plane for  $\delta_{\text{CP}} = 3\pi/2$ . Solid lines are the current bounds, while the dashed lines are the projected sensitivities of upcoming experiments, see Table 4.1 for the numerical values. The colour scheme for the shaded regions is  $\mu \rightarrow 3e$  (blue),  $\mu \rightarrow e\gamma$  (red),  $\mu - e, \text{Ti}$  (yellow) and finally  $\tau \rightarrow 3\mu$  (green).

sign choice, future and current experiments have some sensitivity in the regimes where  $Y_{\Delta}^{(3,3)}$  is close to becoming non-perturbative. Interestingly, due to the increased rate of  $\tau \rightarrow 3\mu$  decays, see the discussion in Section 4.3.2, the corresponding measurement prospects for BELLE II [416, 418] are a little higher than for  $\mu \rightarrow 3e$  despite the unprecedented sensitivity of the Mu3e experiment. The sensitivity for small  $x$  regions is largely unchanged between the sign choices. The best future prospects in this case is through the measurement of  $\mu - e$  conversion.

The last remaining choice studied is  $M_D = V_{\text{CKM}}^\dagger M_{\text{up-type}} V_{\text{CKM}}$ , shown in the bottom row of Fig. 4.16. There is an increase of the LFV observables w.r.t. the  $M_{\text{up-type}}$  case in the region  $\sqrt{v_L/v_R} \gg B_D^{(i,i)}$  due to the CKM multiplication, which boosts sensitivities for the large- $x$  region. With upcoming experiments even regions where  $x \simeq 10^{-2}$  and  $v_L \simeq 1$  GeV will be detectable through these observables, in particular  $\mu - e$  conversion in Titanium. The change in shape of the  $\mu - e$  conversion projections for large  $v_L$  are due to the  $W_{L/R} - \nu_R$  boxes which become important in this region of parameter space, see also Fig. 4.13.

Finally we repeat the same procedure for the case  $\delta_{\text{CP}} = 3\pi/2$  in Fig. 4.17, motivated by recent global fits [433]. As discussed in Section 4.3.2, the differences w.r.t. the  $\delta_{\text{CP}} = 0$  case are most drastic for the same-sign solution and a flavour-diagonal  $M_D$  as the LFV rates obtain a significant boost in the regions with large  $x$  due to the non-orthogonality of the rotation matrix  $R$  in the complex case. Therefore, all six cases shown in Fig. 4.17 also feature measurable LFV rates in the large- $x$  regions. Interestingly, due to different cancellations in the different LFV observables due to the complex phase, see also Fig. 4.15, the relative magnitude of some LFV observables is altered. In particular, all the parameter region above  $x \simeq 10^{-4}$  for  $M_D = x M_{\text{up-type}}$  and  $(+-+)$  probe-able by the Mu3e experiment is already excluded by  $\tau \rightarrow 3\mu$ . Here, BELLE II has the best measurement prospects for the near future. However, also for this maximal CP phase, the best prospects in the long run are found in the  $\mu - e$  conversion rate should the PRISM/PRIME experiment reach its expected sensitivity. The  $M_D \propto \mathbb{1}$  case, however, is best probed by Mu3e.

Finally, for completeness, we show the results of current bounds and future sensitivities using the values of Table 4.1 while varying the neutrino masses and hierarchies. Firstly, we show the effect of altering the lightest neutrino mass to  $m_{\nu_1} = 0.1$  eV resulting in a quasi-degenerate light neutrino mass spectrum. The results of which are shown in Fig. 4.18. We then also consider the case of an inverse hierarchy of the neutrino masses. In this scenario the best-fit values used for the neutrino oscillation parameters are those from [428]. Setting  $\delta_{\text{CP}} = 0$  and assuming  $m_{\nu_3} = 10^{-4}$  eV we obtain the results shown in Fig. 4.19. Modifying both of these parameters we observe that the effects are sub-dominant in comparison to the previous results discussed.

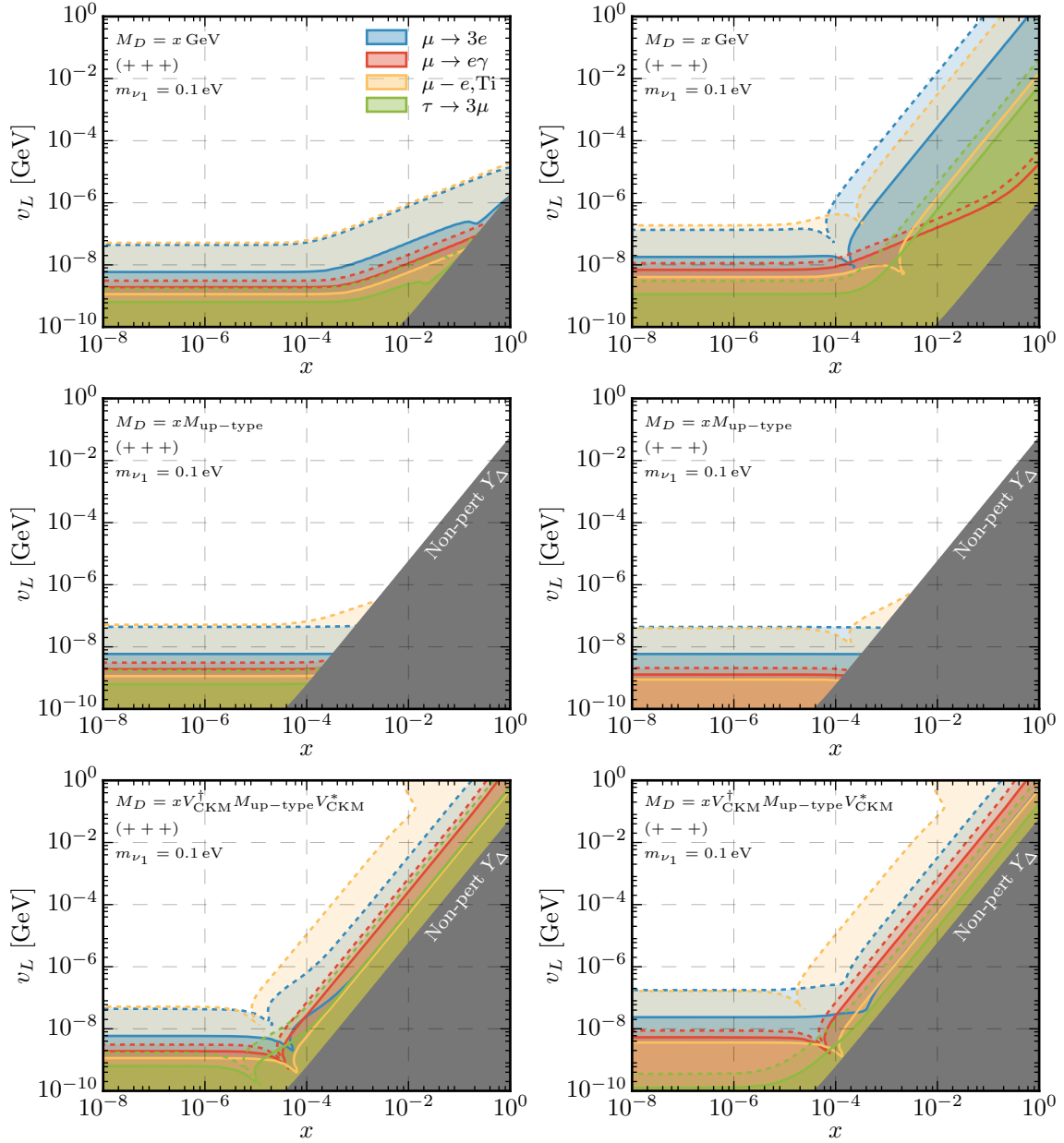


Figure 4.18: Sensitivity of current and future experiments in the  $(x, v_L)$  plane. Here we take  $\delta_{CP} = 0$ , and  $m_{\nu_1} = 0.1 \text{ eV}$  where once again all other model parameters are given in Table 4.2. See Fig. 4.16 for a description of the colours and contours.

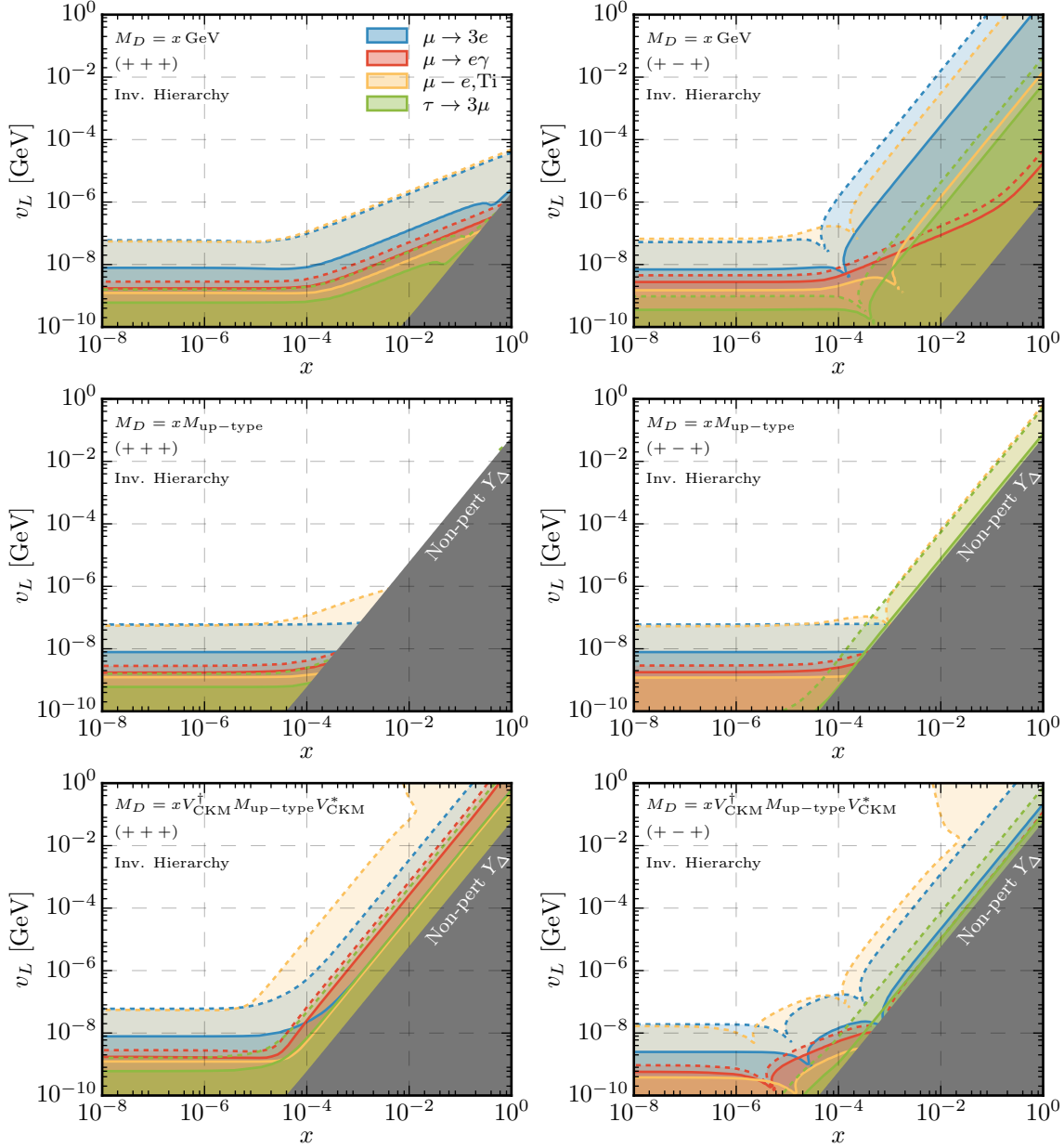


Figure 4.19: Sensitivity of current and future experiments in the  $(x, v_L)$  plane where we assume an inverted neutrino mass hierarchy. Here we take  $\delta_{\text{CP}} = 0$ , and  $m_{\nu_1} = 10^{-4}$  eV where once again all other model parameters are given in Table 4.2. See Fig. 4.16 for a description of the colours and contours.

## 4.4 Conclusion

We have investigated left-right symmetric models containing scalar triplets, paying particular attention to a consistent treatment of the lepton and Higgs sectors. Furthermore, we have advanced a method to consistently calculate the triplet-Yukawa couplings taking into account both the experimental data and the underlying symmetries without any approximations. For a given parameter point in the model there exists an eightfold degeneracy in the solution of the triplet-Yukawas due to different sign choices in the quadratic equations for each fermion generation. We find that these eight cases can be divided into two sub-classes.

The model is completely left-right symmetric in view of its particle content and the differences between the bilinear terms of the scalar potential. We have considered several different realisations of the neutrino Dirac mass term, namely, a flavour diagonal case with either degenerate entries or a hierarchy similar to the up-quark sector as well as a scenario where there is CKM-like mixing. For each case we have studied in detail the consequences for lepton flavour violating observables, considering both classes of sign choice for the triplet-Yukawa solution. Using this knowledge we have surveyed which parts of the parameter space can be probed by upcoming lepton flavour violation experiments. This entailed a calculation of the rates for  $\mu \rightarrow e\gamma$ ,  $\mu \rightarrow 3e$ , their counterparts in the  $\tau$ -sector as well as  $\mu - e$  conversion in heavy nuclei, studying in particular their dependence on the Yukawa couplings as well as on various parameters of the Higgs potential.

Naively one would expect that flavour-violating three-body decays of the leptons, most importantly  $\mu \rightarrow 3e$ , will give the best sensitivity and discovery potential, due to the tree-level contributions via the doubly charged Higgs bosons. While this is correct for some regions of parameter space, we find that there is also a large part where upcoming  $\mu - e$  conversion experiments will be more sensitive. This occurs over the majority of the parameter space due to  $\gamma$ -penguins with charged scalars running in the loops, however for regions where the triplet Yukawas are small, the  $W_{R-\nu_R}$  loop contributions can dominate. These conclusions hold despite the fact that existing electroweak precision data implies that the additional vector bosons are too heavy to be discovered at the 14 TeV LHC.

Given the case that all signs in the solution to the triplet-Yukawa are equal, there are significant differences between the different parametrisations of the Dirac mass term. In particular, the case with a CKM-like flavour mixing in the Dirac mass matrix exhibits LFV rates which are, in most of the parameter space, several orders of magnitude larger than for the other parametrisations. When switching to the other class of sign choices or allowing a non-zero CP phase in the neutrino mixing matrix, the respective differences are reduced.

For completeness we note, that in some parts of the parameter space investigated the doubly charged Higgs bosons are light enough that they might be discovered in the next years at the LHC. However, some are sufficiently heavy that they could only be studied at a 100 TeV  $p$ - $p$  collider.

## Chapter 5

# Supersymmetric Left-Right Models

---

As emphasised throughout this thesis, supersymmetry is one of the leading candidates for BSM physics. However, throughout the previous chapters we have thus far neglected to mention another attractive feature of the MSSM. In contrast to the SM, the MSSM predicts that the three gauge couplings unify in the vicinity of the Planck scale [441–447]. As a result it is often argued that supersymmetry could be the missing ingredient in constructing phenomenologically viable grand unified theories (GUTs) [448]. However, the MSSM alone suffers from two deficiencies. Firstly, as discussed in Chapter 3, there is increasing tension between an acceptable Higgs mass and direct collider constraints with large amounts of fine-tuning necessary [449]. Secondly, the MSSM with the addition of R-parity results in massless neutrinos. Therefore it appears necessary that additional ingredients must be added to the MSSM to rectify these two problems, while also preserving the solution to the hierarchy problem and maintaining gauge coupling unification (GCU).

A possible solution to these problems are supersymmetric variants of the SO(10) GUTs introduced in Chapter 4. In the presence of additional gauge symmetries the Higgs mass can be increased at tree-level leading to enhanced naturalness [450, 451]. Additionally the presence of right-handed neutrinos, as predicted by SO(10) GUT theories, allows for natural see-saw-like mechanisms [452]. A well motivated scenario which has not yet been studied is an SO(10) GUT model which predicts left-right symmetry close to the TeV scale.

There are many different realisations of left-right models proposed in the literature. The most striking difference among different left-right theories can be found in the sector that eventually breaks the larger gauge group down to the SM gauge group. The most appealing choice, as considered in Chapter 4, would be the introduction of  $SU(2)_R$  triplets resulting in an automatic type I see-saw mechanism after left-right symmetry breaking, see, e.g., Refs. [374, 375, 453]. However, the supersymmetric version of this scenario is heavily constrained from vacuum stability arguments [371]. In addition the requirement of gauge coupling unification usually requires the addition of extra intermediate supermultiplets [454]. In the presence of doublets, instead of triplets, supersymmetric models consistent with GCU and a TeV-scale spectrum can be easily found [455, 456].<sup>1</sup> In these models special care must be taken not to destroy the GCU which already works well in the MSSM. In Refs. [455, 456] an exhaustive

---

<sup>1</sup> In the non-supersymmetric case models with triplets and GCU are also possible, see for example Ref. [87].

studies were performed of all possible models exhibiting combinations of the intermediate phases from Eqs. (4.2) to (4.4) with either the left-right symmetric or  $U(1)_{R-L}$ -left-right phase at the TeV-scale. In particular they showed that these intermediate scales, referred to as ‘sliding scales’, could lie anywhere between the GUT and TeV-scale without spoiling GCU. However, requiring these gauge symmetries at the TeV-scale places strong conditions on the particle content of the models.

In this chapter, we study a model where the left-right supersymmetric phase is broken at the TeV-scale. This model is consistent with GCU and contains a minimal set of boundary conditions at the unification scale. The choice of particle content allows the left-right symmetry to be maintained down to energies accessible by the LHC without the need of an intermediate scale. This chapter is organised as follows: First, we discuss the basic model features and the necessary conditions for successful GCU as well as radiative symmetry breaking. We then present the quark and lepton sectors in some detail. In section 5.2, we address the Higgs mass and mixing as well as the expected squark hierarchies which differ from the CMSSM expectations.

## 5.1 The Model

### 5.1.1 Superpotential and Particle Content

We assume that  $SO(10)$  is broken at the GUT scale and below this scale the remaining gauge group is left-right symmetric down to the SUSY scale, i.e.  $\mathcal{G}_{LR} = SU(3)_C \times SU(2)_L \times SU(2)_R \times U(1)_{B-L}$ . The particle content of the model under consideration is given in Table 5.1. Here,  $\Phi$  is a bi-doublet which comes in two generations

$$\Phi^a = \begin{pmatrix} H_d^{a0} & H_u^{a+} \\ H_d^{a-} & H_u^{a0} \end{pmatrix}. \quad (5.1)$$

The SM-like Higgs will be in general a superposition of the four neutral components of these bi-doublets. The conventions for the fields which will be responsible for the breaking of  $SU(2)_R \times U(1)_{B-L}$  are:

$$\chi_c = \begin{pmatrix} \chi_c^0 \\ -\chi_c^- \end{pmatrix}, \quad \bar{\chi}_c = \begin{pmatrix} \bar{\chi}_c^+ \\ -\bar{\chi}_c^0 \end{pmatrix} \quad (5.2)$$

Using this field content the renormalisable superpotential allowed under both the gauge symmetries  $\mathcal{G}_{LR}$  and matter parity [372, 457] is

$$\begin{aligned} W = & Y_{Q_a} Q \Phi^a Q_c + Y_{L_a} L \Phi^a L_c + Y_{\delta_d} Q_c \bar{\chi}_c \delta_d + Y_S L_c \chi_c S + Y_{\Psi} L_c \bar{\chi}_c \Psi_c \\ & + \frac{\mu_S}{2} S^2 + \mu_{\Phi}^{ab} \Phi_a \Phi_b + \mu_{\chi_c} \bar{\chi}_c \chi_c + M_{\delta} \delta_d \bar{\delta}_d + M_{\Psi} \Psi \Psi_c. \end{aligned} \quad (5.3)$$

Here, all generation,  $SU(3)$  and  $SU(2)$  indices are suppressed.

Spontaneous symmetry breaking occurs when the neutral components of  $\Phi$  and  $\chi$ -fields

Field	Multiplicity	$\mathcal{G}_{\text{LR}}$	SO(10) Origin	$\mathbb{Z}_2$
$Q$	3	$(\mathbf{3}, \mathbf{2}, \mathbf{1}, +\frac{1}{3})$	<b>16</b>	-1
$Q_c$	3	$(\bar{\mathbf{3}}, \mathbf{1}, \mathbf{2}, -\frac{1}{3})$	<b>16</b>	-1
$L$	3	$(\mathbf{1}, \mathbf{2}, \mathbf{1}, -1)$	<b>16</b>	-1
$L_c$	3	$(\mathbf{1}, \mathbf{1}, \mathbf{2}, +1)$	<b>16</b>	-1
$S$	3	$(\mathbf{1}, \mathbf{1}, \mathbf{1}, 0)$	<b>1</b>	-1
$\delta_d$	1	$(\mathbf{3}, \mathbf{1}, \mathbf{1}, -\frac{2}{3})$	<b>10</b>	-1
$\bar{\delta}_d$	1	$(\bar{\mathbf{3}}, \mathbf{1}, \mathbf{1}, +\frac{2}{3})$	<b>10</b>	-1
$\Psi, \Psi_c$	2	$(\mathbf{1}, \mathbf{1}, \mathbf{1}, \pm 2)$	<b>120</b>	-1
$\Phi$	2	$(\mathbf{1}, \mathbf{2}, \mathbf{2}, 0)$	<b>10, 120</b>	1
$\chi_c, \bar{\chi}_c$	1	$(\mathbf{1}, \mathbf{1}, \mathbf{2}, \mp 1)$	<b><math>\bar{\mathbf{16}}, \mathbf{16}</math></b>	1

Table 5.1: The matter sector and Higgs sector field content of the supersymmetric left-right model. Generation indices have been suppressed and the index  $c$  refers to the equivalent SM field which transforms under  $SU(2)_R$ . The gauge group is such that  $\mathcal{G}_{\text{LR}} = SU(3)_C \times SU(2)_L \times SU(2)_R \times U(1)_{B-L}$ . Note that We also assume the usual matter parity.

receive vacuum expectation values (VEVs)

$$H_d^{a0} = \frac{1}{\sqrt{2}} (\sigma_d^a + i\varphi_d^a + v_\Phi^{d_a}) , \quad (5.4a)$$

$$H_u^{a0} = \frac{1}{\sqrt{2}} (\sigma_u^a + i\varphi_u^a + v_\Phi^{u_a}) , \quad (5.4b)$$

$$\chi_c^0 = \frac{1}{\sqrt{2}} (\sigma_{\chi_c} + i\varphi_{\chi_c} + v_{\chi_c}) , \quad (5.4c)$$

$$\bar{\chi}_c^0 = \frac{1}{\sqrt{2}} (\bar{\sigma}_{\bar{\chi}_c} + i\bar{\varphi}_{\bar{\chi}_c} + v_{\bar{\chi}_c}) . \quad (5.4d)$$

We make use of the following definitions of the VEVs

$$v_R^2 = v_{\chi_c}^2 + v_{\bar{\chi}_c}^2 , \quad (5.5a)$$

$$v_L^2 = (v_\Phi^{d_1})^2 + (v_\Phi^{d_2})^2 + (v_\Phi^{u_1})^2 + (v_\Phi^{u_2})^2 , \quad (5.5b)$$

where we use three angles to parametrise the VEVs

$$v_\Phi^{u_1} = v_L \sin \beta \sin \beta_u , \quad v_\Phi^{d_1} = v_L \cos \beta \sin \beta_d , \quad (5.6a)$$

$$v_\Phi^{u_2} = v_L \sin \beta \cos \beta_u , \quad v_\Phi^{d_2} = v_L \cos \beta \cos \beta_d . \quad (5.6b)$$

In this parametrisation  $v_L$  is the electroweak VEV and  $\beta$  is the usual mixing angle projecting out the  $SU(2)_L$  would-be-Goldstone bosons as in the MSSM. In general, the gauge symmetries

are broken in two steps

$$\begin{aligned}
 \mathcal{G}_{LR} &\equiv \text{SU}(3)_C \times \text{SU}(2)_L \times \text{SU}(2)_R \times \text{U}(1)_{B-L}, \\
 &\xrightarrow{v_R} \text{SU}(3)_C \times \text{SU}(2)_L \times \text{U}(1)_Y \equiv \mathcal{G}_{SM}, \\
 &\xrightarrow{v_L} \text{SU}(3)_C \times \text{U}(1)_{EM} \equiv \mathcal{G}_{SM}.
 \end{aligned} \tag{5.7}$$

However, if  $v_R$  does not exceed the TeV range, one can assume to a good approximation a one-step breaking  $\mathcal{G}_{LR} \rightarrow \mathcal{G}_{SM}$  which also occurs close to the SUSY breaking scale  $M_{\text{SUSY}} = \sqrt{\tilde{m}_{\tilde{t}_1} \tilde{m}_{\tilde{t}_2}}$ , where  $\tilde{t}_1$  and  $\tilde{t}_2$  are the two mostly stop-like up-type squarks.

We show in Fig. 5.1 the running of the gauge couplings in this model. This shows, the assumption of a left-right breaking close to the TeV scale is consistent with gauge coupling unification. We find that the unification scale is significantly larger than in the MSSM, lying in the range  $(1-4) \times 10^{17}$  GeV. The increased scale of unification arises for two reasons. Firstly, the one-loop threshold corrections are large. This is due to the mass spectrum being spread over several TeV leading to large logarithms in the threshold corrections. Secondly, the beta coefficient of the  $\text{U}(1)_{B-L}$  gauge coupling is large, taking the value  $29/2$ . Consequently the unification scale becomes extremely sensitive on the initial value of  $g_{BL}$ , which also generically receives large corrections due to the thresholds. Subsequently, maintaining gauge coupling unification requires that the mass spectrum of the theory remain as light as possible, leading to the prediction of a small  $\text{SU}(2)_R$  breaking scale. Finally, the running values of the new couplings at  $M_{\text{SUSY}}$  are  $g_{BL} \simeq 0.44$  and  $g_R \simeq 0.59$ .

As a consequence of the symmetry breaking, there are two additional massive gauge boson. Their masses can be approximated by

$$M_{Z'}^2 \simeq \frac{1}{4} \left( (g_{BL}^2 + g_R^2) v_R^2 + \frac{g_R^4}{(g_{BL}^2 + g_R^2)} v_L^2 \right), \tag{5.8a}$$

$$M_{W'\pm}^2 \simeq \frac{1}{4} g_R^2 (v_L^2 + v_R^2). \tag{5.8b}$$

Beside the Weinberg angle, two additional rotation angles for the neutral gauge bosons are required, while only one extra angle is required for the charged gauge bosons. The mixing angles between the mass eigenstates of the new gauge bosons are given by

$$\sin 2\Theta_{ZZ'} \simeq \frac{2g_R^2 v_L^2 \sqrt{g_{BL}^2 g_R^2 + g_L^2 (g_{BL}^2 + g_R^2)}}{(g_{BL}^2 + g_R^2)^2 v_R^2}, \tag{5.9}$$

$$\tan 2\Theta_{WW'} = \frac{4g_L g_R v_L^2}{(g_R^2 (v_L^2 + v_R^2) - g_L^2 v_L^2)} \frac{t_\beta (1 + t_{\beta_d} t_{\beta_u})}{(1 + t_\beta^2) \sqrt{(1 + t_{\beta_d}^2)(1 + t_{\beta_u}^2)}}, \tag{5.10}$$

where we have used the abbreviations  $t_\beta = \tan \beta$ ,  $t_{\beta_u} = \tan \beta_u$  and  $t_{\beta_d} = \tan \beta_d$ .

There are a number of choices for which parameters to solve the six minimisation conditions for the vacuum. Here we solve for the following parameters

$$\{(\mu_\Phi^{(1,1)})^2, B_{\mu_\Phi}^{(1,1)}, B_{\mu_\Phi}^{(1,2)}, B_{\mu_\Phi}^{(2,2)}, \mu_{\chi_c}, B_{\mu_{\chi_c}}\}. \tag{5.11}$$

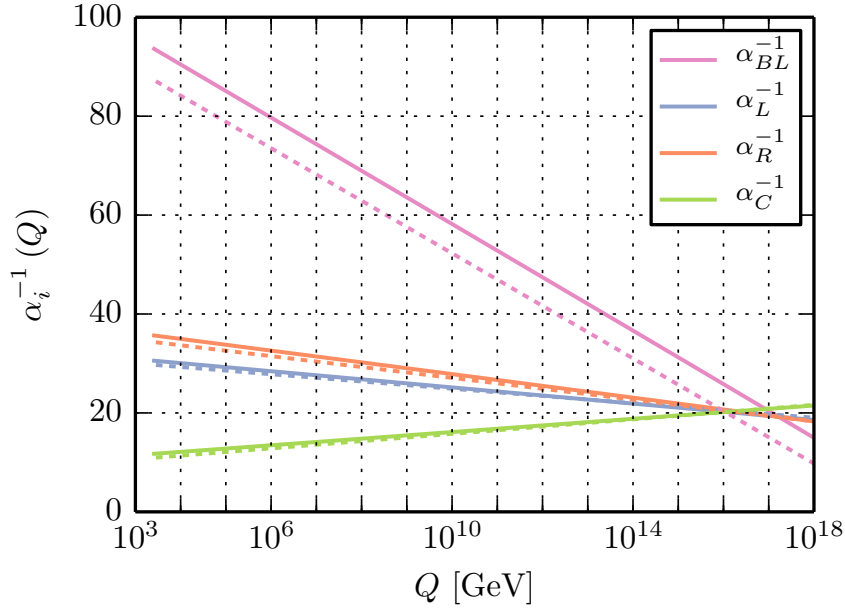


Figure 5.1: Running of the gauge couplings at one-loop (dashed lines) and two-loop (solid lines) in the left-right phase of the model. The two-loop results includes the one-loop threshold corrections arising at both the electroweak and SUSY scales. Additionally the running of the couplings is shown from the SUSY scale rather than the  $SU(2)_R$  breaking scale  $v_R$ . In this figure the GUT normalised  $g_{BL}$  is plotted. The normalisation is given by  $g_{BL} = \sqrt{\frac{3}{2}}g_{BL}^{\text{GUT}}$ . The parameters for the two-loop running are  $t_\beta = 5$ ,  $t_{\beta_u} = 6.5$ ,  $t_{\beta_R} = 0.85$ ,  $m_0 = 1.5$  TeV,  $M_{1/2} = 750$  GeV,  $A_0 = 1$  TeV,  $Y_{\delta_d}^i = 0.15$  and  $v_R = 6$  TeV.

This set of parameters allows for unified soft-masses at the GUT scale while also allowing the minimisation conditions to be solved analytically. The second advantage of this set of parameters is that both  $\mu_{\chi_c}$  and  $B_{\mu_{\chi_c}}$  appear in only two of the six tadpole equations and can therefore be solved independently of the remaining parameters. We obtain

$$|\mu_{\chi_c}|^2 = \frac{1}{2} \left( \left( \Delta m_{\chi_c}^2 - \frac{1}{4} g_R^2 v_L^2 \cos 2\beta \right) \frac{1 + t_{\beta_R}^2}{1 - t_{\beta_R}^2} + \sum m_{\chi_c}^2 - \frac{1}{4} (g_{BL}^2 + g_R^2) v_R^2 \right), \quad (5.12a)$$

$$\simeq \frac{1}{1 - t_{\beta_R}^2} \left( m_{\chi_c}^2 t_{\beta_R}^2 - m_{\tilde{\chi}_c}^2 \right) - \frac{1}{2} M_{Z'}^2, \quad (5.12b)$$

$$B_{\mu_{\chi_c}} = \frac{1}{2} \left( \left( -\Delta m_{\chi_c}^2 + \frac{1}{4} g_R^2 v_L^2 \cos 2\beta \right) \frac{2t_{\beta_R}}{1 - t_{\beta_R}^2} + \frac{1}{4} (g_{BL}^2 + g_R^2) v_R^2 \frac{2t_{\beta_R}}{1 + t_{\beta_R}^2} \right), \quad (5.12c)$$

where  $t_{\beta_R} = \tan \beta_R = v_{\chi_c}/v_{\tilde{\chi}_c}$ ,  $\Delta m_{\chi_c}^2 = m_{\chi_c}^2 - m_{\tilde{\chi}_c}^2$  and  $\sum m_{\chi_c}^2 = -(m_{\chi_c}^2 + m_{\tilde{\chi}_c}^2)$ . We assume that SUSY breaking in the visible sector is triggered by gravity and therefore make use of mSugra-like boundary conditions at the GUT scale, i.e. subsequently we impose the

unification of the following soft-parameters:

$$\begin{aligned} m_0^2 \delta_{ij} &= m_Q^2 \delta_{ij} = m_{Q_c}^2 \delta_{ij} = m_L^2 \delta_{ij} = m_{L_c}^2 \delta_{ij} = m_S^2 \delta_{ij} \\ &= m_\Psi^2 \delta_{ij} = m_{\Psi_c}^2 \delta_{ij} = m_{\delta_d}^2 = m_{\delta_d}^2 m_\Phi^2 \delta_{ij} = m_\chi^2 = m_{\chi_c}^2, \end{aligned} \quad (5.13a)$$

$$M_{1/2} = M_{B-L} = M_R = M_L = M_3. \quad (5.13b)$$

The trilinear soft-breaking couplings are related to the superpotential couplings by a universal parameter  $A_0$

$$T_i = A_0 Y_i, \quad i = Q, L, \delta_d, \Psi, S. \quad (5.14)$$

The resulting free parameters at the GUT scale that are of interest for phenomenological studies<sup>2</sup> are  $m_0, M_{1/2}, A_0, t_\beta, t_{\beta_u}, t_{\beta_R}, (\mu_\Phi^{(2,2)})^2, Y_{\delta_d} Y_S, Y_\Psi$  and  $M_\delta$ .

Using these boundary conditions, the running of the soft masses appearing in Eq. (5.12) can be approximated analytically at the one-loop level. This yields the results

$$\Delta m_{\chi_c}^2 \simeq \frac{1}{4\pi^2} \left( (A_0^2 + 3m_0^2) \left[ 3Y_{\delta_d}^\dagger Y_{\delta_d} - \text{Tr} Y_S^\dagger Y_S + \text{Tr} Y_\Psi^\dagger Y_\Psi \right] \right) \ln \left( \frac{M_{\text{GUT}}}{M_{\text{SUSY}}} \right), \quad (5.15a)$$

$$\begin{aligned} \sum m_{\chi_c}^2 &\simeq -2m_0^2 + \frac{1}{4\pi^2} \left( (A_0^2 + 3m_0^2) \left[ 3Y_{\delta_d}^\dagger Y_{\delta_d} + \text{Tr} Y_S^\dagger Y_S + \text{Tr} Y_\Psi^\dagger Y_\Psi \right] \right. \\ &\quad \left. - (3g_{BL}^2 + 6g_R^2) M_{1/2}^2 \right) \ln \left( \frac{M_{\text{GUT}}}{M_{\text{SUSY}}} \right). \end{aligned} \quad (5.15b)$$

In order to obtain spontaneous symmetry breaking one requires  $\mu_{\chi_c}^2 \geq 0$ , namely the RHS of Eq. (5.12a) must be greater than or equal to zero. This constraint excludes an area of the parameter space as a function of the couplings  $Y_{\delta_d}, Y_\Psi, Y_S$ , the soft-breaking parameters  $m_0, A_0$  and the  $SU(2)_R$  VEV  $v_R$ . As the large  $SU(2)_R$   $D$ -terms in Eq. (5.12a) add negatively to  $|\mu_{\chi_c}^2|$ , the contribution from the soft masses has to account for the positivity requirement. From Eq. (5.15a) one sees that  $m_{\chi_c}^2 > m_{\chi_c}^2$  as long as  $\Delta Y^2 \equiv 3\text{Tr} Y_{\delta_d}^\dagger Y_{\delta_d} + \text{Tr} Y_\Psi^\dagger Y_\Psi - \text{Tr} Y_S^\dagger Y_S > 0$ , so that Eq. (5.12b) requires  $t_{\beta_R}$  close to, but smaller than one. Values of  $t_{\beta_R}$  significantly smaller than unity require a large splitting  $\Delta m_{\chi_c}^2$ , which can be achieved by increasing  $m_0, A_0$  or  $\Delta Y^2$ . We exemplify this behaviour in Fig. 5.2 where we show the contours of different  $\mu_{\chi_c}^2$  values as functions of  $t_{\beta_R}, m_0$  and  $Y_{\delta_d}$ ,<sup>3</sup> highlighting the  $|\mu_{\chi_c}|^2 = 0$  contour in red.

## 5.1.2 RGE Running of the Sfermions and Gauginos

In the CMSSM, which contains similar boundary conditions, one can obtain simple expressions at the one-loop level for the first and second generation sfermion soft-masses relating

<sup>2</sup> We consider here the vector-like leptons  $\Psi, \Psi_c$  and their scalar superpartners as spectator fields only necessary for gauge coupling unification. As such in all numerical studies we chose  $M_\Psi = 1$  TeV and set the corresponding  $B_{\mu_\Psi}$  term to zero. Relaxing this assumption could have interesting consequences for collider phenomenology as well as flavour observables [458].

<sup>3</sup> The approximations applied in Fig. 5.2 do not include the running of  $Y_{\delta_d}$ . Generically, this running increases the size of the couplings, but does not qualitatively modify the behaviour shown in the figure.

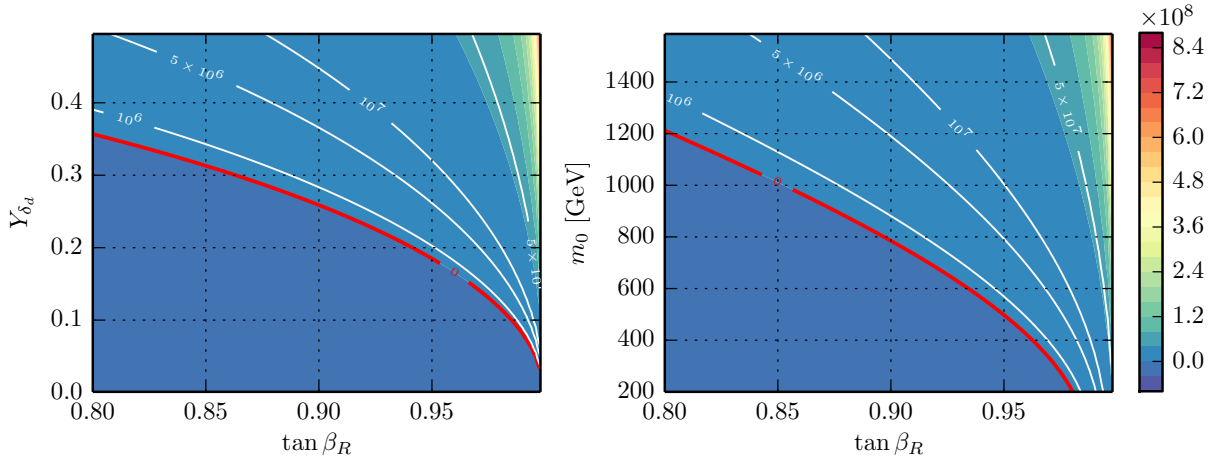


Figure 5.2: Illustration of the constraints on the parameter space arising through the requirement of consistent solutions of the tadpole equations. The figures show contours of the  $\mu_{\chi_c}^2$  values as function of either,  $Y_{\delta_d}$  and  $t_{\beta_R}$  (left) or  $m_0$  and  $t_{\beta_R}$  (right). Here, we have chosen the couplings  $Y_S$  and  $Y_\psi$  to be zero in order to reduce the dimensionality of the parameter space, for a detailed discussion of the effect of these parameters see the text. The red contour corresponds to where  $\mu_{\chi_c}^2 = 0$ , therefore the parameter space underneath this contour is excluded as  $\mu_{\chi_c}^2 < 0$  in this region. The parameter values chosen correspond to left:  $v_R = 7$  TeV,  $m_0 = 750$  GeV and right:  $v_R = 7$  TeV,  $Y_{\delta_d} = 0.25$ . Other parameter values are,  $t_\beta = 10$ ,  $A_0 = 500$  GeV and  $M_{1/2} = 1$  TeV.

their size at  $M_{\text{SUSY}}$  to the high-scale parameters  $m_0$  and  $M_{1/2}$  [49]:

$$m_q^2(M_{\text{SUSY}}) \simeq m_0^2 + 5.2M_{1/2} \quad (5.16a)$$

$$m_d^2(M_{\text{SUSY}}) \simeq m_0^2 + 4.8M_{1/2} \quad (5.16b)$$

$$m_u^2(M_{\text{SUSY}}) \simeq m_0^2 + 4.8M_{1/2} \quad (5.16c)$$

$$m_l^2(M_{\text{SUSY}}) \simeq m_0^2 + 0.50M_{1/2} \quad (5.16d)$$

$$m_e^2(M_{\text{SUSY}}) \simeq m_0^2 + 0.15M_{1/2} \quad (5.16e)$$

Using the same Ansatz in our model, assuming  $M_{\text{SUSY}} \simeq v_R$ , we obtain:

$$m_Q^2(M_{\text{SUSY}}) \simeq m_0^2 + 3.6M_{1/2} \quad (5.17a)$$

$$m_{Q^c}^2(M_{\text{SUSY}}) \simeq m_0^2 + 3.5M_{1/2} \quad (5.17b)$$

$$m_L^2(M_{\text{SUSY}}) \simeq m_0^2 + 0.44M_{1/2} \quad (5.17c)$$

$$m_{L^c}^2(M_{\text{SUSY}}) \simeq m_0^2 + 0.36M_{1/2} \quad (5.17d)$$

Even if one must bear in mind that the correct coefficients get modified at the two-loop level, one can already see two main differences: (i) the mass splitting between left- and right-sleptons and squarks respectively is comparatively smaller than in the CMSSM, (ii) the squark masses don't grow so rapidly with increasing  $M_{1/2}$  as they do in the CMSSM.

For the running gaugino masses one can obtain a rough estimate of the expectations of the CMSSM against this model at one-loop using the relation  $M_a = g_a^2/g_{\text{GUT}}^2 M_{1/2}$ . In the

CMSSM, one obtains

$$M_1 \simeq 0.4M_{1/2}, \quad M_2 \simeq 0.75M_{1/2}, \quad M_3 \simeq 2.15M_{1/2}, \quad (5.18)$$

while this model predicts

$$M_{B-L} \simeq 0.5M_{1/2}, \quad M_L \simeq 0.7M_{1/2}, \quad M_R \simeq 0.6M_{1/2}, \quad M_3 \simeq 1.85M_{1/2}. \quad (5.19)$$

Thus, the lightest gaugino is the one of the  $U(1)_{B-L}$  gauge group. Moreover, the gluino is also lighter for the same value of  $M_{1/2}$  as in the CMSSM despite the increased GUT scale.

### 5.1.3 Quark Masses and Mixing

In the simplest left-right model with only one generation of bi-doublets and no vector-like quarks, the quark mixing is trivial and the CKM matrix can't be generated. An Ansatz often used in literature to cure this problem is to add vector-like quarks which generate the CKM matrix via the mixing with the SM quarks. In the case of vector-like states which mix with the d-quarks and only one generation of bi-doublets, the two mass matrices read

$$M_u = \frac{v_u}{\sqrt{2}} Y, \quad M_d = \begin{pmatrix} \frac{v_d}{\sqrt{2}} Y & \frac{v_{\tilde{\chi}_c}}{\sqrt{2}} Y_{\delta_d} \\ \tilde{m} & M_{\delta_d} \end{pmatrix}. \quad (5.20)$$

To be very general, we kept a term  $\tilde{m}$  which is actually absent in our model.  $M_u$  is diagonalised by two  $3 \times 3$  matrices  $U_u^R, U_d^L$ , and  $M_d$  by  $4 \times 4$  matrices  $U_d^R, U_d^L$ . The measured CKM matrix  $V_{\text{CKM}}$  must be reproduced by the  $3 \times 3$  block related to the usual SM-quarks of the matrix

$$V_{\text{CKM}}^{4 \times 4} = \tilde{U}_L^u (U_L^d)^\dagger, \quad (5.21)$$

where  $\tilde{U}^u$  is  $U^u$  enlarged artificially by a row and column of zeros apart from the (4,4) entry which is set to 1. One can always assume a basis, where  $U^u$  is diagonal and the entire quark mixing is encoded in  $U_L^d$ . In this case and for  $M_{\delta_d} \gg m_b$ , one finds the see-saw condition

$$M = \frac{v_{\tilde{\chi}_c}^2 Y_{\delta_d} Y_{\delta_d}^\dagger}{2} - \tilde{y} \tilde{y}^\dagger, \quad (5.22)$$

with

$$M = V_{\text{CKM}}^* \text{diag}(m_d^2, m_s^2, m_b^2) V_{\text{CKM}}^T - \frac{v_d^2 Y_Q Y_Q^\dagger}{2}, \quad (5.23a)$$

$$\tilde{y} = \frac{v_u Y_Q \tilde{m}^\dagger + M_{\delta_d}^* v_{\tilde{\chi}_c} Y_{\delta_d}}{\sqrt{2(|\tilde{m}|^2 - M_{\delta_d}^2)}}. \quad (5.23b)$$

Using  $\det(A + uv^T) = (1 + v^T A^{-1} u) \det(A)$  for an invertible matrix  $A$  and vectors  $u, v$ , one finds that the determinant of the RHS of Eq. (5.22) always vanishes. This observation together

with the extension of the same lemma where  $u, v$  are  $n \times m$  matrices yields the condition

$$1 - \frac{v_d^2}{2} Y_Q (V_{\text{CKM}}^* \text{diag}(m_d^2, m_s^2, m_b^2) V_{\text{CKM}}^T)^{-1} Y_Q^\dagger = 0, \quad (5.24)$$

for the LHS. Keeping in mind that  $Y_Q$  is diagonal in the chosen basis, we finally find

$$\frac{v_d^2}{2} Y_Q^2 = V_{\text{CKM}}^* \text{diag}(m_d^2, m_s^2, m_b^2) V_{\text{CKM}}^T. \quad (5.25)$$

Thus, there is only a solution to Eq. (5.22) if quark mixing vanishes, otherwise the system is over constrained. We checked numerically that this conclusion holds also independently of the see-saw matrix and that the inclusion of radiative corrections does not alleviate this problem if one demands that all interactions are perturbative. Therefore, the best way to incorporate correct quark mixing in left-right models is to include a second generation of bi-doublets. However, the vector-like quarks in this model play still a crucial role because they are needed for radiative symmetry breaking as discussed below.

In the presence of two generations of bi-doublets, the Yukawa coupling in the left-right phase is related to the usual up- and down-type MSSM Yukawas  $Y_u, Y_d$  via

$$Y_{Q_1} = -\frac{Y_d \sqrt{1+t_{\beta_d}^2} - Y_u \sqrt{1+t_{\beta_u}^2}}{t_{\beta_d} - t_{\beta_u}} \xrightarrow{t_{\beta_d}=0} Y_{Q_1} = \frac{Y_d - Y_u \sqrt{1+t_{\beta_u}^2}}{t_{\beta_u}}, \quad (5.26a)$$

$$Y_{Q_2} = \frac{t_{\beta_u} Y_d \sqrt{1+t_{\beta_d}^2} - Y_u t_{\beta_d} \sqrt{1+t_{\beta_u}^2}}{t_{\beta_d} - t_{\beta_u}} \xrightarrow{t_{\beta_d}=0} Y_{Q_2} = -Y_d. \quad (5.26b)$$

To keep  $Y_{Q_2}^{(3,3)}$  perturbative up to the GUT scale, either  $t_{\beta_u}$  or  $t_{\beta_d}$  is restricted to very small values. Therefore we choose to always take  $t_{\beta_d} = 0$ .

Our Ansatz to calculate  $Y_Q$  numerically is as follows: we derive values for  $Y_d$  and  $Y_u$  to reproduce the known CKM matrix and quark masses. Here, two difficulties have to be taken into account: (i) the mixing with the vector-like quarks which is inevitable because we need a non-vanishing  $Y_{\delta_d}$ , and (ii) the full one-loop radiative corrections to all quarks. From the obtained values of  $Y_d$  and  $Y_u$ ,  $Y_Q$  is calculated. Since  $Y_Q$  affects the one-loop corrections to the quarks entering the calculation of  $Y_d$  and  $Y_u$ , this procedure is iterated until a convergence has been reached.

We now briefly comment on the constraints arising from introducing vector-like quarks. Firstly, let us consider the constraints arising from quark flavour observables due to mixing between the vector-like and down-type quarks. The key point to note is that the introduced vector-like quarks only mix with the right-handed SM quarks due to the superpotential term  $Y_{\delta_d} Q_c \bar{\chi}_c \delta_d$ . The strongest bound stems from the kaon mixing where one also has to include the mixing of heavy vector bosons which scale as  $v_L^2/v_R^2$ , see Eq. (5.9) and (5.10). Recent collider data requires that the  $W'$  mass be at least approximately 2 TeV [459]. Apart from that, it has also been shown that kaon mixing constraints require the  $W'$  boson in left-right models to be at least approximately 3 TeV in the non-supersymmetric case, [401] and at least

2 TeV in supersymmetric models due to gluino contributions [460]. Both of these bounds must be recast for the specific model in question; however, they do not change the conclusion that both the  $W - W'$  and  $Z - Z'$  mixing should be highly suppressed. The mixing in the right-handed  $d$ -quark sector is at most  $m_b/M_\delta \lesssim 10^{-2}$ . In the kaon mixing, both the squares of the quark and vector boson mixing enters, implying that we can easily avoid this bound.

Lastly, one must consider the impact of the vector-like quarks on the electroweak precision observables. Due to the tree-level coupling of the vector-like quarks to  $Z$ -bosons, there will in general be a non-negligible contribution. The corresponding bounds have been obtained in Ref. [461]: while the masses of the vector-like quarks should be  $\gtrsim 600$  GeV, the mixing with the SM quarks is constrained to  $|V_{\text{CKM},34}^{4 \times 4}| \lesssim 0.04$ .<sup>4</sup>

## 5.1.4 Lepton Sector

In the lepton sector, we find equivalent relations between  $Y_{L_1}, Y_{L_2}$  and both the lepton Yukawa coupling  $Y_e$  as well as neutrino Yukawa coupling  $Y_\nu$  as Eqs. (5.26a) and (5.26b) for the quark sector. Because of the additional gauge singlet  $S$  as well as the two generations of extra vector-like leptons  $\Psi, \Psi_c$ , there are more free parameters in the lepton sector as in the quark sector. Thus, the calculation of  $Y_e$  and  $Y_\nu \equiv \sqrt{2}m_D/v_u$  is in general more complicated. In the limit  $v_{\bar{\chi}_c} Y_\Psi M_\Psi^{-1} \rightarrow 0$ , the SM charged leptons decouple from the vector-like states and correspondingly,  $v_d Y_e = -\sum_a v_\Phi^{d_a} Y_{L_a}$  can be diagonalized as usual, which fixes one linear combination of  $Y_{L_1}$  and  $Y_{L_2}$ . The other necessary combination of  $Y_{L_1}$  and  $Y_{L_2}$  can be obtained from neutrino data.

The neutrino masses can be calculated in the see-saw approximation, which give the following expressions for light (heavy) neutrinos [462]:

$$\begin{aligned} m_\nu^{\text{light}} &\simeq \frac{2}{v_{\chi_c}^2} m_D (Y_S^T)^{-1} \mu_S Y_S^{-1} m_D^T, \\ m_{\nu_h} &\simeq \frac{v_{\chi_c}}{\sqrt{2}} Y_S. \end{aligned} \quad (5.27)$$

While the light neutrinos are Majorana states, the six heavy states form three quasi-Dirac pairs.

Since the right-handed neutrinos are part of the  $L_c$  doublets, it is in general not possible to simultaneously diagonalize  $Y_e$  and  $Y_S$ , as opposed to inverse see-saw models with the SM gauge group or with  $U(1)_R \times U(1)_{B-L}$ . However, one can always choose a basis with diagonal  $Y_e, \mu_S$  and  $M_\Psi$ . Therefore, the PMNS matrix can be fitted by the linear combination  $-\sum_a \frac{1}{\sqrt{2}} v_\Phi^{u_a} Y_{L_a} \equiv m_D$ . Alternatively, one can work with diagonal  $m_D$  and use  $Y_S$  to fit neutrino data, or allow off-diagonals in both terms.

---

<sup>4</sup> Interestingly, the bounds from the hadronic ratio  $R_b$  are stronger than those arising from the oblique parameters for the considered case of down-type vector-like quarks.

## 5.2 Phenomenology

In this section we discuss various phenomenological features of the model, focusing on aspects of the mass spectrum that differ compared to the MSSM, as well as on current excesses reported by the LHC experiments. A discussion of the rich flavour phenomenology of this model which provides several new sources for lepton and quark flavour violation, as well as of the dark matter scenarios is beyond the scope of this work and will be given elsewhere.

The numerical results of the model have been calculated using SPheno [104, 105], while the implementation of the model into SPheno was performed using the Mathematica code SARAH [89–94]. This allows one to calculate the full one-loop spectrum as well as the dominant two-loop contributions to the CP-even Higgs masses [97, 98].

### 5.2.1 Higgs Sector

After the would-be Goldstone bosons are rotated out, the Higgs sector comprises six neutral  $CP$ -even states ( $\sigma_i$ , see Eqs. (5.4a – 5.4d)), four neutral  $CP$ -odd and four charged states which each mix among themselves to form the mass eigenstates  $h_i$ ,  $A_i$  and  $H_i^\pm$ . In the following discussion, we will denote the lightest mostly electroweak Higgs state as  $h$  and the lightest mostly right-doublet Higgs as  $h_R$ . In the limit  $t_{\beta_R} \rightarrow 1$ ,  $h_R$  becomes massless at the tree level. In this case, the  $SU(2)_{R-}$  and the electroweak Higgs states decouple from each other and the second-lightest Higgs is purely  $SU(2)_L$ -doublet-like. The tree-level mass of  $h$  is enhanced with respect to the MSSM prediction due to the effect of the extra  $D$ -terms from the enlarged gauge sector. The absolute upper bound on this mass can be evaluated in the limits  $t_{\beta_R} \rightarrow 1$ ,  $t_\beta \rightarrow \infty$ ,  $\tan \beta_u \rightarrow \infty$  and is given by

$$m_{h,\text{tree}}^2 \Big|^{t_{\beta_R} \rightarrow 1} \leq \frac{1}{4}(g_L^2 + g_R^2) v_L^2, \quad (5.28)$$

which is the generic upper limit for supersymmetric left-right theories where electroweak symmetry is broken by bi-doublets [463, 464] as well as in model variants where only the subgroup  $U(1)_R \times U(1)_{B-L}$  survives down to the TeV scale [465, 466].

As soon as  $t_{\beta_R}$  departs from one, a mixing between  $h$  and  $h_R$  sets in which rises with increasing  $\Delta = 1 - t_{\beta_R}$ . This mixing also pushes up the heavier mass of both eigenstates. Treating  $\Delta$  as a small perturbation, one can evaluate the corresponding  $2 \times 2$  mass matrix of said states which reads in the basis  $(h, h_R)$ :

$$m_{h,h_R}^2 = \begin{pmatrix} \frac{v_L^2(D(g_L^2 + g_R^2) - g_R^4 v_R^2)}{4D} & \frac{-m_{A_R}^2 \Delta g_R^2 v_L v_R}{D} \\ \frac{-m_{A_R}^2 \Delta g_R^2 v_L v_R}{D} & m_{A_R}^2 \Delta^2 \end{pmatrix}, \quad (5.29)$$

where  $D \simeq 4(m_{A_R}^2 + M_{Z'}^2)$  and  $m_{A_R}^2 = -2B_{\mu_{\chi_c}} / \sin 2\beta_R \simeq -2B_{\mu_{\chi_c}}$  is the mass of the pseudoscalar Higgs boson of the  $SU(2)_R$  sector. After the level crossing of the eigenstates,  $h_R$  continues getting more massive whereas the mass of the electroweak eigenstate converges

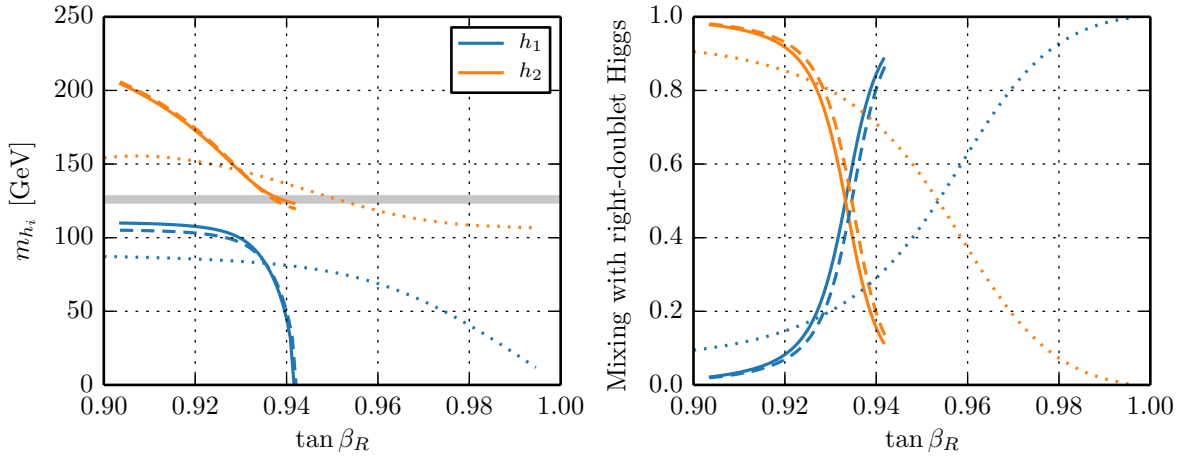


Figure 5.3: Masses of the two lightest Higgs states as a function of  $\tan \beta_R$ . The results are shown at the tree level (dotted) as well as at the one/two loop level (dashed/solid lines). The grey band depicts the approximate mass required for a SM-like Higgs. The remaining parameters have been fixed to  $m_0 = M_{1/2} = 1.2$  TeV,  $A_0 = 1$  TeV,  $\mu_\Phi^{(2,2)} = -2$  TeV,  $v_R = 7$  TeV,  $t_\beta = 15$ ,  $t_{\beta_u} = 10$ ,  $M_\delta = 1$  TeV,  $Y_{\delta_d}^i = 0.09$ .

towards

$$m_{h,\text{tree}}^2 \Big|^{t_{\beta_R} \rightarrow 0} \leq \frac{1}{4} \left( g_L^2 + \frac{g_{BL}^2 g_R^2}{g_{BL}^2 + g_R^2} \right) v_L^2 = M_Z^2, \quad (5.30)$$

which is exactly the same as in the MSSM. The last equality follows because of the relation between the hypercharge coupling  $g_Y$  and the ‘new’ couplings:  $1/g_Y^2 = 1/g_{BL}^2 + 1/g_R^2$ .

Taking into account the measured Higgs properties, the mixing between the Higgs states of the different  $SU(2)$  sectors has to be small. Hence, there are two possibilities in our model:

- values of  $t_{\beta_R}$  close to one, resulting in a light  $SU(2)_R$ -doublet Higgs and a second-lightest Higgs with SM properties and an enhanced tree-level mass
- significant departure from  $t_{\beta_R} = 1$ , in which case the lightest Higgs has SM properties but no  $D$ -term enhancement of the tree-level mass with respect to the MSSM.

In Fig. 5.3, we show the masses as well as admixtures of the two lightest  $CP$ -even Higgs states at the tree level as well as the one- and two-loop level as a function of  $\tan \beta_R$ . Apart from the usual large corrections of several ten per-cent for the SM-like Higgs, the most apparent feature in the loop corrections is the dependence on  $\tan \beta_R$  which is altered at the loop level due to the coupling of  $\chi_c$  to the vector-like coloured sector via  $Y_{\delta_d}$ : Since the average of the scalar masses can be smaller than the corresponding fermion mass, the loop corrections are negative in contrast to the well known feature of large positive (s)quark corrections in the MSSM. In Fig. 5.3 we have chosen  $M_\delta = 1$  TeV as well as a relatively large coupling  $Y_{\delta_d} = 0.09$  (corresponding to  $Y_{\delta_d} = 0.26$  at  $M_{\text{SUSY}}$ ) to maximise these corrections.

As a consequence of those radiative corrections, a second-lightest SM-like Higgs can be accompanied by a very light  $h_R$  state of  $\mathcal{O}(10$  GeV), in contrast to the constrained  $U(1)_R \times U(1)_{B-L}$  model where the loop corrections in the absence of vector-like states always enhance

$m_{h_R}$ , i.e. one finds  $\mathcal{O}(50 \text{ GeV})$  even for  $\tan \beta_R \rightarrow 1$  [466, 467]. We remark that the branching ratio for the decay  $h_2 \rightarrow h_1 h_1$  is below a percent for these points even when the  $h - h_R$  mixing is of  $\mathcal{O}(10 \%)$ .

## 5.2.2 Squark Sector

The down-squark mass matrix is enlarged to an  $8 \times 8$  matrix. The additional entries correspond to the vector-like quarks' scalar superpartners. The addition of these vector-like squarks modifies the expected hierarchy of the light-squark masses in comparison to the MSSM. Namely, we observe that the lightest down-squark is generically lighter than the lightest up-squark which is always the light stop  $\tilde{t}_1$ . This behaviour arises as the vector-like quarks modify the RGE running of the quark soft-masses, and have a potentially large mixing with the standard down-type squarks.

To illustrate this behaviour we consider for the moment only the third-generation of left and right down-type squarks as well as the vector-like squarks. In the basis  $\{\tilde{b}_L, \tilde{b}_R, \tilde{\delta}_d, \tilde{\delta}_d^c\}$  the mass matrix reads

$$m_{\tilde{b}, \tilde{\delta}}^2 \simeq \begin{pmatrix} \left(m_Q^{(3,3)}\right)^2 & 0 & 0 & 0 \\ 0 & \left(m_{Q_c}^{(3,3)}\right)^2 + \frac{1}{4}v_R^2|Y_{\delta_d}^{(3)}|^2 & -\frac{1}{2}v_R \left(T_{Y_{\delta_d}^{(3)}} + \mu_{\chi_c} Y_{\delta_d}^{(3)}\right) & -\frac{1}{2}v_R M_\delta Y_{\delta_d}^{(3)} \\ 0 & -\frac{1}{2}v_R \left(T_{Y_{\delta_d}^{(3)}} + \mu_{\chi_c} Y_{\delta_d}^{(3)}\right) & |M_\delta|^2 + m_{\delta_d}^2 + \frac{1}{4}v_R^2|Y_{\delta_d}^{(3)}|^2 & 0 \\ 0 & -\frac{1}{2}v_R M_\delta Y_{\delta_d}^{(3)} & 0 & |M_\delta|^2 + m_{\delta_d}^2 \end{pmatrix}. \quad (5.31)$$

Here, the electroweak VEVs have been neglected and we have assumed  $t_{\beta_R} \rightarrow 1$  as these quantities give only a shift to the diagonal elements, but play a negligible role in the mixing with the vector-like states. From the form of the mass matrix we arrive at the following conclusions:

- There is no mixing between the left-sbottoms and the vector-like squarks based on these assumptions.
- For fixed values of  $M_\delta$ , the relative size of the mixing between the right-sbottoms and the vector-like states is determined by three parameters, namely  $Y_{\delta_d}$ ,  $A_0$  and  $v_R$ . Typically one requires these parameters to take large values in order to arrive at a phenomenologically viable model<sup>5</sup>. Therefore the right-sbottoms are typically strongly mixed with the vector-like states. This mixing reduces their mass compared to pure  $\tilde{b}_{L/R}$  eigenstates.

In Fig. 5.4 on the left-hand panel the mixing of the lightest sbottom with the vector-like states is shown as a function of  $Y_{\delta_d}$ , where a value of 1.0 corresponds to a purely vector-like squark and zero corresponds to a pure MSSM sbottom state. Here we observe that depending on  $M_\delta$  there exists a minimum value of  $Y_{\delta_d}$  required for significant mixing with the vector-like states. In the right-hand panel we show the effect of  $T_{Y_{\delta_d}}$  on the splitting of the squark masses. As

<sup>5</sup> Here we refer to the constraint that  $Y_{\delta_d}$  must be sufficiently large to allow for spontaneous  $SU(2)_R$  symmetry breaking and  $v_R$  must be of order of several TeV to produce a sufficiently heavy  $W'$ .

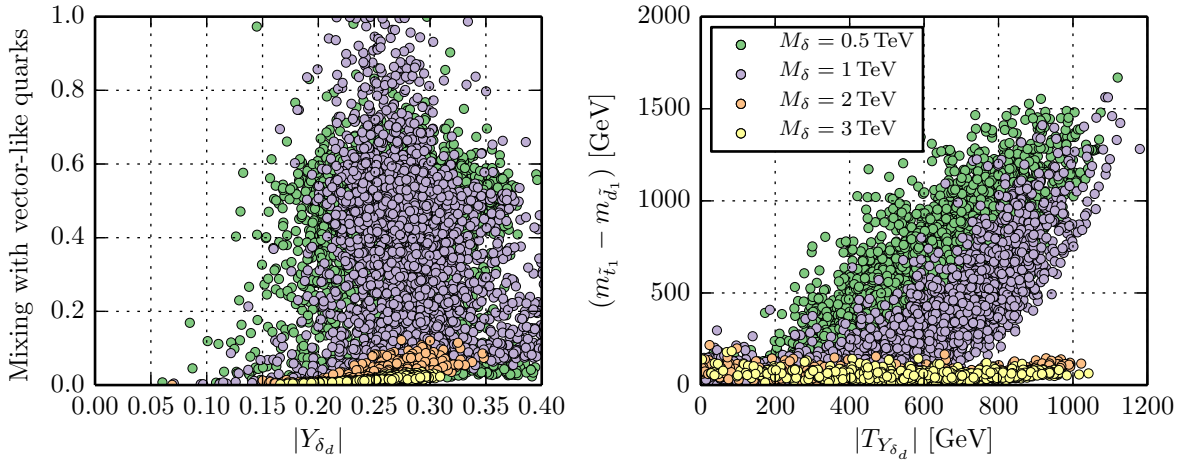


Figure 5.4: The mixing of the lightest down-type squarks (left) and the splitting of both the lightest stop and down-squark masses (right) as functions of  $Y_{\delta_d}$  and  $T_{Y_{\delta_d}}$  at  $M_{\text{SUSY}}$  respectively. Here all input parameters are scanned over randomly for fixed values of  $M_{\delta}$ . The ranges of the parameters scanned over at the GUT scale are  $v_R \in [6.5, 9]\text{TeV}$ ,  $t_{\beta}, t_{\beta_u} \in [1, 30]$ ,  $t_{\beta_R} \in [0.8, 1]$ ,  $m_0, M_{1/2} \in [200, 2000]\text{GeV}$ ,  $A_0 \in [0, 3]\text{TeV}$ ,  $\mu_{\Phi}^{(2,2)} \in [-3, 3]\text{TeV}$  and  $Y_{\delta_d} \in [-0.15, 0.15]$ .

Eq. (5.31) suggests,  $T_{Y_{\delta_d}}$  contributes strongly to this splitting. One should note that the value of this trilinear coupling is strongly correlated with  $M_{1/2}$  due to RGE running, increasing with larger  $M_{1/2}$ .

RGE running effects result in a splitting of the quark soft masses where  $(m_Q^{(3,3)})^2 > (m_{Q_c}^{(3,3)})^2$ . This splitting arises through two main sources. Firstly, the running of the gaugino masses in the left-right sector is asymmetric. This results in the splitting being a function of  $M_{1/2}$  which can be analytically estimated at the one-loop level:

$$\begin{aligned} \Delta m_Q^2 &\equiv (m_Q^{(3,3)})^2 - (m_{Q_c}^{(3,3)})^2 \\ &\simeq \frac{M_{1/2}^2}{4} \left[ 1 + 16\pi^4 \left( \frac{8}{\left(8\pi^2 - 3g_{\text{GUT}}^2 \ln\left(\frac{M_{\text{SUSY}}}{M_{\text{GUT}}}\right)\right)^2} - \frac{3}{\left(-4\pi^2 + g_{\text{GUT}}^2 \ln\left(\frac{M_{\text{SUSY}}}{M_{\text{GUT}}}\right)\right)^2} \right) \right] \\ &\simeq 8.2 \times 10^{-2} M_{1/2}^2 \end{aligned} \quad (5.32)$$

Here,  $g_{\text{GUT}} \simeq 0.8$ ,  $M_{\text{GUT}} \simeq 1.5 \times 10^{17} \text{GeV}$  and  $M_{\text{SUSY}} \simeq 2.5 \text{TeV}$ . In Fig. 5.5 the results of the fully numerical scan are shown. The bold red line corresponds to the above function, whereby we see that this function provides an adequate approximation to the minimal splitting of the soft-masses. Secondly, as is also illustrated by Fig. 5.5, additional splitting occurs due to  $Y_{\delta_d} \neq 0$ . The precise value of this contribution depends strongly upon numerous parameters in the model.

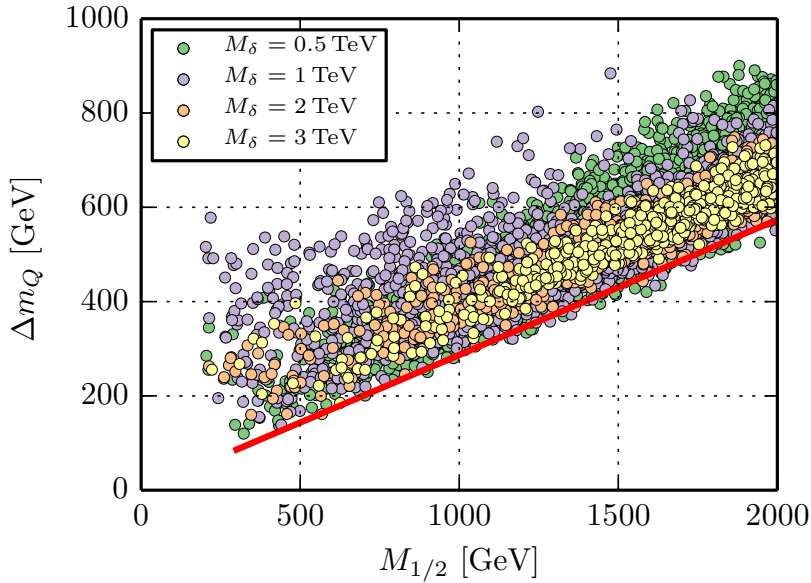


Figure 5.5: A random scan which illustrates the splitting of the squark soft-masses. Also shown in red is the analytic expression based on the asymmetry of the left-right gaugino mass terms. Here all input parameters are scanned over randomly for fixed values of  $M_\delta$ . The ranges of the parameters scanned over at the GUT scale are  $v_R \in [6.5, 9]\text{TeV}$ ,  $t_\beta, t_{\beta_u} \in [1, 30]$ ,  $t_{\beta_R} \in [0.8, 1]$ ,  $m_0, M_{1/2} \in [200, 2000]\text{GeV}$ ,  $A_0 \in [0, 3]\text{TeV}$ ,  $\mu_\Phi^{(2,2)} \in [-3, 3]\text{TeV}$  and  $Y_{\delta_d} \in [-0.15, 0.15]$ .

## 5.3 Conclusion

We have presented a constrained left-right supersymmetric model which predicts a low-scale  $SU(2)_R \times U(1)_{B-L}$  breaking scale. The model is constructed in a manner where gauge coupling unification is maintained, based on the requirement that  $SU(2)_R \times U(1)_{B-L}$  is broken purely through  $SU(2)_R$  doublets. As the left-right breaking scale is assumed to be close to the SUSY scale, gauge coupling unification dictates that additional matter must be introduced. This extra matter takes the form of vector-like quarks and leptons charged under  $U(1)_{B-L}$  but being singlets with respect to the  $SU(2)$  factors.

Due to the fast running of the  $U(1)_{B-L}$  gauge coupling and large one-loop threshold corrections, the model predicts a unification scale close to the string scale. These large threshold corrections are a product of large values of the gauge coupling beta functions in conjunction with a large spread in the mass spectrum. For unification to remain unspoilt by threshold corrections, one naturally predicts the  $SU(2)_R$  breaking scale to lie close to  $M_{\text{SUSY}}$ . Finally, the presence of vector-like quarks are an essential ingredient in driving spontaneous symmetry breaking in the left-right phase: under the assumption of mSUGRA-like boundary conditions, the couplings of these quarks must be non-vanishing to trigger radiative gauge symmetry breaking.

We have demonstrated why the usual paradigm of using vector-like quarks in conjunction with the see-saw mechanism provides insufficient degrees of freedom to fit both the quark

masses and mixings simultaneously. Subsequently, we have implemented both the quark masses and mixing through the introduction of an additional Higgs bi-doublet, raising the total number of electroweak VEVs to four.

The phenomenology of this model contains a number of interesting features. Here, we have focused on the mass spectrum. Firstly the CP-even Higgs sector displays two distinctive tendencies. For  $t_{\beta_R} \rightarrow 1$ , the lightest CP-even Higgs mass tends to  $\mathcal{O}(10)\text{GeV}$  values while the second lightest Higgs becomes SM-like. For sufficient deviation from  $t_{\beta_R} = 1$ , the MSSM-like limit is produced. Note, that the lightest state is essentially a SM gauge singlet. In the squark sector due to both the RGE running and the enlarged down-squark sector the lightest down squark is always lighter than the lightest stop.

## Chapter 6

# Conclusions and Outlook

---

The Standard Model (SM) of particle physics suffers from a number of theoretical and experimental deficiencies. It has been the goal of theorists over the previous decades to remedy these deficiencies and propose testable scenarios for physics beyond the SM (BSM). At the heart of these efforts lie solutions to the *hierarchy problem*. This led to the development of a number of distinct types of theories that could solve this problem. From a phenomenological standpoint, the important consequence of these solutions is the prediction of new TeV-scale physics. However, at the time of writing, both the ATLAS and CMS experiments at the LHC have collected in excess of  $30 \text{ fb}^{-1}$  at centre-of-mass energies of 13 TeV. This data has provided no direct signal of any of these theories, resulting in stringent exclusion limits on new TeV-scale particles. This leads to an interesting impasse with a number of plausible solutions: (i) discard these existing well motivated theories, and set off pursuing ideas that may explain the hierarchy problem without new TeV-scale physics, or (ii) consider non-minimal variants of these theories which modifies the phenomenology such that they remain consistent with observation while preserving their respective solutions to the hierarchy problem.

In this thesis we have pursued the latter option with particular emphasis on supersymmetry as the solution to the hierarchy problem. This however, leads one directly back to a rather daunting reality, that is, the sheer number of possibilities for extending the minimal supersymmetric SM (MSSM). The diverse array of data that any given model must confront leads to a complete dead end if many of the necessary calculations are not automated. Fortunately the last few years have seen significant increases in the number of procedures that have been completely automated. The tool SARAH requires only minimal user input, such as the Lagrangian, field content and symmetries. It gives the user not only useful information like the vertices, mass matrices, RGE and one and two-loop self-energies but also integrates into other high-energy physics codes which can be used to perform a wide range of studies. We refer to this tool chain as the SARAH framework. To demonstrate these capabilities, we have used the diphoton excess seen in December 2015 as a case study in Chapter 2. Here we have emphasised both the ease and speed at which new models can be constructed and immediately confronted with a large cross-section of available data. In particular we have provided a lengthy motivation that examines a number of mistakes observed in the literature and how these tools can be used to aid in preventing such errors and or simplifying assumptions.

In the subsequent chapters we were then interested in two different types of constraints

on BSM theories. In Chapter 3 we have considered BSM effects on the stability of the electroweak vacuum. Here, we have concerned ourselves with minimal supersymmetric models. Supersymmetry results in very complicated scalar potentials due to the large number of new scalar degrees of freedom. To analyse these potentials a large number of assumptions are typically made. The easiest of which, is simply ignoring many of these new scalar directions in the potential, thereby assuming that the potential is stable in these directions. In the first half we have revisited an explanation of the diphoton excess using bound states containing two scalar-top quarks in the context of the MSSM. We find that the requirement of a sufficiently long-lived electroweak vacuum exclude this possibility. We also discuss the impact of non-perturbative effects arising from Higgs exchange. In the second half we revisit the next-to-minimal supersymmetric SM (NMSSM). Here we analyse the effect of including charged Higgs directions in the scalar potential. We find at tree-level additional charge-breaking minima exist which are deeper than other undesirable but charge-conserving minima. However, considering the full one-loop effective potential and performing a full numerical study of the tunnelling time we find that these new minima do not lead to an electroweak vacuum that is further destabilised in comparison to cases where these minima are neglected.

In Chapter 4 we turned to indirect constraints on new physics arising from charge lepton flavour violation (cLFV). Here, we studied a minimal low-scale left-right symmetric model with scalar triplets which naturally gives rise to neutrino masses through a combination of type I and type II see-saw mechanisms. Treating the complete scalar sector in a consistent manner, we examined the cLFV rates considering the combination of both see-saw types. In particular, we developed a parametrisation which utilises either the discrete charge and parity symmetries to determine the triplet Yukawa matrices of the model as a function of only the underlying model parameters and neutrino oscillation data.

One appealing feature of left-right symmetries arises from their compatibility with SO(10) grand unified theories (GUTs). The previous cLFV study considered a low-scale left-right symmetric model which, given the particle content, is incompatible with gauge coupling unification (GCU). In Chapter 5 we therefore constructed a complete supersymmetric SO(10) compatible model containing TeV-scale left-right symmetric gauge symmetries. We find that the two-loop RGEs in conjunction with the one-loop threshold corrections have a large impact on the scale where GCU occurs. We also discussed the phenomenology, particularly in the Higgs and squark sector. We showed, that contrary to previous works, it is not possible to obtain realistic quark masses and mixing values through a single Higgs bi-doublet and vector-like quarks. It is therefore essential that a second Higgs doublet be introduced in a manner similar to two Higgs doublet models.

With a significant amount of 13 TeV LHC data available, even the models explored within this thesis are facing increasing pressure. For example, the scale of supersymmetry breaking is being pushed beyond the TeV-scale which leads to a reintroduction of the hierarchy problem. While for the SO(10) inspired left-right model, a higher left-right breaking scale typically spoils GCU due to large threshold corrections as well as the steep running of the  $U(1)_{B-L}$  gauge coupling. However, possible indirect evidence for BSM physics is beginning to appear. There currently exists a number of small anomalies in the measurements of  $B$ -meson decays. Interestingly all these different measurements point towards specific types of new physics in the mass range 1-35 TeV. If new physics lies at the upper end of this range

---

then this will certainly call for new avenues to explain the hierarchy problem. As a result it is now more tempting than ever to begin exploring option (i), namely the pursuit of brand new solutions to the hierarchy problem. However, there exists a third option not yet discussed. In regards to the hierarchy problem and other theoretical deficiencies of the SM, have we simply been asking the wrong questions all along? Currently we have no definitive answer to this question. However, it appears likely that increasingly precise measurements of portals to new physics will shed further light on this matter. Whether these portals are measurements of the Higgs boson width and couplings,  $B$ -meson decays, or even light neutrino masses and mixings we always gain additional insight into the possible extensions of the SM. Consequently, the absence of direct evidence for new physics, while disappointing, is not the end of the story with the next five years promising a wealth of new data. This data will either pave a clear route forwards pushing us in new exciting directions or finally put many of these long standing questions to rest.



## Appendix A

# Supplementary Information for Chapter 5

---

### A.1 Scalar Mass Matrices

#### Doubly Charged

The mass matrix is written in the basis  $\{\delta_R^{\bar{--}}, \delta_L^{\bar{--}}\}$

$$\mathcal{M}_{H^{\pm\pm}}^2 = \frac{1}{2} \begin{pmatrix} m_{RR} & m_{RL} \\ \dots & m_{LL} \end{pmatrix}, \quad (\text{A.1})$$

with entries

$$m_{RR} = (\rho_3 - 2\rho_1)v_L^2 + \rho_2v_R^2 - \alpha_3v^2 \frac{t_\beta^2 - 1}{t_\beta^2 + 1}, \quad (\text{A.2a})$$

$$m_{LL} = (\rho_3 - 2\rho_1)v_R^2 + \rho_2v_L^2 - \alpha_3v^2 \frac{t_\beta^2 - 1}{t_\beta^2 + 1}, \quad (\text{A.2b})$$

$$m_{RL} = v^2 \left( \beta_3(t_\beta^2 - 1) - \beta_1 \frac{t_\beta}{t_\beta^2 + 1} \right) + v_L v_R (4\rho_4 + (2\rho_1 - \rho_3)t_\beta^2). \quad (\text{A.2c})$$

Expanding in two expansion parameters  $x = v_L/v$  and  $y = v/v_R$  we obtain for the masses to leading order

$$m_{H_1^{\pm\pm}} = 2\rho_2v_R^2 + \frac{1}{2}\alpha_3v^2 \cos 2\beta + \mathcal{O}(x, y^2), \quad (\text{A.3a})$$

$$m_{H_2^{\pm\pm}} = \frac{1}{2}((\rho_3 - 2\rho_1)v_R^2 + \alpha_3v^2 \cos 2\beta) + \mathcal{O}(x, y^2). \quad (\text{A.3b})$$

## Singly Charged

Here the basis is defined as  $\{\phi^-, (\phi^+)^c, (\delta_R^+)^c, (\delta_L^+)^c\}$

$$\mathcal{M}_{H^\pm}^2 = \frac{1}{2} \begin{pmatrix} m_{\phi^-\phi^-} & m_{\phi^-\phi^+} & m_{\phi^-\delta_R^+} & m_{\phi^-\delta_L^+} \\ \dots & m_{\phi^+\phi^+} & m_{\phi^+\delta_R^+} & m_{\phi^+\delta_L^+} \\ \dots & \dots & m_{\delta_R^+\delta_R^+} & m_{\delta_R^+\delta_L^+} \\ \dots & \dots & \dots & m_{\delta_L^+\delta_L^+} \end{pmatrix}, \quad (\text{A.4})$$

with entries

$$m_{\phi^-\phi^-} = \frac{1}{t_\beta^2 - 1} \left( 2v_L v_R t_\beta (2\beta_3 - \beta_1 t_\beta) + \frac{v_L^2 v_R^2}{v^2} (2\rho_1 - \rho_3)(t_\beta^2 + 1) - \alpha_3 (v_L^2 + t_\beta^2 v_R^2) \right), \quad (\text{A.5a})$$

$$m_{\phi^-\phi^+} = \frac{t_\beta^2 + 1}{t_\beta^2 - 1} \left( v_L v_R (2\beta_3 t_\beta - \beta_1) + \frac{2v_L^2 v_R^2}{v^2} t_\beta (2\rho_1 - \rho_3) - \alpha_3 \frac{t_\beta}{t_\beta^2 + 1} (v_L^2 + v_R^2) \right), \quad (\text{A.5b})$$

$$m_{\phi^+\phi^+} = \frac{1}{t_\beta^2 - 1} \left( 2v_L v_R t_\beta (2\beta_3 t_\beta - \beta_1) + \frac{v_L^2 v_R^2}{v^2} (2\rho_1 - \rho_3)(t_\beta^2 + 1) - \alpha_3 (t_\beta^2 v_L^2 + v_R^2) \right), \quad (\text{A.5c})$$

$$m_{\phi^-\delta_R^+} = \frac{\sqrt{2}v}{2\sqrt{t_\beta^2 + 1}} (v_L(\beta_1 - 2\beta_3 t_\beta) + v_R \alpha_3 t_\beta), \quad (\text{A.5d})$$

$$m_{\phi^+\delta_L^+} = \frac{\sqrt{2}v}{2\sqrt{t_\beta^2 + 1}} (v_R(\beta_1 - 2\beta_3 t_\beta) + v_L \alpha_3 t_\beta), \quad (\text{A.5e})$$

$$m_{\phi^-\delta_L^+} = \frac{\sqrt{2}}{2\sqrt{t_\beta^2 + 1}} \left( v v_L \alpha_3 + v v_R t_\beta (\beta_1 - 2\beta_3 t_\beta) - 2 \frac{v_L v_R^2}{v} (2\rho_1 - \rho_3)(t_\beta^2 + 1) \right), \quad (\text{A.5f})$$

$$m_{\phi^+\delta_R^+} = \frac{\sqrt{2}}{2\sqrt{t_\beta^2 + 1}} \left( v v_R \alpha_3 + v v_L t_\beta (\beta_1 - 2\beta_3 t_\beta) - 2 \frac{v_L^2 v_R}{v} (2\rho_1 - \rho_3)(t_\beta^2 + 1) \right), \quad (\text{A.5g})$$

$$m_{RR} = v_L^2 (\rho_3 - 2\rho_1) - \frac{1}{2} v^2 \alpha_3 \frac{t_\beta^2 - 1}{t_\beta^2 + 1}, \quad (\text{A.5h})$$

$$m_{LL} = v_R^2 (\rho_3 - 2\rho_1) - \frac{1}{2} v^2 \alpha_3 \frac{t_\beta^2 - 1}{t_\beta^2 + 1}, \quad (\text{A.5i})$$

$$m_{RL} = \frac{1}{2} \left( 2v_L v_R t_\beta (2\rho_1 - \rho_3) - v^2 (\beta_1 - 2\beta_3 t_\beta) \frac{t_\beta^2 - 1}{t_\beta^2 + 1} \right). \quad (\text{A.5j})$$

Expanding once again in two expansion parameters  $x$  and  $y$  as well as working in the limit  $\tan \beta \rightarrow 0$  we obtain for the masses to leading order

$$m_{H_L^\pm} = \frac{1}{4} \left( v^2 \left[ \alpha_3 \frac{\beta_1^2}{\rho_3 - 2\rho_1 - \alpha_3} \right] + 2v_R^2(\rho_3 - 2\rho_1) \right) + \mathcal{O}(x, y^2), \quad (\text{A.6a})$$

$$m_{H^\pm} = \frac{1}{4} \left( v^2 \left[ \frac{\beta_1^2}{2\rho_1 + \alpha_3 - \rho_3} \right] + \alpha_3(v^2 + 2v_R^2) \right) + \mathcal{O}(x, y^2). \quad (\text{A.6b})$$

## Neutral CP-odd

Here the basis is defined as  $\{\varphi_1, \varphi_2, \varphi_R, \varphi_L\}$

$$\mathcal{M}_A^2 = \frac{1}{2} \begin{pmatrix} m_{\varphi_1\varphi_1} & m_{\varphi_1\varphi_2} & m_{\varphi_1R} & m_{\varphi_1L} \\ \dots & m_{\varphi_2\varphi_2} & m_{\varphi_2R} & m_{\varphi_2L} \\ \dots & \dots & m_{RR} & m_{RL} \\ \dots & \dots & \dots & m_{LL} \end{pmatrix}, \quad (\text{A.7})$$

with entries

$$m_{\varphi_1\varphi_1} = 4v^2 \frac{t_\beta^2}{t_\beta^2 + 1} [2\lambda_2 - \lambda_3] + 2v_L v_R \frac{1}{t_\beta^2 - 1} [\beta_3 t_\beta^2 (t_\beta^2 - 3) - \beta_1 t_\beta (t_\beta^2 - 2)] \\ + \frac{2v_L^2 v_R^2}{v^2} \frac{1}{t_\beta^2 - 1} [(2\rho_1 - \rho_3)(1 + t_\beta^2)((t_\beta^2 - 2))] + \alpha_3 \frac{t_\beta^2}{t_\beta^2 - 1} (v_L^2 + v_R^2), \quad (\text{A.8a})$$

$$m_{\varphi_1\varphi_2} = 4v^2 \frac{t_\beta^2}{t_\beta^2 + 1} [\lambda_3 - 2\lambda_2] + 2v_L v_R \frac{1}{t_\beta^2 - 1} [\beta_3 (t_\beta + t_\beta^3) - \beta_1] \\ + \frac{2v_L^2 v_R^2}{v^2} \frac{(t_\beta + t_\beta^3)}{t_\beta^2 - 1} [(2\rho_1 - \rho_3)(1 + t_\beta^2)((t_\beta^2 - 2))] - \alpha_3 \frac{t_\beta}{t_\beta^2 - 1} (v_L^2 + v_R^2), \quad (\text{A.8b})$$

$$m_{\varphi_2\varphi_2} = 4v^2 \frac{1}{t_\beta^2 + 1} [\lambda_3 - 2\lambda_2] + 2v_L v_R \frac{1}{t_\beta^2 - 1} [(3t_\beta^2 - 1)\beta_3 - \beta_1 t_\beta] \\ + \frac{2v_L^2 v_R^2}{v^2} \frac{t_\beta^2 + 1}{t_\beta^2 - 1} [2\rho_1 - \rho_3] - \alpha_3 \frac{1}{t_\beta^2 - 1} (v_L^2 + v_R^2), \quad (\text{A.8c})$$

$$m_{\varphi_1R} = \frac{1}{\sqrt{t_\beta^2 + 1}} \left( v_L v t_\beta (2\beta_3 t_\beta - \beta_1) + \frac{2v_L^2 v_R}{v} (t_\beta^2 + 1) (2\rho_1 - \rho_3) \right), \quad (\text{A.8d})$$

$$m_{\varphi_1L} = \frac{1}{\sqrt{t_\beta^2 + 1}} \left( v_R v t_\beta (\beta_1 - 2\beta_3 t_\beta) - \frac{2v_L v_R^2}{v} (t_\beta^2 + 1) (2\rho_1 - \rho_3) \right), \quad (\text{A.8e})$$

$$m_{\varphi_2R} = \frac{v_L v}{\sqrt{t_\beta^2 + 1}} (2\beta_3 t_\beta - \beta_1), \quad m_{\varphi_2L} = \frac{v_R v}{\sqrt{t_\beta^2 + 1}} (\beta_1 - 2\beta_3 t_\beta), \quad (\text{A.8f})$$

$$m_{RR} = v_L^2 (\rho_3 - 2\rho_1), \quad m_{LL} = v_R^2 (\rho_3 - 2\rho_1), \quad m_{RL} = v_L v_R (2\rho_1 - \rho_3). \quad (\text{A.8g})$$

Expanding once again in two expansion parameters  $x$  and  $y$  as well as working in the limit  $\tan \beta \rightarrow 0$  we obtain for the masses to leading order

$$m_{A_L}^2 = \frac{1}{2} \left( (\rho_3 - 2\rho_1)v_R^2 - \frac{\beta_1^2}{\alpha_3 + 2\rho_1 - \rho_3} v^2 \right) + \mathcal{O}(x, y^2), \quad (\text{A.9a})$$

$$m_A^2 = \frac{1}{2} \left( 4\alpha_3 v_R^2 + \left[ 4(\lambda_3 - 2\lambda_2) + \frac{\beta_1^2}{\alpha_3 + 2\rho_1 - \rho_3} \right] v^2 \right) + \mathcal{O}(x, y^2). \quad (\text{A.9b})$$

## Neutral CP-even

Here the basis is defined as  $\{\sigma_1, \sigma_2, \sigma_R, \sigma_L\}$

$$\mathcal{M}_A^2 = \frac{1}{2} \begin{pmatrix} m_{\sigma_1\sigma_1} & m_{\sigma_1\sigma_2} & m_{\sigma_1R} & m_{\sigma_1L} \\ \dots & m_{\sigma_2\sigma_2} & m_{\sigma_2R} & m_{\sigma_2L} \\ \dots & \dots & m_{RR} & m_{RL} \\ \dots & \dots & \dots & m_{LL} \end{pmatrix}, \quad (\text{A.10})$$

with entries

$$m_{\sigma_1\sigma_1} = 4v^2 \frac{1}{t_\beta^2 + 1} [\lambda_1 + t_\beta((2\lambda_2 + \lambda_3)t_\beta - 2\lambda_4)] + 2v_L v_R \frac{t_\beta^2}{t_\beta^2 - 1} [\beta_3(t_\beta^2 + 1) - \beta_1 t_\beta] \\ + \frac{2v_L^2 v_R^2}{v^2} \frac{t_\beta^2}{t_\beta^2 - 1} [(2\rho_1 - \rho_3)(t_\beta^2 + 1)] - \alpha_3 \frac{t_\beta^2}{t_\beta^2 - 1} (v_L^2 + v_R^2), \quad (\text{A.11a})$$

$$m_{\sigma_2\sigma_2} = 4v^2 \frac{1}{t_\beta^2 + 1} [2\lambda_2 + \lambda_3 + t_\beta(\lambda_1 t_\beta - 2\lambda_4)] + 2v_L v_R \frac{1}{t_\beta^2 - 1} [\beta_3(t_\beta^2 + 1) - \beta_1 t_\beta] \\ + \frac{2v_L^2 v_R^2}{v^2} \frac{1}{t_\beta^2 - 1} [(2\rho_1 - \rho_3)(t_\beta^2 + 1)] - \alpha_3 \frac{1}{t_\beta^2 - 1} (v_L^2 + v_R^2), \quad (\text{A.11b})$$

$$m_{\sigma_1\sigma_2} = 4v^2 \frac{1}{t_\beta^2 + 1} [t_\beta(\lambda_1 - 2\lambda_2 + \lambda_3) - \lambda_4(1 + t_\beta^2)] + 2v_L v_R \frac{t_\beta}{t_\beta^2 - 1} [\beta_1 t_\beta - \beta_3(t_\beta^2 + 1)] \\ - \frac{2v_L^2 v_R^2}{v^2} \frac{t_\beta}{t_\beta^2 - 1} [(2\rho_1 - \rho_3)(t_\beta^2 + 1)] + \alpha_3 \frac{t_\beta}{t_\beta^2 - 1} (v_L^2 + v_R^2), \quad (\text{A.11c})$$

$$m_{\sigma_1R} = \frac{t_\beta}{\sqrt{1 + t_\beta^2}} \left( v_L v (2\beta_3 t_\beta - \beta_1) + 2v_R v (\alpha_1 - 2\alpha_2 t_\beta) + \frac{2v_L^2 v_R}{v} (t_\beta^2 + 1)(2\rho_1 - \rho_3) \right), \quad (\text{A.11d})$$

$$m_{\sigma_1L} = \frac{1}{\sqrt{1 + t_\beta^2}} \left( v_R v t_\beta (2\beta_3 t_\beta - \beta_1) + 2v_L v (\alpha_1 - 2\alpha_2 t_\beta) + \frac{2v_L v_R^2}{v} (t_\beta^2 + 1)(2\rho_1 - \rho_3) \right), \quad (\text{A.11e})$$

$$m_{\sigma_2R} = \frac{v}{\sqrt{t_\beta^2 + 1}} (v_L [\beta_1 - 2\beta_3 t_\beta] + 2v_R [(\alpha_1 + \alpha_2)t_\beta - 2\alpha_2]), \quad (\text{A.11f})$$

$$m_{\sigma_2 L} = \frac{v}{\sqrt{t_\beta^2 + 1}} (v_R[\beta_1 - 2\beta_3 t_\beta] + 2v_L[(\alpha_1 + \alpha_2)t_\beta - 2\alpha_2]) , \quad (\text{A.11g})$$

$$m_{RR} = (\rho_3 - 2\rho_1)v_L^2 + 4\rho_1v_R^2, \quad m_{LL} = (\rho_3 - 2\rho_1)v_R^2 + 4\rho_1v_L^2, \quad m_{RL} = (2\rho_1 + \rho_3)v_Lv_R. \quad (\text{A.11h})$$

In order to obtain analytic results for the masses one must specify to a region of parameter space where the triplet and bi-doublet scalars do not mix. This corresponds to the limit  $v_L, \alpha_1, \alpha_2, \beta_1 \rightarrow 0$ . Additionally we also once again perform an expansion in the two parameters  $x$  and  $y$  as well as working in the limit  $\tan \beta \rightarrow 0$ . This yields the results

$$m_h^2 \simeq 2\lambda_1 v^2 - \frac{8\lambda_4^2 v^4}{\alpha_3 v_R^2}, \quad m_{H_R}^2 = 2\rho_1 v_R^2, \quad (\text{A.12a})$$

$$m_H^2 = 2(2\lambda_2 + \lambda_3)v^2 + \frac{\alpha_3}{2}v_R^2, \quad m_{H_L}^2 = \frac{1}{2}(\rho_3 - 2\rho_1)v_R^2. \quad (\text{A.12b})$$



# Bibliography

---

- [1] **ATLAS** Collaboration, T. A. collaboration, *Angular analysis of  $B_d^0 \rightarrow K^{*+-}$  decays in  $pp$  collisions at  $\sqrt{s} = 8$  TeV with the ATLAS detector*, 2017.
- [2] **CMS** Collaboration, C. Collaboration, *Measurement of the  $P_1$  and  $P'_5$  angular parameters of the decay  $B^0 \rightarrow K^{*0} \mu^+ \mu^-$  in proton-proton collisions at  $\sqrt{s} = 8$  TeV*, .
- [3] W. Altmannshofer, C. Niehoff, P. Stangl, and D. M. Straub, *Status of the  $B \rightarrow K^* \mu^+ \mu^-$  anomaly after Moriond 2017*, *Eur. Phys. J.* **C77** (2017), no. 6 377, [[arXiv:1703.09189](https://arxiv.org/abs/1703.09189)].
- [4] S. L. Glashow, *Partial Symmetries of Weak Interactions*, *Nucl. Phys.* **22** (1961) 579–588.
- [5] S. Weinberg, *A Model of Leptons*, *Phys. Rev. Lett.* **19** (1967) 1264–1266.
- [6] A. Salam, *Weak and Electromagnetic Interactions*, *Conf. Proc.* **C680519** (1968) 367–377.
- [7] A. Salam and J. C. Ward, *Electromagnetic and weak interactions*, *Phys. Lett.* **13** (1964) 168–171.
- [8] P. W. Higgs, *Broken Symmetries and the Masses of Gauge Bosons*, *Phys. Rev. Lett.* **13** (1964) 508–509.
- [9] P. W. Higgs, *Spontaneous Symmetry Breakdown without Massless Bosons*, *Phys. Rev.* **145** (1966) 1156–1163.
- [10] F. Englert and R. Brout, *Broken Symmetry and the Mass of Gauge Vector Mesons*, *Phys. Rev. Lett.* **13** (1964) 321–323.
- [11] G. S. Guralnik, C. R. Hagen, and T. W. B. Kibble, *Global Conservation Laws and Massless Particles*, *Phys. Rev. Lett.* **13** (1964) 585–587.
- [12] T. W. B. Kibble, *Symmetry breaking in nonAbelian gauge theories*, *Phys. Rev.* **155** (1967) 1554–1561.
- [13] M. Gell-Mann, *A Schematic Model of Baryons and Mesons*, *Phys. Lett.* **8** (1964) 214–215.
- [14] G. Zweig, *An  $SU(3)$  model for strong interaction symmetry and its breaking. Version 1*, .

- [15] H. Fritzsch, M. Gell-Mann, and H. Leutwyler, *Advantages of the Color Octet Gluon Picture*, *Phys. Lett.* **47B** (1973) 365–368.
- [16] D. J. Gross and F. Wilczek, *Ultraviolet Behavior of Nonabelian Gauge Theories*, *Phys. Rev. Lett.* **30** (1973) 1343–1346.
- [17] H. D. Politzer, *Reliable Perturbative Results for Strong Interactions?*, *Phys. Rev. Lett.* **30** (1973) 1346–1349.
- [18] T. E. Jeltema and M. Sher, *The Triple alpha process and the anthropically allowed values of the weak scale*, *Phys. Rev.* **D61** (2000) 017301, [[hep-ph/9905494](#)].
- [19] V. Agrawal, S. M. Barr, J. F. Donoghue, and D. Seckel, *The Anthropic principle and the mass scale of the standard model*, *Phys. Rev.* **D57** (1998) 5480–5492, [[hep-ph/9707380](#)].
- [20] E. Epelbaum, H. Krebs, T. A. Lähde, D. Lee, and U.-G. Meißner, *Viability of Carbon-Based Life as a Function of the Light Quark Mass*, *Phys. Rev. Lett.* **110** (2013), no. 11 112502, [[arXiv:1212.4181](#)].
- [21] E. Witten, *Dynamical Breaking of Supersymmetry*, *Nucl. Phys.* **B188** (1981) 513.
- [22] M. J. G. Veltman, *The Infrared - Ultraviolet Connection*, *Acta Phys. Polon.* **B12** (1981) 437.
- [23] H. P. Nilles, *Dynamically Broken Supergravity and the Hierarchy Problem*, *Phys. Lett.* **115B** (1982) 193.
- [24] G. 't Hooft, *Naturalness, chiral symmetry, and spontaneous chiral symmetry breaking*, *NATO Sci. Ser. B* **59** (1980) 135–157.
- [25] Yu. A. Golfand and E. P. Likhtman, *Extension of the Algebra of Poincare Group Generators and Violation of  $p$  Invariance*, *JETP Lett.* **13** (1971) 323–326. [*Pisma Zh. Eksp. Teor. Fiz.*13,452(1971)].
- [26] D. V. Volkov and V. P. Akulov, *Is the Neutrino a Goldstone Particle?*, *Phys. Lett.* **46B** (1973) 109–110.
- [27] J. Wess and B. Zumino, *A Lagrangian Model Invariant Under Supergauge Transformations*, *Phys. Lett.* **49B** (1974) 52.
- [28] J. Wess and B. Zumino, *Supergauge Transformations in Four-Dimensions*, *Nucl. Phys.* **B70** (1974) 39–50.
- [29] S. Dimopoulos and J. Preskill, *Massless Composites With Massive Constituents*, *Nucl. Phys.* **B199** (1982) 206–222.
- [30] D. B. Kaplan, H. Georgi, and S. Dimopoulos, *Composite Higgs Scalars*, *Phys. Lett.* **136B** (1984) 187–190.

- 
- [31] D. B. Kaplan and H. Georgi, *SU(2) x U(1) Breaking by Vacuum Misalignment*, *Phys. Lett.* **136B** (1984) 183–186.
- [32] H. Georgi and D. B. Kaplan, *Composite Higgs and Custodial SU(2)*, *Phys. Lett.* **145B** (1984) 216–220.
- [33] H. Georgi, D. B. Kaplan, and P. Galison, *Calculation of the Composite Higgs Mass*, *Phys. Lett.* **143B** (1984) 152–154.
- [34] M. J. Dugan, H. Georgi, and D. B. Kaplan, *Anatomy of a Composite Higgs Model*, *Nucl. Phys.* **B254** (1985) 299–326.
- [35] T. Banks, *CONSTRAINTS ON SU(2) x U(1) BREAKING BY VACUUM MISALIGNMENT*, *Nucl. Phys.* **B243** (1984) 125–130.
- [36] L. Randall and R. Sundrum, *A Large mass hierarchy from a small extra dimension*, *Phys. Rev. Lett.* **83** (1999) 3370–3373, [[hep-ph/9905221](#)].
- [37] N. Arkani-Hamed, S. Dimopoulos, and G. R. Dvali, *The Hierarchy problem and new dimensions at a millimeter*, *Phys. Lett.* **B429** (1998) 263–272, [[hep-ph/9803315](#)].
- [38] T. Appelquist, H.-C. Cheng, and B. A. Dobrescu, *Bounds on universal extra dimensions*, *Phys. Rev.* **D64** (2001) 035002, [[hep-ph/0012100](#)].
- [39] N. Arkani-Hamed and M. Schmaltz, *Hierarchies without symmetries from extra dimensions*, *Phys. Rev.* **D61** (2000) 033005, [[hep-ph/9903417](#)].
- [40] Z. Chacko, H.-S. Goh, and R. Harnik, *The Twin Higgs: Natural electroweak breaking from mirror symmetry*, *Phys. Rev. Lett.* **96** (2006) 231802, [[hep-ph/0506256](#)].
- [41] P. W. Graham, D. E. Kaplan, and S. Rajendran, *Cosmological Relaxation of the Electroweak Scale*, *Phys. Rev. Lett.* **115** (2015), no. 22 221801, [[arXiv:1504.07551](#)].
- [42] M. Drees, R. Godbole, and P. Roy, *Theory and phenomenology of sparticles: An account of four-dimensional N=1 supersymmetry in high energy physics*. 2004.
- [43] H. Baer and X. Tata, *Weak scale supersymmetry: From superfields to scattering events*. Cambridge University Press, 2006.
- [44] J. Wess and J. Bagger, *Supersymmetry and supergravity*. 1992.
- [45] H. P. Nilles, *Supersymmetry, Supergravity and Particle Physics*, *Phys. Rept.* **110** (1984) 1–162.
- [46] H. E. Haber and G. L. Kane, *The Search for Supersymmetry: Probing Physics Beyond the Standard Model*, *Phys. Rept.* **117** (1985) 75–263.
- [47] H. E. Haber, *Introductory low-energy supersymmetry*, in *Proceedings, Theoretical Advanced Study Institute (TASI 92): From Black Holes and Strings to Particles: Boulder, USA, June 1-26, 1992*, pp. 589–686, 1993. [hep-ph/9306207](#).

- [48] M. Drees, *An Introduction to supersymmetry*, in *Current topics in physics. Proceedings, Inauguration Conference of the Asia-Pacific Center for Theoretical Physics (APCTP), Seoul, Korea, June 4-10, 1996. Vol. 1, 2, 1996.* [hep-ph/9611409](#).
- [49] S. P. Martin, *A Supersymmetry primer*, [hep-ph/9709356](#). [Adv. Ser. Direct. High Energy Phys.18,1(1998)].
- [50] A. Djouadi, *The Anatomy of electro-weak symmetry breaking. II. The Higgs bosons in the minimal supersymmetric model*, *Phys. Rept.* **459** (2008) 1–241, [[hep-ph/0503173](#)].
- [51] R. Haag, J. T. Lopuszanski, and M. Sohnius, *All Possible Generators of Supersymmetries of the s Matrix*, *Nucl. Phys.* **B88** (1975) 257.
- [52] P. Bechtle et al., *Constrained Supersymmetry after two years of LHC data: a global view with Fittino*, *JHEP* **06** (2012) 098, [[arXiv:1204.4199](#)].
- [53] S. Cassel, D. M. Ghilencea, S. Kraml, A. Lessa, and G. G. Ross, *Fine-tuning implications for complementary dark matter and LHC SUSY searches*, *JHEP* **05** (2011) 120, [[arXiv:1101.4664](#)].
- [54] P. Bechtle et al., *Killing the cMSSM softly*, *Eur. Phys. J.* **C76** (2016), no. 2 96, [[arXiv:1508.05951](#)].
- [55] **Muon g-2** Collaboration, G. W. Bennett et al., *Final Report of the Muon E821 Anomalous Magnetic Moment Measurement at BNL*, *Phys. Rev.* **D73** (2006) 072003, [[hep-ex/0602035](#)].
- [56] **MSSM Working Group** Collaboration, A. Djouadi et al., *The Minimal supersymmetric standard model: Group summary report*, in *GDR (Groupement De Recherche) - Supersymetrie Montpellier, France, April 15-17, 1998, 1998.* [hep-ph/9901246](#).
- [57] C. F. Berger, J. S. Gainer, J. L. Hewett, and T. G. Rizzo, *Supersymmetry Without Prejudice*, *JHEP* **02** (2009) 023, [[arXiv:0812.0980](#)].
- [58] J. A. Conley, J. S. Gainer, J. L. Hewett, M. P. Le, and T. G. Rizzo, *Supersymmetry Without Prejudice at the LHC*, *Eur. Phys. J.* **C71** (2011) 1697, [[arXiv:1009.2539](#)].
- [59] K. J. de Vries et al., *The pMSSM10 after LHC Run 1*, *Eur. Phys. J.* **C75** (2015), no. 9 422, [[arXiv:1504.03260](#)].
- [60] G. Bertone, F. Calore, S. Caron, R. Ruiz, J. S. Kim, R. Trotta, and C. Weniger, *Global analysis of the pMSSM in light of the Fermi GeV excess: prospects for the LHC Run-II and astroparticle experiments*, *JCAP* **1604** (2016), no. 04 037, [[arXiv:1507.07008](#)].
- [61] **ATLAS** Collaboration, A. collaboration, *Search for resonances decaying to photon pairs in  $3.2 \text{ fb}^{-1}$  of  $pp$  collisions at  $\sqrt{s} = 13 \text{ TeV}$  with the ATLAS detector*, .
- [62] **CMS** Collaboration, C. Collaboration, *Search for new physics in high mass diphoton events in proton-proton collisions at 13TeV*, .

- 
- [63] **SNO** Collaboration, B. Aharmim et al., *Combined Analysis of all Three Phases of Solar Neutrino Data from the Sudbury Neutrino Observatory*, *Phys. Rev.* **C88** (2013) 025501, [[arXiv:1109.0763](#)].
- [64] **Super-Kamiokande** Collaboration, J. Hosaka et al., *Solar neutrino measurements in super-Kamiokande-I*, *Phys. Rev.* **D73** (2006) 112001, [[hep-ex/0508053](#)].
- [65] **Super-Kamiokande** Collaboration, J. P. Cravens et al., *Solar neutrino measurements in Super-Kamiokande-II*, *Phys. Rev.* **D78** (2008) 032002, [[arXiv:0803.4312](#)].
- [66] **Super-Kamiokande** Collaboration, K. Abe et al., *Solar neutrino results in Super-Kamiokande-III*, *Phys. Rev.* **D83** (2011) 052010, [[arXiv:1010.0118](#)].
- [67] J. H. Oort, *The force exerted by the stellar system in the direction perpendicular to the galactic plane and some related problems*, *Bull. Astron. Inst. Netherlands* **6** (1932) 249.
- [68] F. Zwicky, *On the Masses of Nebulae and of Clusters of Nebulae*, *Astrophys. J.* **86** (1937) 217–246.
- [69] V. C. Rubin and W. K. Ford, Jr., *Rotation of the Andromeda Nebula from a Spectroscopic Survey of Emission Regions*, *Astrophys. J.* **159** (1970) 379–403.
- [70] D. E. Morrissey and M. J. Ramsey-Musolf, *Electroweak baryogenesis*, *New J. Phys.* **14** (2012) 125003, [[arXiv:1206.2942](#)].
- [71] J. M. Cline, *Baryogenesis*, in *Les Houches Summer School - Session 86: Particle Physics and Cosmology: The Fabric of Spacetime Les Houches, France, July 31-August 25, 2006*, 2006. [hep-ph/0609145](#).
- [72] M. Dine and A. Kusenko, *The Origin of the matter - antimatter asymmetry*, *Rev. Mod. Phys.* **76** (2003) 1, [[hep-ph/0303065](#)].
- [73] M. Trodden, *Electroweak baryogenesis*, *Rev. Mod. Phys.* **71** (1999) 1463–1500, [[hep-ph/9803479](#)].
- [74] P. Huet and E. Sather, *Electroweak baryogenesis and standard model CP violation*, *Phys. Rev.* **D51** (1995) 379–394, [[hep-ph/9404302](#)].
- [75] P. Minkowski,  $\mu \rightarrow e\gamma$  at a Rate of One Out of  $10^9$  Muon Decays?, *Phys. Lett.* **67B** (1977) 421–428.
- [76] M. Gell-Mann, P. Ramond, and R. Slansky, *Complex Spinors and Unified Theories*, *Conf. Proc.* **C790927** (1979) 315–321, [[arXiv:1306.4669](#)].
- [77] R. N. Mohapatra and G. Senjanovic, *Neutrino Mass and Spontaneous Parity Violation*, *Phys. Rev. Lett.* **44** (1980) 912.
- [78] J. Schechter and J. W. F. Valle, *Neutrino Masses in  $SU(2) \times U(1)$  Theories*, *Phys. Rev.* **D22** (1980) 2227.

- [79] T. P. Cheng and L.-F. Li, *Neutrino Masses, Mixings and Oscillations in  $SU(2) \times U(1)$  Models of Electroweak Interactions*, *Phys. Rev.* **D22** (1980) 2860.
- [80] E. K. Akhmedov, A. S. Joshipura, S. Ranfone, and J. W. F. Valle, *Left-right symmetry and neutrino stability*, *Nucl. Phys.* **B441** (1995) 61–75, [[hep-ph/9501248](#)].
- [81] A. Kumar and R. N. Mohapatra, *A Model for Neutrino Decays*, *Phys. Lett.* **150B** (1985) 191–195.
- [82] E. Ma, *Unifiable supersymmetric left-right model with  $E(6)$  particle content*, *Phys. Lett.* **B344** (1995) 164–168, [[hep-ph/9408237](#)].
- [83] H. Fritzsch and P. Minkowski, *Unified Interactions of Leptons and Hadrons*, *Annals Phys.* **93** (1975) 193–266.
- [84] T. E. Clark, T.-K. Kuo, and N. Nakagawa, *A  $SO(10)$  SUPERSYMMETRIC GRAND UNIFIED THEORY*, *Phys. Lett.* **115B** (1982) 26–28.
- [85] C. S. Aulakh and R. N. Mohapatra, *Implications of Supersymmetric  $SO(10)$  Grand Unification*, *Phys. Rev.* **D28** (1983) 217.
- [86] B. Brahmachari, U. Sarkar, and K. Sridhar, *Ruling out low-energy left-right symmetry in unified theories*, *Phys. Lett.* **B297** (1992) 105–110.
- [87] C. Arbeláez, M. Hirsch, M. Malinský, and J. C. Romão, *LHC-scale left-right symmetry and unification*, *Phys. Rev.* **D89** (2014), no. 3 035002, [[arXiv:1311.3228](#)].
- [88] M. Lindner and M. Weiser, *Gauge coupling unification in left-right symmetric models*, *Phys. Lett.* **B383** (1996) 405–414, [[hep-ph/9605353](#)].
- [89] F. Staub, *SARAH*, [[arXiv:0806.0538](#)].
- [90] F. Staub, *From Superpotential to Model Files for FeynArts and CalcHep/CompHep*, *Comput. Phys. Commun.* **181** (2010) 1077–1086, [[arXiv:0909.2863](#)].
- [91] F. Staub, *Automatic Calculation of supersymmetric Renormalization Group Equations and Self Energies*, *Comput. Phys. Commun.* **182** (2011) 808–833, [[arXiv:1002.0840](#)].
- [92] F. Staub, *SARAH 3.2: Dirac Gauginos, UFO output, and more*, *Comput. Phys. Commun.* **184** (2013) 1792–1809, [[arXiv:1207.0906](#)].
- [93] F. Staub, *SARAH 4 : A tool for (not only SUSY) model builders*, *Comput. Phys. Commun.* **185** (2014) 1773–1790, [[arXiv:1309.7223](#)].
- [94] F. Staub, *Exploring new models in all detail with SARAH*, *Adv. High Energy Phys.* **2015** (2015) 840780, [[arXiv:1503.04200](#)].
- [95] N. D. Christensen and C. Duhr, *FeynRules - Feynman rules made easy*, *Comput. Phys. Commun.* **180** (2009) 1614–1641, [[arXiv:0806.4194](#)].

- [96] F. Staub et al., *Precision tools and models to narrow in on the 750 GeV diphoton resonance*, *Eur. Phys. J.* **C76** (2016), no. 9 516, [[arXiv:1602.05581](#)].
- [97] M. D. Goodsell, K. Nickel, and F. Staub, *Two-Loop Higgs mass calculations in supersymmetric models beyond the MSSM with SARAH and SPheno*, *Eur. Phys. J.* **C75** (2015), no. 1 32, [[arXiv:1411.0675](#)].
- [98] M. Goodsell, K. Nickel, and F. Staub, *Generic two-loop Higgs mass calculation from a diagrammatic approach*, *Eur. Phys. J.* **C75** (2015), no. 6 290, [[arXiv:1503.03098](#)].
- [99] M. D. Goodsell and F. Staub, *The Higgs mass in the CP violating MSSM, NMSSM, and beyond*, *Eur. Phys. J.* **C77** (2017), no. 1 46, [[arXiv:1604.05335](#)].
- [100] F. Staub, P. Athron, U. Ellwanger, R. Gröber, M. Mühlleitner, P. Slavich, and A. Voigt, *Higgs mass predictions of public NMSSM spectrum generators*, *Comput. Phys. Commun.* **202** (2016) 113–130, [[arXiv:1507.05093](#)].
- [101] W. Porod, F. Staub, and A. Vicente, *A Flavor Kit for BSM models*, *Eur. Phys. J.* **C74** (2014), no. 8 2992, [[arXiv:1405.1434](#)].
- [102] T. Hahn, *Generating Feynman diagrams and amplitudes with FeynArts 3*, *Comput. Phys. Commun.* **140** (2001) 418–431, [[hep-ph/0012260](#)].
- [103] T. Hahn, *FormCalc 6*, *PoS ACAT08* (2008) 121, [[arXiv:0901.1528](#)].
- [104] W. Porod, *SPheno, a program for calculating supersymmetric spectra, SUSY particle decays and SUSY particle production at  $e^+e^-$  colliders*, *Comput. Phys. Commun.* **153** (2003) 275–315, [[hep-ph/0301101](#)].
- [105] W. Porod and F. Staub, *SPheno 3.1: Extensions including flavour, CP-phases and models beyond the MSSM*, *Comput. Phys. Commun.* **183** (2012) 2458–2469, [[arXiv:1104.1573](#)].
- [106] D. M. Pierce, J. A. Bagger, K. T. Matchev, and R.-j. Zhang, *Precision corrections in the minimal supersymmetric standard model*, *Nucl. Phys.* **B491** (1997) 3–67, [[hep-ph/9606211](#)].
- [107] P. Bechtle, O. Brein, S. Heinemeyer, O. Stål, T. Stefaniak, G. Weiglein, and K. E. Williams, *HiggsBounds – 4: Improved Tests of Extended Higgs Sectors against Exclusion Bounds from LEP, the Tevatron and the LHC*, *Eur. Phys. J.* **C74** (2014), no. 3 2693, [[arXiv:1311.0055](#)].
- [108] P. Bechtle, S. Heinemeyer, O. Stål, T. Stefaniak, and G. Weiglein, *HiggsSignals: Confronting arbitrary Higgs sectors with measurements at the Tevatron and the LHC*, *Eur. Phys. J.* **C74** (2014), no. 2 2711, [[arXiv:1305.1933](#)].
- [109] P. Z. Skands et al., *SUSY Les Houches accord: Interfacing SUSY spectrum calculators, decay packages, and event generators*, *JHEP* **07** (2004) 036, [[hep-ph/0311123](#)].

- [110] J. E. Camargo-Molina, B. O’Leary, W. Porod, and F. Staub, *Vevacious: A Tool For Finding The Global Minima Of One-Loop Effective Potentials With Many Scalars*, *Eur. Phys. J.* **C73** (2013), no. 10 2588, [[arXiv:1307.1477](#)].
- [111] C. L. Wainwright, *CosmoTransitions: Computing Cosmological Phase Transition Temperatures and Bubble Profiles with Multiple Fields*, *Comput. Phys. Commun.* **183** (2012) 2006–2013, [[arXiv:1109.4189](#)].
- [112] P. Bechtle, O. Brein, S. Heinemeyer, G. Weiglein, and K. E. Williams, *HiggsBounds: Confronting Arbitrary Higgs Sectors with Exclusion Bounds from LEP and the Tevatron*, *Comput. Phys. Commun.* **181** (2010) 138–167, [[arXiv:0811.4169](#)].
- [113] P. Bechtle, O. Brein, S. Heinemeyer, G. Weiglein, and K. E. Williams, *HiggsBounds 2.0.0: Confronting Neutral and Charged Higgs Sector Predictions with Exclusion Bounds from LEP and the Tevatron*, *Comput. Phys. Commun.* **182** (2011) 2605–2631, [[arXiv:1102.1898](#)].
- [114] C. Degrande, C. Duhr, B. Fuks, D. Grellscheid, O. Mattelaer, and T. Reiter, *UFO - The Universal FeynRules Output*, *Comput. Phys. Commun.* **183** (2012) 1201–1214, [[arXiv:1108.2040](#)].
- [115] J. Alwall, M. Herquet, F. Maltoni, O. Mattelaer, and T. Stelzer, *MadGraph 5 : Going Beyond*, *JHEP* **06** (2011) 128, [[arXiv:1106.0522](#)].
- [116] G. Cullen, N. Greiner, G. Heinrich, G. Luisoni, P. Mastrolia, G. Ossola, T. Reiter, and F. Tramontano, *Automated One-Loop Calculations with GoSam*, *Eur. Phys. J.* **C72** (2012) 1889, [[arXiv:1111.2034](#)].
- [117] S. Gieseke, A. Ribon, M. H. Seymour, P. Stephens, and B. Webber, *Herwig++ 1.0: An Event generator for e+ e- annihilation*, *JHEP* **02** (2004) 005, [[hep-ph/0311208](#)].
- [118] S. Gieseke, D. Grellscheid, K. Hamilton, A. Ribon, P. Richardson, M. H. Seymour, P. Stephens, and B. R. Webber, *Herwig++ 2.0 Release Note*, [hep-ph/0609306](#).
- [119] J. Bellm et al., *Herwig++ 2.7 Release Note*, [arXiv:1310.6877](#).
- [120] T. Gleisberg, S. Hoeche, F. Krauss, A. Schaliche, S. Schumann, and J.-C. Winter, *SHERPA 1. alpha: A Proof of concept version*, *JHEP* **02** (2004) 056, [[hep-ph/0311263](#)].
- [121] T. Gleisberg, S. Hoeche, F. Krauss, M. Schonherr, S. Schumann, F. Siegert, and J. Winter, *Event generation with SHERPA 1.1*, *JHEP* **02** (2009) 007, [[arXiv:0811.4622](#)].
- [122] S. Höche, S. Kuttimalai, S. Schumann, and F. Siegert, *Beyond Standard Model calculations with Sherpa*, *Eur. Phys. J.* **C75** (2015), no. 3 135, [[arXiv:1412.6478](#)].
- [123] W. Kilian, T. Ohl, and J. Reuter, *WHIZARD: Simulating Multi-Particle Processes at LHC and ILC*, *Eur. Phys. J.* **C71** (2011) 1742, [[arXiv:0708.4233](#)].

- 
- [124] M. Moretti, T. Ohl, and J. Reuter, *O'Mega: An Optimizing matrix element generator*, [hep-ph/0102195](#).
- [125] A. Pukhov, *CalcHEP 2.3: MSSM, structure functions, event generation, batchs, and generation of matrix elements for other packages*, [hep-ph/0412191](#).
- [126] D. Barducci, G. Belanger, J. Bernon, F. Boudjema, J. Da Silva, S. Kraml, U. Laa, and A. Pukhov, *Collider limits on new physics within micrOMEGAs*, [arXiv:1606.03834](#).
- [127] G. Belanger, F. Boudjema, A. Pukhov, and A. Semenov, *MicrOMEGAs: A Program for calculating the relic density in the MSSM*, *Comput. Phys. Commun.* **149** (2002) 103–120, [[hep-ph/0112278](#)].
- [128] T. A. collaboration, *Search for resonances in diphoton events with the ATLAS detector at  $\sqrt{s} = 13$  TeV*, .
- [129] **CMS** Collaboration, C. Collaboration, *Search for new physics in high mass diphoton events in  $3.3 \text{ fb}^{-1}$  of proton-proton collisions at  $\sqrt{s} = 13$  TeV and combined interpretation of searches at 8 TeV and 13 TeV*, .
- [130] **ATLAS** Collaboration, T. A. collaboration, *Search for scalar diphoton resonances with  $15.4 \text{ fb}^{-1}$  of data collected at  $\sqrt{s}=13$  TeV in 2015 and 2016 with the ATLAS detector*, .
- [131] **CMS** Collaboration, V. Khachatryan et al., *Search for high-mass diphoton resonances in proton-proton collisions at 13 TeV and combination with 8 TeV search*, *Phys. Lett.* **B767** (2017) 147–170, [[arXiv:1609.02507](#)].
- [132] M. Chala, M. Duerr, F. Kahlhoefer, and K. Schmidt-Hoberg, *Tricking Landau–Yang: How to obtain the diphoton excess from a vector resonance*, *Phys. Lett.* **B755** (2016) 145–149, [[arXiv:1512.06833](#)].
- [133] L. D. Landau, *On the angular momentum of a system of two photons*, *Dokl. Akad. Nauk Ser. Fiz.* **60** (1948), no. 2 207–209.
- [134] C.-N. Yang, *Selection Rules for the Dematerialization of a Particle Into Two Photons*, *Phys. Rev.* **77** (1950) 242–245.
- [135] Y. Gao, A. V. Gritsan, Z. Guo, K. Melnikov, M. Schulze, and N. V. Tran, *Spin determination of single-produced resonances at hadron colliders*, *Phys. Rev.* **D81** (2010) 075022, [[arXiv:1001.3396](#)].
- [136] J. Ellis and D. S. Hwang, *Does the ‘Higgs’ have Spin Zero?*, *JHEP* **09** (2012) 071, [[arXiv:1202.6660](#)].
- [137] J. Ellis, R. Fok, D. S. Hwang, V. Sanz, and T. You, *Distinguishing ‘Higgs’ spin hypotheses using  $\gamma\gamma$  and  $WW^*$  decays*, *Eur. Phys. J.* **C73** (2013) 2488, [[arXiv:1210.5229](#)].
- [138] M. Bauer, M. Neubert, and A. Thamm, *The “forgotten” decay  $S \rightarrow Zh$  as a CP analyzer*, [arXiv:1607.01016](#).

- [139] M. Bauer, M. Neubert, and A. Thamm, *Analyzing the CP Nature of a New Scalar Particle via  $S\text{-}Z\gamma$  Decay*, *Phys. Rev. Lett.* **117** (2016) 181801, [[arXiv:1610.00009](#)].
- [140] R. Franceschini, G. F. Giudice, J. F. Kamenik, M. McCullough, A. Pomarol, R. Rattazzi, M. Redi, F. Riva, A. Strumia, and R. Torre, *What is the  $\gamma\gamma$  resonance at 750 GeV?*, *JHEP* **03** (2016) 144, [[arXiv:1512.04933](#)].
- [141] H. P. Nilles and M. W. Winkler, *750 GeV Diphotons and Supersymmetric Grand Unification*, *JHEP* **05** (2016) 182, [[arXiv:1604.03598](#)].
- [142] A. Djouadi, *The Anatomy of electro-weak symmetry breaking. I: The Higgs boson in the standard model*, *Phys. Rept.* **457** (2008) 1–216, [[hep-ph/0503172](#)].
- [143] A. D. Martin, W. J. Stirling, R. S. Thorne, and G. Watt, *Parton distributions for the LHC*, *Eur. Phys. J.* **C63** (2009) 189–285, [[arXiv:0901.0002](#)].
- [144] ATLAS Collaboration, G. Aad et al., *Search for new phenomena in the dijet mass distribution using  $p - p$  collision data at  $\sqrt{s} = 8$  TeV with the ATLAS detector*, *Phys. Rev.* **D91** (2015), no. 5 052007, [[arXiv:1407.1376](#)].
- [145] W. Chao, *Neutrino Catalyzed Diphoton Excess*, *Nucl. Phys.* **B911** (2016) 231–245, [[arXiv:1512.08484](#)].
- [146] A. Pilaftsis, *Diphoton Signatures from Heavy Axion Decays at the CERN Large Hadron Collider*, *Phys. Rev.* **D93** (2016), no. 1 015017, [[arXiv:1512.04931](#)].
- [147] R. Martinez, F. Ochoa, and C. F. Sierra, *Diphoton decay for a 750 GeV scalar boson in a  $U(1)_X$  model*, *Nucl. Phys.* **B913** (2016) 64–78, [[arXiv:1512.05617](#)].
- [148] M. Spira, A. Djouadi, D. Graudenz, and P. M. Zerwas, *Higgs boson production at the LHC*, *Nucl. Phys.* **B453** (1995) 17–82, [[hep-ph/9504378](#)].
- [149] C. Hartmann and M. Trott, *On one-loop corrections in the standard model effective field theory; the  $\Gamma(h \rightarrow \gamma\gamma)$  case*, *JHEP* **07** (2015) 151, [[arXiv:1505.02646](#)].
- [150] S. Knapen, T. Melia, M. Papucci, and K. Zurek, *Rays of light from the LHC*, *Phys. Rev.* **D93** (2016), no. 7 075020, [[arXiv:1512.04928](#)].
- [151] A. Falkowski, O. Slone, and T. Volansky, *Phenomenology of a 750 GeV Singlet*, *JHEP* **02** (2016) 152, [[arXiv:1512.05777](#)].
- [152] H. Han, S. Wang, and S. Zheng, *Scalar Explanation of Diphoton Excess at LHC*, *Nucl. Phys.* **B907** (2016) 180–186, [[arXiv:1512.06562](#)].
- [153] H. Han, S. Wang, and S. Zheng, *Dark Matter Theories in the Light of Diphoton Excess*, [arXiv:1512.07992](#).

- 
- [154] F. Wang, W. Wang, L. Wu, J. M. Yang, and M. Zhang, *Interpreting 750 GeV diphoton resonance as degenerate Higgs bosons in NMSSM with vector-like particles*, [arXiv:1512.08434](#).
- [155] F. Goertz, J. F. Kamenik, A. Katz, and M. Nardecchia, *Indirect Constraints on the Scalar Di-Photon Resonance at the LHC*, *JHEP* **05** (2016) 187, [[arXiv:1512.08500](#)].
- [156] M. Son and A. Urbano, *A new scalar resonance at 750 GeV: Towards a proof of concept in favor of strongly interacting theories*, *JHEP* **05** (2016) 181, [[arXiv:1512.08307](#)].
- [157] E. Bertuzzo, P. A. N. Machado, and M. Taoso, *Diphoton excess in the 2HDM: Hastening towards instability and the nonperturbative regime*, *Phys. Rev.* **D94** (2016), no. 11 115006, [[arXiv:1601.07508](#)].
- [158] K. J. Bae, M. Endo, K. Hamaguchi, and T. Moroi, *Diphoton Excess and Running Couplings*, *Phys. Lett.* **B757** (2016) 493–500, [[arXiv:1602.03653](#)].
- [159] A. Salvio, F. Staub, A. Strumia, and A. Urbano, *On the maximal diphoton width*, *JHEP* **03** (2016) 214, [[arXiv:1602.01460](#)].
- [160] C. Gross, O. Lebedev, and J. M. No, *Drell–Yan constraints on new electroweak states: LHC as a  $pp \rightarrow l^+l^-$  precision machine*, *Mod. Phys. Lett.* **A32** (2017), no. 16 1750094, [[arXiv:1602.03877](#)].
- [161] F. Goertz, A. Katz, M. Son, and A. Urbano, *Precision Drell-Yan Measurements at the LHC and Implications for the Diphoton Excess*, *JHEP* **07** (2016) 136, [[arXiv:1602.04801](#)].
- [162] S. Kanemura, K. Nishiwaki, H. Okada, Y. Orikasa, S. C. Park, and R. Watanabe, *LHC 750 GeV diphoton excess in a radiative seesaw model*, *PTEP* **2016** (2016), no. 12 123B04, [[arXiv:1512.09048](#)].
- [163] T. Nomura and H. Okada, *Four-loop Neutrino Model Inspired by Diphoton Excess at 750 GeV*, *Phys. Lett.* **B755** (2016) 306–311, [[arXiv:1601.00386](#)].
- [164] J. Cao, C. Han, L. Shang, W. Su, J. M. Yang, and Y. Zhang, *Interpreting the 750 GeV diphoton excess by the singlet extension of the Manohar–Wise model*, *Phys. Lett.* **B755** (2016) 456–463, [[arXiv:1512.06728](#)].
- [165] R. Ding, Z.-L. Han, Y. Liao, and X.-D. Ma, *Interpretation of 750 GeV Diphoton Excess at LHC in Singlet Extension of Color-octet Neutrino Mass Model*, *Eur. Phys. J.* **C76** (2016), no. 4 204, [[arXiv:1601.02714](#)].
- [166] M. Fabbrichesi and A. Urbano, *750 GeV resonance at the LHC and perturbative unitarity*, *Phys. Rev.* **D94** (2016), no. 3 035004, [[arXiv:1601.02447](#)].
- [167] H. Georgi and M. Machacek, *DOUBLY CHARGED HIGGS BOSONS*, *Nucl. Phys.* **B262** (1985) 463–477.

- [168] P. Kant, R. V. Harlander, L. Mihaila, and M. Steinhauser, *Light MSSM Higgs boson mass to three-loop accuracy*, *JHEP* **08** (2010) 104, [[arXiv:1005.5709](#)].
- [169] B. Dutta, Y. Gao, T. Ghosh, I. Gogoladze, T. Li, Q. Shafi, and J. W. Walker, *Diphoton Excess in Consistent Supersymmetric SU(5) Models with Vector-like Particles*, [arXiv:1601.00866](#).
- [170] K. Nickel and F. Staub, *Precise determination of the Higgs mass in supersymmetric models with vectorlike tops and the impact on naturalness in minimal GMSB*, *JHEP* **07** (2015) 139, [[arXiv:1505.06077](#)].
- [171] J. Baglio, R. Gröber, M. Mühlleitner, D. T. Nhung, H. Rzehak, M. Spira, J. Streicher, and K. Walz, *NMSSMCALC: A Program Package for the Calculation of Loop-Corrected Higgs Boson Masses and Decay Widths in the (Complex) NMSSM*, *Comput. Phys. Commun.* **185** (2014), no. 12 3372–3391, [[arXiv:1312.4788](#)].
- [172] M. Kramer, E. Laenen, and M. Spira, *Soft gluon radiation in Higgs boson production at the LHC*, *Nucl. Phys.* **B511** (1998) 523–549, [[hep-ph/9611272](#)].
- [173] K. G. Chetyrkin, J. H. Kuhn, and C. Sturm, *QCD decoupling at four loops*, *Nucl. Phys.* **B744** (2006) 121–135, [[hep-ph/0512060](#)].
- [174] Y. Schroder and M. Steinhauser, *Four-loop decoupling relations for the strong coupling*, *JHEP* **01** (2006) 051, [[hep-ph/0512058](#)].
- [175] P. A. Baikov and K. G. Chetyrkin, *Top Quark Mediated Higgs Boson Decay into Hadrons to Order  $\alpha_s^5$* , *Phys. Rev. Lett.* **97** (2006) 061803, [[hep-ph/0604194](#)].
- [176] A. Djouadi, J. Kalinowski, and M. Spira, *HDECAY: A Program for Higgs boson decays in the standard model and its supersymmetric extension*, *Comput. Phys. Commun.* **108** (1998) 56–74, [[hep-ph/9704448](#)].
- [177] K. G. Chetyrkin, B. A. Kniehl, and M. Steinhauser, *Hadronic Higgs decay to order  $\alpha_s^{*4}$* , *Phys. Rev. Lett.* **79** (1997) 353–356, [[hep-ph/9705240](#)].
- [178] S. Dawson, A. Djouadi, and M. Spira, *QCD corrections to SUSY Higgs production: The Role of squark loops*, *Phys. Rev. Lett.* **77** (1996) 16–19, [[hep-ph/9603423](#)].
- [179] **LHC Higgs Cross Section Working Group** Collaboration, J. R. Andersen et al., *Handbook of LHC Higgs Cross Sections: 3. Higgs Properties*, [arXiv:1307.1347](#).
- [180] P. Athron, J.-h. Park, D. Stöckinger, and A. Voigt, *FlexibleSUSY—A spectrum generator generator for supersymmetric models*, *Comput. Phys. Commun.* **190** (2015) 139–172, [[arXiv:1406.2319](#)].
- [181] M. D. Goodsell, S. Liebler, and F. Staub, *Generic calculation of two-body partial decay widths at the full one-loop level*, [arXiv:1703.09237](#).

- 
- [182] *Search for production of vector-like quark pairs and of four top quarks in the lepton plus jets final state in  $pp$  collisions at  $\sqrt{s} = 8$  TeV with the ATLAS detector*, Tech. Rep. ATLAS-CONF-2015-012, CERN, Geneva, Mar, 2015.
- [183] C. Anastasiou, C. Duhr, F. Dulat, E. Furlan, T. Gehrmann, F. Herzog, A. Lazopoulos, and B. Mistlberger, *CP-even scalar boson production via gluon fusion at the LHC*, *JHEP* **09** (2016) 037, [[arXiv:1605.05761](#)].
- [184] W. Chao, R. Huo, and J.-H. Yu, *The minimal scalar-vectorlike top interpretation of the diphoton excess*, *Eur. Phys. J. Plus* **132** (2017), no. 1 27, [[arXiv:1512.05738](#)].
- [185] R. Benbrik, C.-H. Chen, and T. Nomura, *Higgs singlet boson as a diphoton resonance in a vectorlike quark model*, *Phys. Rev.* **D93** (2016), no. 5 055034, [[arXiv:1512.06028](#)].
- [186] M. Bauer and M. Neubert, *Flavor anomalies, the 750 GeV diphoton excess, and a dark matter candidate*, *Phys. Rev.* **D93** (2016), no. 11 115030, [[arXiv:1512.06828](#)].
- [187] C.-W. Chiang and A.-L. Kuo, *Can the 750-GeV diphoton resonance be the singlet Higgs boson of custodial Higgs triplet model?*, *Phys. Lett.* **B760** (2016) 634–640, [[arXiv:1601.06394](#)].
- [188] N. Bizot, S. Davidson, M. Frigerio, and J. L. Kneur, *Two Higgs doublets to explain the excesses  $pp \rightarrow \gamma\gamma(750 \text{ GeV})$  and  $h \rightarrow \tau^\pm\mu^\mp$* , *JHEP* **03** (2016) 073, [[arXiv:1512.08508](#)].
- [189] A. Angelescu, A. Djouadi, and G. Moreau, *Scenarii for interpretations of the LHC diphoton excess: two Higgs doublets and vector-like quarks and leptons*, *Phys. Lett.* **B756** (2016) 126–132, [[arXiv:1512.04921](#)].
- [190] S. Jung, J. Song, and Y. W. Yoon, *How Resonance-Continuum Interference Changes 750 GeV Diphoton Excess: Signal Enhancement and Peak Shift*, *JHEP* **05** (2016) 009, [[arXiv:1601.00006](#)].
- [191] M. Badziak, *Interpreting the 750 GeV diphoton excess in minimal extensions of Two-Higgs-Doublet models*, *Phys. Lett.* **B759** (2016) 464–470, [[arXiv:1512.07497](#)].
- [192] X.-F. Han and L. Wang, *Implication of the 750 GeV diphoton resonance on two-Higgs-doublet model and its extensions with Higgs field*, *Phys. Rev.* **D93** (2016), no. 5 055027, [[arXiv:1512.06587](#)].
- [193] S. Moretti and K. Yagyu, *750 GeV diphoton excess and its explanation in two-Higgs-doublet models with a real inert scalar multiplet*, *Phys. Rev.* **D93** (2016), no. 5 055043, [[arXiv:1512.07462](#)].
- [194] P. Ko and T. Nomura, *Dark sector shining through 750 GeV dark Higgs boson at the LHC*, *Phys. Lett.* **B758** (2016) 205–211, [[arXiv:1601.02490](#)].

- [195] K. Das and S. K. Rai, *750 GeV diphoton excess in a  $U(1)$  hidden symmetry model*, *Phys. Rev. D* **93** (2016), no. 9 095007, [[arXiv:1512.07789](#)].
- [196] S. Chang, *A Simple  $U(1)$  Gauge Theory Explanation of the Diphoton Excess*, *Phys. Rev. D* **93** (2016), no. 5 055016, [[arXiv:1512.06426](#)].
- [197] J.-H. Yu, *Hidden Gauged  $U(1)$  Model: Unifying Scotogenic Neutrino and Flavor Dark Matter*, *Phys. Rev. D* **93** (2016), no. 11 113007, [[arXiv:1601.02609](#)].
- [198] T. Modak, S. Sadhukhan, and R. Srivastava, *750 GeV Diphoton excess from Gauged  $B - L$  Symmetry*, *Phys. Lett. B* **756** (2016) 405–412, [[arXiv:1601.00836](#)].
- [199] W. Chao, *Symmetries behind the 750 GeV diphoton excess*, *Phys. Rev. D* **93** (2016), no. 11 115013, [[arXiv:1512.06297](#)].
- [200] P. Ko, Y. Omura, and C. Yu, *Diphoton Excess at 750 GeV in leptophobic  $U(1)$  model inspired by  $E_6$  GUT*, *JHEP* **04** (2016) 098, [[arXiv:1601.00586](#)].
- [201] A. Dasgupta, M. Mitra, and D. Borah, *Minimal Left-Right Symmetry Confronted with the 750 GeV Di-photon Excess at LHC*, [[arXiv:1512.09202](#)].
- [202] F. F. Deppisch, C. Hati, S. Patra, P. Pritimita, and U. Sarkar, *Implications of the diphoton excess on left–right models and gauge unification*, *Phys. Lett. B* **757** (2016) 223–230, [[arXiv:1601.00952](#)].
- [203] P. S. B. Dev, R. N. Mohapatra, and Y. Zhang, *Quark Seesaw, Vectorlike Fermions and Diphoton Excess*, *JHEP* **02** (2016) 186, [[arXiv:1512.08507](#)].
- [204] Q.-H. Cao, S.-L. Chen, and P.-H. Gu, *Strong CP Problem, Neutrino Masses and the 750 GeV Diphoton Resonance*, [[arXiv:1512.07541](#)].
- [205] A. Berlin, *Diphoton and diboson excesses in a left-right symmetric theory of dark matter*, *Phys. Rev. D* **93** (2016), no. 5 055015, [[arXiv:1601.01381](#)].
- [206] U. K. Dey, S. Mohanty, and G. Tomar, *750 GeV resonance in the dark left–right model*, *Phys. Lett. B* **756** (2016) 384–389, [[arXiv:1512.07212](#)].
- [207] S. M. Boucenna, S. Morisi, and A. Vicente, *The LHC diphoton resonance from gauge symmetry*, *Phys. Rev. D* **93** (2016), no. 11 115008, [[arXiv:1512.06878](#)].
- [208] Q.-H. Cao, Y. Liu, K.-P. Xie, B. Yan, and D.-M. Zhang, *Diphoton excess, low energy theorem, and the 331 model*, *Phys. Rev. D* **93** (2016), no. 7 075030, [[arXiv:1512.08441](#)].
- [209] W.-C. Huang, Y.-L. S. Tsai, and T.-C. Yuan, *Gauged Two Higgs Doublet Model confronts the LHC 750 GeV diphoton anomaly*, *Nucl. Phys. B* **909** (2016) 122–134, [[arXiv:1512.07268](#)].
- [210] Y.-L. Tang and S.-h. Zhu, *NMSSM extended with vectorlike particles and the diphoton excess at the LHC*, *Phys. Rev. D* **94** (2016), no. 3 035010, [[arXiv:1512.08323](#)].

- 
- [211] L. J. Hall, K. Harigaya, and Y. Nomura, *750 GeV Diphotons: Implications for Supersymmetric Unification*, *JHEP* **03** (2016) 017, [[arXiv:1512.07904](#)].
- [212] S. Chakraborty, A. Chakraborty, and S. Raychaudhuri, *Diphoton resonance at 750 GeV in the broken  $R$ -symmetric MSSM*, *Phys. Rev.* **D94** (2016), no. 3 035014, [[arXiv:1512.07527](#)].
- [213] Y. Jiang, Y.-Y. Li, and T. Liu, *750 GeV Resonance in the Gauged  $U(1)'$ -Extended MSSM*, *Phys. Lett.* **B759** (2016) 354–360, [[arXiv:1512.09127](#)].
- [214] H. An, T. Liu, and L.-T. Wang, *125 GeV Higgs Boson, Enhanced Di-photon Rate, and Gauged  $U(1)_{PQ}$ -Extended MSSM*, *Phys. Rev.* **D86** (2012) 075030, [[arXiv:1207.2473](#)].
- [215] W. Chao, *The Diphoton Excess from an Exceptional Supersymmetric Standard Model*, [arXiv:1601.00633](#).
- [216] A. Alves, A. G. Dias, and K. Sinha, *The 750 GeV  $S$ -cion: Where else should we look for it?*, *Phys. Lett.* **B757** (2016) 39–46, [[arXiv:1512.06091](#)].
- [217] M. Backovic, A. Mariotti, and D. Redigolo, *Di-photon excess illuminates Dark Matter*, *JHEP* **03** (2016) 157, [[arXiv:1512.04917](#)].
- [218] D. Barducci, A. Goudelis, S. Kulkarni, and D. Sengupta, *One jet to rule them all: monojet constraints and invisible decays of a 750 GeV diphoton resonance*, *JHEP* **05** (2016) 154, [[arXiv:1512.06842](#)].
- [219] B. Bellazzini, R. Franceschini, F. Sala, and J. Serra, *Goldstones in Diphotons*, *JHEP* **04** (2016) 072, [[arXiv:1512.05330](#)].
- [220] L. Berthier, J. M. Cline, W. Shepherd, and M. Trott, *Effective interpretations of a diphoton excess*, *JHEP* **04** (2016) 084, [[arXiv:1512.06799](#)].
- [221] X.-J. Bi, Q.-F. Xiang, P.-F. Yin, and Z.-H. Yu, *The 750 GeV diphoton excess at the LHC and dark matter constraints*, *Nucl. Phys.* **B909** (2016) 43–64, [[arXiv:1512.06787](#)].
- [222] J. Chakraborty, A. Choudhury, P. Ghosh, S. Mondal, and T. Srivastava, *Di-photon resonance around 750 GeV: shedding light on the theory underneath*, [arXiv:1512.05767](#).
- [223] F. D’Eramo, J. de Vries, and P. Panci, *A 750 GeV Portal: LHC Phenomenology and Dark Matter Candidates*, *JHEP* **05** (2016) 089, [[arXiv:1601.01571](#)].
- [224] J. de Blas, J. Santiago, and R. Vega-Morales, *New vector bosons and the diphoton excess*, *Phys. Lett.* **B759** (2016) 247–252, [[arXiv:1512.07229](#)].
- [225] S. Fichtel, G. von Gersdorff, and C. Royon, *Scattering light by light at 750 GeV at the LHC*, *Phys. Rev.* **D93** (2016), no. 7 075031, [[arXiv:1512.05751](#)].

- [226] K. Ghorbani and P. H. Ghorbani, *The LHC upper bounds for  $pp \rightarrow$  diboson,  $t\bar{t}$  cross section on fermionic dark matter*, *Int. J. Mod. Phys. A* **32** (2017), no. 22 1750131, [[arXiv:1601.00602](#)].
- [227] X.-J. Huang, W.-H. Zhang, and Y.-F. Zhou, *A 750 GeV dark matter messenger at the Galactic Center*, *Phys. Rev. D* **93** (2016) 115006, [[arXiv:1512.08992](#)].
- [228] F. P. Huang, C. S. Li, Z. L. Liu, and Y. Wang, *Diphoton and dark matter from cascade decay*, *Phys. Rev. D* **94** (2016), no. 5 055025, [[arXiv:1512.06732](#)].
- [229] S. Kanemura, N. Machida, S. Odori, and T. Shindou, *Diphoton excess at 750 GeV in an extended scalar sector*, [arXiv:1512.09053](#).
- [230] I. Low and J. Lykken, *Implications of Gauge Invariance on a Heavy Diphoton Resonance*, *Submitted to: Phys. Rev. Lett.* (2015) [[arXiv:1512.09089](#)].
- [231] Y. Mambrini, G. Arcadi, and A. Djouadi, *The LHC diphoton resonance and dark matter*, *Phys. Lett. B* **755** (2016) 426–432, [[arXiv:1512.04913](#)].
- [232] C. W. Murphy, *Vector Leptoquarks and the 750 GeV Diphoton Resonance at the LHC*, *Phys. Lett. B* **757** (2016) 192–198, [[arXiv:1512.06976](#)].
- [233] J.-C. Park and S. C. Park, *Indirect signature of dark matter with the diphoton resonance at 750 GeV*, *Phys. Dark Univ.* **14** (2016) 4–10, [[arXiv:1512.08117](#)].
- [234] I. Sahin, *Semi-elastic cross section for a scalar resonance of mass 750 GeV*, [arXiv:1601.01676](#).
- [235] Y. Bai, J. Berger, and R. Lu, *750 GeV dark pion: Cousin of a dark G-parity odd WIMP*, *Phys. Rev. D* **93** (2016), no. 7 076009, [[arXiv:1512.05779](#)].
- [236] N. D. Barrie, A. Kobakhidze, M. Talia, and L. Wu, *750 GeV Composite Axion as the LHC Diphoton Resonance*, *Phys. Lett. B* **755** (2016) 343–347, [[arXiv:1602.00475](#)].
- [237] A. Belyaev, G. Cacciapaglia, H. Cai, T. Flacke, A. Parolini, and H. Serôdio, *Singlets in composite Higgs models in light of the LHC 750 GeV diphoton excess*, *Phys. Rev. D* **94** (2016), no. 1 015004, [[arXiv:1512.07242](#)].
- [238] L. Bian, N. Chen, D. Liu, and J. Shu, *Hidden confining world on the 750 GeV diphoton excess*, *Phys. Rev. D* **93** (2016), no. 9 095011, [[arXiv:1512.05759](#)].
- [239] C.-W. Chiang, M. Ibe, and T. T. Yanagida, *Revisiting Scalar Quark Hidden Sector in Light of 750-GeV Diphoton Resonance*, *JHEP* **05** (2016) 084, [[arXiv:1512.08895](#)].
- [240] J. M. Cline and Z. Liu, *LHC diphotons from electroweakly pair-produced composite pseudoscalars*, [arXiv:1512.06827](#).
- [241] D. Curtin and C. B. Verhaaren, *Quirky Explanations for the Diphoton Excess*, *Phys. Rev. D* **93** (2016), no. 5 055011, [[arXiv:1512.05753](#)].

- 
- [242] K. Harigaya and Y. Nomura, *Composite Models for the 750 GeV Diphoton Excess*, *Phys. Lett.* **B754** (2016) 151–156, [[arXiv:1512.04850](#)].
- [243] K. Harigaya and Y. Nomura, *A Composite Model for the 750 GeV Diphoton Excess*, *JHEP* **03** (2016) 091, [[arXiv:1602.01092](#)].
- [244] J. S. Kim, J. Reuter, K. Rolbiecki, and R. Ruiz de Austri, *A resonance without resonance: scrutinizing the diphoton excess at 750 GeV*, *Phys. Lett.* **B755** (2016) 403–408, [[arXiv:1512.06083](#)].
- [245] W. Liao and H.-q. Zheng, *Scalar resonance at 750 GeV as composite of heavy vector-like fermions*, *Commun. Theor. Phys.* **66** (2016), no. 2 219–223, [[arXiv:1512.06741](#)].
- [246] M. Low, A. Tesi, and L.-T. Wang, *A pseudoscalar decaying to photon pairs in the early LHC Run 2 data*, *JHEP* **03** (2016) 108, [[arXiv:1512.05328](#)].
- [247] S. Matsuzaki and K. Yamawaki, *750 GeV Diphoton Signal from One-Family Walking Technipion*, *Mod. Phys. Lett.* **A31** (2016), no. 17 1630016, [[arXiv:1512.05564](#)].
- [248] E. Molinaro, F. Sannino, and N. Vignaroli, *Minimal Composite Dynamics versus Axion Origin of the Diphoton excess*, *Mod. Phys. Lett.* **A31** (2016), no. 26 1650155, [[arXiv:1512.05334](#)].
- [249] Y. Nakai, R. Sato, and K. Tobioka, *Footprints of New Strong Dynamics via Anomaly and the 750 GeV Diphoton*, *Phys. Rev. Lett.* **116** (2016), no. 15 151802, [[arXiv:1512.04924](#)].
- [250] J. M. No, V. Sanz, and J. Setford, *See-saw composite Higgs model at the LHC: Linking naturalness to the 750 GeV diphoton resonance*, *Phys. Rev.* **D93** (2016), no. 9 095010, [[arXiv:1512.05700](#)].
- [251] S. Abel and V. V. Khoze, *Photo-production of a 750 GeV di-photon resonance mediated by Kaluza-Klein leptons in the loop*, *JHEP* **05** (2016) 063, [[arXiv:1601.07167](#)].
- [252] A. Ahmed, B. M. Dillon, B. Grzadkowski, J. F. Gunion, and Y. Jiang, *Implications of the absence of high-mass radion signals*, *Phys. Rev.* **D95** (2017), no. 9 095019, [[arXiv:1512.05771](#)].
- [253] M. T. Arun and P. Saha, *Gravitons in multiply warped scenarios: At 750 GeV and beyond*, *Pramana* **88** (2017), no. 6 93, [[arXiv:1512.06335](#)].
- [254] M. T. Arun and D. Choudhury, *Bulk gauge and matter fields in nested warping: II. Symmetry Breaking and phenomenological consequences*, *JHEP* **04** (2016) 133, [[arXiv:1601.02321](#)].
- [255] D. Bardhan, D. Bhatia, A. Chakraborty, U. Maitra, S. Raychaudhuri, and T. Samui, *Radion Candidate for the LHC Diphoton Resonance*, [arXiv:1512.06674](#).
- [256] C. Cai, Z.-H. Yu, and H.-H. Zhang, *750 GeV diphoton resonance as a singlet scalar in an extra dimensional model*, *Phys. Rev.* **D93** (2016), no. 7 075033, [[arXiv:1512.08440](#)].

- [257] P. Cox, A. D. Medina, T. S. Ray, and A. Spray, *Implications of diphoton searches for a Radion in the Bulk-Higgs Scenario*, *Int. J. Mod. Phys. A* **32** (2017), no. 04 1750020, [[arXiv:1512.05618](#)].
- [258] H. Davoudiasl and C. Zhang, *750 GeV messenger of dark conformal symmetry breaking*, *Phys. Rev. D* **93** (2016), no. 5 055006, [[arXiv:1512.07672](#)].
- [259] C.-Q. Geng and D. Huang, *Note on spin-2 particle interpretation of the 750 GeV diphoton excess*, *Phys. Rev. D* **93** (2016), no. 11 115032, [[arXiv:1601.07385](#)].
- [260] C. Han, H. M. Lee, M. Park, and V. Sanz, *The diphoton resonance as a gravity mediator of dark matter*, *Phys. Lett. B* **755** (2016) 371–379, [[arXiv:1512.06376](#)].
- [261] E. Megias, O. Pujolas, and M. Quiros, *On dilatons and the LHC diphoton excess*, *JHEP* **05** (2016) 137, [[arXiv:1512.06106](#)].
- [262] J. A. Casas, J. R. Espinosa, and J. M. Moreno, *The 750 GeV Diphoton Excess as a First Light on Supersymmetry Breaking*, *Phys. Lett. B* **759** (2016) 159–165, [[arXiv:1512.07895](#)].
- [263] C. Petersson and R. Torre, *750 GeV Diphoton Excess from the Goldstino Superpartner*, *Phys. Rev. Lett.* **116** (2016), no. 15 151804, [[arXiv:1512.05333](#)].
- [264] S. V. Demidov and D. S. Gorbunov, *On sgoldstino interpretation of the diphoton excess*, *JETP Lett.* **103** (2016), no. 4 219–222, [[arXiv:1512.05723](#)]. [*Pisma Zh. Eksp. Teor. Fiz.*103,no.4,241(2016)].
- [265] R. Ding, Y. Fan, L. Huang, C. Li, T. Li, S. Raza, and B. Zhu, *Systematic Study of Diphoton Resonance at 750 GeV from Sgoldstino*, *Int. J. Mod. Phys. A* **31** (2016), no. 26 1650151, [[arXiv:1602.00977](#)].
- [266] U. Danielsson, R. Enberg, G. Ingelman, and T. Mandal, *Heavy photophilic scalar at the LHC from a varying electromagnetic coupling*, *Nucl. Phys. B* **919** (2017) 569–582, [[arXiv:1601.00624](#)].
- [267] C. T. Potter, *Pseudoscalar Gluino to 750 GeV LHC Diphotons*, [arXiv:1601.00240](#).
- [268] M.-x. Luo, K. Wang, T. Xu, L. Zhang, and G. Zhu, *Squarkonium, diquarkonium, and octetonium at the LHC and their diphoton decays*, *Phys. Rev. D* **93** (2016), no. 5 055042, [[arXiv:1512.06670](#)].
- [269] A. E. Cárcamo Hernández, I. de Medeiros Varzielas, and E. Schumacher, *The 750 GeV diphoton resonance in the light of a 2HDM with  $S_3$  flavour symmetry*, [arXiv:1601.00661](#).
- [270] T. Higaki, K. S. Jeong, N. Kitajima, and F. Takahashi, *The QCD Axion from Aligned Axions and Diphoton Excess*, *Phys. Lett. B* **755** (2016) 13–16, [[arXiv:1512.05295](#)].

- 
- [271] J. E. Kim, *Is an axizilla possible for di-photon resonance?*, *Phys. Lett.* **B755** (2016) 190–195, [[arXiv:1512.08467](#)].
- [272] P. Agrawal, J. Fan, B. Heidenreich, M. Reece, and M. Strassler, *Experimental Considerations Motivated by the Diphoton Excess at the LHC*, *JHEP* **06** (2016) 082, [[arXiv:1512.05775](#)].
- [273] I. Ben-Dayan and R. Brustein, *Hypercharge Axion and the Diphoton 750 GeV Resonance*, [arXiv:1601.07564](#).
- [274] L. Aparicio, A. Azatov, E. Hardy, and A. Romanino, *Diphotons from Diaxions*, *JHEP* **05** (2016) 077, [[arXiv:1602.00949](#)].
- [275] O. Antipin, M. Mojaza, and F. Sannino, *Minimal Coleman-Weinberg theory explains the diphoton excess*, *Phys. Rev.* **D93** (2016), no. 11 115007, [[arXiv:1512.06708](#)].
- [276] L. Marzola, A. Racioppi, M. Raidal, F. R. Urban, and H. Veermäe, *Non-minimal CW inflation, electroweak symmetry breaking and the 750 GeV anomaly*, *JHEP* **03** (2016) 190, [[arXiv:1512.09136](#)].
- [277] T. Nomura and H. Okada, *A four-loop Radiative Seesaw Model*, *Phys. Lett.* **B770** (2017) 307–313, [[arXiv:1601.04516](#)].
- [278] L. A. Anchordoqui, I. Antoniadis, H. Goldberg, X. Huang, D. Lust, and T. R. Taylor, *750 GeV diphotons from closed string states*, *Phys. Lett.* **B755** (2016) 312–315, [[arXiv:1512.08502](#)].
- [279] J. J. Heckman, *750 GeV Diphotons from a D3-brane*, *Nucl. Phys.* **B906** (2016) 231–240, [[arXiv:1512.06773](#)].
- [280] M. Cvetič, J. Halverson, and P. Langacker, *String Consistency, Heavy Exotics, and the 750 GeV Diphoton Excess at the LHC*, *Fortsch. Phys.* **64** (2016), no. 10 748–782, [[arXiv:1512.07622](#)].
- [281] A. E. Faraggi and J. Rizos, *The 750 GeV di-photon LHC excess and extra  $Z'$ 's in heterotic-string derived models*, *Eur. Phys. J.* **C76** (2016), no. 3 170, [[arXiv:1601.03604](#)].
- [282] L. E. Ibanez and V. Martin-Lozano, *A Megaxion at 750 GeV as a First Hint of Low Scale String Theory*, *JHEP* **07** (2016) 021, [[arXiv:1512.08777](#)].
- [283] S. Ferrara, L. Girardello, and F. Palumbo, *A General Mass Formula in Broken Supersymmetry*, *Phys. Rev.* **D20** (1979) 403.
- [284] K. Harada and N. Sakai, *SOFTLY BROKEN SUPERSYMMETRIC THEORIES*, *Prog. Theor. Phys.* **67** (1982) 1877.
- [285] L. Girardello and M. T. Grisaru, *Soft Breaking of Supersymmetry*, *Nucl. Phys.* **B194** (1982) 65.

- [286] S. Dimopoulos and H. Georgi, *Softly Broken Supersymmetry and SU(5)*, *Nucl. Phys.* **B193** (1981) 150–162.
- [287] R. Barbieri, S. Ferrara, and C. A. Savoy, *Gauge Models with Spontaneously Broken Local Supersymmetry*, *Phys. Lett.* **119B** (1982) 343.
- [288] A. H. Chamseddine, R. L. Arnowitt, and P. Nath, *Locally Supersymmetric Grand Unification*, *Phys. Rev. Lett.* **49** (1982) 970.
- [289] G. L. Kane, C. F. Kolda, L. Roszkowski, and J. D. Wells, *Study of constrained minimal supersymmetry*, *Phys. Rev.* **D49** (1994) 6173–6210, [[hep-ph/9312272](#)].
- [290] H. K. Dreiner, H. E. Haber, and S. P. Martin, *Practical Supersymmetry*. 2017.
- [291] M. T. Grisaru, W. Siegel, and M. Rocek, *Improved Methods for Supergraphs*, *Nucl. Phys.* **B159** (1979) 429.
- [292] N. Seiberg, *Naturalness versus supersymmetric nonrenormalization theorems*, *Phys. Lett.* **B318** (1993) 469–475, [[hep-ph/9309335](#)].
- [293] S. Weinberg, *Varieties of Baryon and Lepton Nonconservation*, *Phys. Rev.* **D22** (1980) 1694.
- [294] H. K. Dreiner, C. Luhn, and M. Thormeier, *What is the discrete gauge symmetry of the MSSM?*, *Phys. Rev.* **D73** (2006) 075007, [[hep-ph/0512163](#)].
- [295] J. E. Camargo-Molina, B. O’Leary, W. Porod, and F. Staub, *Stability of the CMSSM against sfermion VEVs*, *JHEP* **12** (2013) 103, [[arXiv:1309.7212](#)].
- [296] A. J. Bordner, *Parameter bounds in the supersymmetric standard model from charge / color breaking vacua*, [hep-ph/9506409](#).
- [297] P. M. Ferreira, *A Full one loop charge and color breaking effective potential*, *Phys. Lett.* **B509** (2001) 120–130, [[hep-ph/0008115](#)]. [Erratum: *Phys. Lett.*B518,333(2001)].
- [298] A. Barroso, P. M. Ferreira, and R. Santos, *Charge and CP symmetry breaking in two Higgs doublet models*, *Phys. Lett.* **B632** (2006) 684–687, [[hep-ph/0507224](#)].
- [299] M. Maniatis, A. von Manteuffel, O. Nachtmann, and F. Nagel, *Stability and symmetry breaking in the general two-Higgs-doublet model*, *Eur. Phys. J.* **C48** (2006) 805–823, [[hep-ph/0605184](#)].
- [300] I. P. Ivanov, *Minkowski space structure of the Higgs potential in 2HDM*, *Phys. Rev.* **D75** (2007) 035001, [[hep-ph/0609018](#)]. [Erratum: *Phys. Rev.*D76,039902(2007)].
- [301] A. Sommese and C. Wampler, *The numerical solution of systems of polynomials arising in engineering and science*. 2005.
- [302] L. T, *Handbook of numerical analysis*. 2003.

- 
- [303] M. Maniatis and D. Mehta, *Minimizing Higgs Potentials via Numerical Polynomial Homotopy Continuation*, *Eur. Phys. J. Plus* **127** (2012) 91, [[arXiv:1203.0409](#)].
- [304] T. L. Lee, T. Y. Li, and C. H. Tsai, *HOM4PS-2.0: a software package for solving polynomial systems by the polyhedral homotopy continuation method*, *Computing* **83** (2008), no. 2 109–133.
- [305] H. P. Nilles, M. Srednicki, and D. Wyler, *Weak Interaction Breakdown Induced by Supergravity*, *Phys. Lett.* **120B** (1983) 346.
- [306] L. Alvarez-Gaume, J. Polchinski, and M. B. Wise, *Minimal Low-Energy Supergravity*, *Nucl. Phys.* **B221** (1983) 495.
- [307] J. P. Derendinger and C. A. Savoy, *Quantum Effects and  $SU(2) \times U(1)$  Breaking in Supergravity Gauge Theories*, *Nucl. Phys.* **B237** (1984) 307–328.
- [308] M. Claudson, L. J. Hall, and I. Hinchliffe, *Low-Energy Supergravity: False Vacua and Vacuum Predictions*, *Nucl. Phys.* **B228** (1983) 501–528.
- [309] C. Kounnas, A. B. Lahanas, D. V. Nanopoulos, and M. Quiros, *Low-Energy Behavior of Realistic Locally Supersymmetric Grand Unified Theories*, *Nucl. Phys.* **B236** (1984) 438–466.
- [310] J. A. Casas, A. Lleyda, and C. Munoz, *Strong constraints on the parameter space of the MSSM from charge and color breaking minima*, *Nucl. Phys.* **B471** (1996) 3–58, [[hep-ph/9507294](#)].
- [311] C. Le Mouél, *Charge and color breaking conditions associated to the top quark Yukawa coupling*, *Phys. Rev.* **D64** (2001) 075009, [[hep-ph/0103341](#)].
- [312] J. F. Gunion, H. E. Haber, and M. Sher, *Charge / Color Breaking Minima and  $a$ -Parameter Bounds in Supersymmetric Models*, *Nucl. Phys.* **B306** (1988) 1–13.
- [313] N. Chamoun, H. K. Dreiner, F. Staub, and T. Stefaniak, *Resurrecting light stops after the 125 GeV Higgs in the baryon number violating CMSSM*, *JHEP* **08** (2014) 142, [[arXiv:1407.2248](#)].
- [314] S. R. Coleman, *The Fate of the False Vacuum. 1. Semiclassical Theory*, *Phys. Rev.* **D15** (1977) 2929–2936. [Erratum: *Phys. Rev.* **D16**, 1248(1977)].
- [315] C. G. Callan, Jr. and S. R. Coleman, *The Fate of the False Vacuum. 2. First Quantum Corrections*, *Phys. Rev.* **D16** (1977) 1762–1768.
- [316] W. G. Hollik, *A new view on vacuum stability in the MSSM*, *JHEP* **08** (2016) 126, [[arXiv:1606.08356](#)].
- [317] J. E. Camargo-Molina, B. Garbrecht, B. O’Leary, W. Porod, and F. Staub, *Constraining the Natural MSSM through tunneling to color-breaking vacua at zero and non-zero temperature*, *Phys. Lett.* **B737** (2014) 156–161, [[arXiv:1405.7376](#)].

- [318] V. Branchina, E. Messina, and M. Sher, *Lifetime of the electroweak vacuum and sensitivity to Planck scale physics*, *Phys. Rev.* **D91** (2015) 013003, [[arXiv:1408.5302](#)].
- [319] Z. Lalak, M. Lewicki, and P. Olszewski, *Higher-order scalar interactions and SM vacuum stability*, *JHEP* **05** (2014) 119, [[arXiv:1402.3826](#)].
- [320] ATLAS Collaboration, *Search for resonances decaying to photon pairs in  $3.2 \text{ fb}^{-1}$  of  $pp$  collisions at  $\sqrt{s} = 13 \text{ TeV}$  with the ATLAS detector*, *ATLAS-CONF-2015-081* (2015).
- [321] CMS Collaboration, C. Collaboration, *Search for resonant production of high mass photon pairs using  $12.9 \text{ fb}^{-1}$  of proton-proton collisions at  $\sqrt{s} = 13 \text{ TeV}$  and combined interpretation of searches at 8 and 13 TeV*, .
- [322] Y. Kats and M. J. Strassler, *Resonances from QCD bound states and the 750 GeV diphoton excess*, *JHEP* **05** (2016) 092, [[arXiv:1602.08819](#)]. [Erratum: JHEP07,044(2016)].
- [323] D. Choudhury and K. Ghosh, *The LHC Diphoton excess at 750 GeV in the framework of the Constrained Minimal Supersymmetric Standard Model*, [arXiv:1605.00013](#).
- [324] G. F. Giudice and A. Kusenko, *A Strongly interacting phase of the minimal supersymmetric model*, *Phys. Lett.* **B439** (1998) 55, [[hep-ph/9805379](#)].
- [325] Z. Kang, *Bound states via Higgs exchanging and heavy resonant di-Higgs*, *Phys. Lett.* **B771** (2017) 313–317, [[arXiv:1606.01531](#)].
- [326] H. E. Haber and R. Hempfling, *The Renormalization group improved Higgs sector of the minimal supersymmetric model*, *Phys. Rev.* **D48** (1993) 4280–4309, [[hep-ph/9307201](#)].
- [327] M. Carena, M. Quiros, and C. E. M. Wagner, *Effective potential methods and the Higgs mass spectrum in the MSSM*, *Nucl. Phys.* **B461** (1996) 407–436, [[hep-ph/9508343](#)].
- [328] S. Heinemeyer, W. Hollik, and G. Weiglein, *The Masses of the neutral CP - even Higgs bosons in the MSSM: Accurate analysis at the two loop level*, *Eur. Phys. J.* **C9** (1999) 343–366, [[hep-ph/9812472](#)].
- [329] S. Heinemeyer, W. Hollik, and G. Weiglein, *The Mass of the lightest MSSM Higgs boson: A Compact analytical expression at the two loop level*, *Phys. Lett.* **B455** (1999) 179–191, [[hep-ph/9903404](#)].
- [330] M. Carena, H. E. Haber, S. Heinemeyer, W. Hollik, C. E. M. Wagner, and G. Weiglein, *Reconciling the two loop diagrammatic and effective field theory computations of the mass of the lightest CP - even Higgs boson in the MSSM*, *Nucl. Phys.* **B580** (2000) 29–57, [[hep-ph/0001002](#)].
- [331] S. P. Martin, *Diphoton decays of stoponium at the Large Hadron Collider*, *Phys. Rev.* **D77** (2008) 075002, [[arXiv:0801.0237](#)].
- [332] M. Drees and M. M. Nojiri, *Production and decay of scalar stoponium bound states*, *Phys. Rev.* **D49** (1994) 4595–4616, [[hep-ph/9312213](#)].

- 
- [333] **ATLAS** Collaboration, T. A. collaboration, *A search for resonant Higgs-pair production in the  $b\bar{b}b\bar{b}$  final state in  $pp$  collisions at  $\sqrt{s} = 8$  TeV*, .
- [334] M. R. Buckley, *Wide or narrow? The phenomenology of 750 GeV diphotons*, *Eur. Phys. J.* **C76** (2016), no. 6 345, [[arXiv:1601.04751](#)].
- [335] J. M. Cornwall, A. Kusenko, L. Pearce, and R. D. Peccei, *Can supersymmetry breaking lead to electroweak symmetry breaking via formation of scalar bound states?*, *Phys. Lett.* **B718** (2013) 951–956, [[arXiv:1210.6433](#)].
- [336] **CMS** Collaboration, V. Khachatryan et al., *Search for new physics with the  $M_{T2}$  variable in all-jets final states produced in  $pp$  collisions at  $\sqrt{s} = 13$  TeV*, *JHEP* **10** (2016) 006, [[arXiv:1603.04053](#)].
- [337] **ATLAS** Collaboration, G. Aad et al., *Search for pair production of gluinos decaying via stop and sbottom in events with  $b$ -jets and large missing transverse momentum in  $pp$  collisions at  $\sqrt{s} = 13$  TeV with the ATLAS detector*, *Phys. Rev.* **D94** (2016), no. 3 032003, [[arXiv:1605.09318](#)].
- [338] A. Djouadi, J.-L. Kneur, and G. Moultaka, *SuSpect: A Fortran code for the supersymmetric and Higgs particle spectrum in the MSSM*, *Comput. Phys. Commun.* **176** (2007) 426–455, [[hep-ph/0211331](#)].
- [339] **ATLAS** Collaboration, G. Aad et al., *Observation of a new particle in the search for the Standard Model Higgs boson with the ATLAS detector at the LHC*, *Phys. Lett.* **B716** (2012) 1–29, [[arXiv:1207.7214](#)].
- [340] **CMS** Collaboration, S. Chatrchyan et al., *Observation of a new boson at a mass of 125 GeV with the CMS experiment at the LHC*, *Phys. Lett.* **B716** (2012) 30–61, [[arXiv:1207.7235](#)].
- [341] A. Brignole, *Radiative corrections to the supersymmetric neutral Higgs boson masses*, *Phys. Lett.* **B281** (1992) 284–294.
- [342] P. H. Chankowski, S. Pokorski, and J. Rosiek, *Charged and neutral supersymmetric Higgs boson masses: Complete one loop analysis*, *Phys. Lett.* **B274** (1992) 191–198.
- [343] A. Dabelstein, *The One loop renormalization of the MSSM Higgs sector and its application to the neutral scalar Higgs masses*, *Z. Phys.* **C67** (1995) 495–512, [[hep-ph/9409375](#)].
- [344] N. Blinov and D. E. Morrissey, *Vacuum Stability and the MSSM Higgs Mass*, *JHEP* **03** (2014) 106, [[arXiv:1310.4174](#)].
- [345] D. Chowdhury, R. M. Godbole, K. A. Mohan, and S. K. Vempati, *Charge and Color Breaking Constraints in MSSM after the Higgs Discovery at LHC*, *JHEP* **02** (2014) 110, [[arXiv:1310.1932](#)].

- [346] U. Ellwanger, C. Hugonie, and A. M. Teixeira, *The Next-to-Minimal Supersymmetric Standard Model*, *Phys. Rept.* **496** (2010) 1–77, [[arXiv:0910.1785](#)].
- [347] U. Ellwanger and C. Hugonie, *The Upper bound on the lightest Higgs mass in the NMSSM revisited*, *Mod. Phys. Lett.* **A22** (2007) 1581–1590, [[hep-ph/0612133](#)].
- [348] M. Bastero-Gil, C. Hugonie, S. F. King, D. P. Roy, and S. Vempati, *Does LEP prefer the NMSSM?*, *Phys. Lett.* **B489** (2000) 359–366, [[hep-ph/0006198](#)].
- [349] R. Dermisek and J. F. Gunion, *Consistency of LEP event excesses with an  $h \rightarrow aa$  decay scenario and low-fine-tuning NMSSM models*, *Phys. Rev.* **D73** (2006) 111701, [[hep-ph/0510322](#)].
- [350] R. Dermisek, J. F. Gunion, and B. McElrath, *Probing NMSSM Scenarios with Minimal Fine-Tuning by Searching for Decays of the Upsilon to a Light CP-Odd Higgs Boson*, *Phys. Rev.* **D76** (2007) 051105, [[hep-ph/0612031](#)].
- [351] R. Dermisek and J. F. Gunion, *The NMSSM Solution to the Fine-Tuning Problem, Precision Electroweak Constraints and the Largest LEP Higgs Event Excess*, *Phys. Rev.* **D76** (2007) 095006, [[arXiv:0705.4387](#)].
- [352] U. Ellwanger, G. Espitalier-Noel, and C. Hugonie, *Naturalness and Fine Tuning in the NMSSM: Implications of Early LHC Results*, *JHEP* **09** (2011) 105, [[arXiv:1107.2472](#)].
- [353] G. G. Ross and K. Schmidt-Hoberg, *The Fine-Tuning of the Generalised NMSSM*, *Nucl. Phys.* **B862** (2012) 710–719, [[arXiv:1108.1284](#)].
- [354] G. G. Ross, K. Schmidt-Hoberg, and F. Staub, *The Generalised NMSSM at One Loop: Fine Tuning and Phenomenology*, *JHEP* **08** (2012) 074, [[arXiv:1205.1509](#)].
- [355] A. Kaminska, G. G. Ross, and K. Schmidt-Hoberg, *Non-universal gaugino masses and fine tuning implications for SUSY searches in the MSSM and the GNMSSM*, *JHEP* **11** (2013) 209, [[arXiv:1308.4168](#)].
- [356] U. Ellwanger, M. Rausch de Traubenberg, and C. A. Savoy, *Phenomenology of supersymmetric models with a singlet*, *Nucl. Phys.* **B492** (1997) 21–50, [[hep-ph/9611251](#)].
- [357] U. Ellwanger and C. Hugonie, *Constraints from charge and color breaking minima in the  $(M+1)$ SSM*, *Phys. Lett.* **B457** (1999) 299–306, [[hep-ph/9902401](#)].
- [358] Y. Kanehata, T. Kobayashi, Y. Konishi, O. Seto, and T. Shimomura, *Constraints from Unrealistic Vacua in the Next-to-Minimal Supersymmetric Standard Model*, *Prog. Theor. Phys.* **126** (2011) 1051–1076, [[arXiv:1103.5109](#)].
- [359] T. Kobayashi, T. Shimomura, and T. Takahashi, *Constraining the Higgs sector from False Vacua in the Next-to-Minimal Supersymmetric Standard Model*, *Phys. Rev.* **D86** (2012) 015029, [[arXiv:1203.4328](#)].

- [360] K. Agashe, Y. Cui, and R. Franceschini, *Natural Islands for a 125 GeV Higgs in the scale-invariant NMSSM*, *JHEP* **02** (2013) 031, [[arXiv:1209.2115](#)].
- [361] J. Beuria, U. Chattopadhyay, A. Datta, and A. Dey, *Exploring viable vacua of the  $Z_3$ -symmetric NMSSM*, *JHEP* **04** (2017) 024, [[arXiv:1612.06803](#)].
- [362] M. Muhlleitner, M. O. P. Sampaio, R. Santos, and J. Wittbrodt, *The N2HDM under Theoretical and Experimental Scrutiny*, *JHEP* **03** (2017) 094, [[arXiv:1612.01309](#)].
- [363] M. D. Goodsell, K. Nickel, and F. Staub, *Two-loop corrections to the Higgs masses in the NMSSM*, *Phys. Rev.* **D91** (2015) 035021, [[arXiv:1411.4665](#)].
- [364] T. L. Lee, T. Y. Li, and C. H. Tsai, *HOM4PS-2.0: a software package for solving polynomial systems by the polyhedral homotopy continuation method*, *Computing* **83** (2008), no. 2 109–133.
- [365] F. James and M. Roos, *Minuit: A System for Function Minimization and Analysis of the Parameter Errors and Correlations*, *Comput. Phys. Commun.* **10** (1975) 343–367.
- [366] A. Djouadi and A. Pilaftsis, *Enhanced Rates for Diphoton Resonances in the MSSM*, *Phys. Lett.* **B765** (2017) 175–180, [[arXiv:1605.01040](#)].
- [367] R. Slansky, *Group Theory for Unified Model Building*, *Phys. Rept.* **79** (1981) 1–128.
- [368] J. C. Pati and A. Salam, *Unified Lepton-Hadron Symmetry and a Gauge Theory of the Basic Interactions*, *Phys. Rev.* **D8** (1973) 1240–1251.
- [369] C. S. Aulakh, A. Melfo, A. Rasin, and G. Senjanovic, *Supersymmetry and large scale left-right symmetry*, *Phys. Rev.* **D58** (1998) 115007, [[hep-ph/9712551](#)].
- [370] F. F. Deppisch, T. E. Gonzalo, and L. Graf, *Surveying the  $SO(10)$  Model Landscape: The Left-Right Symmetric Case*, [arXiv:1705.05416](#).
- [371] L. Basso, B. Fuks, M. E. Krauss, and W. Porod, *Doubly-charged Higgs and vacuum stability in left-right supersymmetry*, *JHEP* **07** (2015) 147, [[arXiv:1503.08211](#)].
- [372] P. S. B. Dev and R. N. Mohapatra, *TeV Scale Inverse Seesaw in  $SO(10)$  and Leptonic Non-Unitarity Effects*, *Phys. Rev.* **D81** (2010) 013001, [[arXiv:0910.3924](#)].
- [373] M. Hirsch, M. E. Krauss, T. Opferkuch, W. Porod, and F. Staub, *A constrained supersymmetric left-right model*, *JHEP* **03** (2016) 009, [[arXiv:1512.00472](#)].
- [374] K. S. Babu and R. N. Mohapatra, *Minimal Supersymmetric Left-Right Model*, *Phys. Lett.* **B668** (2008) 404–409, [[arXiv:0807.0481](#)].
- [375] M. Cvetič and J. C. Pati,  *$N = 1$  Supergravity Within the Minimal Left-right Symmetric Model*, *Phys. Lett.* **135B** (1984) 57–62.

- [376] D. Chang, R. N. Mohapatra, and M. K. Parida, *Decoupling Parity and SU(2)-R Breaking Scales: A New Approach to Left-Right Symmetric Models*, *Phys. Rev. Lett.* **52** (1984) 1072.
- [377] D. Chang, R. N. Mohapatra, and M. K. Parida, *A New Approach to Left-Right Symmetry Breaking in Unified Gauge Theories*, *Phys. Rev.* **D30** (1984) 1052.
- [378] N. G. Deshpande, J. F. Gunion, B. Kayser, and F. I. Olness, *Left-right symmetric electroweak models with triplet Higgs*, *Phys. Rev.* **D44** (1991) 837–858.
- [379] M. Raidal and A. Santamaria, *Muon electron conversion in nuclei versus  $\mu \rightarrow e\gamma$ : An Effective field theory point of view*, *Phys. Lett.* **B421** (1998) 250–258, [[hep-ph/9710389](#)].
- [380] **SINDRUM** Collaboration, U. Bellgardt et al., *Search for the Decay  $\mu^+ \rightarrow e^+e^+e^-$* , *Nucl. Phys.* **B299** (1988) 1–6.
- [381] A. Blondel et al., *Research Proposal for an Experiment to Search for the Decay  $\mu \rightarrow eee$* , [arXiv:1301.6113](#).
- [382] M. Hirsch, H. V. Klapdor-Kleingrothaus, and O. Panella, *Double beta decay in left-right symmetric models*, *Phys. Lett.* **B374** (1996) 7–12, [[hep-ph/9602306](#)].
- [383] R. L. Awasthi, M. K. Parida, and S. Patra, *Neutrino masses, dominant neutrinoless double beta decay, and observable lepton flavor violation in left-right models and SO(10) grand unification with low mass  $W_R, Z_R$  bosons*, *JHEP* **08** (2013) 122, [[arXiv:1302.0672](#)].
- [384] J. Barry and W. Rodejohann, *Lepton number and flavour violation in TeV-scale left-right symmetric theories with large left-right mixing*, *JHEP* **09** (2013) 153, [[arXiv:1303.6324](#)].
- [385] R. L. Awasthi, P. S. B. Dev, and M. Mitra, *Implications of the Diboson Excess for Neutrinoless Double Beta Decay and Lepton Flavor Violation in TeV Scale Left Right Symmetric Model*, *Phys. Rev.* **D93** (2016), no. 1 011701, [[arXiv:1509.05387](#)].
- [386] G. Bambhaniya, P. S. B. Dev, S. Goswami, and M. Mitra, *The Scalar Triplet Contribution to Lepton Flavour Violation and Neutrinoless Double Beta Decay in Left-Right Symmetric Model*, *JHEP* **04** (2016) 046, [[arXiv:1512.00440](#)].
- [387] V. Tello, M. Nemevsek, F. Nesti, G. Senjanovic, and F. Vissani, *Left-Right Symmetry: from LHC to Neutrinoless Double Beta Decay*, *Phys. Rev. Lett.* **106** (2011) 151801, [[arXiv:1011.3522](#)].
- [388] Y. Zhang, H. An, X. Ji, and R. N. Mohapatra, *General CP Violation in Minimal Left-Right Symmetric Model and Constraints on the Right-Handed Scale*, *Nucl. Phys.* **B802** (2008) 247–279, [[arXiv:0712.4218](#)].
- [389] M. Nemevsek, F. Nesti, G. Senjanovic, and Y. Zhang, *First Limits on Left-Right Symmetry Scale from LHC Data*, *Phys. Rev.* **D83** (2011) 115014, [[arXiv:1103.1627](#)].

- 
- [390] J. C. Helo and M. Hirsch, *LHC dijet constraints on double beta decay*, *Phys. Rev.* **D92** (2015), no. 7 073017, [[arXiv:1509.00423](#)].
- [391] M. Lindner, F. S. Queiroz, and W. Rodejohann, *Dilepton bounds on left–right symmetry at the LHC run II and neutrinoless double beta decay*, *Phys. Lett.* **B762** (2016) 190–195, [[arXiv:1604.07419](#)].
- [392] R. N. Mohapatra and Y. Zhang, *LHC accessible second Higgs boson in the left-right model*, *Phys. Rev.* **D89** (2014), no. 5 055001, [[arXiv:1401.0018](#)].
- [393] G. Bambhaniya, J. Chakraborty, J. Gluza, M. Kordiaczyńska, and R. Szafron, *Left-Right Symmetry and the Charged Higgs Bosons at the LHC*, *JHEP* **05** (2014) 033, [[arXiv:1311.4144](#)].
- [394] G. Bambhaniya, J. Chakraborty, J. Gluza, T. Jelinski, and R. Szafron, *Search for doubly charged Higgs bosons through vector boson fusion at the LHC and beyond*, *Phys. Rev.* **D92** (2015), no. 1 015016, [[arXiv:1504.03999](#)].
- [395] P. S. B. Dev, R. N. Mohapatra, and Y. Zhang, *Probing the Higgs Sector of the Minimal Left-Right Symmetric Model at Future Hadron Colliders*, *JHEP* **05** (2016) 174, [[arXiv:1602.05947](#)].
- [396] S. P. Das, F. F. Deppisch, O. Kittel, and J. W. F. Valle, *Heavy Neutrinos and Lepton Flavour Violation in Left-Right Symmetric Models at the LHC*, *Phys. Rev.* **D86** (2012) 055006, [[arXiv:1206.0256](#)].
- [397] C.-Y. Chen, P. S. B. Dev, and R. N. Mohapatra, *Probing Heavy-Light Neutrino Mixing in Left-Right Seesaw Models at the LHC*, *Phys. Rev.* **D88** (2013) 033014, [[arXiv:1306.2342](#)].
- [398] M. Lindner, F. S. Queiroz, W. Rodejohann, and C. E. Yaguna, *Left-Right Symmetry and Lepton Number Violation at the Large Hadron Electron Collider*, *JHEP* **06** (2016) 140, [[arXiv:1604.08596](#)].
- [399] J. Gluza, T. Jelinski, and R. Szafron, *Lepton number violation and ‘Diracness’ of massive neutrinos composed of Majorana states*, *Phys. Rev.* **D93** (2016), no. 11 113017, [[arXiv:1604.01388](#)].
- [400] M. Blanke, A. J. Buras, K. Gemmler, and T. Heidsieck,  *$\Delta F = 2$  observables and  $B \rightarrow X_q \gamma$  decays in the Left-Right Model: Higgs particles striking back*, *JHEP* **03** (2012) 024, [[arXiv:1111.5014](#)].
- [401] S. Bertolini, A. Maiezza, and F. Nesti, *Present and Future K and B Meson Mixing Constraints on TeV Scale Left-Right Symmetry*, *Phys. Rev.* **D89** (2014), no. 9 095028, [[arXiv:1403.7112](#)].
- [402] **ATLAS** Collaboration, T. A. collaboration, *Search for New Phenomena in Dijet Events with the ATLAS Detector at  $\sqrt{s}=13$  TeV with 2015 and 2016 data*, .

- [403] **CMS** Collaboration, V. Khachatryan et al., *Search for narrow resonances decaying to dijets in proton-proton collisions at  $\sqrt{s} = 13$  TeV*, *Phys. Rev. Lett.* **116** (2016), no. 7 071801, [[arXiv:1512.01224](#)].
- [404] **Gfitter Group** Collaboration, M. Baak, J. Cúth, J. Haller, A. Hoecker, R. Kogler, K. Mönig, M. Schott, and J. Stelzer, *The global electroweak fit at NNLO and prospects for the LHC and ILC*, *Eur. Phys. J.* **C74** (2014) 3046, [[arXiv:1407.3792](#)].
- [405] **Particle Data Group** Collaboration, C. Patrignani et al., *Review of Particle Physics*, *Chin. Phys.* **C40** (2016), no. 10 100001.
- [406] M. E. Peskin and T. Takeuchi, *Estimation of oblique electroweak corrections*, *Phys. Rev.* **D46** (1992) 381–409.
- [407] L. Lavoura and L.-F. Li, *Making the small oblique parameters large*, *Phys. Rev.* **D49** (1994) 1409–1416, [[hep-ph/9309262](#)].
- [408] J. F. Gunion, R. Vega, and J. Wudka, *Naturalness problems for  $\rho = 1$  and other large one loop effects for a standard model Higgs sector containing triplet fields*, *Phys. Rev.* **D43** (1991) 2322–2336.
- [409] A. Arhrib, R. Benbrik, M. Chabab, G. Moulataka, M. C. Peyranere, L. Rahili, and J. Ramadan, *The Higgs Potential in the Type II Seesaw Model*, *Phys. Rev.* **D84** (2011) 095005, [[arXiv:1105.1925](#)].
- [410] S. Kanemura and K. Yagyu, *Radiative corrections to electroweak parameters in the Higgs triplet model and implication with the recent Higgs boson searches*, *Phys. Rev.* **D85** (2012) 115009, [[arXiv:1201.6287](#)].
- [411] A. Maiezza, M. Nemevšek, and F. Nesti, *Perturbativity and mass scales in the minimal left-right symmetric model*, *Phys. Rev.* **D94** (2016), no. 3 035008, [[arXiv:1603.00360](#)].
- [412] E. K. Akhmedov and M. Frigerio, *Duality in Left-Right Symmetric Seesaw Mechanism*, *Phys. Rev. Lett.* **96** (2006) 061802, [[hep-ph/0509299](#)].
- [413] **MEG** Collaboration, A. M. Baldini et al., *Search for the lepton flavour violating decay  $\mu^+ \rightarrow e^+\gamma$  with the full dataset of the MEG experiment*, *Eur. Phys. J.* **C76** (2016), no. 8 434, [[arXiv:1605.05081](#)].
- [414] A. M. Baldini et al., *MEG Upgrade Proposal*, [arXiv:1301.7225](#).
- [415] **BaBar** Collaboration, B. Aubert et al., *Searches for Lepton Flavor Violation in the Decays  $\tau^\pm \rightarrow e^\pm\gamma$  and  $\tau^\pm \rightarrow \mu^\pm\gamma$* , *Phys. Rev. Lett.* **104** (2010) 021802, [[arXiv:0908.2381](#)].
- [416] T. Aushev et al., *Physics at Super B Factory*, [arXiv:1002.5012](#).

- 
- [417] K. Hayasaka et al., *Search for Lepton Flavor Violating Tau Decays into Three Leptons with 719 Million Produced Tau+Tau- Pairs*, *Phys. Lett.* **B687** (2010) 139–143, [[arXiv:1001.3221](#)].
- [418] B. Golob, L. Trabelsi, and P. Urquijo, *Impact of Belle II on flavour physics*, BELLE2-NOTE-0021, 2015.
- [419] **SINDRUM II** Collaboration, C. Dohmen et al., *Test of lepton flavor conservation in  $\mu u - e$  conversion on titanium*, *Phys. Lett.* **B317** (1993) 631–636.
- [420] **PRISM/PRIME** Collaboration, *Search for the  $\mu \rightarrow e$  Conversion Process at an Ultimate Sensitivity of the Order of  $10^{-18}$  with PRISM*, [http://j-parc.jp/researcher/Hadron/en/pac\\_0606/pdf/p20-Kuno.pdf](http://j-parc.jp/researcher/Hadron/en/pac_0606/pdf/p20-Kuno.pdf), 2006.
- [421] R. J. Barlow, *The PRISM/PRIME project*, *Nucl. Phys. Proc. Suppl.* **218** (2011) 44–49.
- [422] **SINDRUM II** Collaboration, W. H. Bertl et al., *A Search for muon to electron conversion in muonic gold*, *Eur. Phys. J.* **C47** (2006) 337–346.
- [423] **Mu2e** Collaboration, L. Bartoszek et al., *Mu2e Technical Design Report*, [arXiv:1501.05241](#).
- [424] **COMET** Collaboration, Y. G. Cui et al., *Conceptual design report for experimental search for lepton flavor violating mu- - e- conversion at sensitivity of  $10^{*-}(-16)$  with a slow-extracted bunched proton beam (COMET)*, .
- [425] **COMET** Collaboration, A. Kurup, *The COherent Muon to Electron Transition (COMET) experiment*, *Nucl. Phys. Proc. Suppl.* **218** (2011) 38–43.
- [426] **DeeMe** Collaboration, M. Aoki, *An experimental search for muon-electron conversion in nuclear field at sensitivity of  $10^{*-}(-14)$  with a pulsed proton beam*, *AIP Conf. Proc.* **1441** (2012) 599–601.
- [427] A. Maiezza, M. Nemevsek, F. Nesti, and G. Senjanovic, *Left-Right Symmetry at LHC*, *Phys. Rev.* **D82** (2010) 055022, [[arXiv:1005.5160](#)].
- [428] D. V. Forero, M. Tortola, and J. W. F. Valle, *Neutrino oscillations refitted*, *Phys. Rev.* **D90** (2014), no. 9 093006, [[arXiv:1405.7540](#)].
- [429] M. C. Gonzalez-Garcia, M. Maltoni, and T. Schwetz, *Updated fit to three neutrino mixing: status of leptonic CP violation*, *JHEP* **11** (2014) 052, [[arXiv:1409.5439](#)].
- [430] F. Capozzi, G. L. Fogli, E. Lisi, A. Marrone, D. Montanino, and A. Palazzo, *Status of three-neutrino oscillation parameters, circa 2013*, *Phys. Rev.* **D89** (2014) 093018, [[arXiv:1312.2878](#)].
- [431] H. K. Dreiner, H. E. Haber, and S. P. Martin, *Two-component spinor techniques and Feynman rules for quantum field theory and supersymmetry*, *Phys. Rept.* **494** (2010) 1–196, [[arXiv:0812.1594](#)].

- [432] J. A. Casas and A. Ibarra, *Oscillating neutrinos and  $\mu \rightarrow e\gamma$* , *Nucl. Phys.* **B618** (2001) 171–204, [[hep-ph/0103065](#)].
- [433] I. Esteban, M. C. Gonzalez-Garcia, M. Maltoni, I. Martinez-Soler, and T. Schwetz, *Updated fit to three neutrino mixing: exploring the accelerator-reactor complementarity*, *JHEP* **01** (2017) 087, [[arXiv:1611.01514](#)].
- [434] A. Abada, M. E. Krauss, W. Porod, F. Staub, A. Vicente, and C. Weiland, *Lepton flavor violation in low-scale seesaw models: SUSY and non-SUSY contributions*, *JHEP* **11** (2014) 048, [[arXiv:1408.0138](#)].
- [435] A. Ilakovac and A. Pilaftsis, *Supersymmetric Lepton Flavour Violation in Low-Scale Seesaw Models*, *Phys. Rev.* **D80** (2009) 091902, [[arXiv:0904.2381](#)].
- [436] R. Alonso, M. Dhen, M. B. Gavela, and T. Hambye, *Muon conversion to electron in nuclei in type-I seesaw models*, *JHEP* **01** (2013) 118, [[arXiv:1209.2679](#)].
- [437] D. N. Dinh, A. Ibarra, E. Molinaro, and S. T. Petcov, *The  $\mu - e$  Conversion in Nuclei,  $\mu \rightarrow e\gamma$ ,  $\mu \rightarrow 3e$  Decays and TeV Scale See-Saw Scenarios of Neutrino Mass Generation*, *JHEP* **08** (2012) 125, [[arXiv:1205.4671](#)]. [Erratum: JHEP09,023(2013)].
- [438] A. Ilakovac, A. Pilaftsis, and L. Popov, *Charged lepton flavor violation in supersymmetric low-scale seesaw models*, *Phys. Rev.* **D87** (2013), no. 5 053014, [[arXiv:1212.5939](#)].
- [439] L. Clavelli, T. Gajdosik, and W. Majerotto, *Gaugino mass dependence of electron and neutron electric dipole moments*, *Phys. Lett.* **B494** (2000) 287–296, [[hep-ph/0007342](#)].
- [440] W. C. Griffith, *Plenary talk at 'Interplay between Particle & Astroparticle physics 2014'*, <https://indico.ph.qmul.ac.uk/indico/conferenceDisplay.py?confId=1>, 2014.
- [441] S. Dimopoulos, S. Raby, and F. Wilczek, *Supersymmetry and the Scale of Unification*, *Phys. Rev.* **D24** (1981) 1681–1683.
- [442] L. E. Ibanez and G. G. Ross, *Low-Energy Predictions in Supersymmetric Grand Unified Theories*, *Phys. Lett.* **105B** (1981) 439–442.
- [443] W. J. Marciano and G. Senjanovic, *Predictions of Supersymmetric Grand Unified Theories*, *Phys. Rev.* **D25** (1982) 3092.
- [444] M. B. Einhorn and D. R. T. Jones, *The Weak Mixing Angle and Unification Mass in Supersymmetric SU(5)*, *Nucl. Phys.* **B196** (1982) 475–488.
- [445] U. Amaldi, W. de Boer, and H. Furstenau, *Comparison of grand unified theories with electroweak and strong coupling constants measured at LEP*, *Phys. Lett.* **B260** (1991) 447–455.

- 
- [446] P. Langacker and M.-x. Luo, *Implications of precision electroweak experiments for  $M_t$ ,  $\rho_0$ ,  $\sin^2 \theta_W$  and grand unification*, *Phys. Rev.* **D44** (1991) 817–822.
- [447] J. R. Ellis, S. Kelley, and D. V. Nanopoulos, *Probing the desert using gauge coupling unification*, *Phys. Lett.* **B260** (1991) 131–137.
- [448] R. N. Mohapatra, *Supersymmetric grand unification: An Update*, in *Proceedings, Summer School in Particle Physics: Trieste, Italy, June 21–July 9, 1999*, pp. 336–394, 1999. [hep-ph/9911272](#).
- [449] M. Papucci, J. T. Ruderman, and A. Weiler, *Natural SUSY Endures*, *JHEP* **09** (2012) 035, [[arXiv:1110.6926](#)].
- [450] P. Batra, A. Delgado, D. E. Kaplan, and T. M. P. Tait, *The Higgs mass bound in gauge extensions of the minimal supersymmetric standard model*, *JHEP* **02** (2004) 043, [[hep-ph/0309149](#)].
- [451] A. Maloney, A. Pierce, and J. G. Wacker, *D-terms, unification, and the Higgs mass*, *JHEP* **06** (2006) 034, [[hep-ph/0409127](#)].
- [452] M. Malinsky, J. C. Romao, and J. W. F. Valle, *Novel supersymmetric  $SO(10)$  seesaw mechanism*, *Phys. Rev. Lett.* **95** (2005) 161801, [[hep-ph/0506296](#)].
- [453] R. Kuchimanchi and R. N. Mohapatra, *No parity violation without  $R$ -parity violation*, *Phys. Rev.* **D48** (1993) 4352–4360, [[hep-ph/9306290](#)].
- [454] S. K. Majee, M. K. Parida, A. Raychaudhuri, and U. Sarkar, *Low intermediate scales for leptogenesis in SUSY  $SO(10)$  GUTs*, *Phys. Rev.* **D75** (2007) 075003, [[hep-ph/0701109](#)].
- [455] V. De Romeri, M. Hirsch, and M. Malinsky, *Soft masses in SUSY  $SO(10)$  GUTs with low intermediate scales*, *Phys. Rev.* **D84** (2011) 053012, [[arXiv:1107.3412](#)].
- [456] C. Arbelaez, R. M. Fonseca, M. Hirsch, and J. C. Romao, *Supersymmetric  $SO(10)$ -inspired GUTs with sliding scales*, *Phys. Rev.* **D87** (2013), no. 7 075010, [[arXiv:1301.6085](#)].
- [457] P. S. Bhupal Dev and R. N. Mohapatra, *Electroweak Symmetry Breaking and Proton Decay in  $SO(10)$  SUSY-GUT with TeV  $W(R)$* , *Phys. Rev.* **D82** (2010) 035014, [[arXiv:1003.6102](#)].
- [458] A. Falkowski, D. M. Straub, and A. Vicente, *Vector-like leptons: Higgs decays and collider phenomenology*, *JHEP* **05** (2014) 092, [[arXiv:1312.5329](#)].
- [459] ATLAS Collaboration, G. Aad et al., *Search for new phenomena in dijet mass and angular distributions from  $pp$  collisions at  $\sqrt{s} = 13$  TeV with the ATLAS detector*, *Phys. Lett.* **B754** (2016) 302–322, [[arXiv:1512.01530](#)].

- [460] Y. Zhang, H. An, and X.-d. Ji, *Constraining the right-handed scale through kaon mixing in the supersymmetric left-right model*, *Phys. Rev.* **D78** (2008) 035006, [[arXiv:0710.1454](#)].
- [461] J. A. Aguilar-Saavedra, R. Benbrik, S. Heinemeyer, and M. Pérez-Victoria, *Handbook of vectorlike quarks: Mixing and single production*, *Phys. Rev.* **D88** (2013), no. 9 094010, [[arXiv:1306.0572](#)].
- [462] D. V. Forero, S. Morisi, M. Tortola, and J. W. F. Valle, *Lepton flavor violation and non-unitary lepton mixing in low-scale type-I seesaw*, *JHEP* **09** (2011) 142, [[arXiv:1107.6009](#)].
- [463] K. Huitu, P. N. Pandita, and K. Puolamaki, *Mass of the lightest Higgs boson in supersymmetric left-right models*, *Phys. Lett.* **B423** (1998) 97–103, [[hep-ph/9708486](#)].
- [464] K. S. Babu and A. Patra, *Higgs Boson Spectra in Supersymmetric Left-Right Models*, *Phys. Rev.* **D93** (2016), no. 5 055030, [[arXiv:1412.8714](#)].
- [465] M. E. Krauss, W. Porod, and F. Staub, *SO(10) inspired gauge-mediated supersymmetry breaking*, *Phys. Rev.* **D88** (2013), no. 1 015014, [[arXiv:1304.0769](#)].
- [466] M. Hirsch, M. Malinsky, W. Porod, L. Reichert, and F. Staub, *Hefty MSSM-like light Higgs in extended gauge models*, *JHEP* **02** (2012) 084, [[arXiv:1110.3037](#)].
- [467] M. Hirsch, W. Porod, L. Reichert, and F. Staub, *Phenomenology of the minimal supersymmetric  $U(1)_{B-L} \times U(1)_R$  extension of the standard model*, *Phys. Rev.* **D86** (2012) 093018, [[arXiv:1206.3516](#)].